Final Report

CONTAMINANT TRANSPORT

IN

COASTAL AQUIFERS

By

Yuan Ding
Yong Peng

Department of Civil and Environmental Engineering
New Jersey Institute of Technology
Newark, NJ

Submitted

To

New Jersey Department of Environmental Protection

Division of Science, Research and Technology

Trenton, New Jersey

April 2009

Contract Number SR02-035

Research Team

Department of Civil and Environmental Engineering
New Jersey Institute of Technology

Paul C. Chan, Ph.D., Professor
Yuan Ding, Ph.D., Associate Professor
Robert Dresnack, Ph.D., Professor
John R. Schuring, Ph.D., Professor
Yong Peng, Ph.D.

ABSTRACT

CONTAMINANT TRANSPORT IN COASTAL AQUIFERS

Coastal aquifers are distinguished from other aquifers because of tidal effects which cause complicated groundwater flow and contaminant transport phenomena in regions immediately adjacent to the coast. This study is designed to address the significance of tidal influence on contaminant transport by focusing on one-dimensional homogeneous coastal aquifers.

This study formulates a conceptual model and corresponding flow and transport equations, analyzes coastal boundary conditions, solves numerically the transport equation, and uses experiments to verify the numerical results.

Results of the numerical and experimental studies conclude that tides can have a significant impact on contaminant transport, especially when under unconfined aquifer conditions, subject to moderate to high tidal amplitude, with low groundwater flow velocity in the aquifer, and within areas adjacent to the coastal boundary. Quantitatively, under these favorable conditions, contaminant discharge can be enhanced by tides by a factor of two or three during the early stages of discharge, and the enhanced discharge can still be substantial during later stages by 30 to 50 percent. When the groundwater flow is close to stagnant, as demonstrated in the case study, the tidal impact is most apparent, resulting in significant discharge tens of years ahead of the case without tides.

TABLE OF CONTENTS

TABLE OF CONTENTS
(Continued)

Chapter **Page**

TABLE OF CONTENTS
(Continued)

Chapter **Page**

LIST OF TABLES

LIST OF TABLES

LIST OF FIGURES

LIST OF FIGURES
(Continued)

LIST OF FIGURES
(Continued)

LIST OF FIGURES
(Continued)

LIST OF FIGURES
(Continued)

LIST OF FIGURES
(Continued)

CHAPTER 1

INTRODUCTION

This chapter introduces the background of the current study, including a general description of contaminant transport in coastal aquifers, the current research status with regard to the tidal influence on contaminant transport and its limitations, and an outline of the objective and scope of study for the current research.

1.1 Contamination Problem in Coastal Waters

Coastal waters and estuaries have served as important ecological and economic centers for human beings, fostering the development of shipping, industry, fisheries, and commerce. The quality of coastal and estuarine waters is affected not only by activities occurring directly in the waters, but also by industrial, agricultural and land use practices throughout regional watersheds contributing water and sediment to the coastal water bodies. Efforts have been made to track the sources of contamination in coastal waters and major attention has been given to the contribution by tributary inputs, storm water, combined sewer overflows (CSO), municipal/industrial discharges and atmospheric deposition. The state of knowledge on contaminant transport as well as other environmental problems encountered in estuarine waters has been summarized in two authoritative treatises (Ippen, 1966; Fischer et al., 1979). Beyond these sources, the effects of groundwater on coastal environments are not as well known as those of river flow and storm water. In most cases of coastal aquifers, contaminant sources are released either on the ground or directly into the subsurface, with contaminants penetrating into

the underlying inland aquifers and eventually transporting to surface water bodies such as rivers, harbors and oceans. Consequently, groundwater containing pollutants can have a significant influence on coastal ecosystems, especially when pollutant concentration is high in groundwater or the quantity of submarine groundwater discharge (SGWD) is relatively large.

Recently, several studies have indicated that groundwater seepage can be a significant component of the total outflow discharge to the coasts (e.g., Moore, 1999; Cambareri and Eichner, 1998; Church, 1996; Moore, 1996; Reilly and Goodman, 1985). Therefore, if the fresh groundwater source is contaminated with pollutants derived from inland, such as those by hazardous industrial waste, by leachate from landfills, by oil spills, by agricultural activities, and by sites of radioactive waste repositories (to mention but a few of the more acute pollution sources), these contaminant sources can become a potential threat to the coastal water environment. There are, indeed, numerous coastal waters that have encountered the problem with regard to groundwater discharge of pollutants. For example, groundwater seepage has a major influence on nutrient levels on the Guam fringing reef flat (Marsh, 1977), Great South Bay, New York (Capone and Bautista, 1985), Nauset Marsh estuary, Massachusetts (Portnoy et al., 1998), and Mid-Atlantic coastal waters (Gallagher et al., 1996). And others have reported other pollutant loading via groundwater flow along other coastlines (e.g., Johannes, 1980; Sewell, 1982; Nixon et al., 1986; Giblin and Gaines, 1990; Valiela et al., 1978, 1992; Simmons, 1990; Simmons et al., 1992).

Thus, it is important to correctly identify the path and fate of contaminants in groundwater systems in coastal areas. The significance includes good management of

water resources to protect the population who depends on contaminated groundwater supply, successful soil and groundwater remediation, pollution source release control, and pursuing potential responsible polluters, among many others.

1.2 Limitations in Previous Studies

It is generally recognized that groundwater flow and contaminant transport in coastal aquifers are rather complicated due to the presence of coastal dynamic boundary conditions in the open sea, which are characterized by the oscillations of tidal fluctuations, wave activities, beach seepage, and saltwater intrusion (Nielsen, 1990; Baird and Horn, 1996; Zhang et al., 2001, 2002). These oscillations are transmitted into the aquifers, with the amplitude decreasing in the landward direction. The groundwater fluctuations induced by the sea level oscillations are termed "groundwater waves". In unconfined aquifers, this leads to water table fluctuations corresponding to tidal frequencies, whereas in confined aquifers, this results in the amplitude of piezometric fluctuation within the aquifer. This study focuses on understanding the transport of contaminants in coastal aquifers subject to tidal fluctuations.

The general framework of the problem can be modeled by a pair of partial differential equations, the first of which is for the groundwater flow subject to tidal fluctuations and the second is for contaminant transport. The solution of these two equations, either in closed form or in numerical solution, must be accompanied with appropriate boundary conditions in order to provide the proper perspective of the problem. Some limitations of the investigations are summarized as follows:

1. Although three types of boundary conditions namely, the Dirichlet, Cauchy, and Neumann, are well known in boundary value problems, no comparative

analysis has been found for contaminant concentration or flux representation in tidal boundary conditions. Thus, a comparative study of these conditions is necessary.

2. Estimation of the potential impact area induced by tidal fluctuations on water table or piezometric head fluctuation appears to be inconsistent in groundwater literature, ranging from the order of ten meters for some studies to several kilometers for some others. An analytical evaluation of the potential effect by tides regarding water table or piezometric head fluctuation inland is necessary for the consideration of the potential effect by tides regarding contaminant transport to and from proximate aquifers.

3. In groundwater engineering, the confined aquifer is considered in general as a "standard" unit in most analyses. Thus, it is of importance to consider tide-induced fluctuations of contaminant transport in confined aquifers. As a result, a comparison can be made for the tidal influence in unconfined and confined aquifers.

4. The relative significance of the tidal effect on contaminant transport has been barely analyzed. The significance of tidal effect can be quantified by potential impact area. Only the potential impact area is of concern when we consider the tidal influence, and successful identification of this area is important. Also, tidal influence may be significant under certain conditions but less so under others. It is necessary to identity what these conditions are.

5. No experimental study on contaminant transport induced by tidal fluctuations has been found in currently available literature, except that Zhang and Volker's recent study (Zhang et al., 2001, 2002; Volker et al., 2002) included tidal fluctuations in an unconfined aquifer. But with a main focus on variable density flow, they neither addressed the significance of tidal influence as compared to the zero-tide case, nor compared tidal impact in unconfined aquifers with that in confined aquifers.

1.3 Objective and Scope of Study

The main objective of this study is to investigate contaminant transport and its corresponding discharge in coastal aquifers subject to tidal fluctuations.

The scope of study is as follows:

1. To formulate the governing equations of the groundwater flow and contaminant transport in a coastal aquifer and to analyze the corresponding

boundary conditions of contaminant concentration or flux in coastal water due to tidal fluctuations;

2. To derive a finite difference solution for the governing equations formulated in (1) incorporating tidal fluctuations;

3. To conduct numerical simulations addressing the tidal impact on contaminant transport;

4. To identify quantitatively the area of influence by tides in both confined and unconfined coastal aquifers;

5. To conduct laboratory experiments investigating contaminant transport subject to tidal fluctuations, including both closed- and unconfined-condition experiments simulating confined and unconfined situations, respectively; and

6. To compare the experimental and numerical results and draw conclusions based on the comparison.

CHAPTER 2

LITERATURE REVIEW

In this chapter, an exhaustive literature review is presented regarding both groundwater flow and contaminant transport in coastal aquifers. It considers various factors that influence groundwater flow and contaminant transport and outlines the conclusions made by prior authors as to the various aspects of how each factor, or the combination of these factors, affect the flow and transport pattern in coastal aquifers.

2.1 Groundwater Dynamics in Coastal Aquifers

The study of groundwater flow and contaminant transport in coastal aquifers is a crucial part of the investigation of the contribution of contamination from pollution sources along coastlines to coastal water bodies. Groundwater flow and contaminant transport in coastal aquifers are fairly complicated, and Figure 2.1 gives a schematic illustration of a typical coastal aquifer-sea water exchange system.

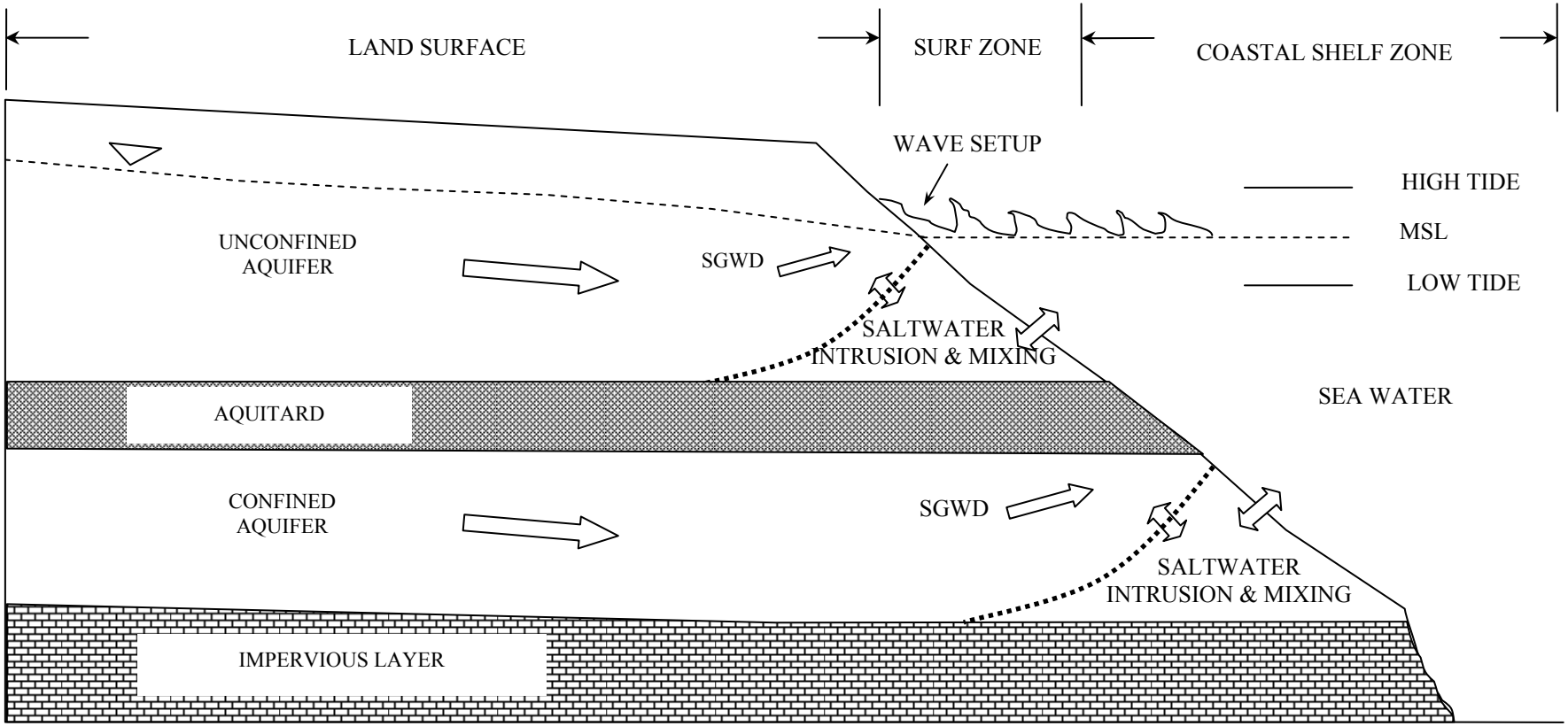

Figure 2.1 Schematic Illustration of Coastal Aquifers and the Open Sea.

Water seeping from the land into the coastal ocean is considered ground water, regardless of its salinity or history. The coastal aquifer, defined as the "subterranean estuary" by Moore (1999), is the subsurface region where ground water derived from land drainage measurably dilutes sea water that has invaded the aquifer through a free connection to the sea. Several mechanisms have been proposed to explain the interaction between sea water and fresh ground water in coastal sediments. Interactions between fresh water and sea water through coastal aquifers may be driven by a seaward hydraulic gradient, i.e., fresh submarine groundwater discharge (SGWD) near the shoreline or in deeper sea water through confined aquifers (See Figure 2.1). Secondly, the cycling of fresh ground water and sea water can be due to variable density flow: sea water intrusion and mixing occurs in regions immediately adjacent to the sea. This interaction can be predicted by the classic Ghyben-Hezberg relation, and can be analyzed or modeled by improved methods proposed by theoreticians such as Hubbert, Muskat, Cooper, Glover, and Henry (Reilly and Goodman, 1985). Thirdly, circulation of the two fluids can also be accelerated by tidal pumping and wave setups (Li and Barry, 2000). During rising tide or wave buildup, sea water enters the aquifer; during falling tide or wave setback, it flows back to the sea. Through each tidal cycle, the net movement of the fresh water-saltwater interface may be small (depending on average hydraulic gradient), but the preferential flow caused by anisotropic permeability may produce irregular saltwater and fresh water mixing (Moore, 1999). Furthermore, the cyclic flow of sea water through coastal aquifers could be driven by geothermal heating (Kohout, 1965), deep pressure force (Manheim, 1967), sea water evaporation (Adams and Rhodes, 1960; Simms, 1984), and sea level change (Moore, 1999).

In addition to the general factors that influence the groundwater flow in a common aquifer system, i.e., hydraulic gradient, hydraulic conductivity, anisotropy, porosity, boundary conditions, recharge, pumping, and other geological settings (e.g., Bear, 1972, 1979; Freese and Cherry, 1979; Silliman, 1995; Gerke and van Genuchten, 1996; Kim and Parizek, 1997; Whitaker and Smart, 1997; Bakker et al., 1999; Kim et al., 2000; Lambrakis and Kallergis, 2001; Simmons et al., 2001), the presence of the coastal boundary makes coastal aquifers even more complex and thus distinct from other aquifer systems. The rise and ebb of tides along coastlines produce periodical fluctuations of the groundwater table in coastal aquifers. The fluctuations of the groundwater table, in turn, drive surface water into or out of the aquifers. Experimental studies as well as mathematical solutions have long been adopted in the investigation of the temporal and spatial conditions of groundwater flow regimes adjacent to coastal areas (Ferris, 1951; Gregg, 1966; Serfes, 1987). The major factors that are critical to coastal aquifer studies include tides and tide-introduced estuarine waves, moving boundary conditions resulting from tidal fluctuations, beach slope and seepage dynamics, density variable flow, and the saltwater-freshwater interface introduced by saltwater intrusion. These topics have been intensively addressed by a number of studies in recent years (Baird and Horn, 1996; Barry et al., 1996; Li et al., 1997; Nielsen et al., 1997; Naji et al., 1998; Ataie-Ashtiani et al., 1999; Bower et al., 1999; Jiao and Tang, 1999; Li et al., 1999; Trefry, 1999; Li and Barry, 2000; Li et al., 2000a; Li et al., 2000b; Li and Jiao, 2003). Some important results regarding these factors are outlined in the following paragraphs.

There are three distinct features of the local water table fluctuations caused by oceanic tides identified by Nielsen (1990): (1) Asymmetric water table fluctuation - steep rising phase versus flat falling phase, which is caused by different effective transmissivities and sloping beach faces; (2) The amplitude of water table fluctuation shows an exponential decay with increasing distance from the coastline because of the dissipative characteristics of the system; (3) There exists a linear phase lag between the water table fluctuations at different locations in the cross-shore direction due to the increase of traveling time of wave propagation. Later, Li et al. (1997) reached the same conclusions by using numerical modeling of tide-induced beach water table fluctuations. The results are also confirmed by the field observations of Erskine (1991) and Serfes (1991), and were found to be consistent with the theoretical relationship between the tide and the piezometric response (Todd, 1959).

The distance away from the coastline that can be affected by tidal fluctuations varies depending upon both aquifer and tide characteristics. The numerical study of Yim and Mohsen (1992) implies that the effect of tides is significant only over a short distance, i.e., approximately 40 feet from the bank of the estuary for the unconfined aquifer considered in the study. A numbers of studies, however, have shown that the influence distance varies for unconfined and confined aquifers. Tidal waves propagate much further inland in confined aquifers than in unconfined aquifers because unconfined aquifers have storage capacity several orders of magnitude larger than the confined aquifer storage, and thus unconfined aquifers have a much larger capacity of damping pressure waves over a short distance (Serfes, 1991; Erskine, 1991). White and Robert (1994) conclude, “The attenuation of the tidal response with distance varies markedly for

confined and unconfined aquifers. Confined aquifers even of medium to low permeability have a stiff response and exhibit low attenuation with fluctuations potentially extending to a hundred meters or more from open water. Unconfined aquifers are heavily damped and unless the permeability is above about 10 m/s (8.64 m/d) significant fluctuations are unlikely to extend to more than about 20 or 30 m from open water." The range affected can be even larger when cross-shore estuarine waves induced by tides are also considered (Li et al, 2000). These studies are somewhat inconsistent in magnitude with Lanyon et al. (1982), who have shown that a typical damping distance for tidal water table fluctuations in an unconfined aquifer is several hundred meters, whereas the tidal influence on a confined aquifer can extend landward by several thousand meters.

Oceanic tides not only directly contact aquifers from the coast lines, but also propagate into an estuary forming cross-shore estuarine waves. Both the oceanic tides and estuarine waves can influence the aquifer behaviors at natural coasts regarding the groundwater head fluctuation. More interestingly and significantly, in their study Li et al (2000) include both the effects of oceanic and estuarine tides on aquifer dynamics. The study demonstrates that the interaction between the cross- and along-shore tidal waves in the aquifer area near the estuary entry and the interaction zone can reach as far both inland and from estuary interface as one and a half kilometers. As the distance from the estuary or coastline increases, the wave interaction is weakened and the aquifer response is reduced. The study also suggests that the tidal wave interactions are non-linear, in the sense that the net effect of both oceanic tides and estuarine waves is not simply the superposition of the individual effects of oceanic tides and estuarine waves.

Water density is another important factor affecting coastal groundwater flow. The density of pure fresh groundwater in natural aquifer systems is 0.9982 kgl^{-1} at 20 °C (White et al., 1963), while the density of "average" surface seawater ranges between 1.022 and 1.028 kgl^{-1} which is partly dependent on the temperature and the contaminant concentration (Chow, 1964). In relatively homogeneous porous media in a coastal area, the denser saltwater tends to remain separated from the overlying freshwater. A mixing zone, which is known as the zone of diffusion or dispersion, forms between the two fluids. To enable a reasonable and quantitative description of the system, various simplifying assumptions have been made, which are categorized into two major approaches: sharp interface (immiscible fluids) and dispersed interface (miscible fluids) (Reilly and Goodman, 1985). From the perspective of groundwater flow, a major consequence that results from the presence of a saltwater-freshwater interface is that not only a circulation of saltwater beneath the interface forms, but also the fresh groundwater travels upwards towards the beach along the freshwater-saltwater interface (vertical flow) and exits the aquifer around the coastline instead of deep under the seawater (Glover, 1959; Volker et al., 2002). Studies have been conducted to investigate the impact of different parameters on the shape and location of the interface (Reilly and Goodman, 1985; Volker and Rushton, 1982). However, the presence of the interface may not significantly affect net mass discharge in coastal aquifers from the perspective of mass balance in the long run.

Fluid density variations may also occur because of changes in the contaminant or colloidal concentration, temperature, and pressure of the groundwater. These conditions include high-level radioactive waste disposal, groundwater contamination, and

geothermal energy production in addition to seawater intrusion (Pinder and Cooper, 1970; Schincariol and Schwartz, 1990; Herber et al., 1988). In most of such situations, groundwater dynamics are strongly influenced by destabilizing density differences producing convective currents, called "free convection" (Ghebart et al., 1988). The significant impacts induced by the free convection process are: (1) the total quantity of contaminant transport involved in the convective process is typically far greater than that of diffusion transport, (2) the time scales associated with the mixing process are significantly reduced, and (3) the dimensions of the mixing zone are typically larger and, therefore, enable contaminants to spread over much greater distances (Simmons et al., 2001). The coupling of groundwater flow and contaminant transport, however, can be simplified to advective and velocity-dependent dispersion in usual low-concentration situations if all contaminant properties such as density and viscosity are nearly constant and the overall fluid motion is independent of the motion of individual species (Kolditz et al., 1998).

A few authors have also studied the tidal effect under different beach slopes (Nielson, 1990; Li et al., 2000; Li and Jiao, 2003). The cases in Teo et al. (2003), for example, demonstrate the influence of beach slope on the tide-induced water table fluctuations. In general, water table level increases as beach slope decreases.

2.2 Contaminant Transport in Coastal Aquifers

Since contaminants in aquifer systems migrate with ground water flow, any factors that may affect groundwater flow are also likely to influence the migration of contaminants in aquifers. As a result, the tidal influence on flow pattern discussed in the previous section

applies in general to contaminant transport patterns in coastal aquifers. One should, however, approach it with caution. Because contaminants are chemicals or bacteria or virus which are mostly physically, chemically and biologically active, the transport of contaminants are subject to physical, chemical and biological activities, such as contaminant density (Kolditz et al., 1998), adsorption and desorption (Serrano, 2001), retardation (Sen et al., 2002), degradation (Sandrin et al., 2001), and chemical-biological reactions (Baverman et al., 1995). Furthermore, the spatial and temporal distribution of contamination sources may also have a significant impact on contamination transport and plume distribution in the subsurface.

To date, contamination transport in coastal aquifers subject to tidal fluctuation has been barely investigated. A major contribution to the study of contamination transport in coastal aquifers, as the author is aware, comes from Yim and Mohsen (1992), Li et al. (1999), Zhang et al. (2001, 2002), and Volker et al. (2002), each of whom considered only a few characteristics of the geological conditions or contaminant properties deemed important by the individual investigators. A summary review of their works follows.

Yim and Mohsen (1992) first develop a one-dimensional numerical model to simulate the migration process of a contaminant plume within tidally influenced unconfined aquifers. They take into consideration both oscillating groundwater velocities and contaminant dispersions. Model simulations demonstrate that a major effect that tidal fluctuation has on the migration process of the contaminant plume is on the exit concentration discharging to the tidal estuary. The results show that tidal fluctuation causes the exit contaminant concentration to be significantly diluted by the estuarine water body.

Because of the relatively high advective, dispersive and convective fluxes induced by tides, contaminant transport in the tidally active zone is hastened by tide activities. Yim and Mohsen (1992) observe that tidal fluctuation hastens the rate of plume migration near the bank of the estuary (thus the rate of contaminant discharge into the estuary). Zhang et al. (2001, 2002), by experimental and mathematical modeling, also find that the contaminant plume is more diffusive when it reaches the interactive zone of saltwater and freshwater. Wrenn et al. (1997) study the nutrient movement process in a bioremediation zone in a sandy beach on the southwestern shore of Delaware Bay. Their study further demonstrates that the washout process of nutrients in the sandy beach is not only accelerated by tides but also by ocean waves especially during storms.

Similar to the tidal influence on groundwater flow, however, the effect of tides on contaminant transport is significant only over a short distance (the tidally active zone). The effective distance is approximately 40 feet inland from the bank of the estuary in the case of Yim and Mohsen (1992). For the case of Wrenn et al. (1997), it is about 60 feet inland from the shoreline (only within the remediation zone on the sandy beach). Zhang et al. (2001, 2002) also indicate that tides are effective only close to and at the saltwater-freshwater interface. Away from the tidally active zone, contaminant plume migration is barely influenced by tidal fluctuation or saltwater-freshwater interaction (Zhang et al, 2001, 2002; Volker et al., 2002). All these cases address tidal effects in unconfined aquifers, while no one, to the author's knowledge, has studied it within confined aquifers.

The study of Yim and Mohsen (1992) indicates that tide fluctuations not only accelerate the mixing process and discharge rate of contaminants at the tide-groundwater interface, but also tend to increase the total amount of contamination discharged into the

estuary over a given period of time. With different tidal amplitudes, the study suggests the difference in the amount of contamination discharged may vary up to more than 30% compared to each other depending upon the regional hydraulic gradient, hydraulic conductivity, and other factors (Yim and Mohsen, 1992). In the study of Li et al. (1999), however, modeling results show that groundwater circulation and oscillating flow, caused by wave setup and tides, may constitute up to 96% of submarine groundwater discharge compared with 4% due to the net groundwater discharge. That means that these local flow processes do not change the total amount of land-derived chemical input to the ocean over a long period (e.g., yearly), while they do induce fluctuations of the chemical transfer rate as the aquifer undergoes saltwater intrusion. For long periods of time, contamination in coastal water contributed by submarine groundwater discharge is derived totally from net fresh groundwater discharge. Tidal circulation accelerates the contaminant washout in a relatively short period of time. Thus, tidal effects may result in a substantial increase in chemical fluxes to the ocean over a short period (e.g., monthly and by a factor of up to 20 times above the average level) (Li et al., 1999; Moore, 1999).

As discussed earlier, the existence of a saltwater-freshwater interface and the groundwater circulation in the tidally active zone may change the flow path of groundwater flow (Glover, 1959; Volker et al., 2002). This, in turn, would impact the transport path, exit point, and even discharge rate of contaminant fluxes. This is especially true when the contaminant is denser than the ambient groundwater (Zhang et al., 2001, 2002). As to the impact of contaminant density, the studies of Volker et al. (2002) and Zhang et al. (2001, 2002) show that the denser the contaminant plume, the more diffusive the plume front is towards the coastline and the freshwater-saltwater

interface zone, and that a denser contaminant plume travels significantly more quickly in the vertical direction than a less dense one does, which results in a much thicker polluted area in the vertical direction for the denser contaminant plume. Furthermore, instability in the form of fingers of the contaminant plume may also occur for a density difference of 1.2% or larger between the contaminant and ambient groundwater (Zhang et al., 2002).

With seawater density considered, when a contaminant plume travels to the saltwater-freshwater interface, it tends to travel upwards towards the beach along the interface (vertical flow) and exit the aquifer around the coastline. The contaminant plume would otherwise travel through and exit deep under the seawater if no density difference between seawater and freshwater is taken into account (thus there is no saltwater-freshwater interface) (Zhang et al., 2001, 2002). Therefore, neglect of seawater density, thus the saltwater-freshwater interface, will result in an underestimate of contaminant mass transport rate exiting around the coastline (but not the total discharge). However, the neglect of the freshwater-saltwater interface and tidal fluctuations does not noticeably affect the horizontal migration rate of the contaminant plume before it reaches the interface and tidally active zone, as suggested by the studies of Volker et al. (2002) and Zhang et al. (2001, 2002).

With regard to the influence on groundwater flow and contaminant transport, the significance of the factors varies. Among the factors, regional groundwater velocity (determined by the combination of hydraulic gradient and hydraulic conductivity) has the most significant influence on the groundwater flow rate, while tidal amplitude, aquifer thickness, specific yield, and upstream boundary condition (constant or changing freely with water table fluctuation), etc., have relatively less effects on aquifer behaviors (Yim

and Mohsen, 1992; Li et al., 1997). Despite that fact, tide-induced water table and flow fluctuations adjacent to the coastline can be significant, especially in the case of a small regional hydraulic gradient and thus low net groundwater discharge rate, which could be the case for many coastal aquifers. For an even extreme situation, when the mean regional gradient is zero and thus net inland groundwater discharge is also zero, oceanic tides may, more apparently, cause seawater and groundwater circulation in coastal areas and drive contaminant washout and saltwater intrusion (Li and Jiao, 2003).

As a summary, when the areas immediately adjacent to the coastline and relatively short-time transient flow and transport problems are considered, the tidal effect is important and has significant practical implications. In the current study, considered are contaminant release problems by landfills and industrial waste sites near the coastline, for example, tens of meters away from coast water or even right above beach water. Consequently, tides play an important role in these problems and they are addressed specifically by this study.

2.3 Study Approaches

Analytical solutions, numerical simulations, and experiment and field observations are used to address groundwater flow and contaminant transport problems in coastal aquifers. Analytical methods basically provide solutions to governing equations of groundwater flow and contaminant transport with simplified boundary conditions and hydrogeological and chemical properties. Limitations for analytical solutions of groundwater flow and contaminant transport in coastal aquifers include: assumptions of a uniform thickness of aquifer, a constant beach face angle, a uniform hydraulic conductivity and specific yield,

a single inland boundary condition, and a single-phase homogeneous fluid, among others (Ataie-Ashtiani et al., 1999). More complicated analytical solutions may take into consideration multiple aquifer layers and tidal fluctuations (Li et al., 1997; Li et al., 2000; Townley, 1995; Nielsen, 1990). But among these studies, most attention has been given to groundwater flow rather than to solute transport. It is extremely difficult or even impossible to derive analytical solutions to solute transport when a more complex system is considered, e.g., a system with one or more aspects among moving and periodic boundary conditions, variable-density flow, heterogeneity of geological settings, physical, chemical, and biological degradations, and multiple dimensions.

Numerical modeling has been given more and more attention recently only with the aid of computers. It is more powerful than analytical analysis of a complex system. Unfortunately, even though numerical simulation has the potential to undertake the tasks, a comprehensive simulation model that can account for all the factors has not yet been constructed. Still, numerous numerical models have been developed dealing with one or more facets concerning groundwater flow and contaminant transport in coastal aquifers. The major topics that are most frequently considered and intensively studied in numerical modeling include variable density flow and contaminant transport (Kolditz et al., 1998 and Simmons et al., 2001), tidally influenced water table fluctuation or periodic boundary conditions (Volker et al., 2002; Li et al., 1997; Townley, 1995), saltwater-freshwater interface or saltwater intrusion (Oude Essink, 2001; Naji et al., 1998), and sloping beaches and seepage dynamics (Li et al., 1997).

One of the most successful models is the saturated-unsaturated transport finite-element ground-water simulation model (SUTRA), developed by Voss (1984), which can

be used to simulate variable-density flow with chemically reactive single species contaminant transport in saturated-unsaturated formations. Later, Ataie-Ashtiani et al. (1999) modified SUTRA such that it can account for periodic boundary conditions and sloping beach faces, in addition to variable density and variably saturated flow. A potential problem embedded in the exiting models is that the built-in boundary conditions are fixed and as indicated in a later analysis, this boundary condition is not appropriate for the particular problem considered in this study. As a result, a numerical solution will be developed to solve the flow and transport equations directly, incorporating the correct boundary conditions pertinent to the coastal boundary.

The widely used models for groundwater flow and solute transport, such as MODFLOW and SUTRA, or the others developed by various authors, do not account for tidal fluctuations. Even though SUTRA modified by Ataie-Ashtiani et al. (1999) can incorporate tidal fluctuations, it is based on a boundary condition describing contaminant concentration or flux at the coastal boundary that is deemed inappropriate for the problem in this study (refer to boundary condition analysis in Chapter 3). These limitations in the existing numerical models and the relative affordable complexity of developing numerical solutions and program codes allow this study to derive numerical solutions to the flow and transport equations and run simulations to study tidal fluctuations.

Laboratory experimentation is another important and useful tool for the study of groundwater flow and contaminant transport. Hydrologists have a long history of utilizing laboratory experiments in the study of groundwater flow and contaminant transport. The laboratory experiments, known as intermediate scale experiments, or ISEs, have been able to investigate contaminant advection, diffusion, dispersion, and fluid flow

in saturated and partially saturated systems, flow and transport in homogeneous and heterogeneous media, transport of contaminants under uniform- and variable-density flow fields, multiphase transport, chemical reactions, particle transport, and microbial interactions, as summarized by Silliman et al. (1998). The experimental study of tidal impact on flow and transport, however, has been barely conducted by investigators. The few include Volker et al. (2002) and Zhang et al. (2001, 2002). Both Volker and Zhang actually consider only saltwater density and use the same experiment results. Even though a tide is included in the studies, variation in tidal amplitude is not considered and the results are not compared to a no-tide baseline for the identification of the significance of tidal impact. However, the experimental design and processes in their studies are a good starting point for the proposed study, except that this study will focus more on tidal fluctuations than variable density flow and beach slope, and that confined-aquifer situations are included to be compared with the unconfined-aquifer situations.

CHAPTER 3

PROBLEM FORMULATION AND SOLUTION

Equation Chapter 3 Section 1In this chapter, the research problem is formulated from the conceptual model illustration to the solution to the problem. Equations of groundwater flow and contaminant transport are formulated, which consider both the case subject with no tide, and the case with tidal fluctuations. Contaminant input, initial conditions, and boundary conditions are described in order, and an important discussion with regard to the baseline selection is presented as well.

3.1 Conceptual Model of the Research Problem

From the discussions in Chapter 2, it is recognized that the coastal groundwater flow and contaminant discharge problem includes a number of potential issues such as tidal fluctuations, variable density flow, beach seepage, and oceanic waves. It would be ideal if a study could incorporate all of these aspects at the same time, as in the real world. However, since each of these aspects itself is a big topic and needs elaborative study to fully understand, it is beyond the limit of the current study to incorporate all factors. On the other hand, taking into consideration one aspect and leaving the others constant or ignored is a common way of addressing complicated problems, and this can still lead to an understanding of this particular facet of the problem. Specifically in this study, focus is put on tidal fluctuations only. It is believed that by doing this important and correct information can be gained with regard to the actual tidal impact on contaminant transport, because, to the author's knowledge, superposition theory applies to groundwater flow and

contaminant transport; that is, if the information on purely tidal impact is gained, it can be used in conjunction with the information regarding the impact by saltwater intrusion, beach slope, and oceanic waves to help gain a better understanding of the whole picture of contaminant transport in coastal aquifers. Based on this logic, this study makes the following the assumptions in order to focus on tidal fluctuations:

- one-dimensional saturated flow
- homogeneous and isotropic geological settings
- constant density flow
- vertical beach face
- zero oceanic waves
- pulse-type contaminant source release

The conceptual model is illustrated in Figure 3.1 (refer to Figure 2.1 for a comparison to the conceptual model of more complicated real situations). Groundwater flows from the inland (left) to the coast (right). Contaminant source is released at the left boundary of the aquifer system. In the following sections, presented in order are the equations describing the groundwater flow and contaminant transport, and the corresponding initial and boundary conditions for the problem considered.

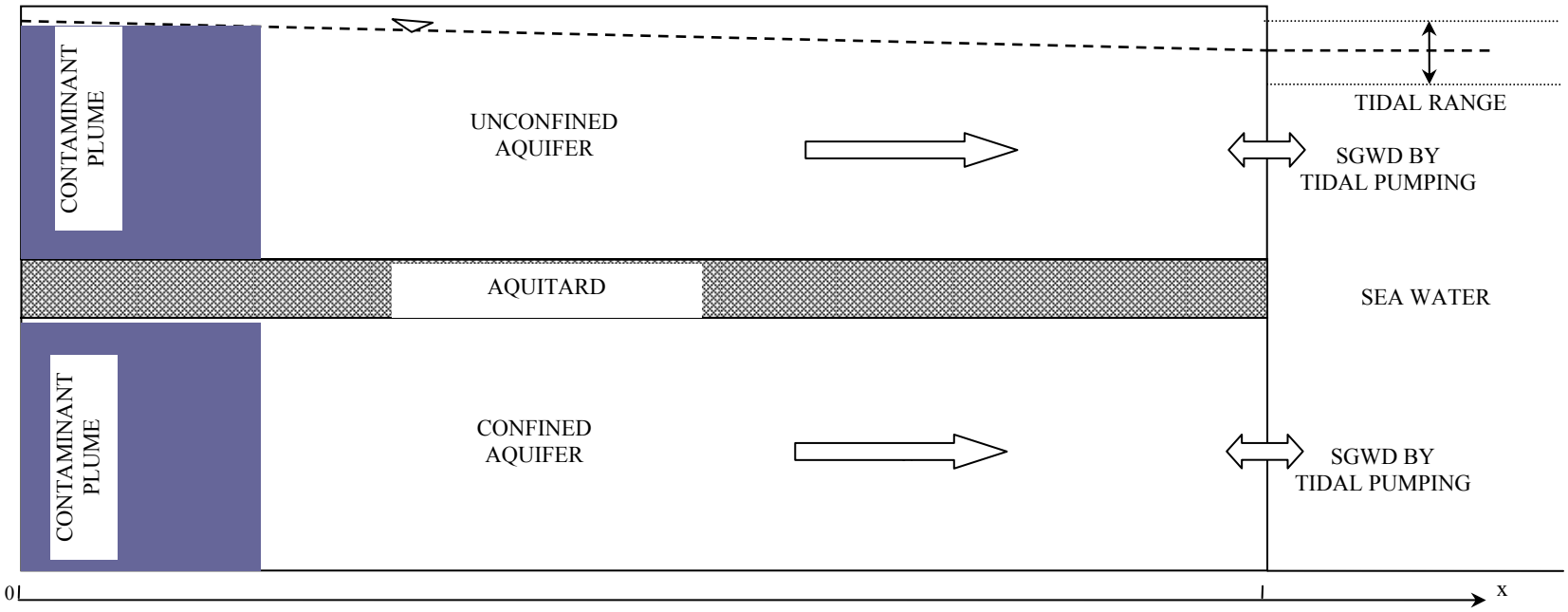

Figure 3.1 Conceptual Model of the Study Problem.

3.2 Flow and Transport Equations

3.2.1 Groundwater Flow Equation

The equation describing the one-dimensional groundwater level change over time and location in a confined aquifer (refer to Figure 3.1) is given as (Todd, 1980)

$$\frac{S}{T}\frac{\partial h}{\partial t} = \frac{\partial^2 h}{\partial x^2} \tag{3.1}$$

where:

h = hydraulic head [L],

S = the storage coefficient of the aquifer [dimensionless],

T = the transmissivity [L^2/T],

x = the distance from a base point inland [L], and

t = the time [T].

The equation also applies, as a good approximation, to water table fluctuations of the unconfined aquifer as long as groundwater table fluctuations are small in comparison with the saturated aquifer thickness (Todd, 1980). In the case of unconfined groundwater flow, simply replace the terms, S and T, in equation (3.1) by S_y and K·b, where S_y is the specific yield [dimensionless], K is the hydraulic conductivity [L/T], and b is the average saturated thickness [L].

In the case when the oscillation of the water table is dramatic in the unconfined aquifer, the following equation should be used to describe the flow (Fetter, 1994)

$$\frac{S_y}{K}\frac{\partial h}{\partial t} = \frac{\partial}{\partial x}\left(h\frac{\partial h}{\partial x}\right) \tag{3.2}$$

This is the case especially when the thickness of the aquifer is relatively small or the tidal range is large compared to the aquifer thickness and in the adjacent area near the

coastline where water table oscillation manifests. It is necessary to consider it if, in the experiment, substantial water level fluctuations are encountered when relatively large tide amplitudes are used. This is because the conditions used in the experiment are divergent from the field conditions such that the water table may drop dramatically compared to the thickness of the porous medium in the unconfined-condition experiment.

3.2.2 Contaminant Transport Equation

The one-dimensional advective-dispersive contaminant-transport equation, describing the time rate of change of contaminant concentration subject to variable flow velocity and thus dispersion coefficient, has the form as proposed by Domenico and Schwartz (1997)

$$R_f \frac{\partial C}{\partial t} = \frac{\partial}{\partial x}\left(D_x \cdot \frac{\partial C}{\partial x} \right) - \frac{\partial}{\partial x}\left(V_x \cdot C \right) - \lambda R_f C \qquad (3.3)$$

where:

C = contaminant concentration [M/L^3],

V_x = interstitial groundwater flow velocity [L/T],

R_f = retardation factor (equilibrium absorption)[dimensionless],

D_x = longitudinal dispersion coefficient [L^2/T],

λ = first-order decay, biodegradation, or kinetic reaction factor (constant) [T^{-1}],

x = the x coordinate axis assumed to be parallel with flow [L],

t = time [T].

Notice that D_x is dispersion only and equals the product of α and V_x where α is the longitudinal dispersivity [L]. When groundwater flow velocity is large enough, molecular diffusion is negligible (Domenico and Schwartz, 1997).

3.2.3 Tides

Oceanic tides produce sinusoidal fluctuations of the groundwater table in coastal aquifers in contact with the ocean. Water table fluctuations in turn cause fluctuations in groundwater flow velocity. With the interstitial velocity varying, the solution to the flow equation (3.1) or (3.2) provides the interstitial velocity field, which couples the contaminant-transport equation to the groundwater flow equation.

For a simple and harmonic sinusoidal tide with amplitude, or half range of the tide, of A [L], and an angular velocity of ω [T^{-1}], it can be represented by

$$h_{tide} = A\sin\omega t, \text{ and } \delta = \frac{2\pi}{\omega} \tag{3.4}$$

where δ is the tidal period [T].

If it is assumed the mean sea level (MSL) is h_0, the applicable flow boundary condition at the coast boundary is h_0+h_{tide} for the flow equation (see Figure 3.2). Taking into consideration a regional groundwater gradient, i_r (it is negative if assuming a flow from the inland towards the coast) due to recharge from rainfall, etc., the solution to the flow equation (3.1) is (modified from Todd, 1980)

$$h = h_0 - i_r\left(L - x\right) + Ae^{-\beta(L-x)}\sin\left(\omega t - \beta\left(L - x\right)\right) \tag{3.5}$$

where $\beta = \sqrt{\pi S / \delta T}$.

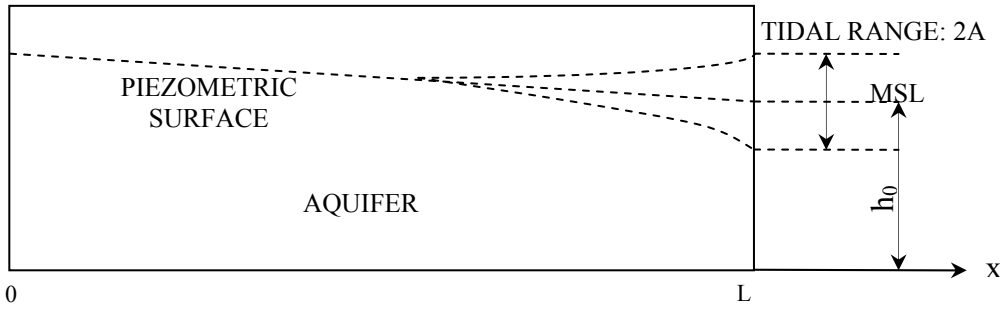

Figure 3.2 Groundwater Level Fluctuations Induced by Tides.

For a more complicated tidal variation with the Fourier series (Nielsen, 1990),

$$h_{tide} = \sum A_j \sin(j\omega t - \varphi_j) \tag{3.6}$$

the corresponding solution is

$$h = h_0 - i_r (L - x) + \sum A_j e^{-\sqrt{j}\beta(L-x)} \sin\left(j\omega t - \varphi j - \sqrt{j}\beta(L-x)\right) \tag{3.7}$$

Flow equation (3.1) is solved to derive the velocity field in a confined aquifer and in an unconfined aquifer where water table fluctuations are negligible compared to aquifer thickness. When water table fluctuations are not negligible, flow equation (3.2) should be used for the unconfined aquifer and solved accordingly using a numerical method to derive flow velocity field.

The oscillating groundwater flow velocity can be derived by differentiating equation (3.5) using Darcy's Law:

$$V_x = -\frac{K}{n}\frac{\partial h}{\partial x} \tag{3.8}$$

which gives

$$V_x = -\frac{K}{n}\left[i_r + \sqrt{2}\beta A e^{-\beta(L-x)} \sin\left(\omega t - \beta(L-x) + \frac{\pi}{4}\right)\right] \tag{3.9}$$

Now that the flow velocity is solved, to derive the solution to contaminant transport equation (3.3), appropriate initial and boundary conditions are needed to be incorporated with the equation. These conditions are described in the following subsections.

3.2.4 Initial Condition

The initial condition considered is

$$C(x,t)\big|_{t=0} = f(x) \tag{3.10}$$

where f(x) is only a function of the location along the flow system. Commonly used initial conditions include a constant value representing a uniform initial distribution of contaminant over the entire aquifer, or a value of zero representing no contaminant at all initially, or an exponentially increasing or decreasing function for a more realistic distribution after a certain period of time since the first release of contamination. In the current study, the initial condition is chosen to be zero contaminant concentration over the entire aquifer. This is used in conjunction with an appropriate boundary condition to simulate pollution release at some time point (for example at t = 0) and consequent movement along the aquifer corridor.

3.2.5 Influent Boundary Condition

Three types of boundary conditions are generally associated with the contaminant-transport equation, the Dirichlet (or first-type), Neumann (or second-type), and Cauchy (or third-type) boundary conditions. For a one-dimensional problem, they can be described as follows.

- The first-type boundary condition specifies the value of the concentration along a cross-section of the flow and transport boundary as

$$C(x,t)\big|_{x=boundary} = g(t) \tag{3.11}$$

where g(t) is the measured concentration in the influent or effluent water as a function of time.

- The second-type boundary condition specifies the gradient in solute concentration along a cross-section of the boundary as

$$\left.\frac{\partial C}{\partial x}\right|_{x=boundary} = p(t) \tag{3.12}$$

where p(t) is the measured concentration gradient in the influent or effluent water as a function of time.

- The third-type boundary condition specifies the flux of solute across the boundary as

$$\left.\left(V_x C - D_x \frac{\partial C}{\partial x}\right)\right|_{x=boundary} = V_x g(t) \tag{3.13}$$

where g(t) is the measured concentration in the flow as a function of time.

These three types of boundary conditions are used to describe conditions at both the influent and effluent ends of a flow system. The influent boundary is generally assigned with the first- or third-type boundary condition to specify a constant or variant influent of contaminant source. Application of the first-type boundary condition presumes that the concentration gradient across the boundary equals zero as soon as flow begins, which may lead to overestimation of the mass of contaminant in the system at early times. The third-type boundary condition allows for contaminant concentration at

the influent boundary to be lower than the influent concentration initially, and then to increase as more contaminant enters the system. Over time, the concentration gradient across the boundary decreases as the concentration at the influent boundary approaches the influent concentration, which eventually reaches the case of the first-type boundary condition. Gershon and Nir (1969), van Genuchten and Alves (1982), and Parker and van Genuchten (1984) present more discussions and the relative advantages and disadvantages of the three boundary conditions at the influent end of a system.

In this study, the influent boundary is taken to be sufficiently far away from the coastal boundary such that the coastal boundary would not affect the condition at the influent end. In this case, the influent boundary condition can be approximated by the first-type boundary condition. The aquifer domain chosen in this study is variable so as to account for the possible case in which tidal fluctuations can propagate far inland.

3.2.6 Contaminant Input

For the influent end of an aquifer, the first- or the third-type boundary conditions are generally used to specify a constant input of contaminant source. For example, a continuous contaminant input at the influent boundary at a constant rate may be simply represented by (3.14), assuming it is well-mixed instantly over the entire vertical section,

$$C\big|_{x=0} = C_0 \tag{3.14}$$

And, a pulse-type input can be represented by

$$C\big|_{x=0} = \begin{cases} C_0, & 0 < t < t_0 \\ 0, & t > t_0 \end{cases} \tag{3.15}$$

where t_0 is the time span of the contaminant release (assuming release starts at time zero).

When considering the contamination release and discharge problem in coastal industrial sites, this situation is realistic in the sense that generally industries or waste sites release pollution in a finite time period, either because industrial firms have a finite life or the pollution problem is controlled after a certain time with the awareness of the contamination or government regulation. Contaminant concentration at the boundary can be set to vary over time as a result of a variable discharge rate, but it would be more convenient to set it as a constant to simplify the problem without resulting in significant detriment to this study.

3.3 Coastal Boundary Conditions and Baseline Selection

3.3.1 Coastal Boundary Conditions

The influent boundary condition is presented in Section 3.2.5, but the coastal (effluent) boundary condition was not included there because the coastal boundary condition is so important to the current problem that it is necessary to address it here as a separate section.

For a system with the effluent boundary far away from the contaminant source, the boundary would not affect contaminant concentrations within the aquifer of interest, i.e., the potential impact area by tides. Such a system can be treated as semi-infinite, and either a first-type or second-type boundary condition can be specified as (Domenico and Schwartz, 1997)

$$\left(C,\ and/or\ \frac{\partial C}{\partial x} \right)\Bigg|_{x=\infty} = 0 \qquad (3.16)$$

When the system has a finite length, however, contaminant concentrations near the effluent boundary are much more likely to be effected by the boundary conditions used, and thus selection of an appropriate boundary condition becomes more important and difficult.

Van Genuchten and Alves (1982) analyze the effect of boundary conditions on predicted concentrations comparing a semi-infinite system using (3.16) with a finite system having a second-type boundary condition of

$$\left.\frac{\partial C}{\partial x}\right|_{x=L} = 0 \qquad (3.17)$$

where L is the length of a finite aquifer system.

They find that the predicted concentrations at points near the effluent boundary begin to differ significantly when the contaminant front moves closer to the effluent boundary. The magnitude of the difference and the distance inland from the effluent boundary at which the solutions diverge decreases as the value of VL/D increases.

Another potential option to describe the effluent boundary is the first-type boundary condition (3.18) at the effluent end of the system,

$$C\big|_{x=L} = C_L \qquad (3.18)$$

where C_L is a constant concentration at the effluent boundary. The condition (with C_L=0) is believed to be more realistic when contaminant discharges into a large, well-mixed reservoir like the coastal water and additional contaminant will not significantly change the contaminant concentration in the water body. This boundary condition is believed to be the case for the discharge problem in coastal aquifers (refer to the next subsection, BASELINE SELECTION, for detailed analysis). Later this section will analyze how

different boundary conditions affect the solutions to contaminant distribution and discharge patterns, and will discuss the selection of the appropriate baseline (i.e., which boundary condition should be used for the baseline problem) for the identification of tidal effects.

3.3.2 Baseline Selection

Conventional work concerning contaminant discharge into surface water bodies through groundwater flow favored the second-type boundary condition of constant mass flux (generally specified as zero flux). This boundary condition is widely adopted in problems concerning soil-column experiments and solute discharge into small no-mixing water bodies (Gershon and Nir, 1969), but for the large well-mixing coastal water encountered in this study, it is suspected that it would yield considerable deviation from reality. The first-type boundary condition, constant concentration, is believed to better represent the case studied. Even though each of the boundary conditions mentioned herein has been intensively used in various problems, it is interesting to find that no work has compared them in the use for situations like those considered in this study.

On the other hand, in order to identify the tidal effect on contaminant transport, obviously a baseline solution is needed for contaminant transport subject to no tidal fluctuations. It is reasonable to choose a uniform flow system subject to no tides as the baseline problem as illustrated in Figure 3.3. For the baseline problem, it is necessary to use an appropriate boundary condition at the coastal boundary as well. The boundary conditions discussed in the previous subsection are potential candidates, and as mentioned before the first-type boundary condition (3.18) is used for the baseline. Here it is demonstrated that the difference in the solution associated with the selection of

different boundary conditions is significant and thus the error induced by the selection of a wrong boundary condition for the baseline can be dramatic.

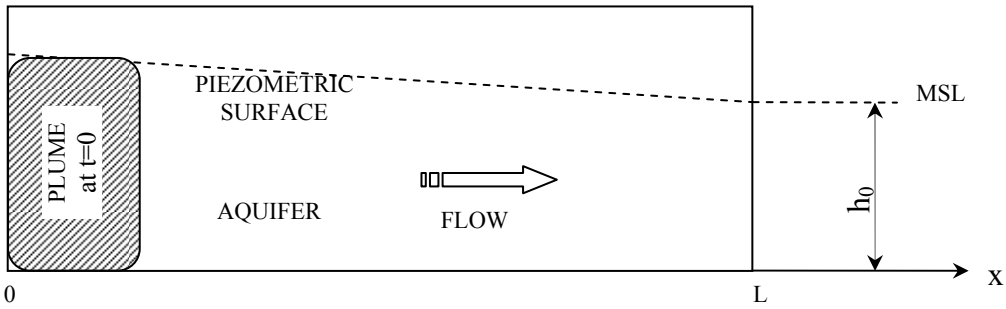

Figure 3.3 Illustration of the Baseline Problem without Tides.

3.3.3 Solutions to the Baseline Problem

Given in the schematic illustration (Figure 3.3) is the baseline problem: the finite aquifer system (both confined and unconfined) goes from x = 0 to the coastal boundary at x = L. Initially there is no contaminant in the aquifer. At t = 0, the contaminant source is released at the left boundary which is far enough away from the right boundary such that the right boundary does not affect the flow and transport behavior at the left boundary. Contaminant transport for this problem can be generally represented by equation (3.19), taking into consideration of advection, dispersion, equilibrium adsorption and ion exchange, and first-order kinetic reactions (Domenico and Schwartz, 1997),

$$R_f \frac{\partial C}{\partial t} = D_x \frac{\partial^2 C}{\partial x^2} - V_x \frac{\partial C}{\partial x} - \lambda R_f C \qquad (3.19)$$

where:

C = contaminant concentration [M/L^3],

V_x = interstitial groundwater flow velocity [L/T],

R_f = retardation factor (equilibrium absorption and ion exchange) [dimensionless],

D_x = longitudinal dispersion coefficient [L^2/T],

λ = first-order decay, biodegradation, or kinetic reaction factor (constant) [T^{-1}],

x = the x coordinate axis assumed to be parallel with flow [L], and

t = time [T].

To compare the effect of coastal boundary conditions, the solutions with different representations of the boundary conditions are listed in Table 3.1 and presented in this subsection. All these solutions are based on the same initial condition of (3.10) with f(x) = 0, and the same input scheme (3.15) presented in Section 3.2. Retardation factor is not included in the following solutions. To consider the retardation, one can simply replace V_x and D_x with $\frac{V_x}{R_f}$ and $\frac{D_x}{R_f}$ in the solutions.

Table 3.1 Analytical Solutions of the Baseline Problem

Solution No.	Initial Cond.	Aquifer Domain	Influent B.C.	Effluent B.C.
1	C(x,0)=0	Semi-Infinite	Eq. (3.15)	Eq. (3.16)
2	C(x,0)=0	Finite	Eq. (3.15)	Eq. (3.17)
3	C(x,0)=0	Finite	Eq. (3.15)	Eq. (3.18)

- Solution No. 1

The first solution presented is for the case of semi-infinite domain with the second-type boundary condition at the effluent end. In this case, the analytical solution to equation (3.19) is given as by Bear (1972), van Genuchten and Alves (1982), and Wexler (1992)

$$C(x,t)=\frac{C_0}{2}\left\{\exp\left(\frac{x}{2D_x}(V_x-U)\right)erfc\left(\frac{x-Ut}{2\sqrt{D_xt}}\right)+\exp\left(\frac{x}{2D_x}(V_x+U)\right)erfc\left(\frac{x+Ut}{2\sqrt{D_xt}}\right)\right\} \tag{3.20}$$

where $U=\sqrt{V_x^2+4\lambda D_x}$, and erfc(x) is the complimentary error function.

- Solution No. 2

The second solution presented is for the case of finite domain with the second-type boundary condition at the effluent end. In this case, the analytical solution of equation (3.19) is modified from van Genuchten and Alves (1982) and Wexler (1992) as

$$C(x,t)=\begin{cases}C_0A(x,t), 0<t\le t_0\\ C_0A(x,t)-C_0A(x,t-t_0), t>t_0\end{cases} \tag{3.21}$$

with,

$$A(x,t)=\left\{\frac{\exp\left(\frac{(V_x-U)x}{2D_x}\right)+\left(\frac{U-V_x}{U+V_x}\right)\exp\left(\frac{(V_x+U)x}{2D_x}-\frac{UL}{D_x}\right)}{\left(1+\left(\frac{U-V_x}{U+V_x}\right)\exp\left(\frac{-UL}{D}\right)\right)}\right.$$
$$\left.-2\exp\left(\frac{xV_x}{2D_x}-\lambda t-\frac{V_x^2t}{4D_x}\right)\cdot\sum_{i=1}^{\infty}\frac{\beta_i\sin\left(\frac{\beta_ix}{L}\right)\left[\beta_i^2+\left(\frac{V_xL}{2D_x}\right)^2\exp\left(-\frac{\beta_i^2D_xt}{L^2}\right)\right]}{\left[\beta_i^2+\left(\frac{V_xL}{2D_x}\right)^2+\frac{V_xL}{2D_x}\right]\left[\beta_i^2+\left(\frac{V_xL}{2D_x}\right)^2+\frac{\lambda L^2}{D_x}\right]}\right\},$$

where $U=\sqrt{V_x^2+4\lambda D_x}$, and β_i are the roots of equation $\beta \bullet cot\beta + V_xL/2D_x = 0$.

Values of the first six roots of the equation, $a \bullet cot(a)+c=0$, are tabulated in Carslaw and Jaeger (1959) for various values of the constant c. Additional roots of the equation can be found through standard root-search techniques.

- Solution No. 3

The final solution presented is for the case of finite domain with the first-type boundary condition at the effluent end. In this case, the analytical solution of equation (3.19) is derived according to the methodology presented by Churchill (1971) (see appendix for the details of the derivation of the solution)

$$C(x,t)=\begin{cases} C_0 \exp\left(\dfrac{xV_x}{2D_x}\right)B(x,t)+C_L \exp\left(\dfrac{V_x(L-x)}{2D_x}\right)B(L-x,t), & t \le t_0 \\ C_0 \exp\left(\dfrac{xV_x}{2D_x}\right)\left[B(x,t)-B(x,t-t_0)\right]+C_L \exp\left(\dfrac{V_x(L-x)}{2D_x}\right)B(L-x,t), & t > t_0 \end{cases} \tag{3.22}$$

with

$$B(x,t)=\frac{L-x}{L}-\frac{2}{\pi}\sum_{n=1}^{\infty}\frac{\sin(\eta x)}{n}\exp\left[-(\beta+\eta^2 D_x)t\right] + \frac{2}{\pi}\sum_{n=1}^{\infty}\frac{\beta\sin(\eta x)}{n(\beta+\eta^2 D_x)}\left\{\exp\left[-(\beta+\eta^2 D_x)t\right]-1\right\}$$

where $\beta=\dfrac{V_x^2}{4D_x}+\lambda$ and $\eta=\dfrac{n\pi}{L}$.

For a finite system, the concentration distribution and mass discharge at the effluent boundary are compared for all three solutions (for the case with semi-infinite aquifer domain, concentration distribution in the first part of the system and mass flow across the location with a distance equivalent to the finite system are considered).

Results are compared in terms of the dimensionless variables as given by van Genuchten and Alves (1982):

$$P = VL/D,\ T = Vt/L,\ \text{and}\ Z = x/L \tag{3.23}$$

Here, P is the column Peclet number, T the number of displaced pore volumes, and Z the reduced distance (van Genuchten and Alves, 1982). All these dimensionless variables are used for convenience of comparison. And physically, the Peclet number measures the relative magnitude of convection versus dispersion. The number of displaced pore volumes measures the movement of contaminant plume front, for example, T = 1 indicates the contaminant plume front reaches the effluent boundary (x = L). To make the comparison applicable to a semi-infinite system, the reduced distance, Z, cannot exceed one because $0 \leq x \leq L$ (as it is defined in Figure 3.3 the aquifer domain goes from x = 0 to x = L).

Special attention is given to the effect of effluent boundary conditions regardless of the influent boundary condition (which is chosen to be the same, i.e., constant concentration of C_0, for all these solutions). All the other parameters for the comparison study are listed in Table 3.2 and the initial condition f(x) is set to be zero.

Table 3.2 Parameter Values Used in Boundary Condition Study

Case No.	Solution No.	V_x m/day	t_0 years	α_x m	D_x m^2/day	λ day^{-1}	R_f /	L m	P /
A1	1	1.0	1	20	20	0.0	1.0	500	25
A2	2	1.0	1	20	20	0.0	1.0	500	25
A3	3	1.0	1	20	20	0.0	1.0	500	25
A4	1	0.5	1	20	10	0.0	1.0	100	5
A5	2	0.5	1	20	10	0.0	1.0	100	5
A6	3	0.5	1	20	10	0.0	1.0	100	5

Figure 3.4 gives the concentration distributions at different pore volumes with Peclet number equal to 25.

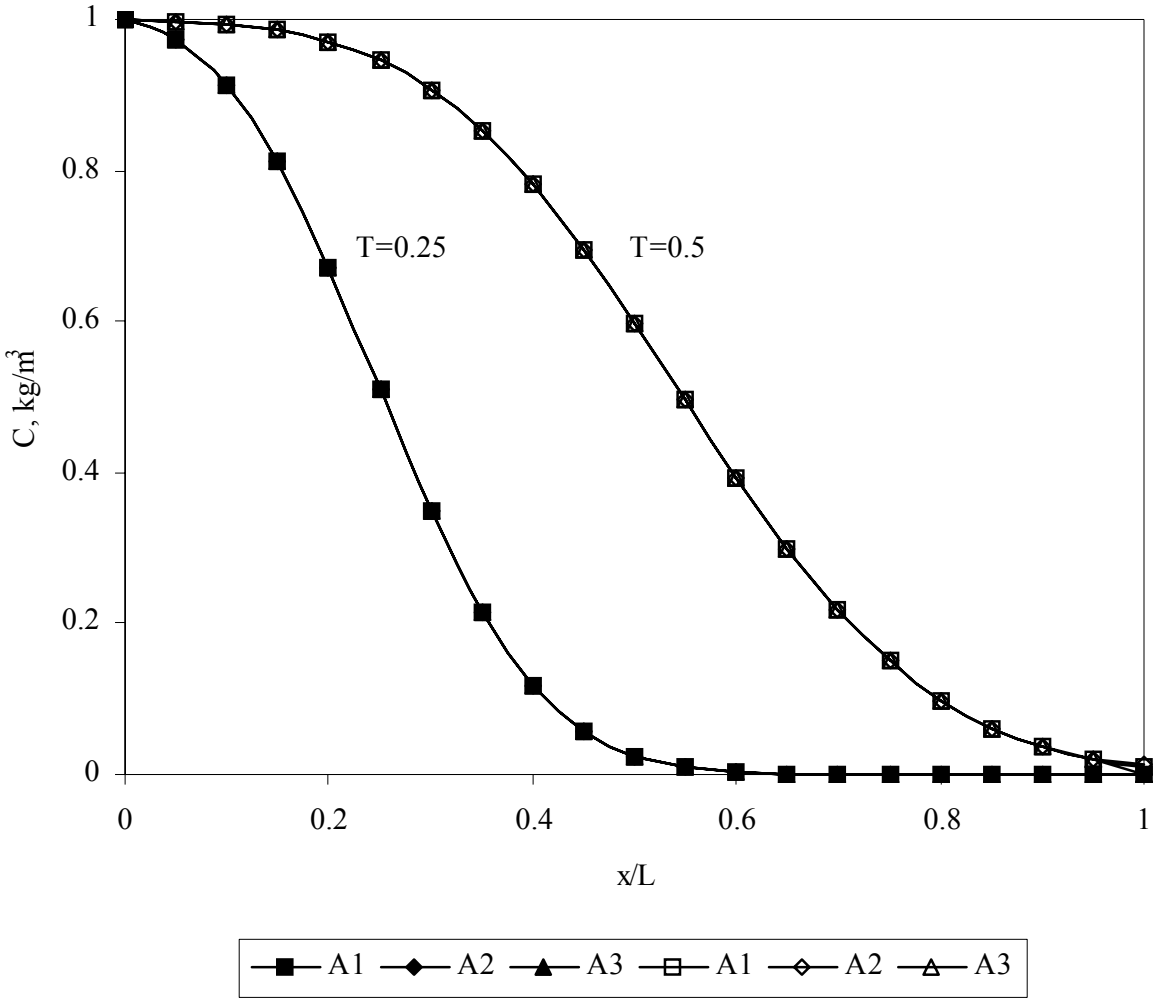

Figure 3.4 Concentration Profile Comparison for Peclet Number P=25.

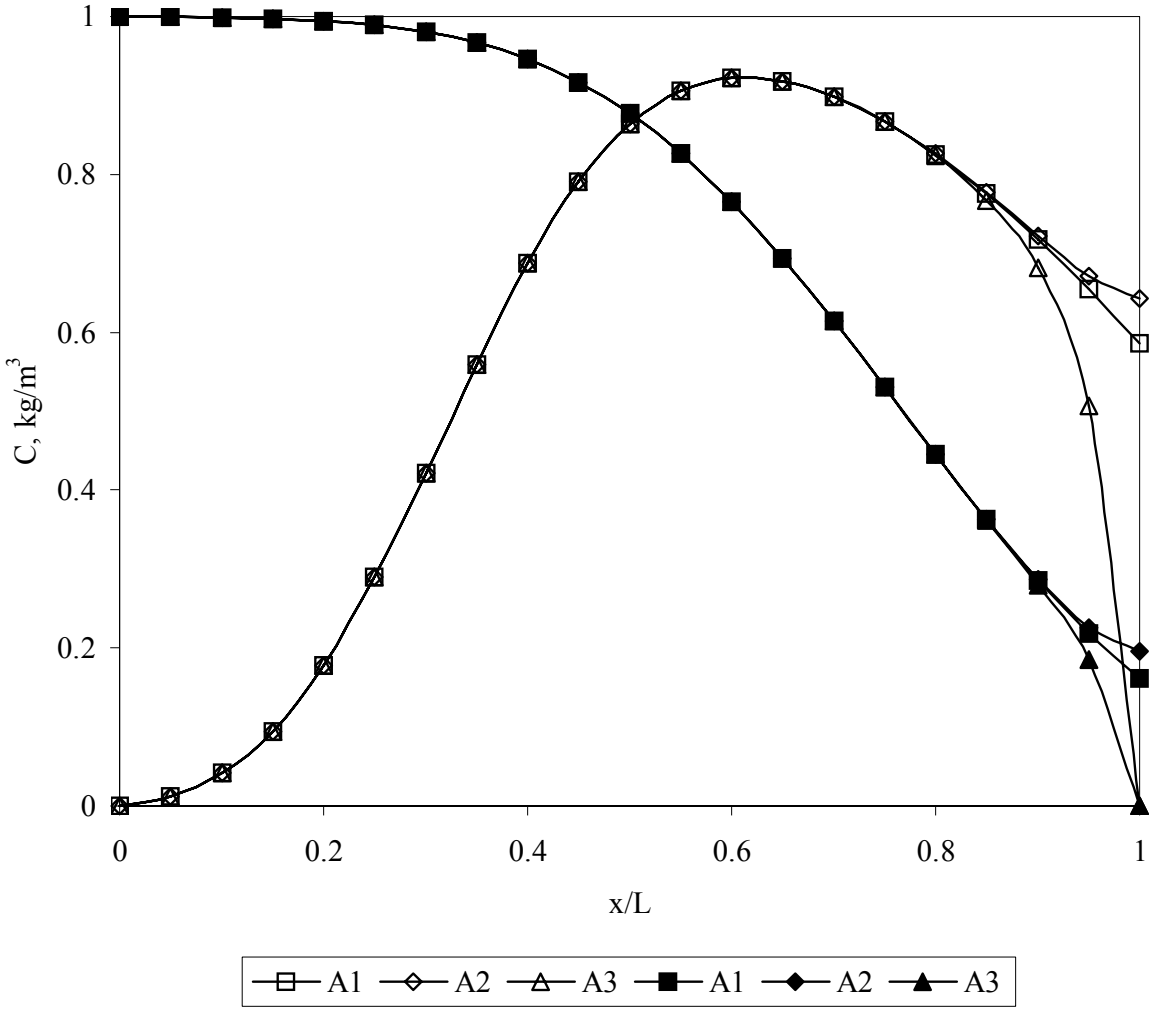

Figure 3.4 Concentration Profile Comparison for Peclet Number P=25 (Continued).

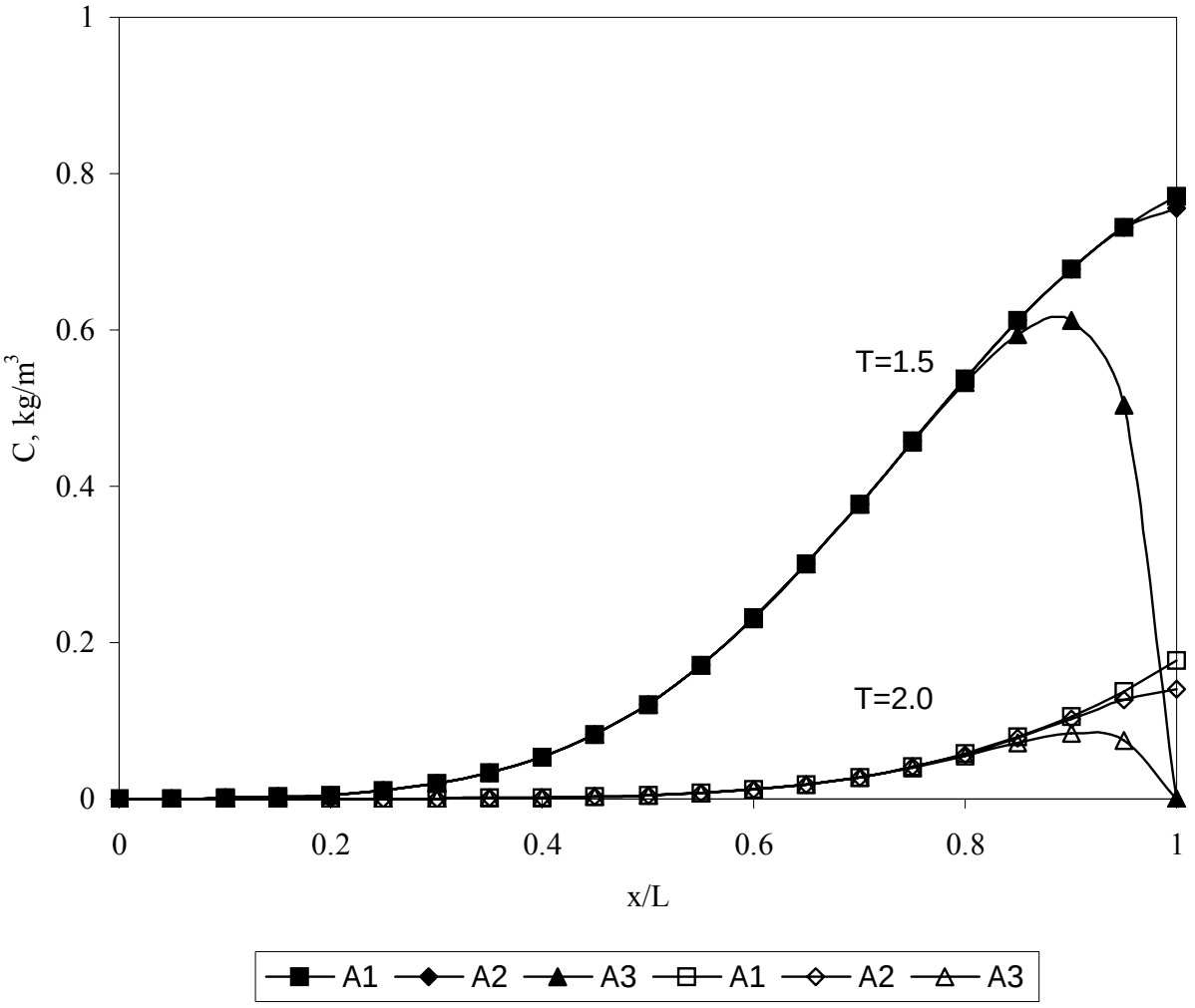

Figure 3.4 Concentration Profile Comparison for Peclet Number P=25 (Continued).

Figure 3.5 gives the concentration distributions at different pore volumes with Peclet number equal to 5.

A similar difference trend is observed as was found by van Genuchten and Alves (1982). The analytical solution No.1 and No.2, represented by case A1 and A2, and case A4 and A5, respectively, corresponding to the finite and semi-infinite systems with second-type boundary condition, are almost identical when T is small enough, i.e., before the contaminant front gets close to the effluent boundary. The difference between the two solutions increases as T goes up and it reaches a maximum when T gets to 1.0. Thereafter the difference drops again along with the increase of T value. Also observed from Figure 3.4 and Figure 3.5 is that the difference becomes more significant when the Peclet number decreases. Notice from these figures that the impact of the boundary condition extends inward from the boundary over a relative distance up to 80% of the entire domain, that is, the relative inward location from the effluent boundary at which the solutions diverge may reach as far as to Z = 0.2. This relative distance increases as the value of the Perclet number decreases, which means the effect of boundary conditions becomes more significant as the Perclet number gets smaller. But interestingly, even though the relative distance represented by Z changes, the absolute physical distance from which the solutions diverge has almost the same magnitude (about 50 meters from the effluent boundary for both situations with P equal to 25 and 5). This observation is practically important because it represents the actual potential of the effect by boundary conditions. This fact, however, is not mentioned by van Genuchten and Alves (1982).

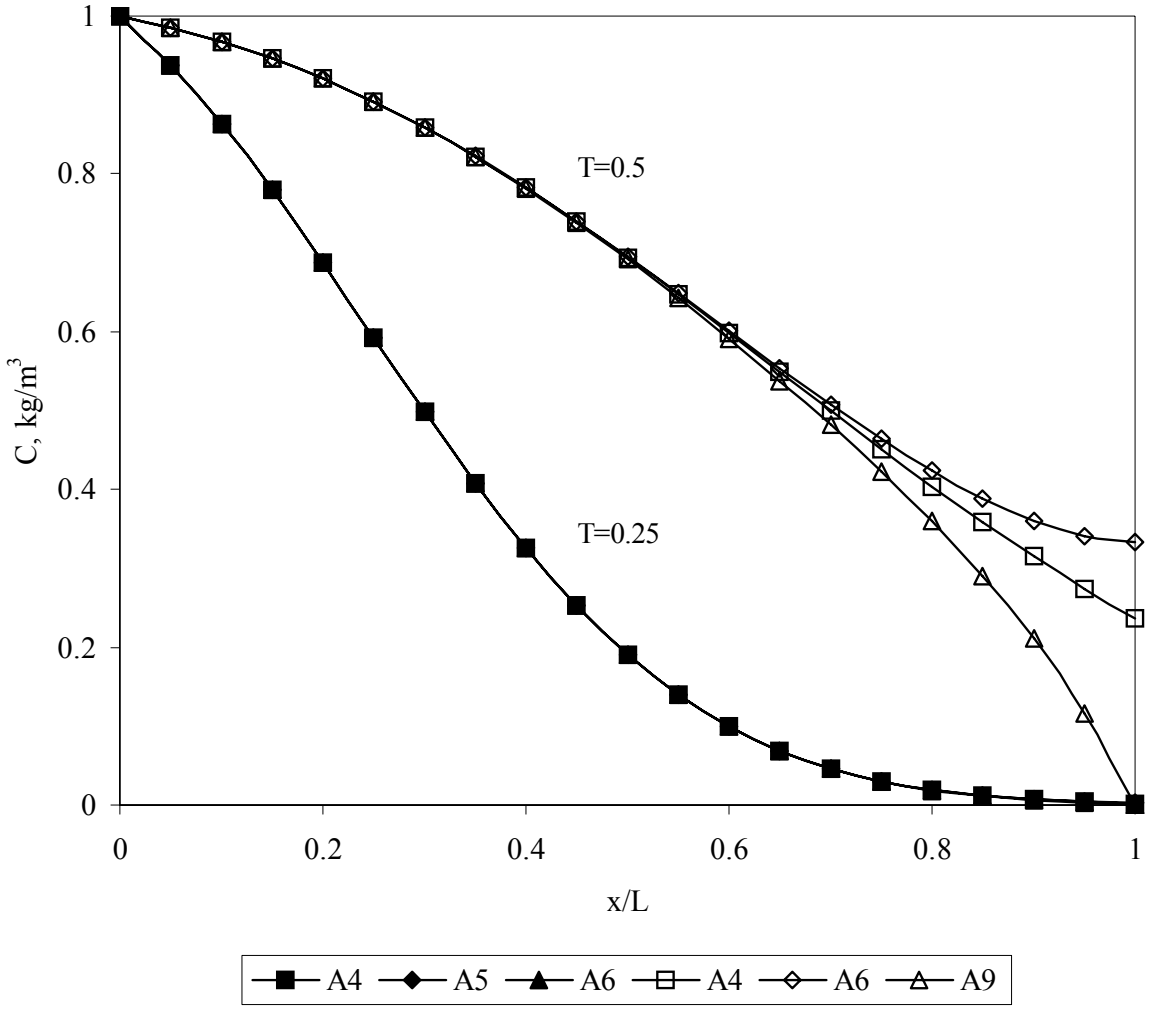

Figure 3.5 Concentration Profile Comparison for Peclet Number P=5.

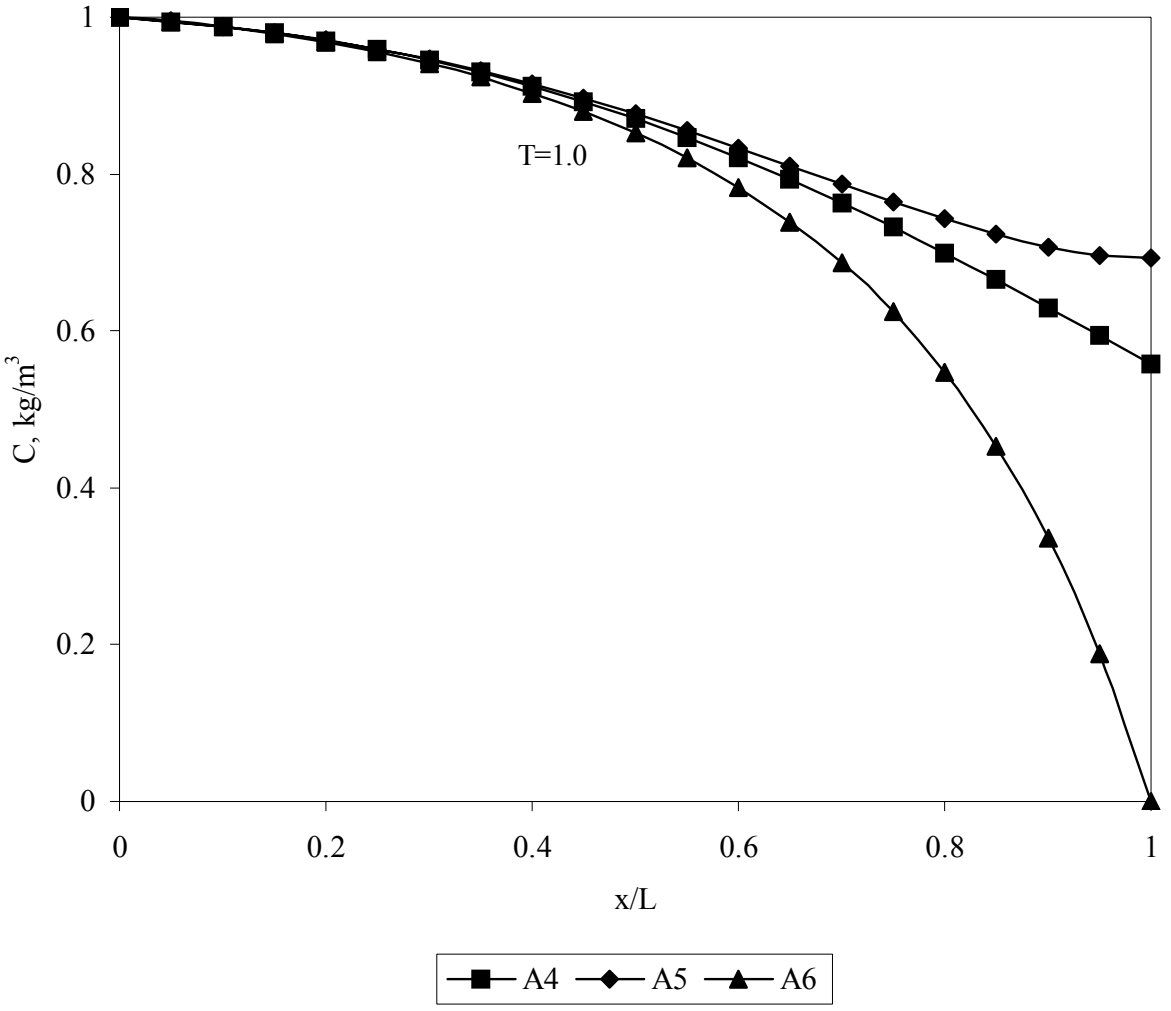

Figure 3.5 Concentration Profile Comparison for Peclet Number P=5 (Continued).

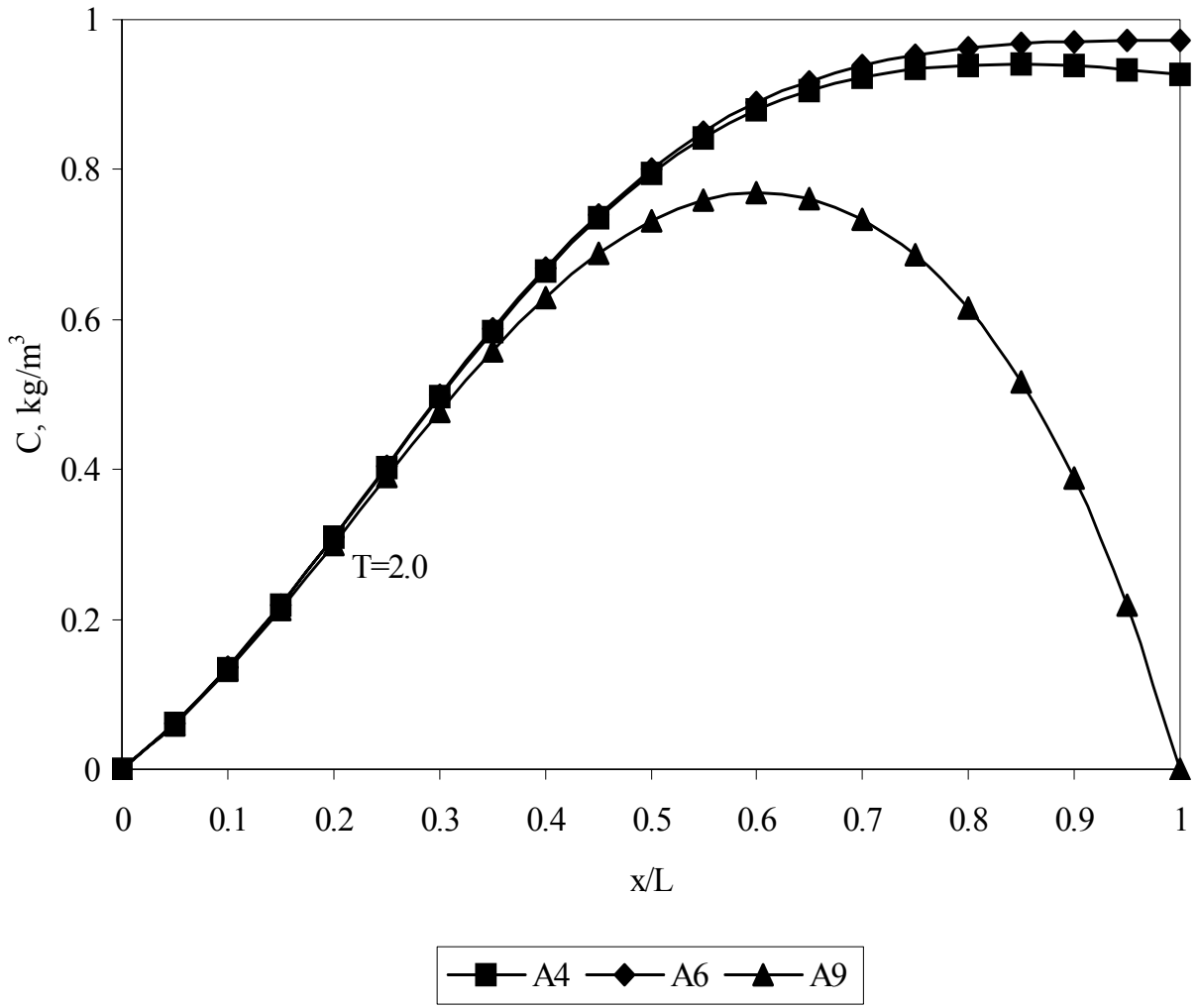

Figure 3.5 Concentration Profile Comparison for Peclet Number P=5 (Continued).

As mentioned earlier, an important solution with regard to contaminant transport in coastal aquifers, denoted in this study by solution No.3, is not studied comparatively with the other two solutions. This solution is considered here since it is critical and physically more realistic than the other two solutions for the problem, as will be demonstrated later.

Solution No. 3 corresponds to a finite aquifer domain with the first-type boundary condition. The curves representing solution No. 3 are included in Figure 3.4 and Figure 3.5 denoted by case A3 and A6 corresponding to Peclet number 25 and 5, respectively. From these figures, dramatic differences, which are much more significant than the difference between solution No. 1 and No. 2, are observed between solution No.3 and the other two solutions regardless of the Peclet number used. The most significant concentration divergence occurs when the contaminant front gets close to the effluent boundary. The concentration for solution No.3 always drops to zero at the right boundary (as specified by the boundary condition), while the other two do not. The difference between solution No.3 and the other two solutions changes with T and P, as was observed for the difference between solution No.1 and No.2 discussed earlier. But the magnitude of the difference and inward distance at which the solutions diverge are much more dramatic, especially for the portion of the profiles close to the effluent boundary.

However, with all these differences mentioned, the three solutions are similar when T is small, i.e., in the region far from the effluent boundary where the impact of boundary conditions are minimal. It also holds true that the two solutions, No.2 and No.3, for the finite aquifer domain but with different effluent boundary conditions, can be approximated with good accuracy by solution No. 1, with the semi-infinite aquifer

domain, for small Z with all values of T, and for larger Z with relatively small T (van Genuchten and Alves, 1982).

The considerable differences between the solution profiles, especially those between solution No.3 and the other two solutions, are only one aspect of interest. The other aspect of interest, in this study, is the variation in contaminant mass discharge out of the system at the effluent boundary.

Figure 3.6 and Figure 3.7 show the mass discharge at the effluent boundary versus pore volume, T, for different Peclet numbers. Opposite to the observations of concentration profiles for the three solutions, the mass discharge profiles for all solutions are considerably close to each other when the Peclet number is relatively large (the difference is negligible when compared to general experimental errors). When the Peclet number is small (for instance, P = 5 as shown in Figure 3.7), however, the profile for solution No. 3 with the first-type boundary condition is shifted to the left with a difference of approximately 10% from the other two profiles with the second-type boundary condition. That tells us the first-type boundary condition tends to accelerate the contaminant mass discharge, while eventually the total discharge will be the same, i.e., 100% of the total mass input, as time goes to infinite (this time frame will be discussed later). The discharge profiles are almost identical for solutions No.1 and No.2 in this case, which is consistent with the conclusion reached by van Genuchten and Alves (1982).

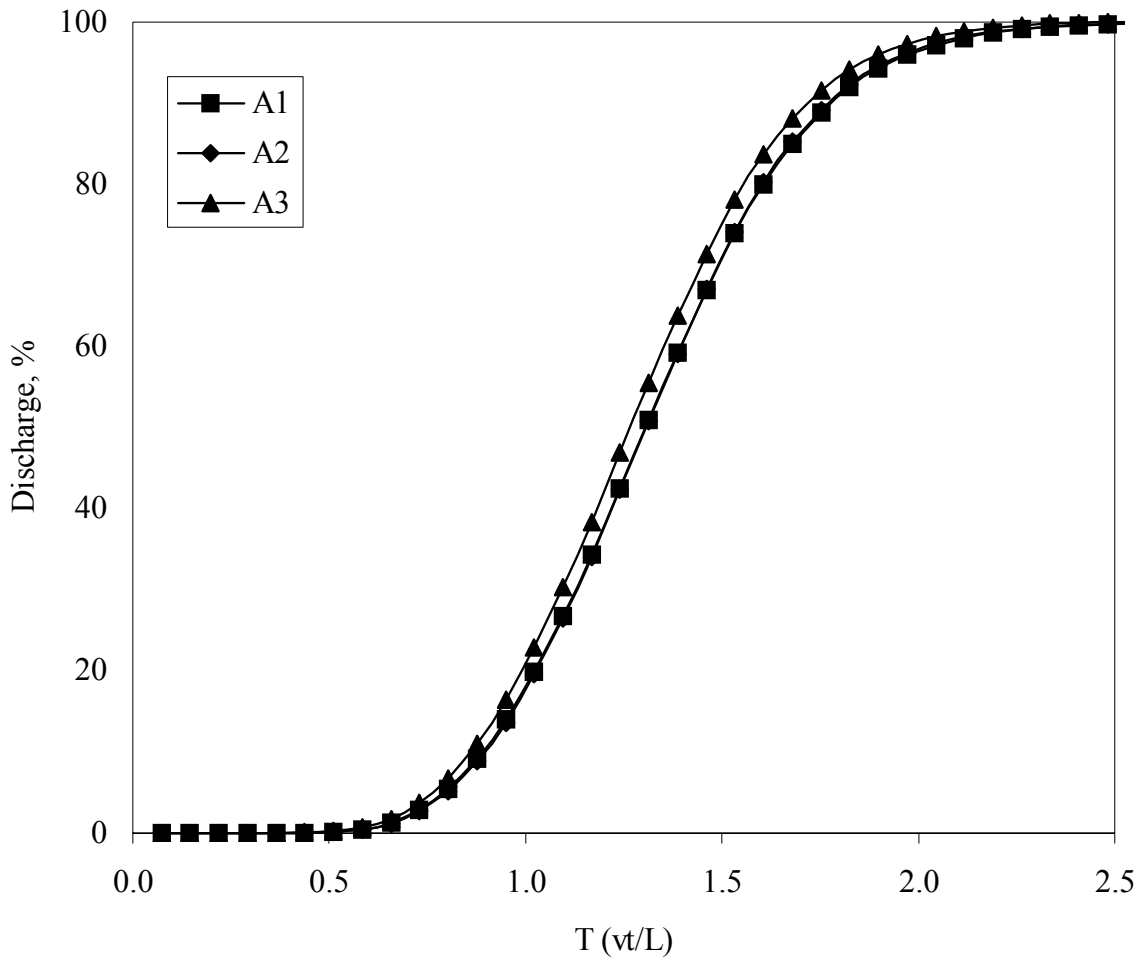

Figure 3.6 Discharge Profile Comparison for Peclet Number P=25.

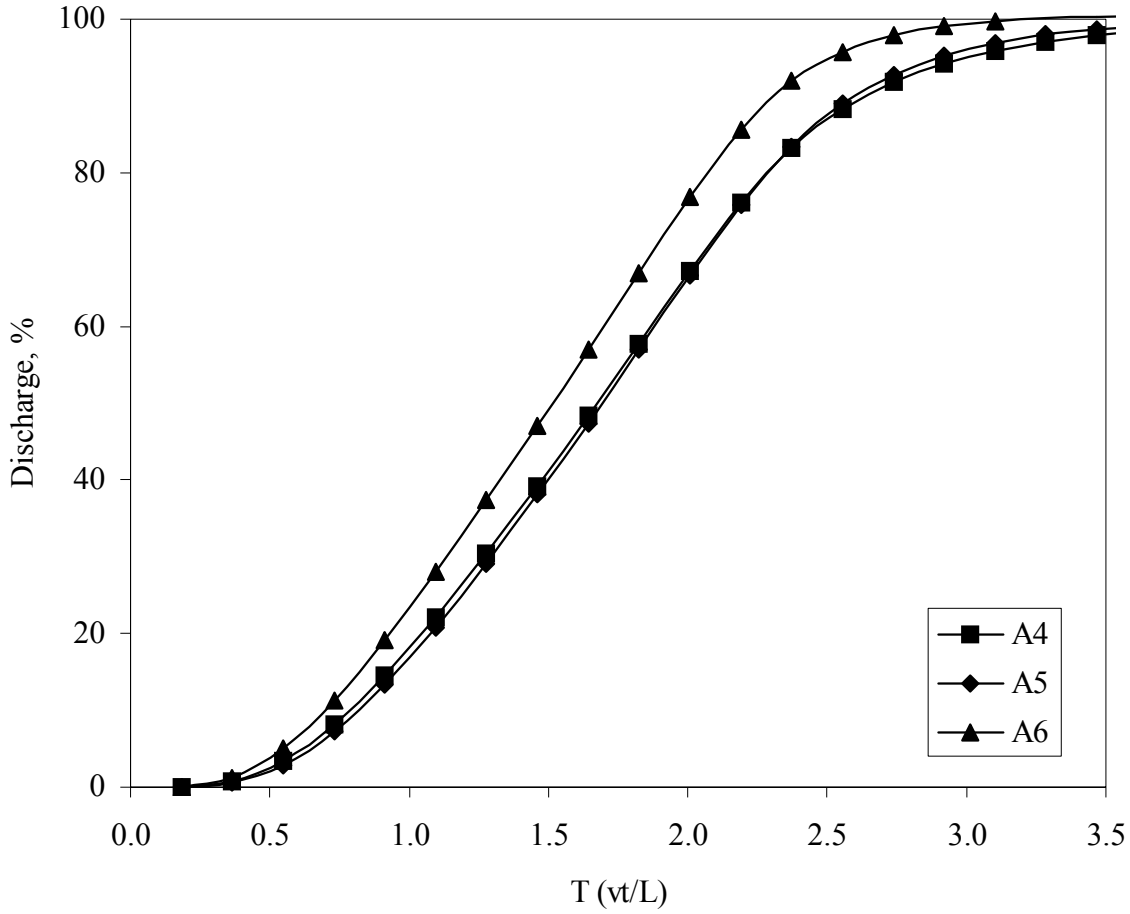

Figure 3.7 Discharge Profile Comparison for Peclet Number P=5.

Next, the contaminant transport mechanism at the coastal boundary is analyzed for further comparison of the effect by boundary conditions. Figure 3.8 shows how the contaminant transport through convection and dispersion changes with the distance away from the effluent boundary for both models with a finite system. Recall that case A2 represents the solution with the second-type boundary condition at the effluent boundary while case A3 represents the solution with the first-type boundary condition at the effluent boundary (see Table 3.2 for other parameters used).

Demonstrated here is how contaminant-transport components – dispersion and convection – change at different locations for the two cases subject to the first-type (zero concentration) and the second-type (zero concentration gradient) boundary conditions. With the second-type boundary condition, the dispersion component smoothes out slowly as the location goes towards the effluent boundary, while the convection component remains dominant with no noticeable change at all. With the first-type boundary condition, however, the convection component drops dramatically as the location goes towards the effluent boundary, as a result of the dramatic decrease of contaminant concentration. The dispersion component, on the other hand, increases as quickly as the convection component drops, and finally, at the boundary, dispersion with the first-type boundary condition reaches the magnitude of the convection with the second-type boundary condition. Thus, convection and dispersion compensate with each other, and as discussed earlier, for a large Peclet number, this does not significantly affect the overall mass transport rate, which is the summation of convection and dispersion. The first-type boundary condition, however, does have an effect on the contaminant transport rate for a smaller Peclet number. Quick and well mixing at the effluent boundary causes a dramatic

drop in concentration over a relatively short distance close to the boundary, which accelerates the contaminant discharge out of the system. The acceleration may lead to up to a 10% increase of mass discharge versus that with the second-type boundary condition when the contaminant front reaches the boundary.

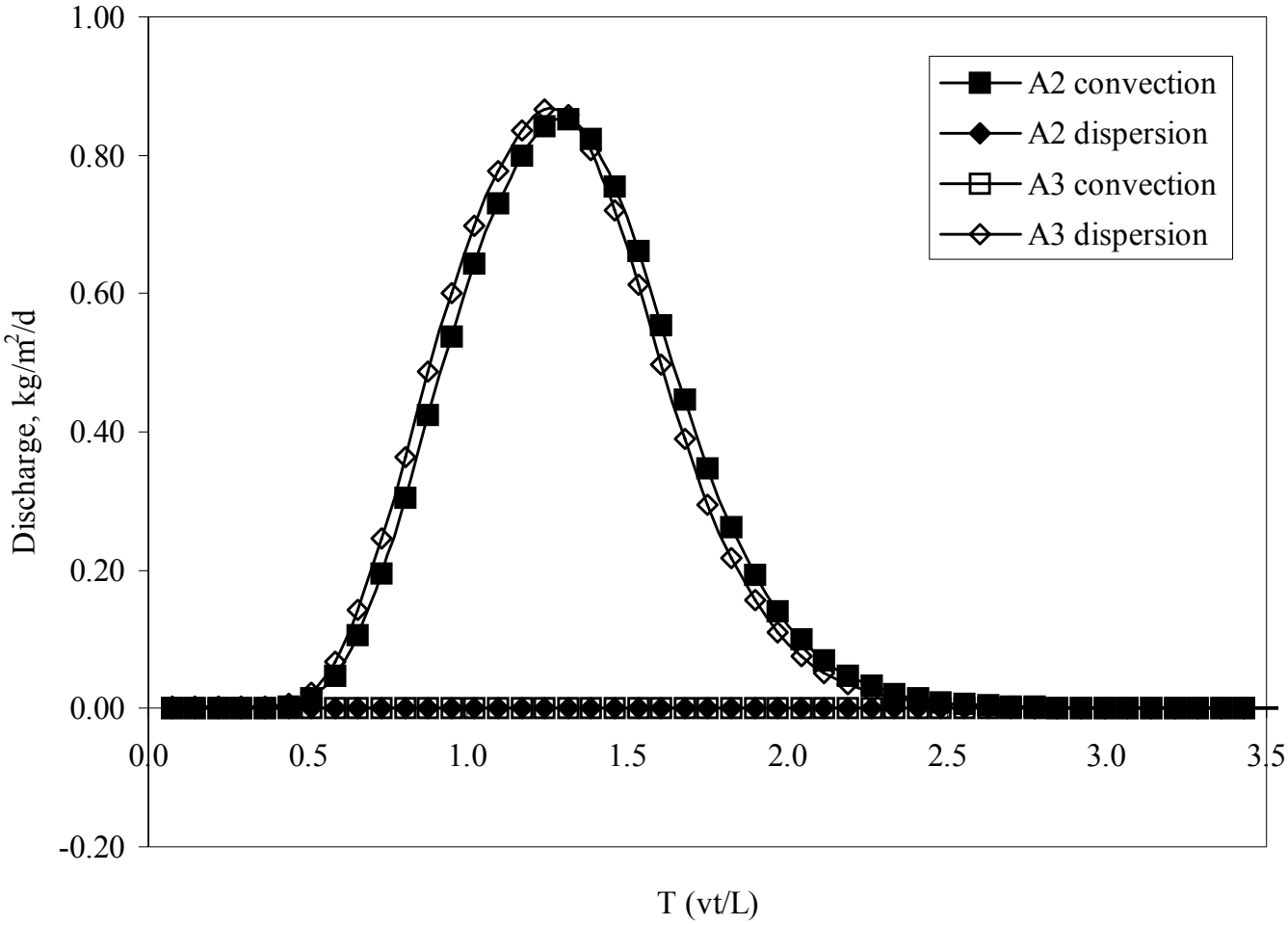

Figure 3.8 Convection vs. Dispersion: At the Coastal Boundary.

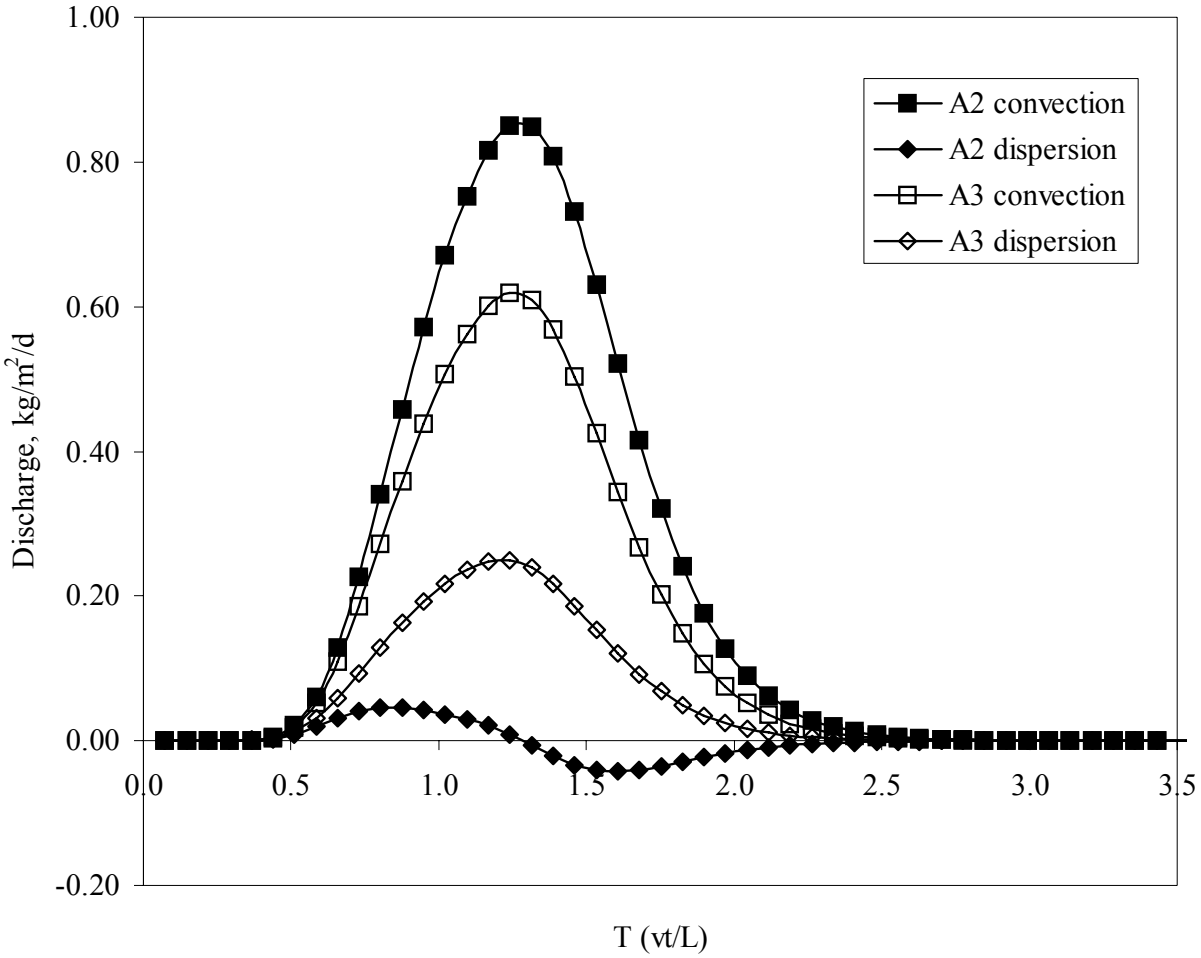

Figure 3.8 Convection vs. Dispersion: 0.05L away from the Boundary (Continued).

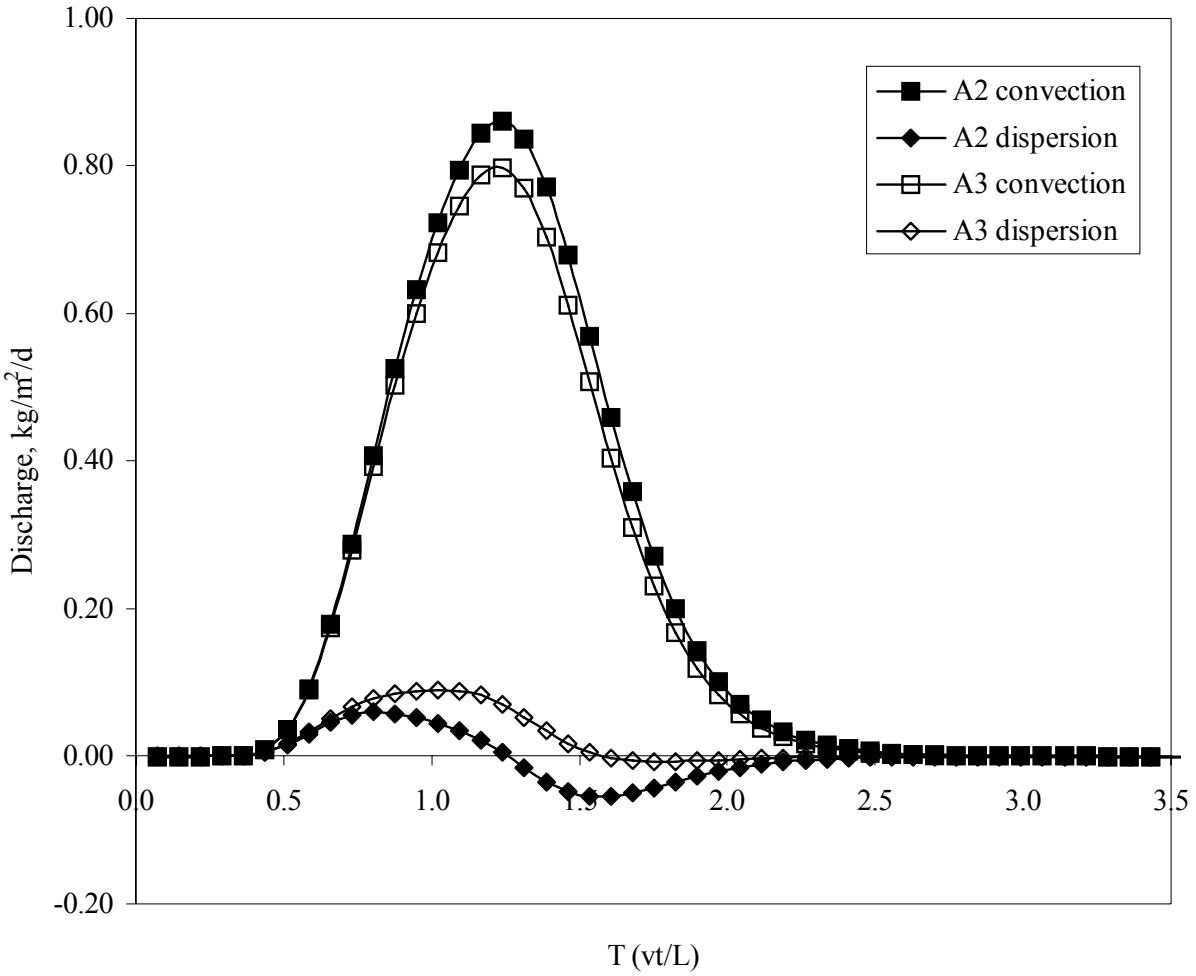

Figure 3.8 Convection vs. Dispersion: 0.1L away from the Boundary (Continued).

3.3.4 Discussion and Conclusion to Baseline Selection

The discussions above indicate that a second-type boundary condition at the coastline results in a significantly higher contaminant concentration in the coastal water when the contaminant reaches the boundary. Because of its properties of voluminous capacity and quick and well mixing, coastal water tends to dilute the contaminant immediately to a sufficiently low concentration as the contaminant reaches the boundary. Consequently, it is believed the coastal water boundary is better represented by a zero concentration condition, i.e., the first-type boundary condition. Thus, it is suspected to be unsuitable that Yim and Mohsen (1992) chose the solution derived from a second-type boundary condition as the baseline to study the tidal effect. Suppose, for example, the tidal effect on the concentration distribution is to be considered for the case studied in Section 3.3.3 (see Table 3.2). Potentially there are three solutions, i.e. case A1, A2, and A3, that can be used as the baseline. Yim and Mohsen (1992) selected case A2 as the baseline, but it is known from the discussion above that case A3 is more appropriate for coastal boundary conditions. Consequently, the tidal effect shall be represented by area III only (refer to Figure 3.9; the numerical solution incorporating tidal fluctuations is presented in the next section, and the results are used here for the discussion of baseline selection). However, as Yim and Mohsen (1992) compare with baseline A2, the tidal effect is represented by three pieces, areas I, II, and III. As a result, the tidal effect is significantly exaggerated due to the selection of an inappropriate baseline.

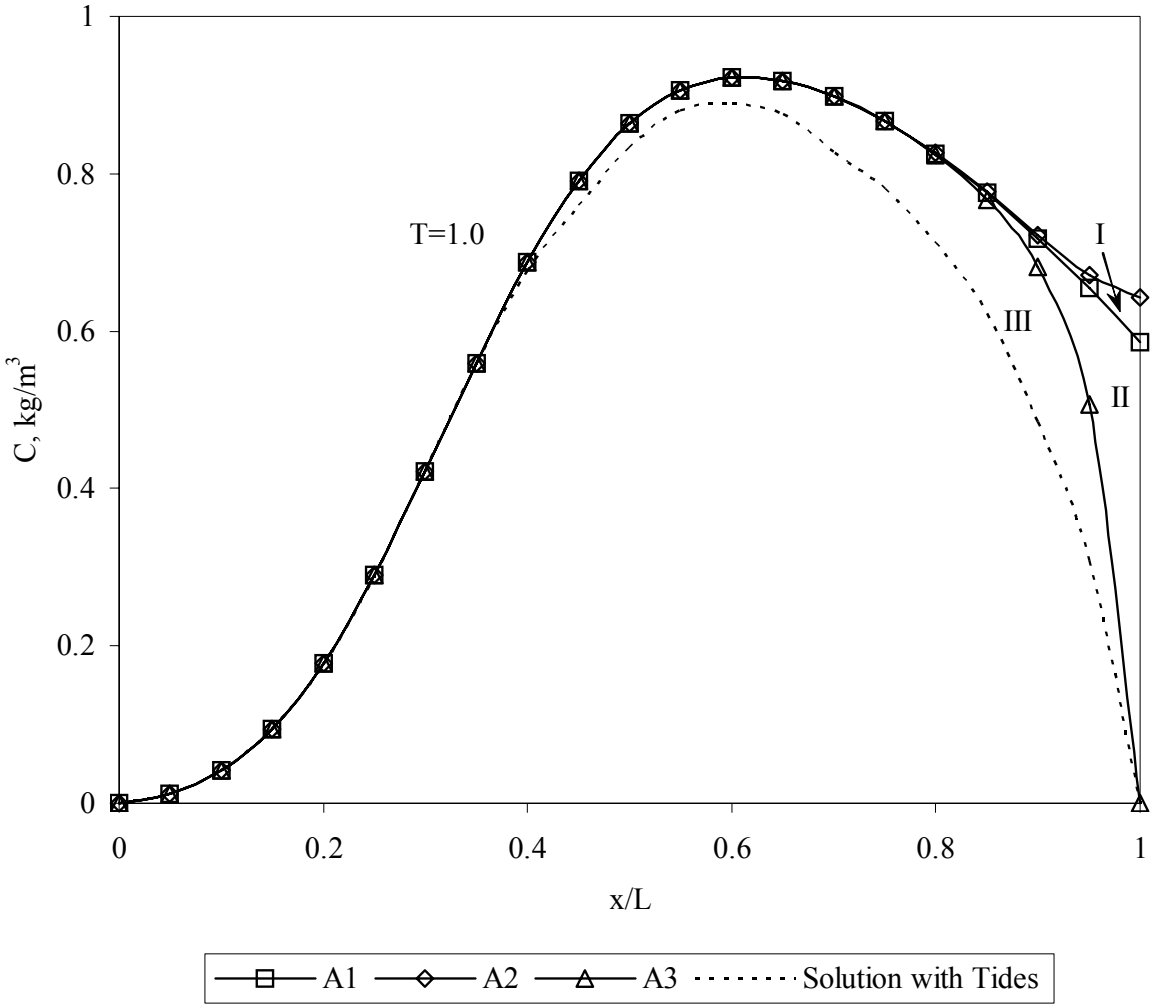

Figure 3.9 Different Tidal Effects Revealed by Selection of Different Baseline Solutions.

The conclusion of the baseline selection is that the correct boundary condition for the coastal boundary problem is the first-type boundary condition instead of the second-type boundary condition, and the analytical solution No. 3 based on the first-type boundary condition should be used as the baseline. In the numerical study of this document, tidal fluctuations are incorporated and compared with the results by analytical solution No. 3 derived here, rather than the analytical solution No. 2. By using solution No. 3 as the baseline, it is believed that the effect of tidal fluctuations will be better understood.

3.4 Numerical Solution

Among the many different approaches to solving partial differential equations, the finite difference method is one of the most widely used methods.

Finite difference methods apply a grid over the system of interest and solve relevant partial differential equations by approximating the derivatives via the Taylor series expansion and using differences as an approximation. For this method it is important that a uniform grid is applied over the region to reduce the errors by the differencing method. The benefits of finite difference methods are that they are easy to understand, easy to explain, easy to program, meshing is simple, and the error is known in terms of the remainder from the Taylor series expansion of the derivatives. Furthermore, the availability of fast and inexpensive computers allows problems that are intractable using analytic or mechanical methods to be solved in a straightforward manner using finite difference methods.

In this study, a finite difference scheme is applied to solve the equation of interest. Since a finite difference solution is only an approximation of the actual solution, which, however, might be unknown, it is important for the approximate solution to converge to the real solution and it is also important to know precisely of what accuracy is the solution. In order to reach the goal of sufficient accuracy, it is necessary to study the convergence, consistency, and stability of the finite difference solution.

3.4.1 Development of a Finite Difference Solution

For convenient solution derivation and presenting the results, the numerical solution of the nondimensionalized equation will be used. The following nondimensional variables are used to derive a nondimensional partial differential equation for the contaminant transport.

$$\tilde{x} = \frac{x}{L},\ \tilde{t} = \frac{V_r t}{L},\ \tilde{C} = \frac{C}{C_0},\ \tilde{V} = \frac{V}{R_f V_r},\ \tilde{\alpha} = \frac{\alpha}{L},\ \tilde{D} = \tilde{\alpha}\tilde{V} = \frac{\alpha}{L}\frac{V}{R_f V_r},\ \text{and}\ \tilde{\lambda} = \frac{\lambda L}{V_r} \qquad (3.24)$$

Recall that the variables in (3.3) are defined as:

x = the distance [L],

t = the time [T],

L = the length of the aquifer domain [L],

C = the concentration of contaminant (mass of contaminant per unit volume of fluid) [M/L^3],

C_0 = the concentration of contaminant source (mass of contaminant per unit volume of fluid) [M/L^3],

V = the average interstitial fluid velocity vector [L/T],

D = the hydrodynamic dispersion coefficient [L^2/T],

K = the hydraulic conductivity [L/T],

n = the effective porosity [dimensionless],

α = the longitudinal dispersivity [L], and

λ = the degradation reaction rate [1/T].

$V_r = -\frac{K \cdot i_r}{n}$, [L/T], the average interstitial flow velocity corresponding the regional hydraulic gradient, i_r.

Using the dimensionless variables given in (3.24), the contaminant transport equation (3.3) becomes

$$\frac{\partial \tilde{C}}{\partial \tilde{t}} = \frac{\partial}{\partial \tilde{x}}\left(\tilde{D} \cdot \frac{\partial \tilde{C}}{\partial \tilde{x}} \right) - \frac{\partial}{\partial \tilde{x}}\left(\tilde{V} \cdot \tilde{C} \right) - \tilde{\lambda} \tilde{C} \tag{3.25}$$

such that the limits become

$$\tilde{x} \in [0,1] \; and \; \tilde{C} \in [0,1]. \tag{3.26}$$

Now the derivative terms in (3.25) can be approximated as

$$\frac{\partial}{\partial \tilde{x}}\left(\tilde{D} \cdot \frac{\partial \tilde{C}}{\partial \tilde{x}} \right) = p(1) + p(2), \; and \; \frac{\partial}{\partial \tilde{x}}\left(\tilde{V} \cdot \tilde{C} \right) = q(1) + q(2) \tag{3.27}$$

where

$$p(1) = \frac{\theta}{\Delta x^2}\left[\tilde{D}^{n+1}_{m+\frac{1}{2}}\left(\tilde{C}^{n+1}_{m+1} - \tilde{C}^{n+1}_{m} \right) - \tilde{D}^{n+1}_{m-\frac{1}{2}}\left(\tilde{C}^{n+1}_{m} - \tilde{C}^{n+1}_{m-1} \right) \right],$$

$$p(2) = \frac{1-\theta}{\Delta x^2}\left[\tilde{D}^{n}_{m+\frac{1}{2}}\left(\tilde{C}^{n}_{m+1} - \tilde{C}^{n}_{m} \right) - \tilde{D}^{n}_{m-\frac{1}{2}}\left(\tilde{C}^{n}_{m} - \tilde{C}^{n}_{m-1} \right) \right],$$

$$q(1) = \frac{\theta}{2\Delta x}\left[\tilde{V}^{n+1}_{m+1}\tilde{C}^{n+1}_{m+1} - \tilde{V}^{n+1}_{m-1}\tilde{C}^{n+1}_{m-1} \right], \; and$$

$$q(2) = \frac{1-\theta}{2\Delta x}\left[\tilde{V}^{n}_{m+1}\tilde{C}^{n}_{m+1} - \tilde{V}^{n}_{m-1}\tilde{C}^{n}_{m-1} \right],$$

$$with \; m = 1, \cdots, M-1, \; and \; n = 0, \; 1, \cdots$$

Note that in the finite difference scheme (3.27), θ is the implicit factor with $0 \le \theta \le 1$, m and n denote the space grid and tine step, respectively, and M is the number of grid points of space discretization.

Then the finite difference equation approximating equation (3.25) can be written as

$$\frac{\tilde{C}_m^{n+1} - \tilde{C}_m^n}{\Delta \tilde{t}} = p(1) + p(2) - q(1) - q(2) - \tilde{\lambda}\tilde{C}_m^n \tag{3.28}$$

Rearranging it becomes

$$\tilde{C}_m^{n+1} - p'(1) + q'(1) = p'(2) - q'(2) - \Delta t \tilde{\lambda}\tilde{C}_m^n + \tilde{C}_m^n \tag{3.29}$$

where

$$p'(1) = \theta\mu\left[\tilde{D}_{m+\frac{1}{2}}^{n+1}\left(\tilde{C}_{m+1}^{n+1} - \tilde{C}_m^{n+1}\right) - \tilde{D}_{m-\frac{1}{2}}^{n+1}\left(\tilde{C}_m^{n+1} - \tilde{C}_{m-1}^{n+1}\right)\right],$$

$$p'(2) = (1-\theta)\mu\left[\tilde{D}_{m+\frac{1}{2}}^{n}\left(\tilde{C}_{m+1}^{n} - \tilde{C}_m^{n}\right) - \tilde{D}_{m-\frac{1}{2}}^{n}\left(\tilde{C}_m^{n} - \tilde{C}_{m-1}^{n}\right)\right],$$

$$q'(1) = \frac{\theta}{2}\nu\left[\tilde{V}_{m+1}^{n+1}\tilde{C}_{m+1}^{n+1} - \tilde{V}_{m-1}^{n+1}\tilde{C}_{m-1}^{n+1}\right], \text{ and}$$

$$q'(2) = \frac{1-\theta}{2}\nu\left[\tilde{V}_{m+1}^{n}\tilde{C}_{m+1}^{n} - \tilde{V}_{m-1}^{n}\tilde{C}_{m-1}^{n}\right],$$

$$\text{where } \mu = \frac{\Delta t}{\Delta x^2},\ \nu = \frac{\Delta t}{\Delta x},\ m = 1, \cdots, M-1, \text{ and } n = 0,\ 1, \cdots$$

- Initial and Boundary Conditions

In order to solve the finite difference equation (3.29), initial and boundary conditions are needed. The following initial and boundary conditions are given in the Section 3 and Section 4 of this chapter.

Initial condition:

$$C\big|_{t=0} = 0 \tag{3.30}$$

Boundary condition:

$$C\big|_{x=0} = C_0,\ and\ \ C\big|_{x=L} = C_L = 0 \tag{3.31}$$

These give

$$\tilde{C}\big|_{\tilde{t}=0} = 0 \tag{3.32}$$

And

$$\tilde{C}\big|_{\tilde{x}=0} = 1.0,\ and\ \ \tilde{C}\big|_{\tilde{x}=1} = 0 \tag{3.33}$$

The finite difference approximation of the initial and boundary conditions is then given by the following:

$$\begin{aligned} &\tilde{C}_m^0 = 0,\ m = 0,\cdots,M \\ &\tilde{C}_0^{n+1} = 1.0\ and\ \tilde{C}_M^{n+1} = 0,\ n = 0,\cdots \end{aligned} \tag{3.34}$$

- The Solution

Now equation (3.29) can be rearranged to put the equation in matrix form, A $\underline{c}$ = $\underline{r}$, for convenient computation of the solution.

$$\begin{aligned} &\left(-\frac{\theta}{2}\nu\tilde{V}_{m-1}^{n+1} - \theta\mu\tilde{D}_{m-\frac{1}{2}}^{n+1}\right)\tilde{C}_{m-1}^{n+1} + \left(1 + \theta\mu\tilde{D}_{m+\frac{1}{2}}^{n+1} + \theta\mu\tilde{D}_{m-\frac{1}{2}}^{n+1}\right)\tilde{C}_m^{n+1} + \left(\frac{\theta}{2}\nu\tilde{V}_{m+1}^{n+1} - \theta\mu\tilde{D}_{m+\frac{1}{2}}^{n+1}\right)\tilde{C}_{m+1}^{n+1} \\ &= (1-\theta)\mu\left[\tilde{D}_{m+\frac{1}{2}}^{n}\left(\tilde{C}_{m+1}^{n} - \tilde{C}_m^{n}\right) - \tilde{D}_{m-\frac{1}{2}}^{n}\left(\tilde{C}_m^{n} - \tilde{C}_{m-1}^{n}\right)\right] \\ &\quad -\frac{1-\theta}{2}\nu\left(\tilde{V}_{m+1}^{n}\tilde{C}_{m+1}^{n} - \tilde{V}_{m-1}^{n}\tilde{C}_{m-1}^{n}\right) + \left(1 - \Delta\tilde{t}\,\tilde{\lambda}\right)\tilde{C}_m^{n} \\ &with\ m = 1,\cdots,M-1 \end{aligned} \tag{3.35}$$

Specifically, when m=1:

$$\begin{aligned}
&\left(1+\theta\mu\tilde{D}_{\frac{3}{2}}^{n+1}+\theta\mu\tilde{D}_{\frac{1}{2}}^{n+1}\right)\tilde{C}_1^{n+1}+\left(\frac{\theta}{2}\nu\tilde{V}_2^{n+1}-\theta\mu\tilde{D}_{\frac{3}{2}}^{n+1}\right)\tilde{C}_2^{n+1}\\
&=-\left(-\frac{\theta}{2}\nu\tilde{V}_0^{n+1}-\theta\mu\tilde{D}_{\frac{1}{2}}^{n+1}\right)\tilde{C}_0^{n+1}\\
&+(1-\theta)\mu\left[\tilde{D}_{\frac{3}{2}}^{n}\left(\tilde{C}_2^{n}-\tilde{C}_1^{n}\right)-\tilde{D}_{\frac{1}{2}}^{n}\left(\tilde{C}_1^{n}-\tilde{C}_0^{n}\right)\right]\\
&-\frac{1-\theta}{2}\nu\left(\tilde{V}_2^{n}\tilde{C}_2^{n}-\tilde{V}_0^{n}\tilde{C}_0^{n}\right)+\left(1-\Delta\tilde{t}\,\tilde{\lambda}\right)\tilde{C}_1^{n}
\end{aligned}\tag{3.36}$$

And when m=M-1:

$$\begin{aligned}
&\left(-\frac{\theta}{2}\nu\tilde{V}_{M-2}^{n+1}-\theta\mu\tilde{D}_{M-\frac{3}{2}}^{n+1}\right)\tilde{C}_{M-2}^{n+1}+\left(1+\theta\mu\tilde{D}_{M-\frac{1}{2}}^{n+1}+\theta\mu\tilde{D}_{M-\frac{3}{2}}^{n+1}\right)\tilde{C}_{M-1}^{n+1}\\
&=-\left(\frac{\theta}{2}\nu\tilde{V}_M^{n+1}-\theta\mu\tilde{D}_{M-\frac{1}{2}}^{n+1}\right)\tilde{C}_M^{n+1}\\
&+(1-\theta)\mu\left[\tilde{D}_{M-\frac{1}{2}}^{n}\left(\tilde{C}_M^{n}-\tilde{C}_{M-1}^{n}\right)-\tilde{D}_{M-\frac{3}{2}}^{n}\left(\tilde{C}_{M-1}^{n}-\tilde{C}_{M-2}^{n}\right)\right]\\
&-\frac{1-\theta}{2}\nu\left(\tilde{V}_M^{n}\tilde{C}_M^{n}-\tilde{V}_{M-2}^{n}\tilde{C}_{M-2}^{n}\right)+\left(1-\Delta\tilde{t}\,\tilde{\lambda}\right)\tilde{C}_{M-1}^{n}
\end{aligned}\tag{3.37}$$

Thus if writing in the form of A $\underline{c}$ = $\underline{r}$, A[i_m, j_m, k_m] is a tridiagonal matrix with the m^{th} three diagonal terms as

$$\begin{aligned}
i_m&=-\frac{\theta}{2}\nu\tilde{V}_{m-1}^{n+1}-\theta\mu\tilde{D}_{m-\frac{1}{2}}^{n+1},\quad m=2,\cdots,M-1\\
j_m&=1+\theta\mu\tilde{D}_{m+\frac{1}{2}}^{n+1}+\theta\mu\tilde{D}_{m-\frac{1}{2}}^{n+1},\quad m=1,\cdots,M-1\\
k_m&=\frac{\theta}{2}\nu\tilde{V}_{m+1}^{n+1}-\theta\mu\tilde{D}_{m+\frac{1}{2}}^{n+1},\quad m=1,\cdots,M-2
\end{aligned}\tag{3.38}$$

and the solution vector $\underline{c}$ at time step n+1 as

$$\underline{c}=\left[\tilde{C}_1^{n+1}\quad\tilde{C}_2^{n+1}\quad\cdots\quad\tilde{C}_{M-2}^{n+1}\quad\tilde{C}_{M-1}^{n+1}\right]^T\tag{3.39}$$

And the right hand side vector $\underline{r}[h_m]^T$ as a function of the solution at time step n with the m^{th} term is

$$h_m = (1-\theta)\mu\left[\tilde{D}^n_{m+\frac{1}{2}}\left(\tilde{C}^n_{m+1}-\tilde{C}^n_m\right)-\tilde{D}^n_{m-\frac{1}{2}}\left(\tilde{C}^n_m-\tilde{C}^n_{m-1}\right)\right]$$
$$-\frac{1-\theta}{2}\nu\left(\tilde{V}^n_{m+1}\tilde{C}^n_{m+1}-\tilde{V}^n_{m-1}\tilde{C}^n_{m-1}\right)+\left(1-\Delta\tilde{t}\,\tilde{\lambda}\right)\tilde{C}^n_m \qquad (3.40)$$
$$m = 2,\cdots,M-2$$

with two end terms as

$$h_1 = -\left(-\frac{\theta}{2}\nu\tilde{V}^{n+1}_0-\theta\mu\tilde{D}^{n+1}_{\frac{1}{2}}\right)\tilde{C}^{n+1}_0$$
$$+(1-\theta)\mu\left[\tilde{D}^n_{\frac{3}{2}}\left(\tilde{C}^n_2-\tilde{C}^n_1\right)-\tilde{D}^n_{\frac{1}{2}}\left(\tilde{C}^n_1-\tilde{C}^n_0\right)\right] \qquad (3.41)$$
$$-\frac{1-\theta}{2}\nu\left(\tilde{V}^n_2\tilde{C}^n_2-\tilde{V}^n_0\tilde{C}^n_0\right)+\left(1-\Delta\tilde{t}\,\tilde{\lambda}\right)\tilde{C}^n_1$$

$$h_{M-1} = -\left(\frac{\theta}{2}\nu\tilde{V}^{n+1}_M-\theta\mu\tilde{D}^{n+1}_{M-\frac{1}{2}}\right)\tilde{C}^{n+1}_M$$
$$+(1-\theta)\mu\left[\tilde{D}^n_{M-\frac{1}{2}}\left(\tilde{C}^n_M-\tilde{C}^n_{M-1}\right)-\tilde{D}^n_{M-\frac{3}{2}}\left(\tilde{C}^n_{M-1}-\tilde{C}^n_{M-2}\right)\right] \qquad (3.42)$$
$$-\frac{1-\theta}{2}\nu\left(\tilde{V}^n_M\tilde{C}^n_M-\tilde{V}^n_{M-2}\tilde{C}^n_{M-2}\right)+\left(1-\Delta\tilde{t}\,\tilde{\lambda}\right)\tilde{C}^n_{M-1}$$

With the given initial and boundary conditions (3.34), the finite difference equation (3.35) can be solved recursively to reach the solution at any given time of $\tilde{t} = (n+1)\Delta\tilde{t}$.

- Adjustment for Dispersion

The numerical solution to (3.35) is not stable since the dispersion term, D, can be negative as a result of the negative flow velocity, which in turn is a result of tidal fluctuation. In this case, the convective-dispersion equation (3.25) is bad-posed such that the numerical solution would blow up and deviate unacceptably from the exact solution (Thomas, 1995). A study of dispersion reveals that dispersion is caused by velocity heterogeneity, and it is symmetrical about the contaminant front and thus independent of

flow direction (Domenico and Schwartz, 1997). As a result, the dispersion term can be adjusted as

$$D = \alpha |V|, \text{ and } \tilde{D} = \tilde{\alpha} |\tilde{V}| = \frac{\alpha}{L} \frac{|V|}{R_f V_r} \tag{3.43}$$

With this adjustment, the convective-dispersion equation (3.25) is well-posed such that a numerical solution is achievable.

3.4.2 Accuracy and Convergence of Numerical Solution

It is important that the numerical solution accurately satisfies the partial differential contaminant-transport equation. The accuracy generally means that the numerical solution sufficiently converges to the real solution of the partial differential equation. This can be typically verified by comparing it to the closed-form (or analytical) solution. If the closed-form solution is evaluated correctly, any discrepancies between the numerical and analytical solutions can be attributed to errors in the numerical algorithm. However, when a closed-form solution is not available, some other options are needed to fulfill this task. A number of options are routinely used for this purpose. One is mass conservation, and another to examine the behavior of the numerical solution as its spatial grid and time step are progressively refined (Ruan, et al., 1999), i.e., a convergence study. Convergence is most commonly obtained through the concepts of consistency and stability and the Lax Theorem (Thomas, 1995, p. 41). The Lax Theorem allows one to prove convergence of a difference scheme by showing that the scheme is both consistent and stable. In the following sections these methods are used to demonstrate the validity of the numerical solution developed.

- Consistency

A numerical scheme is consistent if the original partial differential equation is obtained as both the time and space increments approach zero. A numerical method is convergent if the results obtained as both the time and space increments are reduced approach a limiting value and that value matches the true solution of the governing equations. Consistency relates to the governing equation and convergence relates to the exact solution of the equation.

Through Taylor series analysis, the finite difference scheme is, approximating the modified transport equation (3.25), consistent and accurate within two orders of magnitude with regard to space, and accurate within one order of magnitude with regard to time. When the implicitness factor, θ, equals 0.5, which represents the Crank-Nicolson Scheme, the finite difference scheme is convergent and accurate within two orders of magnitude with regard to both space and time. This is also the desirable scheme to be used to solve the transport equation.

- Stability

A numerical method is computationally stable if rounding-off and truncation errors do not accumulate such that the solution diverges. The stability of the finite difference scheme prescribed in equation (3.35) can be demonstrated by analyzing the matrix A defined by (3.38).

Notice that since the entries in matrix $A[i_m, j_m, k_m]$ are not constant the traditional Von Neumann stability analysis no longer applies. And notice also that this is a linear problem, and if it can be demonstrated that the matrix $A[i_m, j_m, k_m]$ is diagonally

dominant or if diagonal dominance can be achieved by constraining the values of ν and μ, the solution would be stable (Thomas, 1995).

Diagonal dominance implies that in (3.38)

$$j_m \geq |i_m| + |k_m|, \quad m = 1, \cdots, M-1 \tag{3.44}$$

That is

$$1 + \theta\mu\tilde{D}^{n+1}_{m+\frac{1}{2}} + \theta\mu\tilde{D}^{n+1}_{m-\frac{1}{2}} \geq \left| -\frac{\theta}{2}\nu\tilde{V}^{n+1}_{m-1} - \theta\mu\tilde{D}^{n+1}_{m-\frac{1}{2}} \right| + \left| \frac{\theta}{2}\nu\tilde{V}^{n+1}_{m+1} - \theta\mu\tilde{D}^{n+1}_{m+\frac{1}{2}} \right| \tag{3.45}$$

The right hand side of the above inequality can be rearranged to show

$$\begin{aligned} &\left| -\frac{\theta}{2}\nu\tilde{V}^{n+1}_{m-1} - \theta\mu\tilde{D}^{n+1}_{m-\frac{1}{2}} \right| + \left| \frac{\theta}{2}\nu\tilde{V}^{n+1}_{m+1} - \theta\mu\tilde{D}^{n+1}_{m+\frac{1}{2}} \right| \\ &\leq \left| \frac{\theta}{2}\nu\tilde{V}^{n+1}_{m-1} \right| + \left| \theta\mu\tilde{D}^{n+1}_{m-\frac{1}{2}} \right| + \left| \frac{\theta}{2}\nu\tilde{V}^{n+1}_{m+1} \right| + \left| \theta\mu\tilde{D}^{n+1}_{m+\frac{1}{2}} \right| \\ &\leq \frac{\theta}{2}\nu\left(\left|\tilde{V}^{n+1}_{m-1}\right| + \left|\tilde{V}^{n+1}_{m+1}\right| \right) + \left| \theta\mu\tilde{D}^{n+1}_{m-\frac{1}{2}} \right| + \left| \theta\mu\tilde{D}^{n+1}_{m+\frac{1}{2}} \right| \\ &\leq \theta\nu\left|\tilde{V}\right|_{\max} + \left| \theta\mu\tilde{D}^{n+1}_{m-\frac{1}{2}} \right| + \left| \theta\mu\tilde{D}^{n+1}_{m+\frac{1}{2}} \right| \end{aligned} \tag{3.46}$$

Notice from (3.43) that $\tilde{D} \geq 0$, such that (3.45) can be satisfied if the following stands true

$$1 + \theta\mu\tilde{D}^{n+1}_{m+\frac{1}{2}} + \theta\mu\tilde{D}^{n+1}_{m-\frac{1}{2}} \geq \theta\nu\left|\tilde{V}\right|_{\max} + \left| \theta\mu\tilde{D}^{n+1}_{m-\frac{1}{2}} \right| + \left| \theta\mu\tilde{D}^{n+1}_{m+\frac{1}{2}} \right| \tag{3.47}$$

which is rearranged to give

$$\nu \leq \frac{1}{\theta\left|\tilde{V}\right|_{\max}} \tag{3.48}$$

From (3.9) the velocity is given as a function of time and space. Combined with (3.24), it gives

$$\begin{aligned}\left|\tilde{V}\right| &= \left|\frac{K}{nR_fV_r}\left[i_r+\sqrt{2}\beta Ae^{-\beta(L-x)}\sin\left(\omega t-\beta\left(L-x\right)+\frac{\pi}{4}\right)\right]\right| \\ &\le \frac{1}{R_f}+\left|\frac{K}{nR_fV_r}\left[\sqrt{2}\beta Ae^{-\beta(L-x)}\sin\left(\omega t-\beta\left(L-x\right)+\frac{\pi}{4}\right)\right]\right| \\ &\le \frac{1}{R_f}+\frac{\sqrt{2}K\beta A}{nR_fV_r}e^{-\beta(L-x)}\end{aligned} \tag{3.49}$$

Since x is always less than or equal to L and β is positive, the above inequality leads to

$$\left|\tilde{V}\right|_{\max} = \frac{1}{R_f}+\frac{\sqrt{2}K\beta A}{nR_fV_r} \tag{3.50}$$

Then (3.48) and (3.50) together give a sufficient condition for stability as

$$\nu \le \frac{1}{\theta\left(\frac{1}{R_f}+\frac{\sqrt{2}K\beta A}{nR_fV_r}\right)} = \nu_{\max} \tag{3.51}$$

This means that if condition (3.51) is met, the stability requirement for the finite difference solution of equation (3.35) is automatically satisfied.

- Convergence

The simultaneous satisfaction of consistency and stability implies that the numerical solution is convergent to the true solution of the transport equation (Thomas, 1995). The next step is to refine the size of both the space grid and the time step according to the relationship obtained from the stability analysis, i.e., the restriction of the value of ν and μ. The "converged solution" achieved by doing so is the solution that will be finally used.

Next we test the convergence using two sets of tests. One involves comparing the numerical solution to the analytical solution for the uniform flow case, while the other

involves keeping a fixed time horizon and reducing the size of the time step to see if a "converged solution" could be reached for the case with tides. While doing this, the space discretion is also refined according to the restriction of stability.

In the first test the analytical solution attained in Chapter 3 is used with parameters set A listed in Table 3.2. Note that in the test an error defined as follows is used to represent the divergence of the finite difference solution from the analytical solution:

$$E = \sqrt{\Delta x \sum_{m=1}^{M} \left| \tilde{C}_m - \tilde{c}(x_m, t) \right|^2} \qquad (3.52)$$

where M is the number of space grid nodes, $\tilde{c}$ denotes the analytical solution and $\tilde{C}$ the numerical solution.

Since the stability constraint is critical to the problem, a series of values for ν is evaluated in the test to see how error varies with the refined space and time steps. The time horizon is chosen to be T=1.5. Recall T is the number of displaced pore volumes defined in (3.23). From Table 3.3 it is observed that the error diminishes as the space and time grids are reduced, except that there is some oscillation in the trend in how the error decreases due to the performance of numerical solution. From this test, for the current study, a space grid of 51 and a corresponding time discretization is thus an acceptable refinement level.

Table 3.3 Convergence Test for the Case without Tides (T=1.5)

E (Divergence)	$\Delta t = 0.9\nu_{max}\Delta x$	$\Delta t = 0.5\nu_{max}\Delta x$	$\Delta t = 0.2\nu_{max}\Delta x$
M = 11 (Δx = 0.1)	0.057447	0.075635	0.051052
21 (Δx = 0.05)	0.024599	0.011420	0.013527
51 (Δx = 0.02)	0.002304	0.001984	0.001403
101 (Δx = 0.01)	0.011245	0.004403	0.000442
201 (Δx = 0.005)	0.000575	0.006737	0.000877
501 (Δx = 0.002)	0.002052	0.000957	0.000714

In the next test it is considered how the numerical solution converges (it will converge because of the consistency and stability demonstrated earlier). The same conditions, except for non-zero tide amplitude, and the same refining schedule are used. This time the divergence between solutions is visualized and compared in the following plots. Figure 3.10 shows the overview of the concentration distribution over the entire flow domain with $\Delta t = 0.2\nu_{max}\Delta x$ ending at time T=1.5, while in Figure 3.11 it is zoomed in to show what is happening close to the effluent boundary. More attention is given to this portion of the domain since as tides fluctuate, most of the divergence would happen locally adjacent to the tidal boundary.

It is observed that the numerical solution oscillates up and down about the "converged solution" as the size of the space and time grids are reduced. And in this case the "converged solution" is the approximate solution when space grid M reaches 501 or more. However, the solutions corresponding to M equal to 101 and 201 are sufficiently close the "converged solution" such that a higher grid refinement would not justify the expense of computation (see Table 3.4).

Table 3.4 Convergence Test for the Case with Tides (T=1.5)

Computation Time (s)	$\Delta t = 0.9\nu_{max}\Delta x$	$\Delta t = 0.5\nu_{max}\Delta x$	$\Delta t = 0.2\nu_{max}\Delta x$
M = 11 ($\Delta x = 0.1$)	0.2810	0.3280	0.4060
21 ($\Delta x = 0.05$)	0.4060	0.5780	0.8120
51 ($\Delta x = 0.02$)	1.0320	1.9370	4.5470
101 ($\Delta x = 0.01$)	3.9690	7.0930	17.8280
201 ($\Delta x = 0.005$)	16.6250	29.5630	73.6880
501 ($\Delta x = 0.002$)	109.4370	203.3910	508.0320

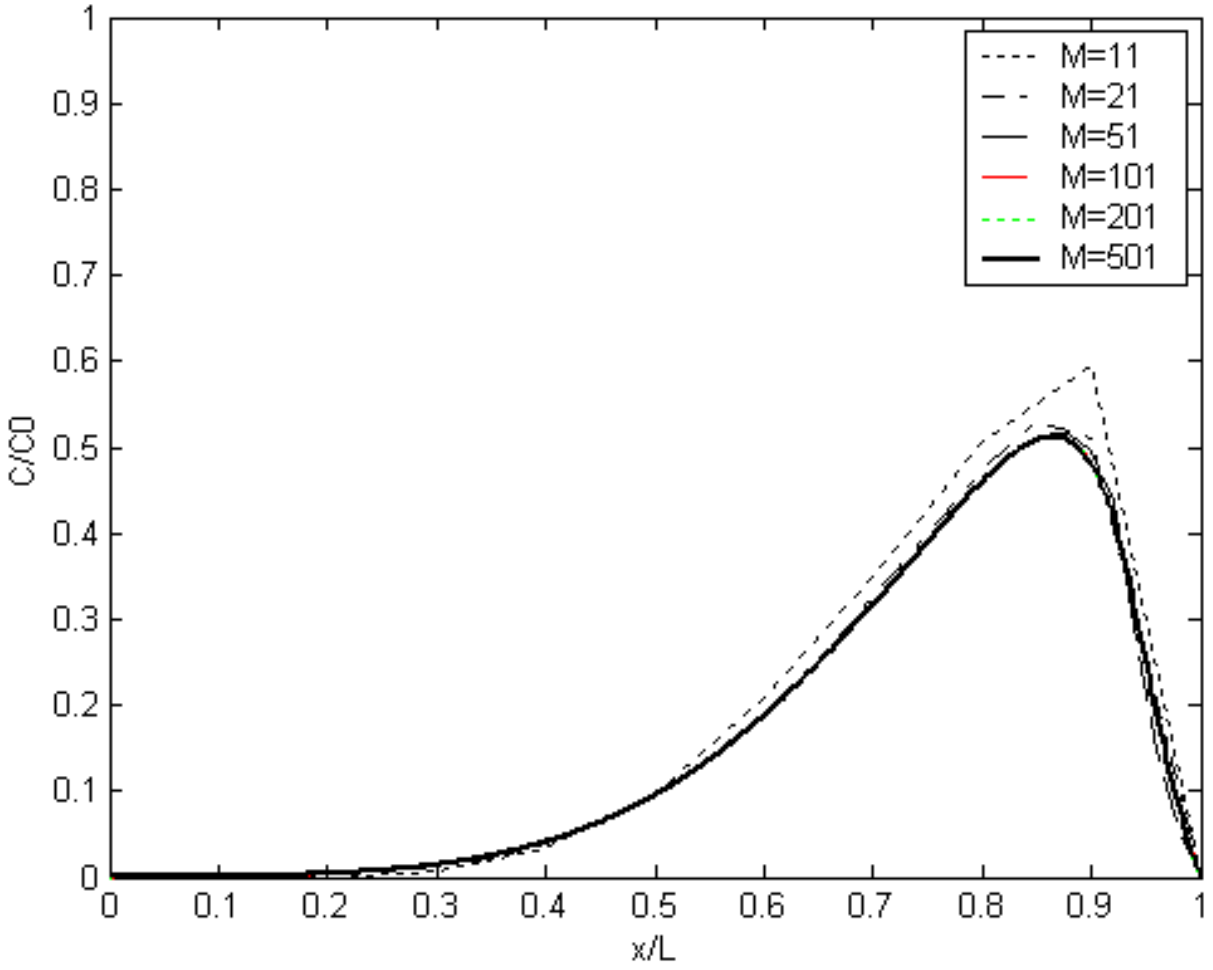

Figure 3.10 Numerical Solution Convergence Test with $\Delta t = 0.2 v_{max} \Delta x$.

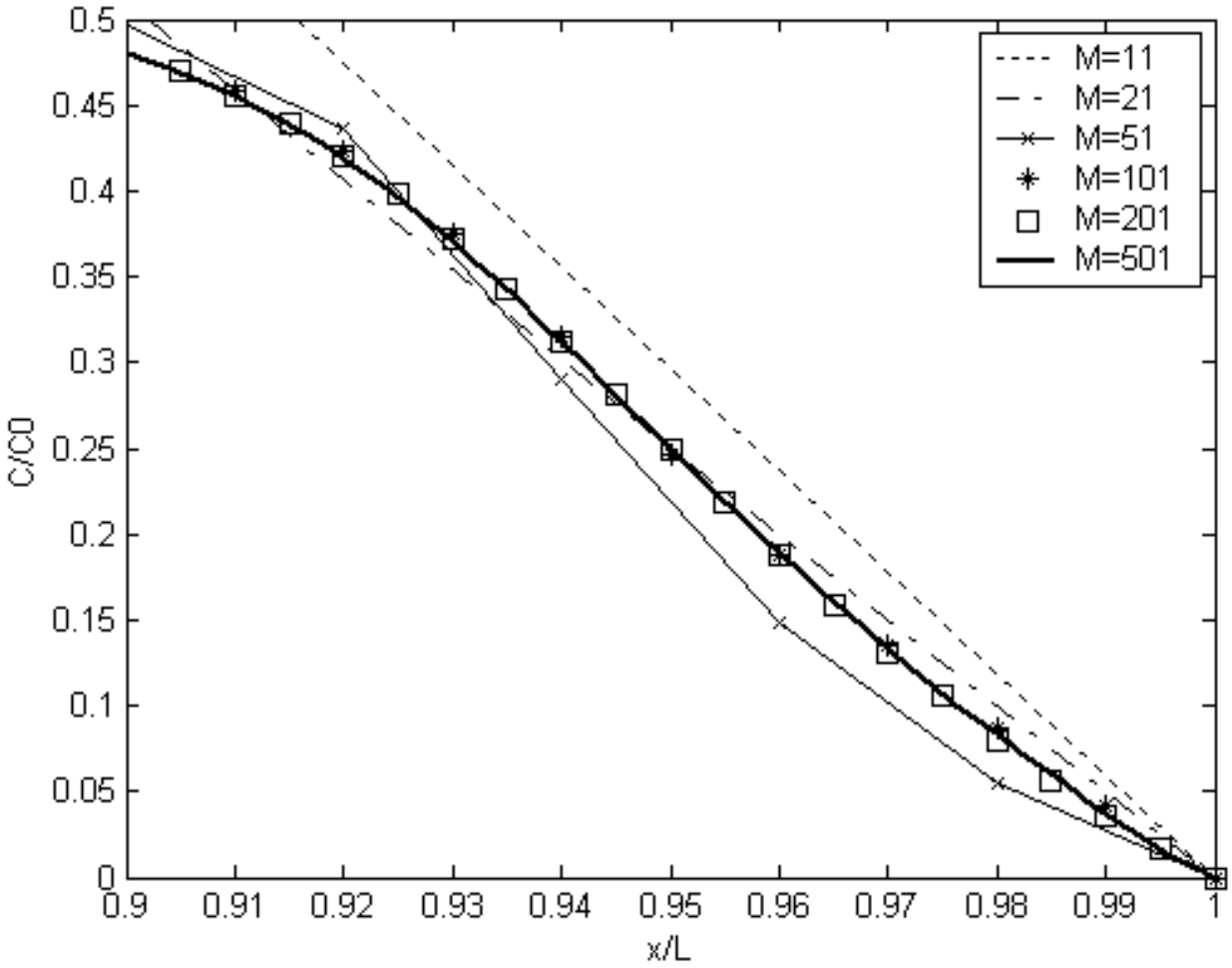

Figure 3.11 Numerical Solution Convergence Test with $\Delta t = 0.2 v_{max} \Delta x$ (zoomed in).

It is further tested for the cases with $\Delta t = 0.5\nu_{max}\Delta x$ and $\Delta t = 0.9\nu_{max}\Delta x$ with the solution profiles presented in Figure 3.12 and Figure 3.13, respectively. Since Δt gets larger, the convergence gets more difficult to achieve. That is, in the former case, the solution begins to converge only after the space grid M reaches 501, while in the latter case, the solution diverges significantly from the possible "converged solution" when M is small, and the solution could be on the way close to the "converged solution" after M hits 501 and above, which, however, is not continued without necessity. A much finer grid would not justify the increased cost in computation time (refer to Table 3.4).

These results conclude that in the case with tides, a space grid of 101 combined with a time step of $\Delta t = 0.2\nu_{max}\Delta x$ is all that is needed to reach a sufficiently accurate solution (an error of the order 10^{-3} is assumed to be sufficient for this study).

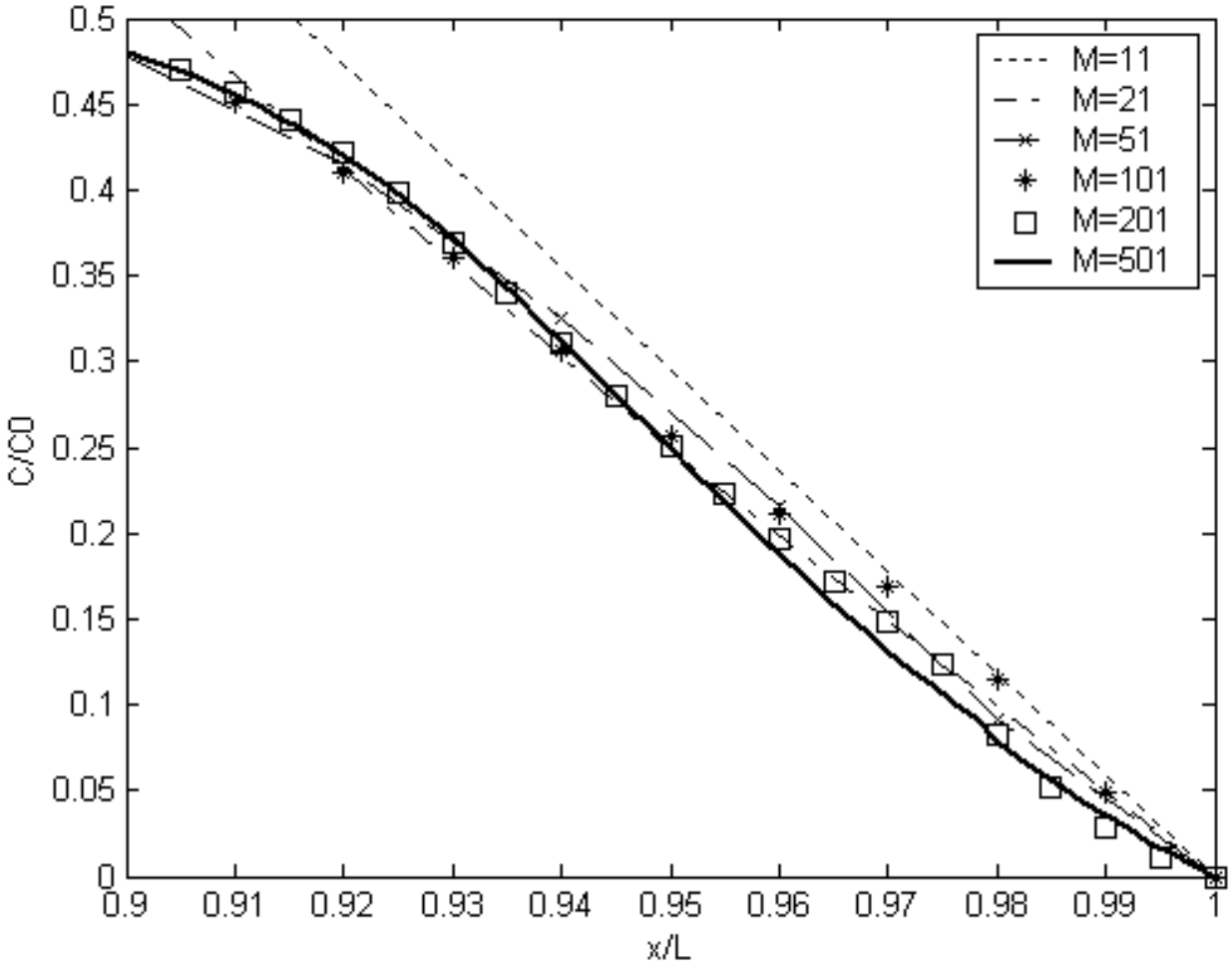

Figure 3.12 Numerical Solution Convergence Test with $\Delta t = 0.5 v_{max} \Delta x$ (zoomed in).

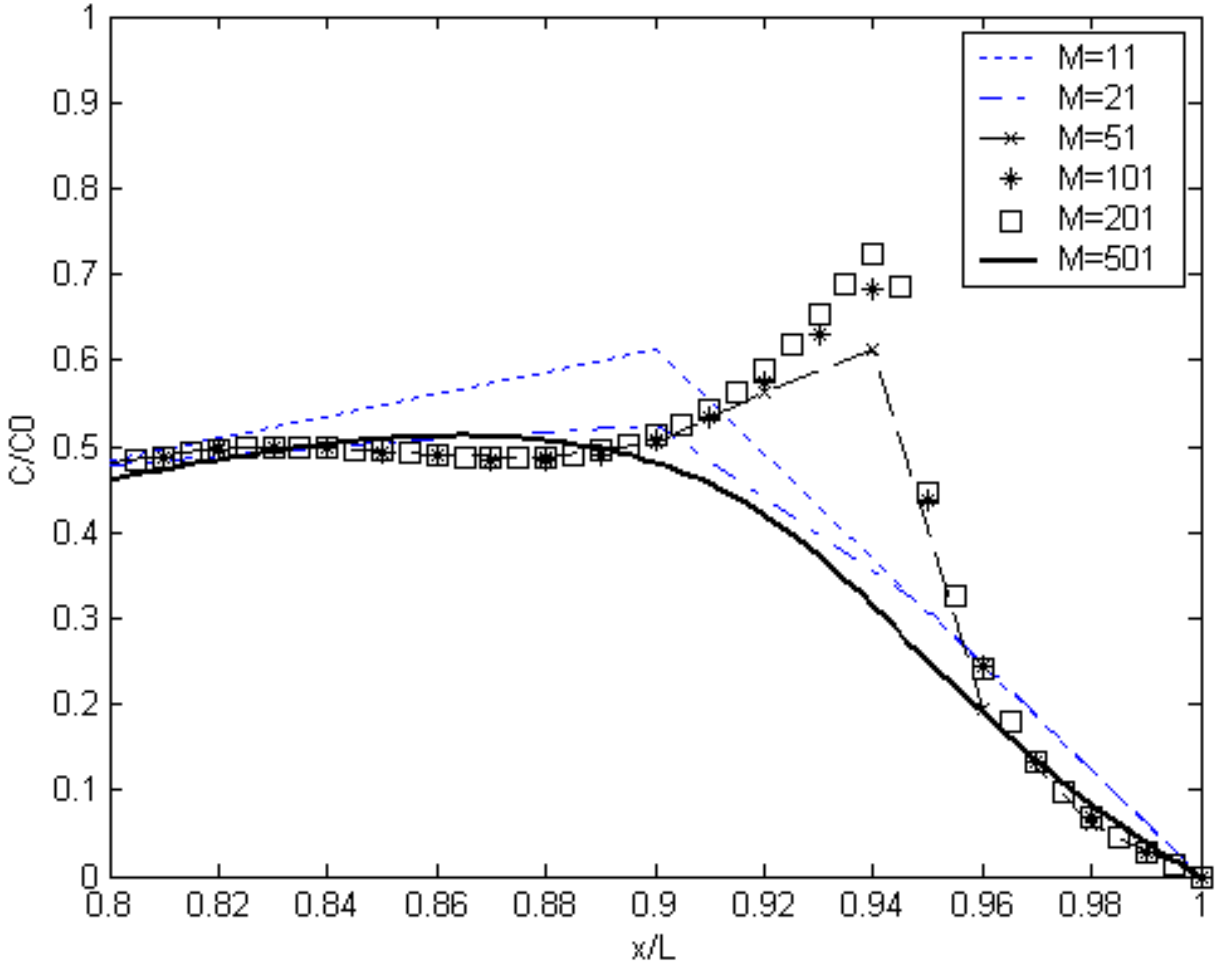

Figure 3.13 Numerical Solution Convergence Test with $\Delta t = 0.9\nu_{max}\Delta x$ (zoomed in).

In summary, the numerical scheme used here is demonstrated to be consistent with the partial differential equation and accurate to at least one order of magnitude with regard to time, and accurate within two orders of magnitude with regard to space. The numerical solution is also stable if certain conditions are met. Starting from this point, different contaminant transport parameters can then be applied into the numerical scheme to study the impact of each of these factors. And more importantly, tidal fluctuations are able to be incorporated into the solution such that its influence can be investigated. Numerical results will be presented in Chapter 5.

CHAPTER 4

EXPERIMENTAL STUDY

Recall that the numerical and analytical solutions of the groundwater flow and contaminant transport equations are solved based on a number of assumptions. All of these assumptions might give biased results and thus need to be verified by experiments. Obviously the results coming out of experiments are not absolutely correct because of systematic as well as operational errors, but they can provide insight into the physical transport phenomena, and if both the experimental and numerical results agree well with each other, then conclusions can be reached accordingly.

4.1 Experimental Setup

4.1.1 Experimental Scale

Since the laboratory experiment is only a small and simplified model of the full-size field condition (prototype) for the groundwater flow problem in this study, the dimension of the model is chosen to be much smaller but reasonable in order to achieve the goals of cost saving and operational convenience. Thus, the law of similitude or similarity is used in this study to determine the appropriate selection of the model scale.

Three similarities are desirable in model studies, geometric similarity, kinematic similarity, and dynamic similarity (Finnemore and Franzini, 2002). Geometric similarity means that the model and its prototype have identical shapes but differ only in size, i.e., geometrically similar. Kinematic similarity implies that, in addition to geometric similarity, the ratio of the velocities at all corresponding points in the flows are the same.

Two systems have dynamic similarity if, in addition to kinematic similarity, corresponding forces are in the same ratio in both the model and the prototype. Depending on which force(s) is most important in the flow problem, one or more ratios, such as Reynolds number, Froulde number, and Mach number, may be selected for the similarity comparison (Finnemore and Franzini, 2002).

To ensure the flows in the experimental model and the prototype are comparable, dynamic similarity shall be applied for the model setup. In groundwater systems, contaminant transport occurs predominantly through groundwater flow (when advection is dominant over diffusion) which complies with the Darcy's law. The dominant driving forces in groundwater flow are inertial and viscous forces. Thus the Reynolds number, R, may be used, which expresses the dimensionless ratio of inertial to viscous forces and serves as a criterion to distinguish between laminar and turbulent flow, and a way to identify the validity of Darcy's law. For this characteristic of groundwater flow, two groundwater flow systems have dynamic similarity when they have the same Reynolds number. The Reynolds number is defined as (Todd, 1980)

$$R = \frac{\rho V D}{\mu} \tag{4.1}$$

where ρ is the fluid density, V the flow velocity, D the diameter (of pipe, in groundwater flow the interstitial flow pathway between soil grains), and μ the absolute contaminant viscosity of the fluid. To adopt this criterion, an effective grain size (d_{10}) is substituted for D to approximate the flow tube diameter.

Letting subscripts p and m denote prototype and model, respectively, dynamic similarity is met when

$$\left(\frac{\rho VD}{\mu}\right)_m = R_m = R_p = \left(\frac{\rho VD}{\mu}\right)_p \qquad (4.2)$$

In both the model and the field condition (prototype) the fluid, fresh water, is considered to have similar properties, which means that the terms, ρ and μ, in equation (4.2) are the same. Thus in order to achieve dynamic similarity, the grain-size distribution of the porous medium and the flow velocity in the model are chosen selectively according to typical field conditions.

Dynamic similarity means geometric and kinematic similarities at the same time, as indicated by the definitions. Complete geometric similarity, however, is not practically feasible to attain. For example, in this study, the same scale can not be used both horizontally and vertically, because this would produce an aquifer system so shallow that capillarity would have a significant effect on the flow and transport patterns, and the head difference would be too small for flow to occur. In this case, a distorted model is needed, which means that the vertical scale is larger than the horizontal scale.

Let λ denote the model length scale (the ratio of model length to prototype length). For a distorted model as in this study, two model length scales imply: horizontal length scale, λ_h, and vertical length scale, λ_v, as defined by

$$\lambda_h = \frac{L_m}{L_p}, \ and \ \lambda_v = \frac{B_m}{B_p} \qquad (4.3)$$

where B is the vertical dimension (aquifer thickness).

By kinematic similarity the velocity scale is

$$V_s = \frac{V_m}{V_p} \qquad (4.4)$$

As time T is dimensionally L/V, the time scale is thus

$$T_s = \frac{\lambda_h}{V_s} \tag{4.5}$$

Here λ_h is used because the flow is dominantly horizontal in the flow system.

The knowledge of the length and time scales helps when studying the cyclic phenomenon of tides. The application is that the amplitude and period of the tide will be chosen accordingly using the same vertical length scale, λ_v, and time scale, T_s. Typical data of coastal aquifer systems and tides, and coincident values used in the experimental model are listed in Table 4.1.

Table 4.1 Aquifer Parameter Values Considered in Prototype and Model

Parameters	Prototype (typical value)	Scale	Model value
Aquifer Length, ft	1200 (10^2~10^4)	λ_h=0.01	12
Aquifer Thickness, ft	30 (10^1~10^2)	λ_v=0.1	3
Hydraulic Conductivity, ft/d	300 (10^1~10^2)	K_s=1.0	[a]300
Hydraulic Gradient	0.005 (10^{-3}~10^{-2})	i_s= 10 (λ_v/λ_h)	[b]0.05
Flow Velocity, ft/d	5 (10^{-1}~10^1)	V_s=10 (K_s i_s)	[b]50
Tidal Period, hr	12 (12 / 24)	T_s=0.001 (λ_h/ V_s)	[b]1 min
Tidal Amplitude, ft	2 (0.5~3)	λ_v=0.1	[b]0.2

[a] Values are estimated.
[b] Values are to be changed within certain range to study the effects.

4.1.2 Experimental Facility

The experimental facility is illustrated in Figure 4.1. The sand tank is designed such that it can be used to simulate groundwater flow and contaminant transport in both unconfined and confined aquifers by switching the seal cover, and with a periodic boundary condition (tidal fluctuations) imposed at the effluent end. The sand tank is constructed with cast acrylic sheets and is chosen to have a dimension of 12 feet long, 3 feet high, and 6 inches wide. The water level in each end of the tank is controlled such that tidal fluctuations can be simulated.

The cover of the sand tank can be bolted to the walls of the sand tank, with a rubber band used to seal the tank. By doing this, the water level in the sand tank can be raised to be above the tank such that confined groundwater flow can be simulated. However, when the cover is unsealed, groundwater flow in the sand tank is unconfined.

Sand is filled between the two mesh lattices embedded in the side walls of the sand tank. Through the meshes water enters and exits the porous medium. At the influent chamber of the tank, water level is controlled through a perforated pipe of 12 inch diameter connected to a constant-head water-supply box (see the left end of Figure 4.1). The water level in the water-supply box is controlled to be constant by a fixed weir at the center of the box, with overflow water from the weir directed to a sink by a 12 inch diameter PVC pipe. The elevation of the box can also be adjusted to set a constant head at any level required. At the effluent chamber of the tank, water level is controlled through a similar fashion except that the water-supply box is movable vertically controlled by a mechanical mechanism to impose a periodic-head boundary condition (see the TIDAL TANK in Figure 4.1).

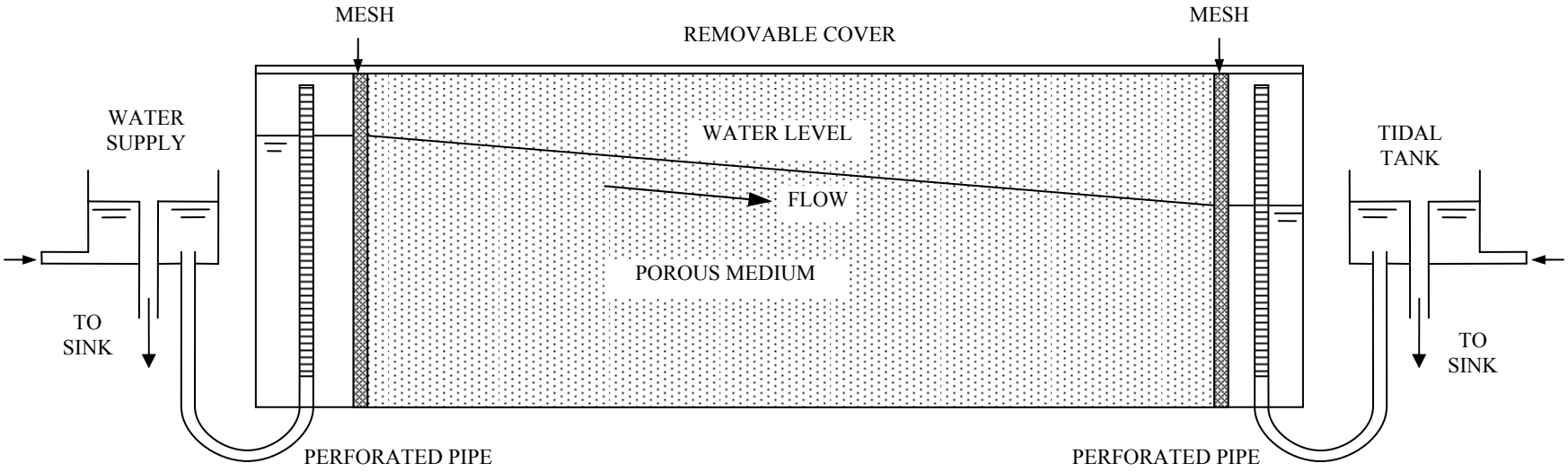

Figure 4.1 Experimental Facility Layout.

4.1.3 Porous Medium

Ottawa sand is used as the porous medium. Sand is packed in the flow tank using the method outlined by Waygal (1963). It is poured into a 20 to 30 mm layer of water through a packer box. The water layer is assumed not to produce any size segregation of the sand.

The porosity of the sand medium can be estimated using the formula

$$n = 1 - \frac{W_s}{V_0 \rho_b} \tag{4.6}$$

where n is the porosity, W_s is the weight of the amount of sand used to fill a known tank volume of V_0, and ρ_b is the sand particle density which is approximately 2.65 g/cm^3. The value of the saturated hydraulic conductivity, K, is determined using a standard head permeameter and is measured directly in the sand tank.

The specific yield of the porous medium is needed for the unconfined case, while the storage coefficient is needed for the confined case. The specific yield of a saturated soil is the ratio of the volume of water which it will yield by gravity, to its total volume. The storativity of a saturated soil is the ratio of the volume of water which it will yield by water elasticity, to its total volume (Fetter, 1994). Standard methods in groundwater textbooks are used to measure these parameters.

A constant head permeameter or falling head permeameter (Todd, 1980) can be used to determine the permeability of the sand used. For a constant head permeameter, water enters the porous medium from the bottom and is collected as overflow after passing upward through the material. The hydraulic conductivity can be obtained from Darcy's law that

$$K = \frac{L}{Ah}\frac{V}{t} \tag{4.7}$$

where L is the length of sand sample [L], h the heads difference [L], V the overflow volume [L^3] in time t [T], and A the horizontal area of the sample [L^2], which is equal to πR^2 with R being the radius of the sand sample. For a falling head permeameter, water is added to the tall tube and flows upward through the sample medium and collected as overflow. If it takes time t for the water level in the tube to fall from h_1 to h_2, the permeability can be calculated as

$$K = \frac{r^2 L}{R^2 t}\ln\left(\frac{h_1}{h_2}\right) \tag{4.8}$$

Permeameter results may bear little information for actual field hydraulic conductivities as the samples are disturbed with packing and the porosity changed (Todd, 1980). The permeameter results in this study, however, are useful since both the samples and the sand condition in the experiment tank are similar and thus the values are expected to be comparable. Sample tests and experimental runs in the actual sand tank indicate a porosity and hydraulic conductivity of the sand medium to be approximately 0.45 and 17.2 cm/min, respectively.

4.1.4 Experiment Equipments and Procedures

Two arrays of penetration ports are used, one for sampling tracer solution and the other for water heads measurement. The locations of the sampling and measurement nodes are illustrated in Figure 4.2.

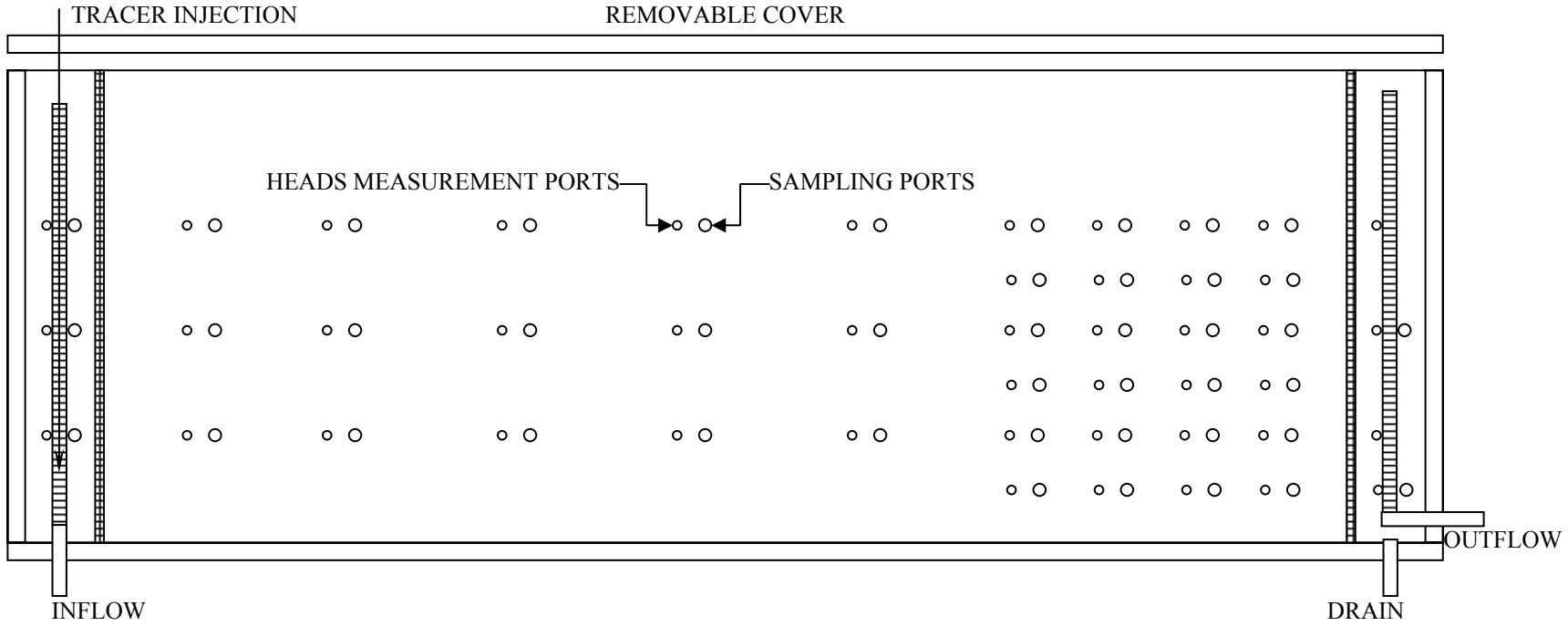

Figure 4.2 Positions of Tracer Sampling and Heads Measurement Ports.

The piezometers consist of 1/8 inch I.D. copper tubing which are installed in the acrylic tank wall through commercial liquid-tight fittings. The copper tubing extends approximately 5 mm into the tank, and this portion of the tubing would not significantly influence the flow field (Silliman, 2003). On the exterior of the tank, 3/16-inch I.D. PVC tubing is connected to the copper tubing, unionized and run to a manometer board. It is estimated that the precision of water level measurements is approximately 0.5 mm on the manometer board (using new tubing), but that this precision decays with time as biological growth changes the inner surface properties of the tube (thereby influencing surface tension and observed water level in the manometer) (Silliman, 2003).

A similar design is used for tracer sample collection except that smaller tubing, i.e., 1/16 inch I.D. tubing, is used in order not to expend too much solution (thereby introducing experiment error by interfering with the solution concentration downstream from the sampling ports). Again, copper tubing is used and extends about 5mm into the tank. Outside the tank wall 1/8 inch I.D. PVC tubing is connected to the copper tubing, and the PVC tubing is only half to one inch long, with plugs used to control flow.

In the experiment, food color (red) is used as the tracer. The food color used has the advantages of not being adsorbed onto the sand grains (Ottawa Sand) and is easily washed off. It is a conservative chemical solution with the convenience of visual observation and concentration measurement. A UV-Visible Spectroscopy System (Hewlett-Packard Model HP 8453) is utilized to measure the concentration of the color solution (Huber, 1993). The HP 8453 system is based on the HP 8453 UV-Visible spectrophotometer. This spectrophotometer has no optically-active moving parts and has proven to be extremely reproducible and stable both in the short and long term. The

system's excellent reliability, stability, and its built-in self-verification make frequent, full verification unnecessary. The operating software for HP ChemStations undergoes extensive validation during development, and the advanced software for the HP 8453 system includes tools that simplify the validation of an analytical method. The system has the ability of generating a calibration curve based on standard samples and applies the curve for sample measurements.

The experiment procedures are as follow, for each given case,

1. Set water levels at boundaries as required;
2. Let water flow for at least 12 hours to reach steady state prior to tracer application;
3. Start color solution injection, and set time to t=0. In cases with tides, start tidal fluctuations at t=0;
4. Collect samples and get hydraulic heads reading every 30 minutes;
5. Measure samples within 24 hours following SOPs for the UV-Visible Spectroscopy system; and
6. Record and interpret experimental data.

4.2 Experimental Results

Experimental results are important with regard to understanding the physical transport phenomenon and to the verification of the analytical and numerical results. With the limitations of experiment itself, the experiment study will not take into account as many factors as was done in the numerical analysis. The major considerations include the tidal fluctuations at the effluent boundary, and the comparison between the unconfined (unconfined-condition experiment) and confined situations (confined-condition experiment). The experimental results will verify the validity of the selection of the boundary condition for the baseline and numerical solutions, and these results are expected to be consistent with the numerical results, provided that the numerical

solutions perform sufficiently accurate. Table 4.2 and Table 4.3 give the parameters values and case numbers for the cases considered in the experiments.

Table 4.2 Cases Considered in the Unconfined-Condition Experiments

Case #	Average Hydraulic Gradient (i)	Tidal Period (δ) min	Tidal Amplitude (A) cm	Dilution Factor (DF)
B16/18	0.05	NA	NA	1.0
B16X	0.05	NA	NA	9.48
T16	0.05	5.0	20.00	9.48
T18	0.05	5.0	10.00	9.48
U2	0.05	2.0	20.00	9.48
U3	0.05	2.0	10.00	9.48

Table 4.3 Cases Considered in the Confined-Condition Experiments

Case #	Average Hydraulic Gradient (i)	Tidal Period (δ), min	Tidal Amplitude (A),cm	Dilution Factor (DF)
B19	0.1	NA	NA	1.0
B19X	0.1	NA	NA	8.13
T19	0.1	5.0	20.00	8.44
CON3	0.1	1.0	30.00	8.44
CON4	0.1	1.0	20.00	8.44
B20	0.05	NA	NA	1.0
B20X	0.05	NA	NA	29.39
T20	0.05	5.0	20.0	29.39
CON1	0.05	1.0	30.0	29.39
CON2	0.05	1.0	20.0	29.39

4.2.1 Experiment Consistency Tests

A series of experimental runs are conducted to investigate the stability and consistency of the experimental results. The first runs are conducted with regard to hydraulic heads distribution in the sand tank, and results are compared to the analytical solution derived in Chapter 3.

Figure 4.3 and Figure 4.4 show the comparison of the experimental results with the analytical results regarding the hydraulic heads distribution for the unconfined case and confined case, respectively. These results demonstrate that the experimental and analytical results match each other fairly well.

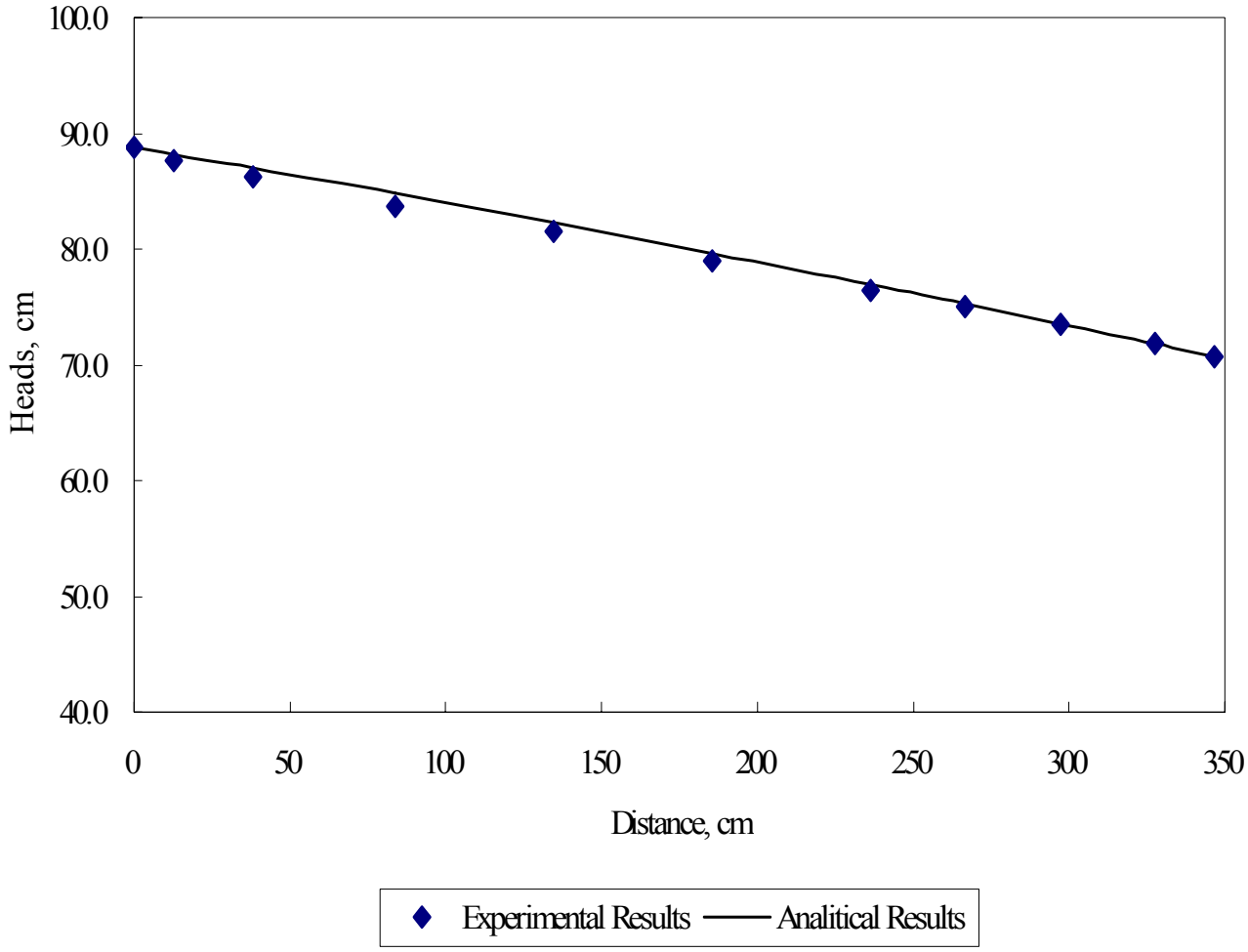

Figure 4.3 Experimental Results in Unconfined Situation-Hydraulic Heads.

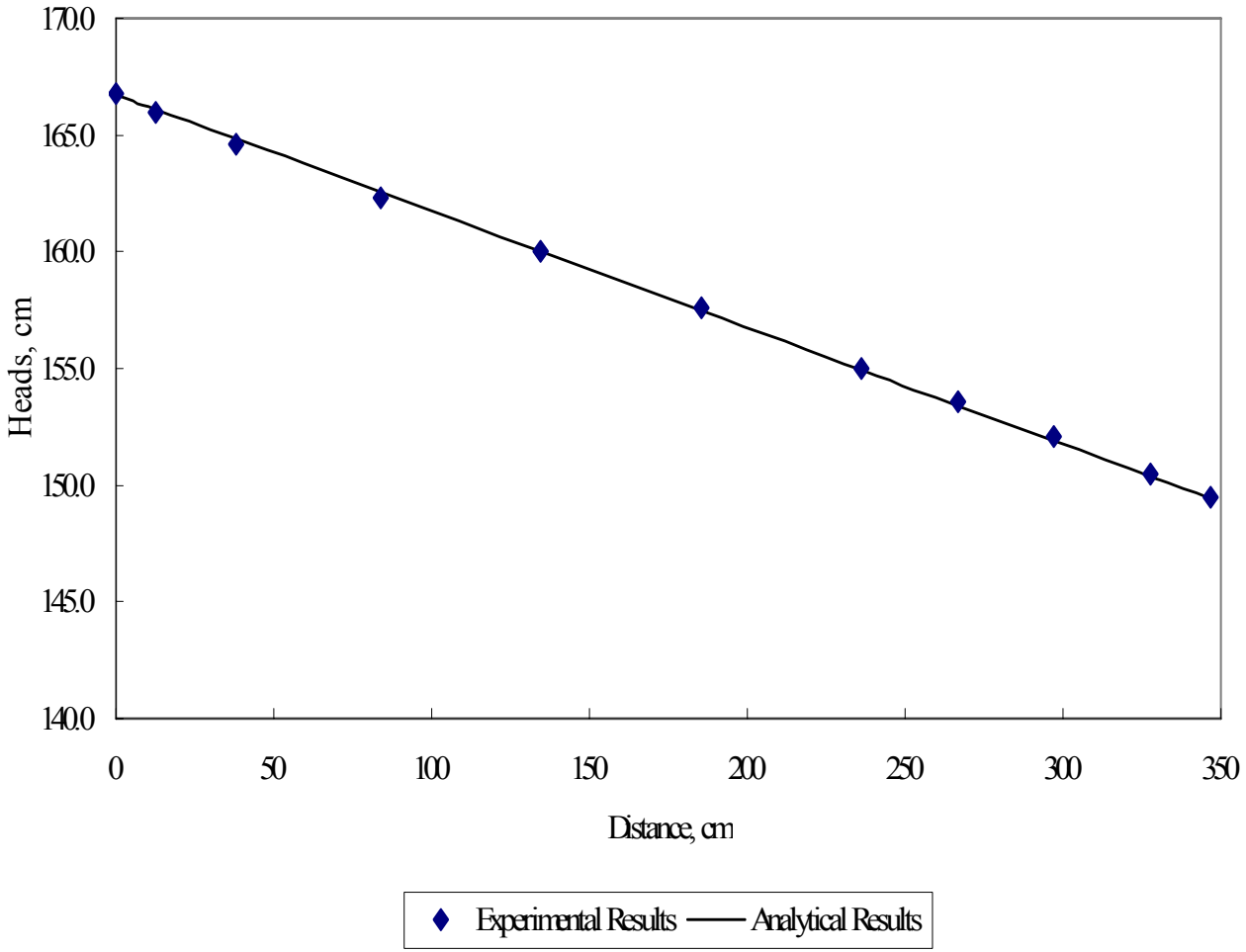

Figure 4.4 Experimental Results in Confined Situation-Hydraulic Heads.

Next, the experimental runs investigating contaminant concentration distribution are carried out under two conditions: one, the baseline without tides but dilution at the effluent boundary, and the second, the case with both tides and dilution. The corresponding case numbers are B16X and T16 (refer to Table 4.2 on page 88 for details of the experimental parameters used). Under each condition, three experiment runs are conducted, and both contaminant distribution and discharge are quantified and compared.

From Figure 4.5 it is observed that under identical conditions (case B16X), the contaminant concentration distribution stays reasonably close together, with an acceptable fluctuation error negligible compared to the concentration distribution itself. Figure 4.6 further gives the contaminant discharge profiles under the same condition for all three runs, and the profile is shown with the error bar represented by one standard deviation. The fluctuation error in the discharge, quantified by the standard deviation, is between 1% and 3% and has an average of 2.1%. If this error is compared with the tidal influence identified in later sections of the magnitude of over 30%, the experimental errors are negligible.

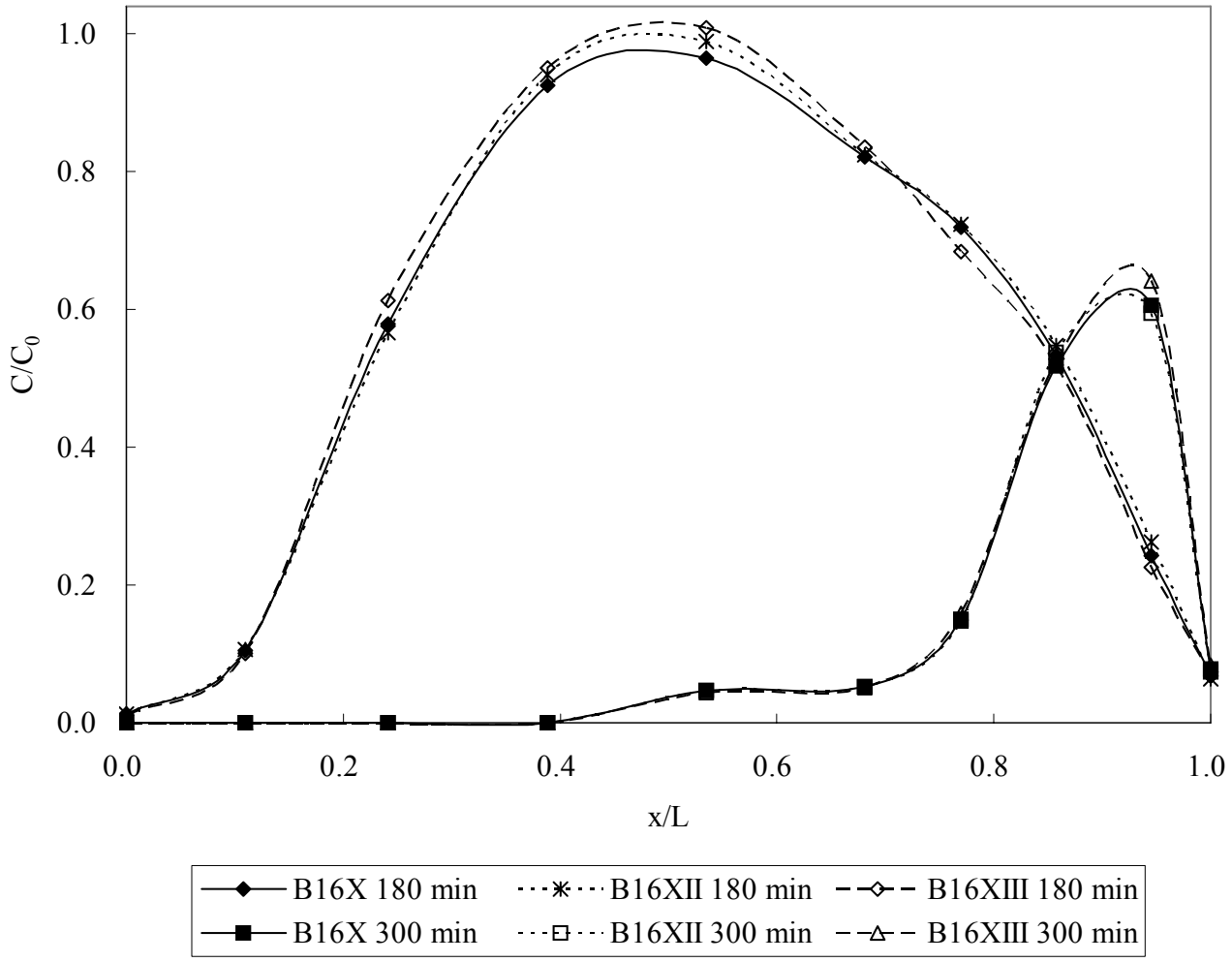

Figure 4.5 Experimental Repeating Tests for Case B16X.

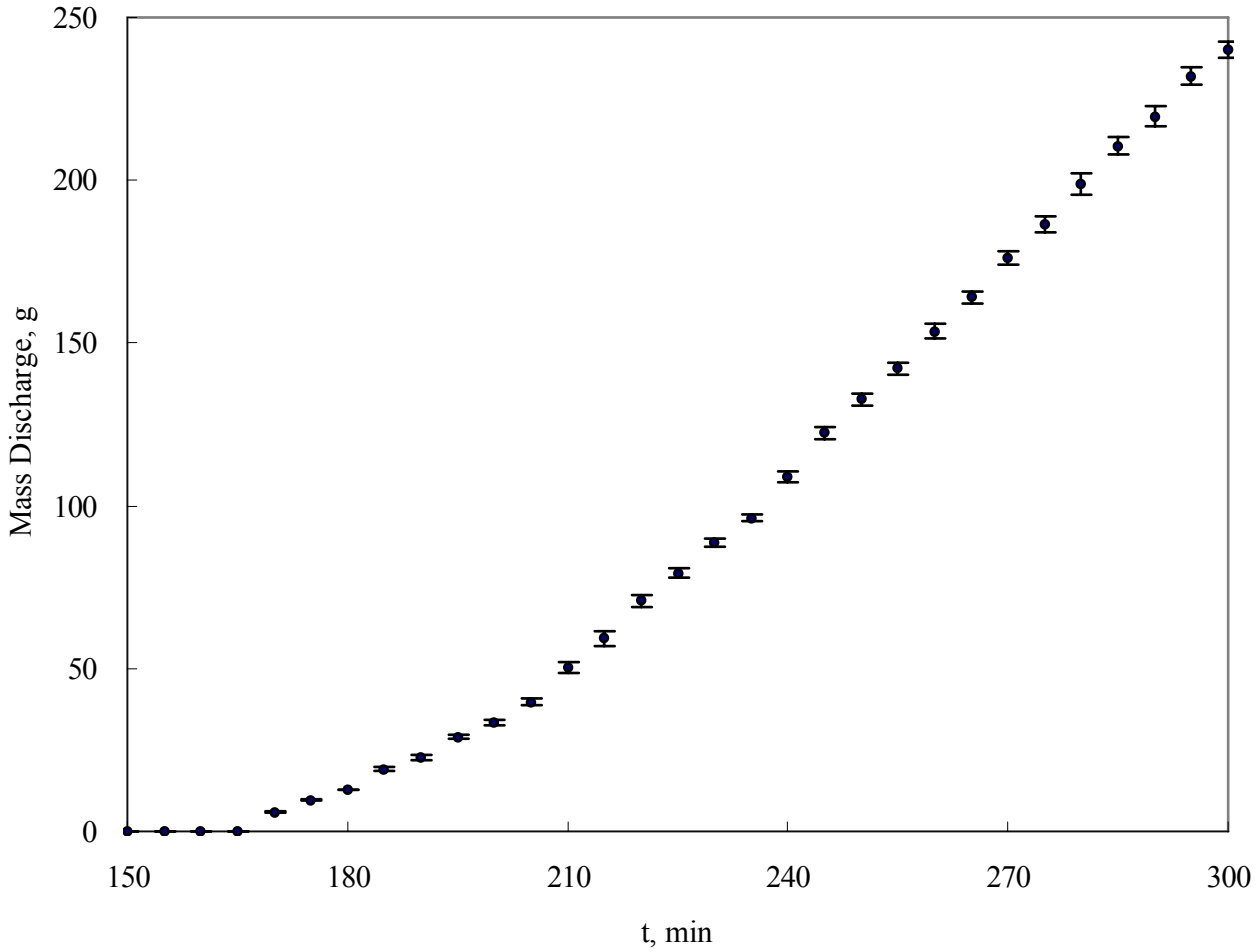

Figure 4.6 Experimental Repeating Tests for Case B16X (mean and standard deviation).

Figure 4.7 and Figure 4.8 demonstrate that the experimental errors resulting in case T16 are similarly negligible, with a magnitude of 1.75% average in the discharge variation.

These results regarding both hydraulic heads and contaminant distribution prove that the experiments are accurate at an acceptable level, and thus can be used to correctly quantify the contaminant concentration distribution and discharge.

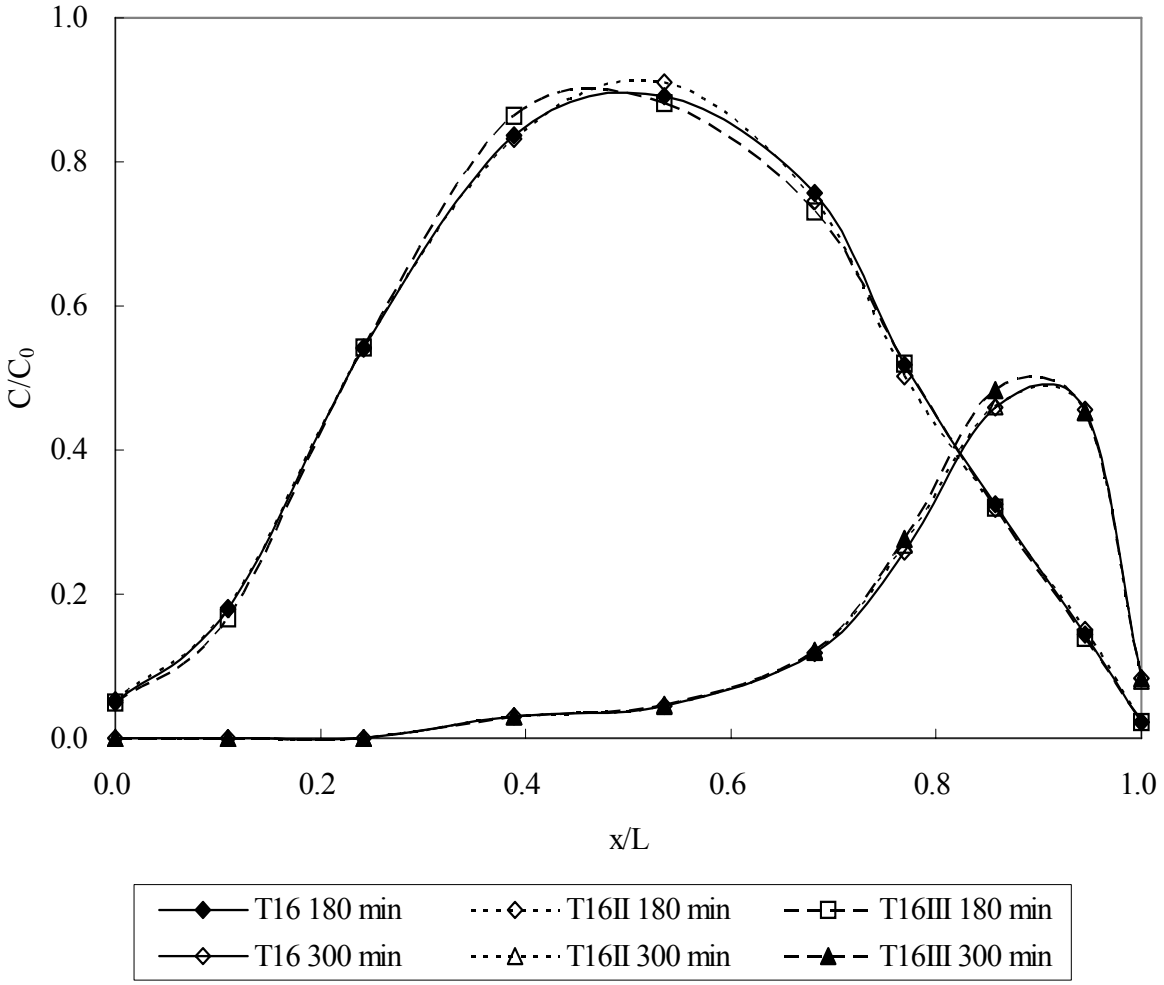

Figure 4.7 Experimental Repeating Tests for Case T16.

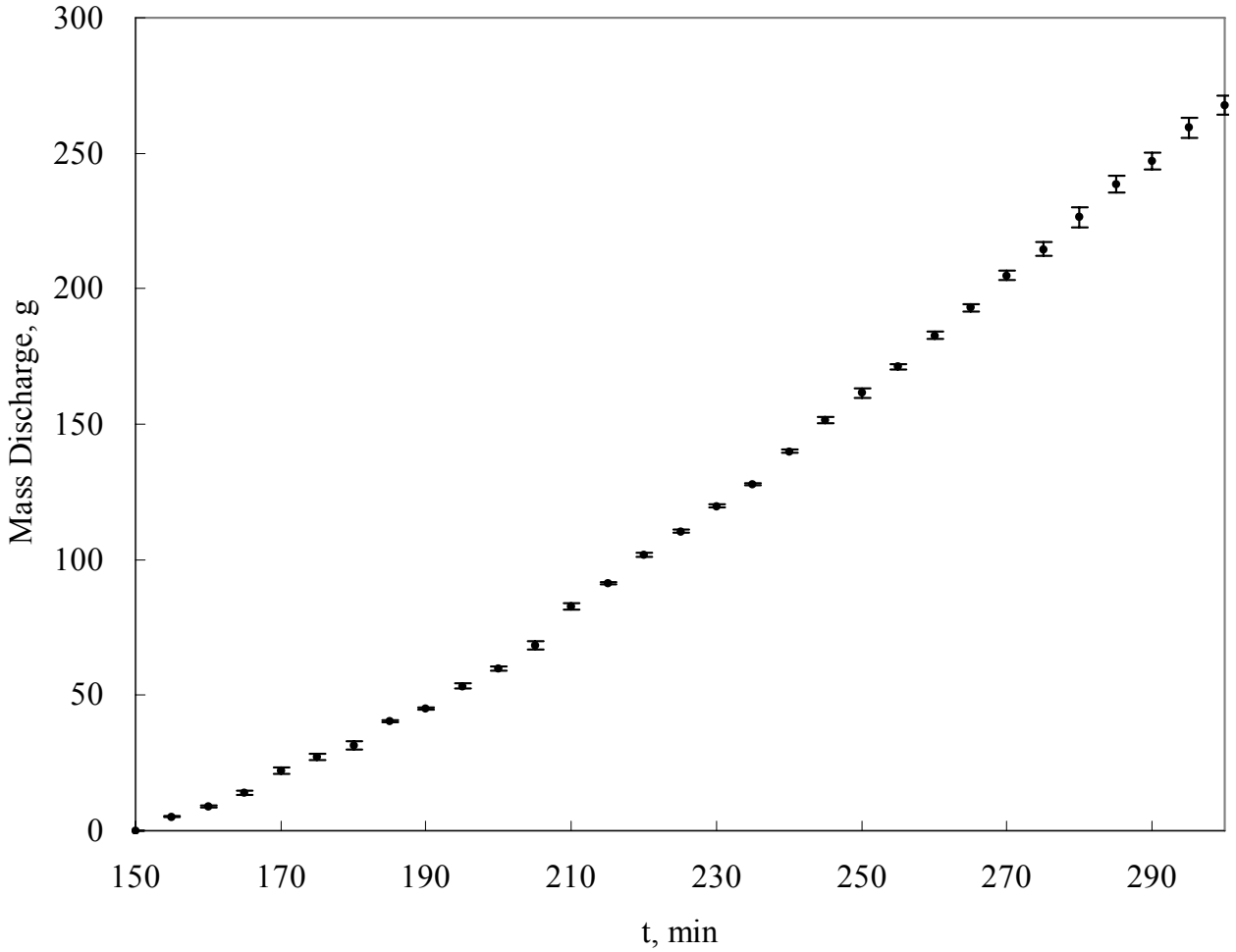

Figure 4.8 Experimental Repeating Tests for Case T16 (mean and standard deviation).

To demonstrate that the experimental study is reasonably accurate, experimental results are also compared with the numerical results. The numerical model is first calibrated based on the base case, B20X, subject to no tides, and the numerical model is then used to predict contaminant transport under other conditions (refer to Table 4.2 and Table 4.3 on page 88 for the parameters used for these cases).

The detailed procedures used to derive the numerical results are listed as follows:

- The base case (the case subject to no tides) is used for the calibration of the numerical model with measured values assigned to parameters which can be accurately measured in the experiment. These parameters include porous medium geometry, hydraulic conductivity, hydraulic gradient, etc.;

- The parameters which are not quantified in the experiment, including aquifer storativity, dispersivity, and retardation factor, are adjusted subsequently in the numerical model such that the numerical results with regard to the base case are matched with the experimental results;

- The adjusted parameter values are then used in the numerical model to generate results for the case subject to tidal fluctuations.

- These results are then compared to the experimental results in order to verify that both the numerical and experimental simulations are consistent and stable.

Table 4.4 gives the values used for calibrating the numerical model. Figure 4.9 and Figure 4.10 gives the calibrated results based on case B20X.

Table 4.4 Calibration of the Numerical Model Based on Case B20X

Parameters	Measured Value	Calibrated Value
Aquifer Length, cm	346.71	NA
Aquifer Thickness, cm	91.4	NA
Hydraulic Gradient	0.05	NA
Hydraulic Conductivity, cm/min	17.20	NA
Porosity	0.45	NA
Retardation Factor	NA	1.3
Dispersivity, cm	NA	7.5
Storativity	NA	0.005

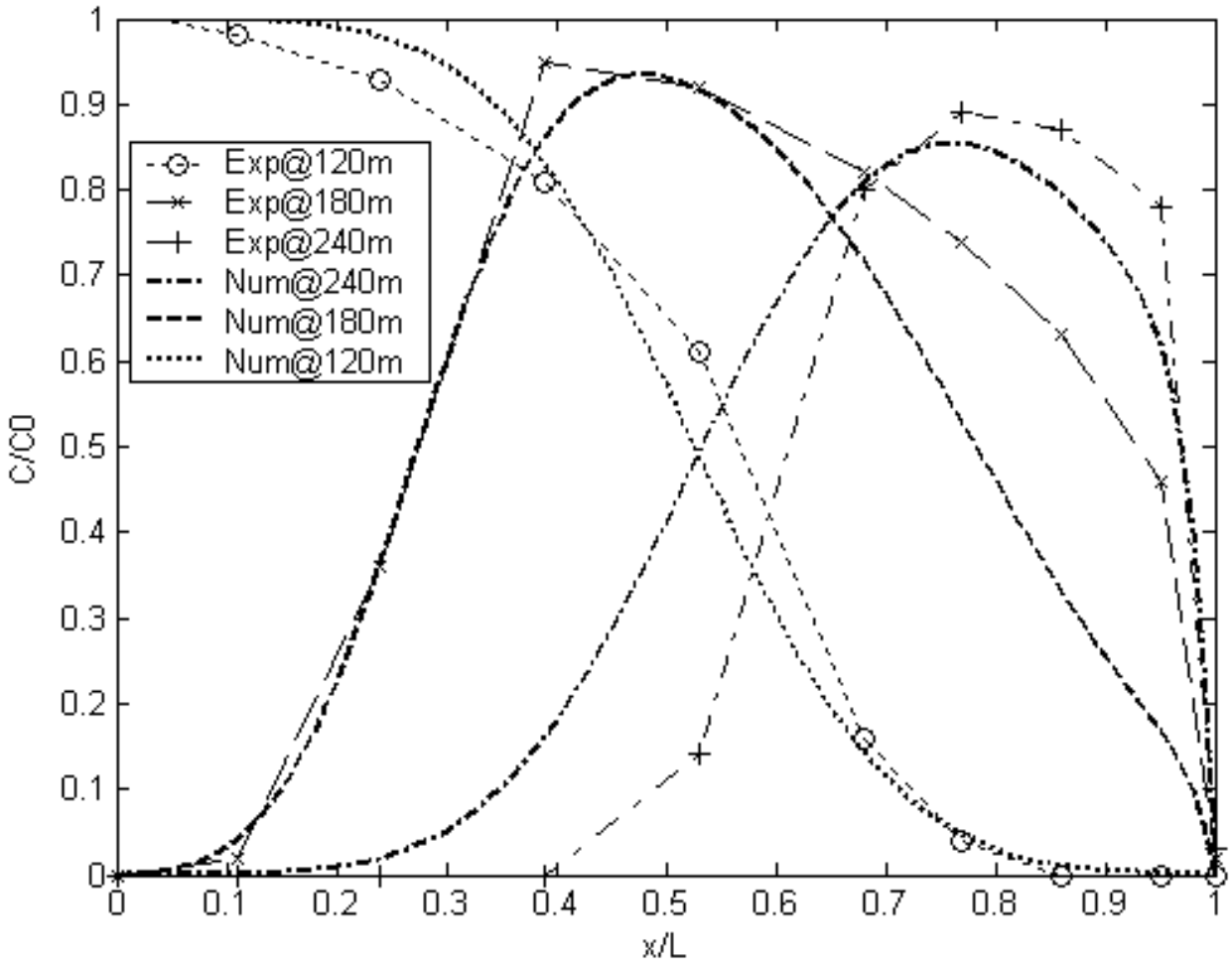

Figure 4.9 Calibration of Numerical Model Based on Case B20X.

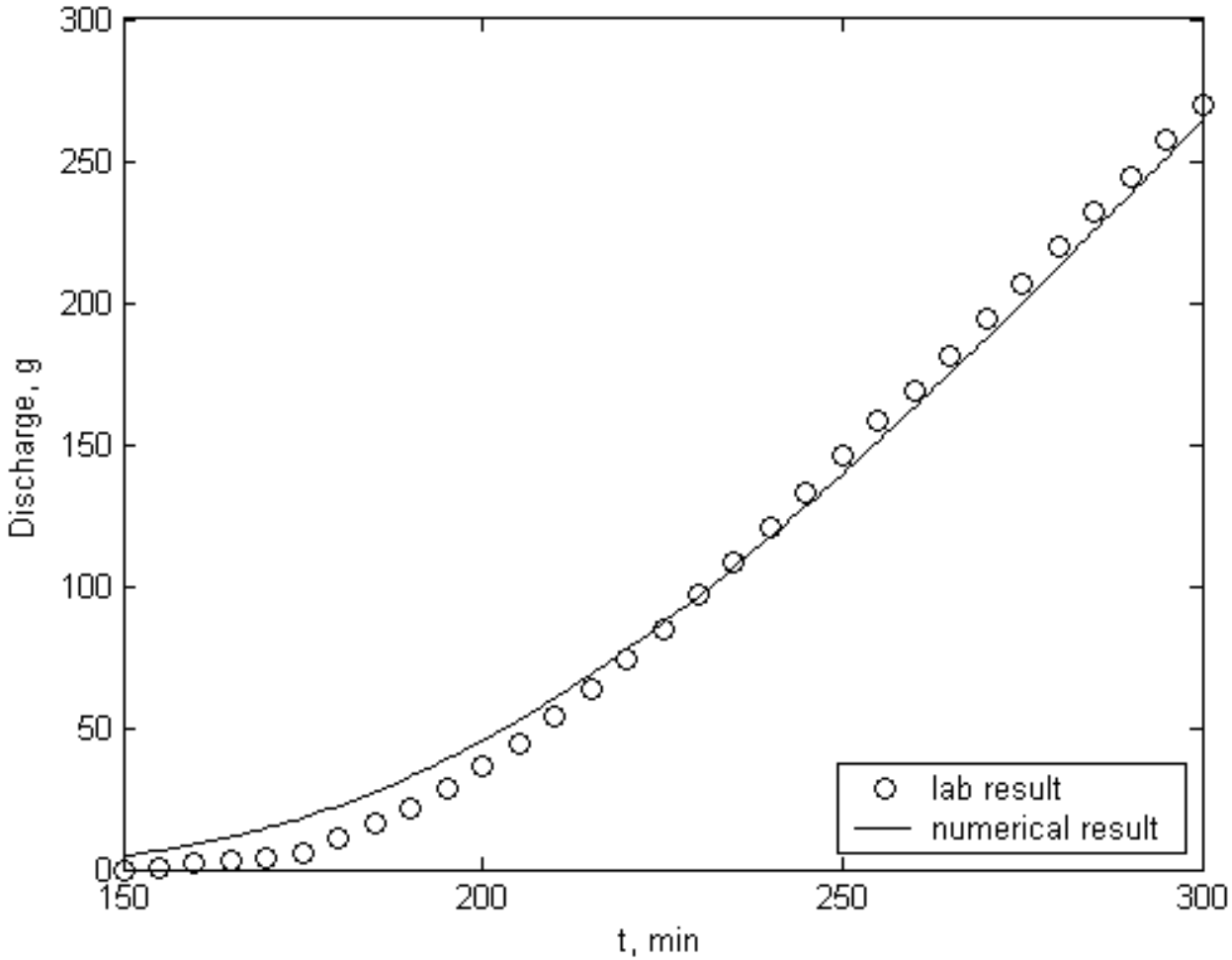

Figure 4.10 Calibration of Numerical Model Based on Case B20X.

Figure 4.11, Figure 4.12 and Figure 4.13 give the numerical results for case T20, case CON2, and case CON1, respectively, using the calibrated numerical model and compare the numerical results with the experimental results under the same conditions.

The cases discussed above are based on a hydraulic gradient of 0.05. A relatively larger hydraulic gradient of 0.1 is considered next with all of the other parameters (except the dilution factor) considered the same as used before. Figure 4.14 first compares the numerical results with the experiment for case T19 with a tidal period of 5 minutes. The comparison demonstrates the good match between the numerical and experimental results under these conditions.

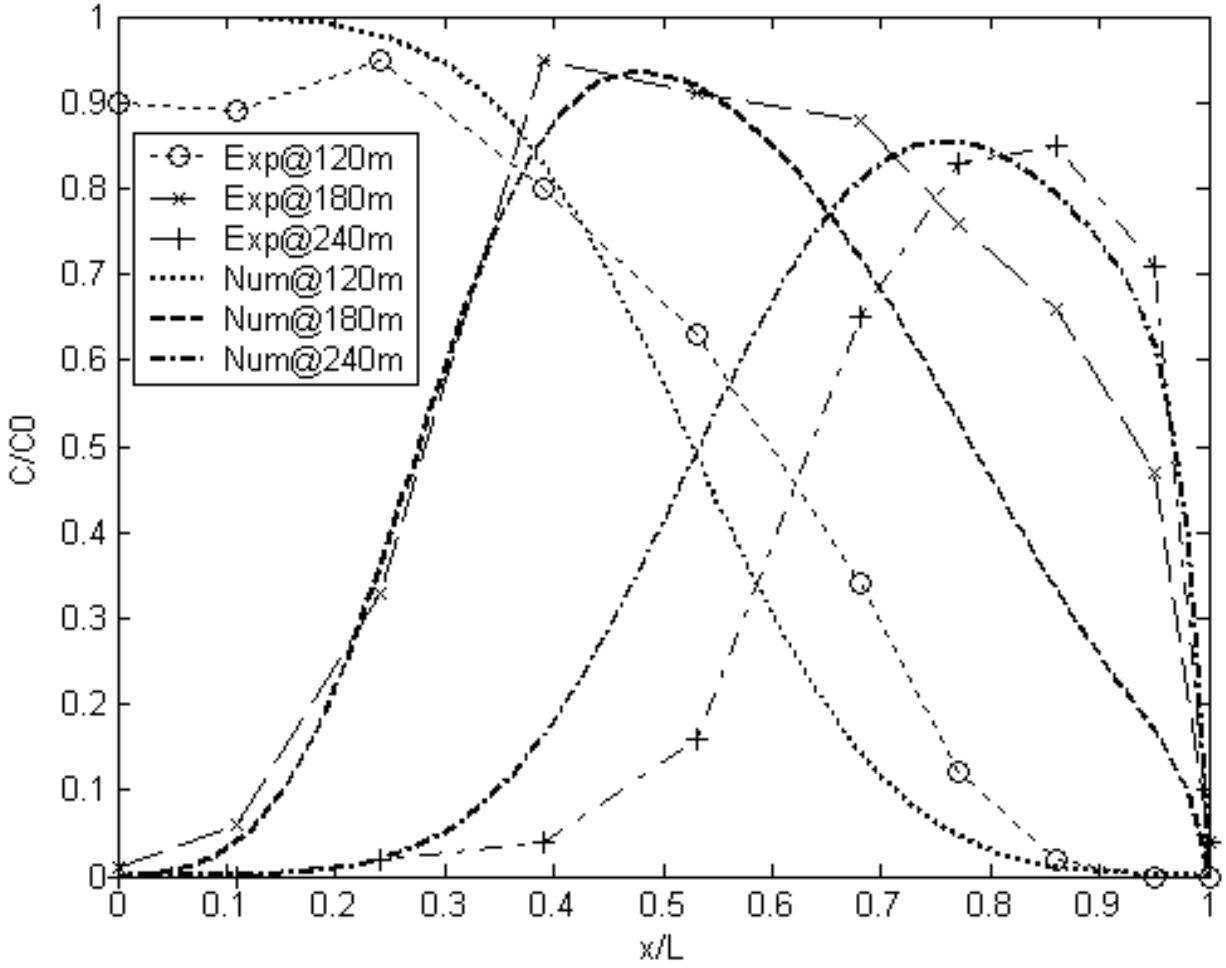

Figure 4.11 Comparison of Experimental and Numerical Results for Case T20.

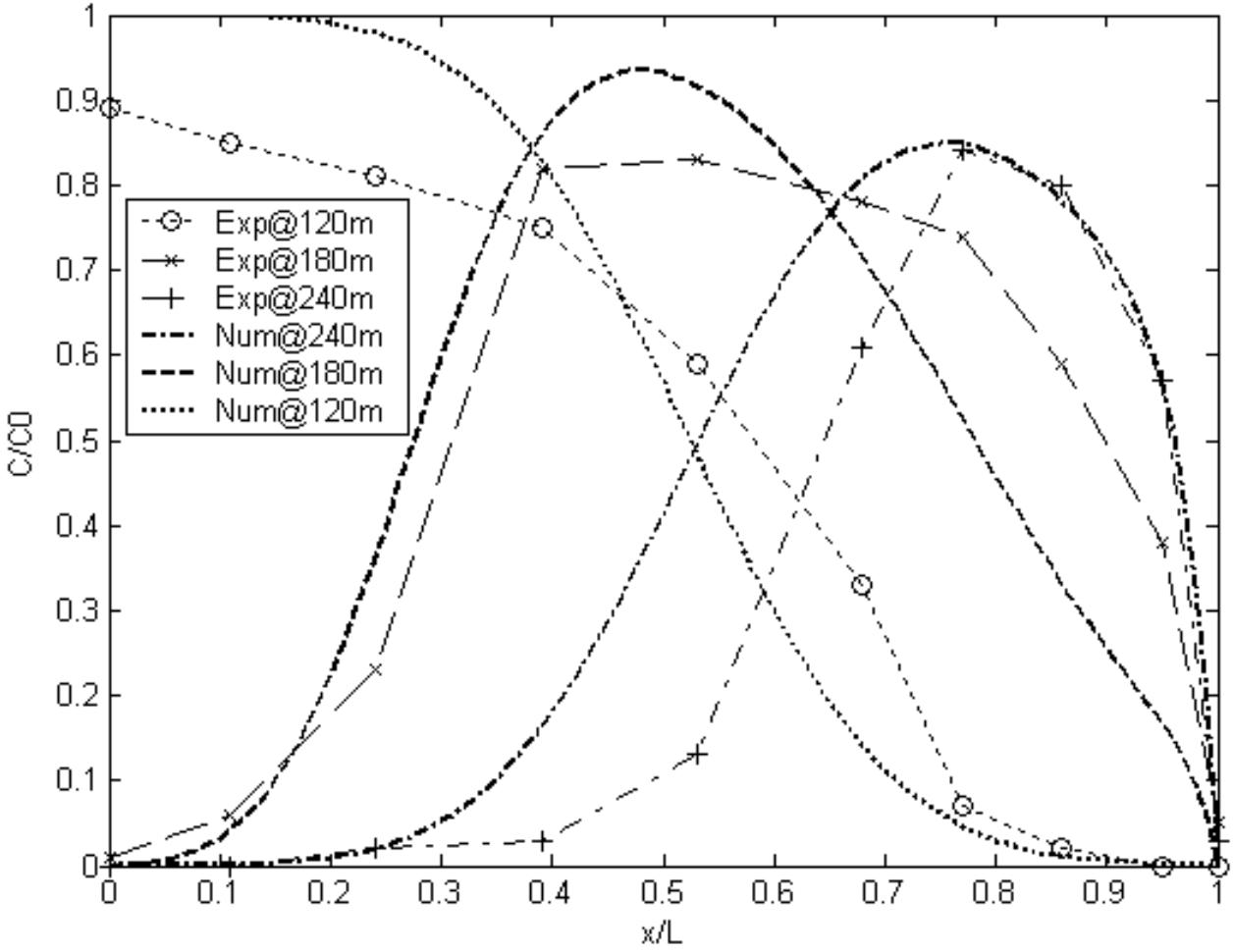

Figure 4.12 Comparison of Experimental and Numerical Results for Case CON2.

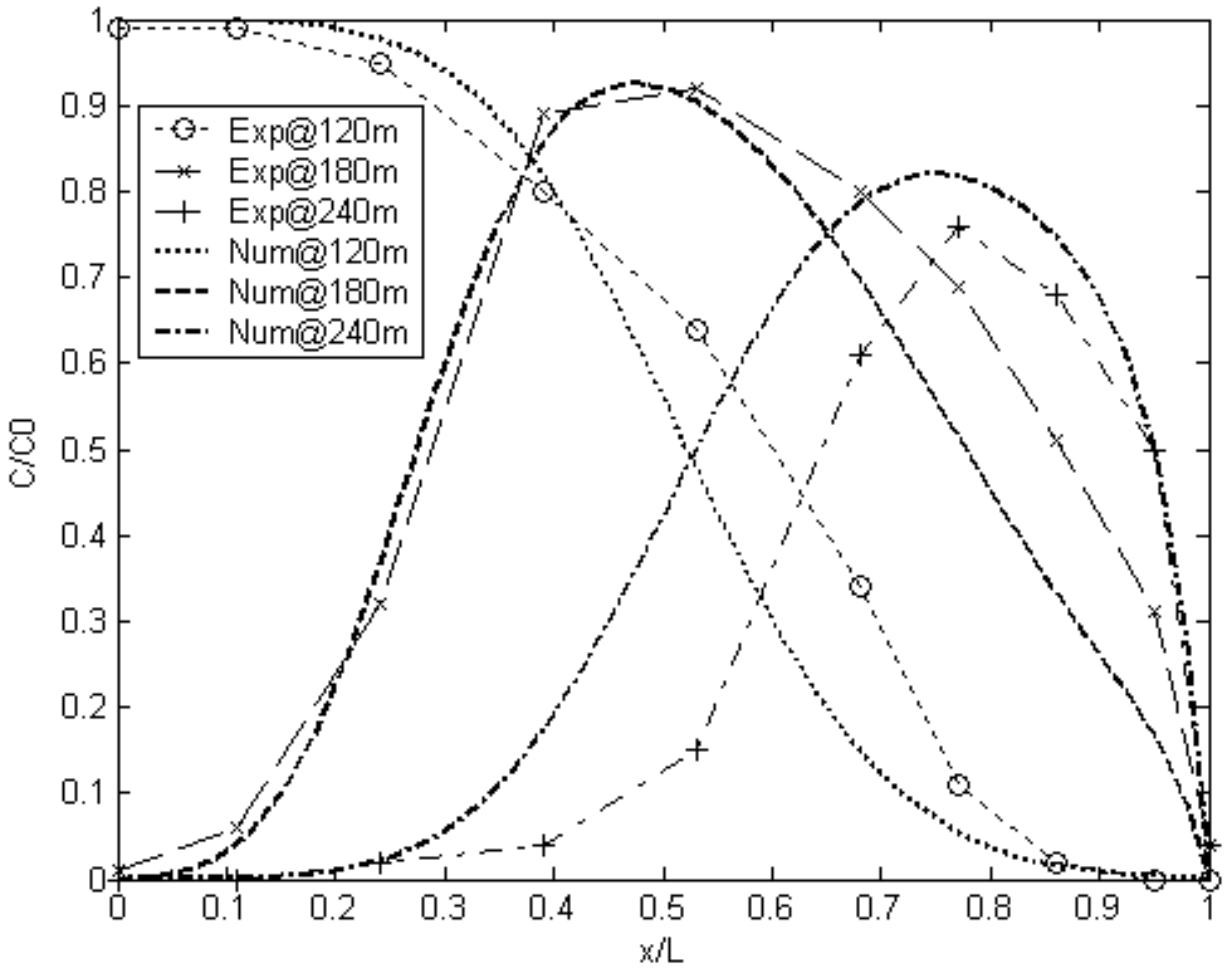

Figure 4.13 Comparison of Experimental and Numerical Results for Case CON1.

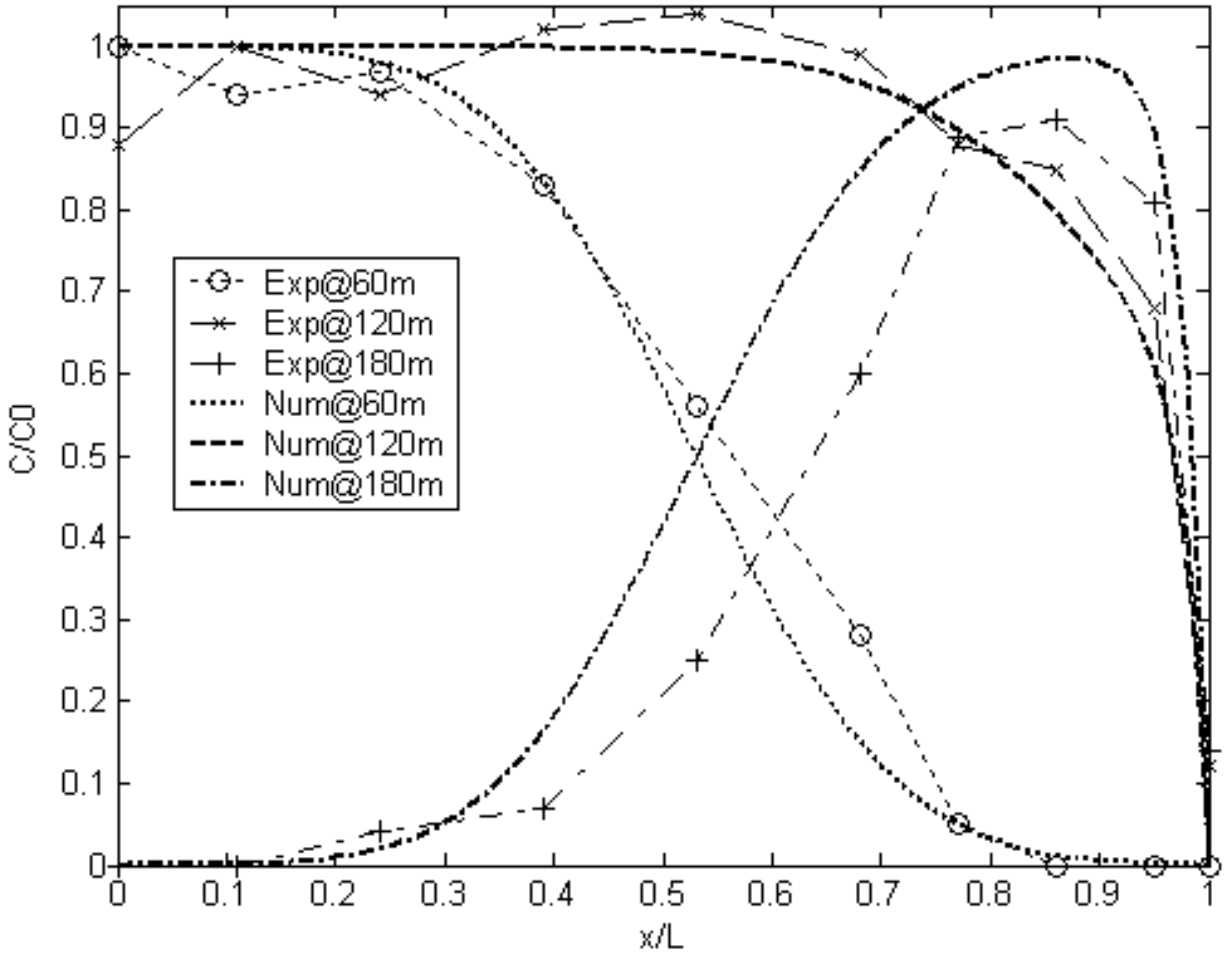

Figure 4.14 Comparison of Experimental and Numerical Results for Case T19.

Figure 4.15 and Figure 4.16 further give the numerical results for case CON4 and case CON3 with a tidal period of one minute using the calibrated numerical model and compare the numerical results with the experimental results under the same conditions. The observed differences in cases CON3 and CON4 at a time of 180 minutes are due to larger uncertainties in the experiment with larger tidal amplitude and a smaller tidal period.

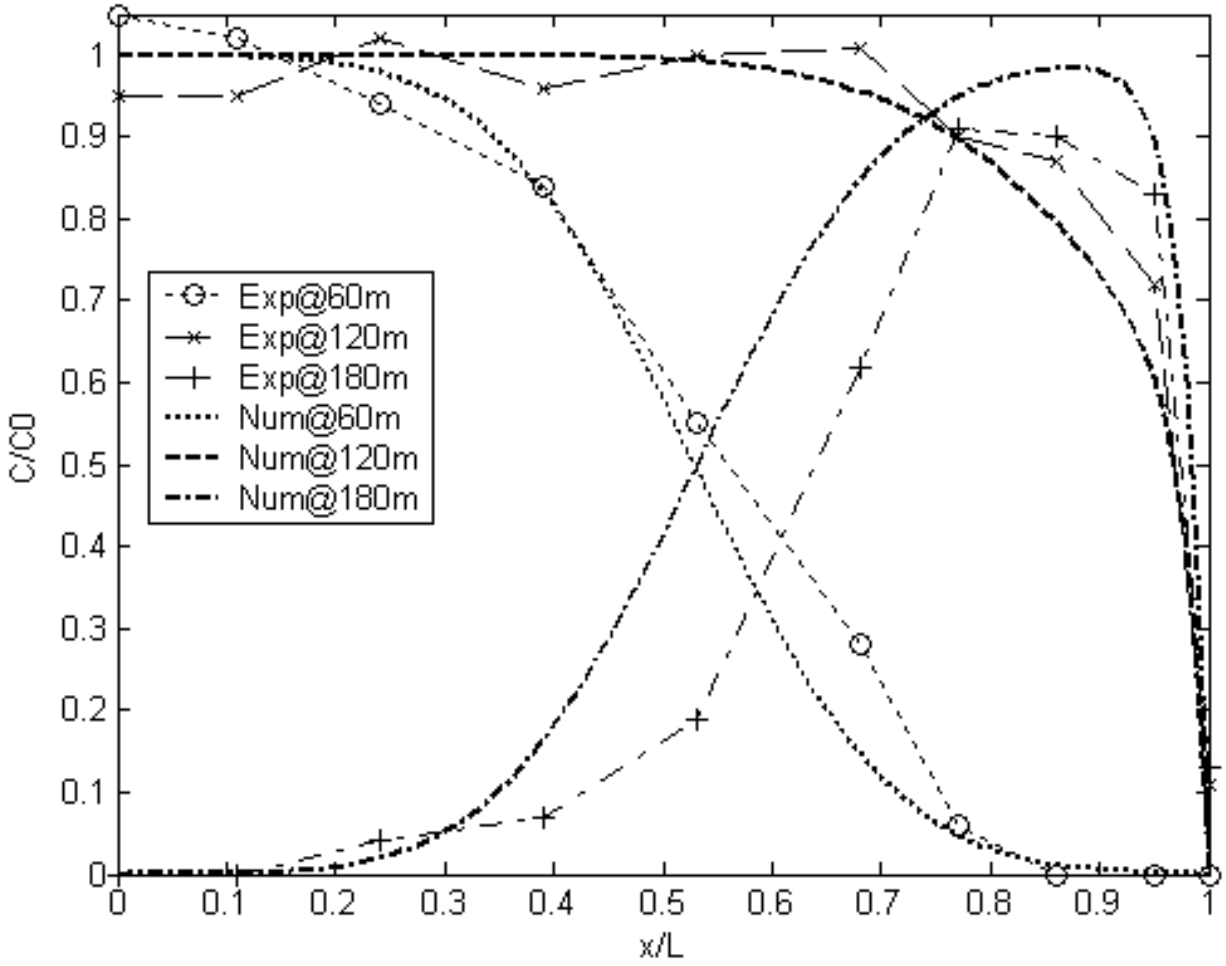

Figure 4.15 Comparison of Experimental and Numerical Results for Case CON4.

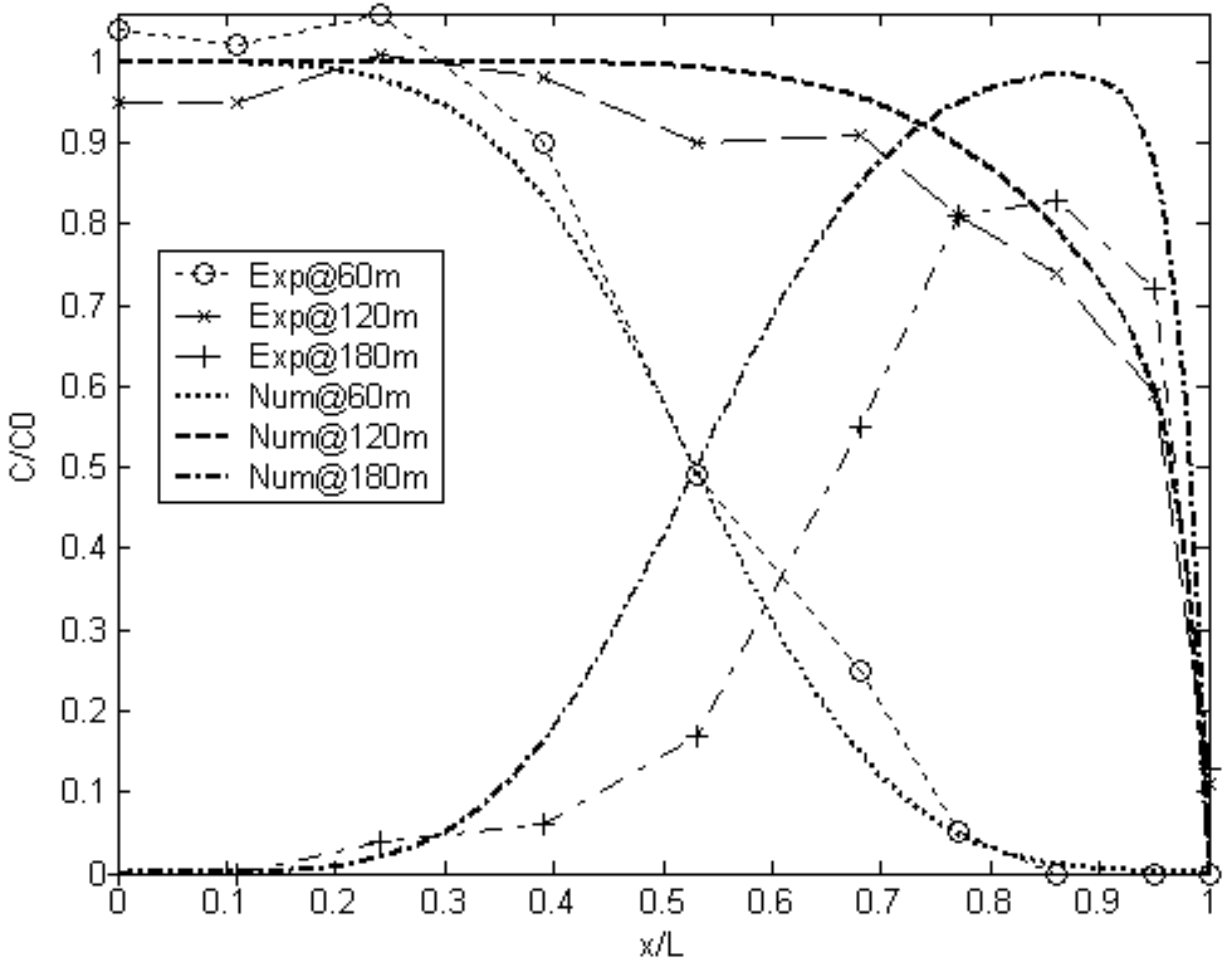

Figure 4.16 Comparison of Experimental and Numerical Results for Case CON3.

The profiles of the numerical and experimental results are illustrated in Figure 4.11 through Figure 4.16. Table 4.5 also gives the correlations between the numerical and experimental results (correlation coefficient = $\frac{\frac{1}{n}\sum_{i}^{n}(x_i-\bar{x})(y_i-\bar{y})}{\sigma_x\sigma_y}$). The comparison demonstrates the good match between the experimental and numerical results, with minor exceptions under some of the conditions. The deviation can be attributable to the larger uncertainties in the experiment with larger tidal amplitude and smaller tidal period, under which conditions experimental operations become more difficult. Despite the discrepancy in the discharge profiles, the experimental and numerical results are deemed to be reasonably consistent and stable. As a result, the experiment is believed to be valid to the extent that it generates stable results which are also consistent with the numerical simulations.

Table 4.5 Correlation Coefficient for Experimental and Numerical Results

Case #		T20	CON2	CON1	T19	CON4	CON3
Correlation Coefficient	At 120min or 60min	0.978	0.978	0.984	0.996	0.994	0.997
	At 180min or 120min	0.932	0.964	0.976	0.981	0.979	0.992
	At 240min or 180min	0.947	0.966	0.956	0.982	0.972	0.957

4.2.2 Experimental Study of Boundary Conditions

As mentioned earlier in Chapter 3, the first-type boundary condition is more appropriate for the coast boundary problem considered in this study. It was also demonstrated in that chapter that the second-type boundary condition is characterized by increasing contaminant concentration, with the contaminant accumulating in the boundary water to a high concentration. In contrast, the first-type boundary condition is characterized by the

opposite, i.e., the contaminant concentration in the boundary water remains very low, and thus can be specified as a small constant, generally zero.

In addition, the coastal boundary condition considered in this study has the characteristics of a large volume and well- and quick-mixing. As a result, as long as the contaminant reaches the coastal water, it would not accumulate to a significantly high concentration, and instead would be diluted immediately and remain at a very low concentration.

In the experiment, the boundary condition is studied in order to verify the conclusion made in Chapter 3 regarding the boundary condition. In the effluent chamber of the sand tank, a water supply pipe is used to supply a large volume of water in order to obtain a similar effect as in the coastal water (see Figure 4.17). As shown in Figure 4.17, the original groundwater water discharge into the discharge chamber through the sand medium is Q_1. Water supply of rate Q_2 through the water supply pipe is used to dilute the contaminant in the chamber just as the coastal water would dilute groundwater discharged into the coast. The total water discharge of Q_{1+2} is drained through the water discharge pipe. A dilution factor is defined to measure the degree of dilution in the chamber as

$$\text{dilution factor (DF)} = \frac{Q_{1+2}}{Q_1} \tag{4.9}$$

Obviously, the larger the dilution factor, the greater the contaminant is diluted in the discharge chamber.

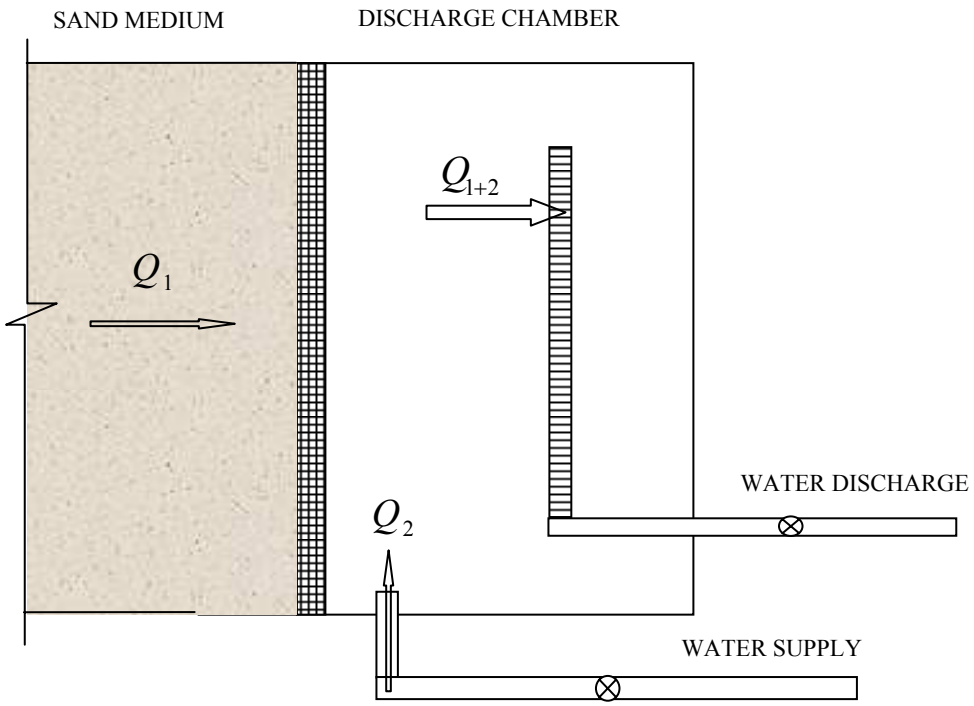

Figure 4.17 Dilution and Mixing in the Effluent Chamber Simulating Coastal Boundary Condition.

A series of experiments are conducted to see how the contaminant concentration behaves in the discharge chamber with different dilution factors. Figure 4.18 gives the concentration variation over time in the discharge chamber for the cases in the confined-condition experiment with a hydraulic gradient of 0.05 (Experimental results under other conditions lead to the same conclusions reached herein, so they are not included). It is also worth noting that this experiment is done without tidal fluctuations at the boundary. The graph suggests that a large dilution factor can cause the contaminant concentration in the discharge chamber to be significantly lower than the case without dilution. Obviously, the larger the dilution factor, the more dramatic is its impact on the contaminant concentration at the boundary. And, as the dilution factor increases to a certain level, the discharge contaminant concentration would be diluted to a significantly low level such

that it can be neglected. This is believed to resemble the case with the first-type boundary condition which specifies a constant contaminant concentration (commonly zero) at the boundary. On the other hand, in the cases without dilution, the contaminant concentration in the discharge chamber varies with time similarly as when the second-type boundary condition is specified, as discussed in Chapter 3. Again, coastal water is characterized by significant dilution and quick mixing, and consequently, it should be represented by the first-type, not the second-type, boundary condition.

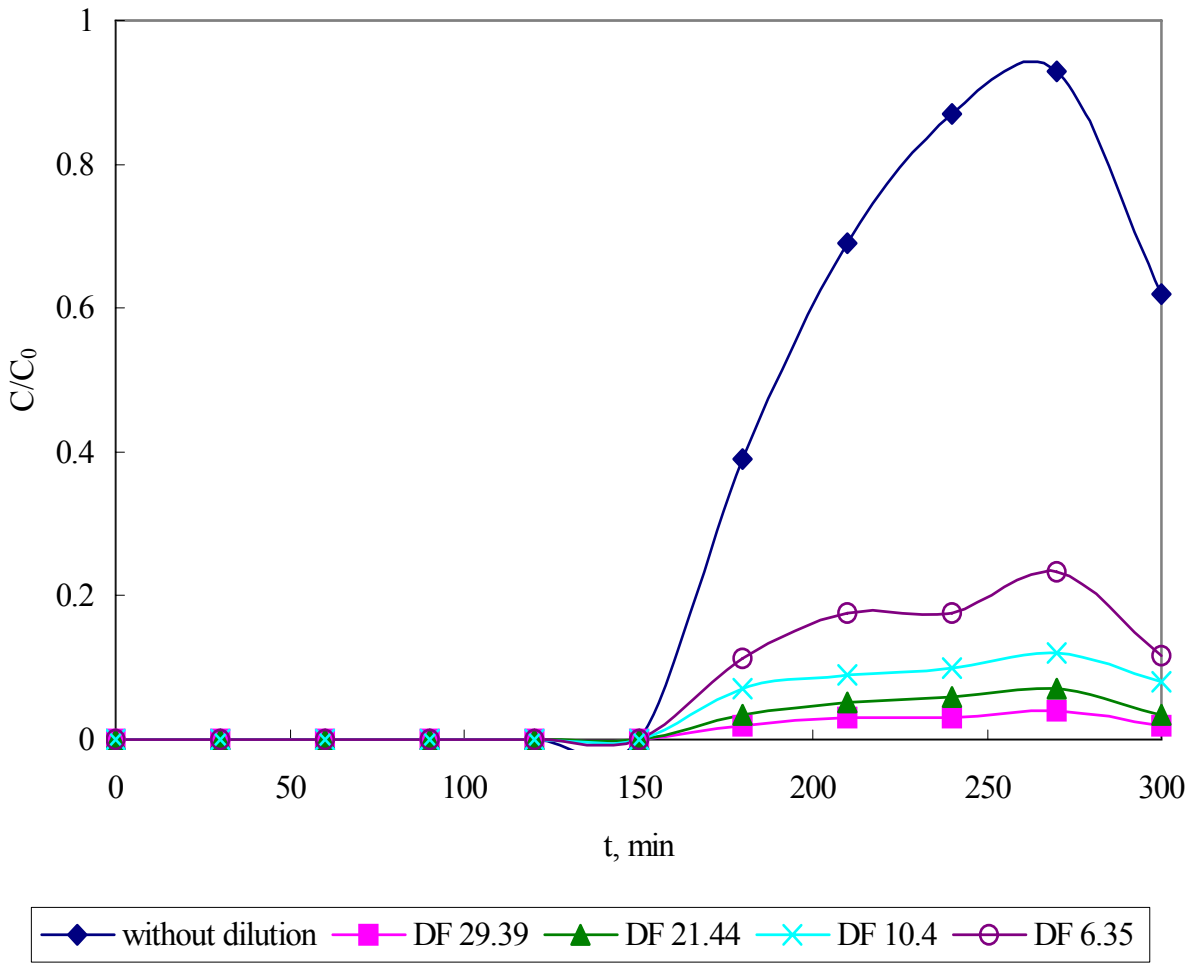

Figure 4.18 Contaminant Concentration Varies over Time in the Discharge Chamber Showing Lower Concentration Resulted from Dilution and Mixing.

In Chapter 3, it is also mentioned that the dilution and mixing at the coastal boundary would affect the contaminant concentration distribution in the area adjacent to the coastline and impact the discharge over time even without tidal activities. That leads to the conclusion that the first-type boundary condition is not only more appropriate for the case subject to tidal fluctuations, but also for the baseline selected.

Figure 4.19 shows an example of the experimental results in terms of contaminant concentration distribution compared for the cases with and without dilution. The results are consistent with the analytical analysis in Chapter 3 with regard to the trend by which the contaminant concentration is lowered near and at the boundary as a result of dilution. The dilution at the boundary would also cause a slight acceleration of contaminant discharge. The experimental results demonstrating the discharge acceleration are shown in Figure 4.20.

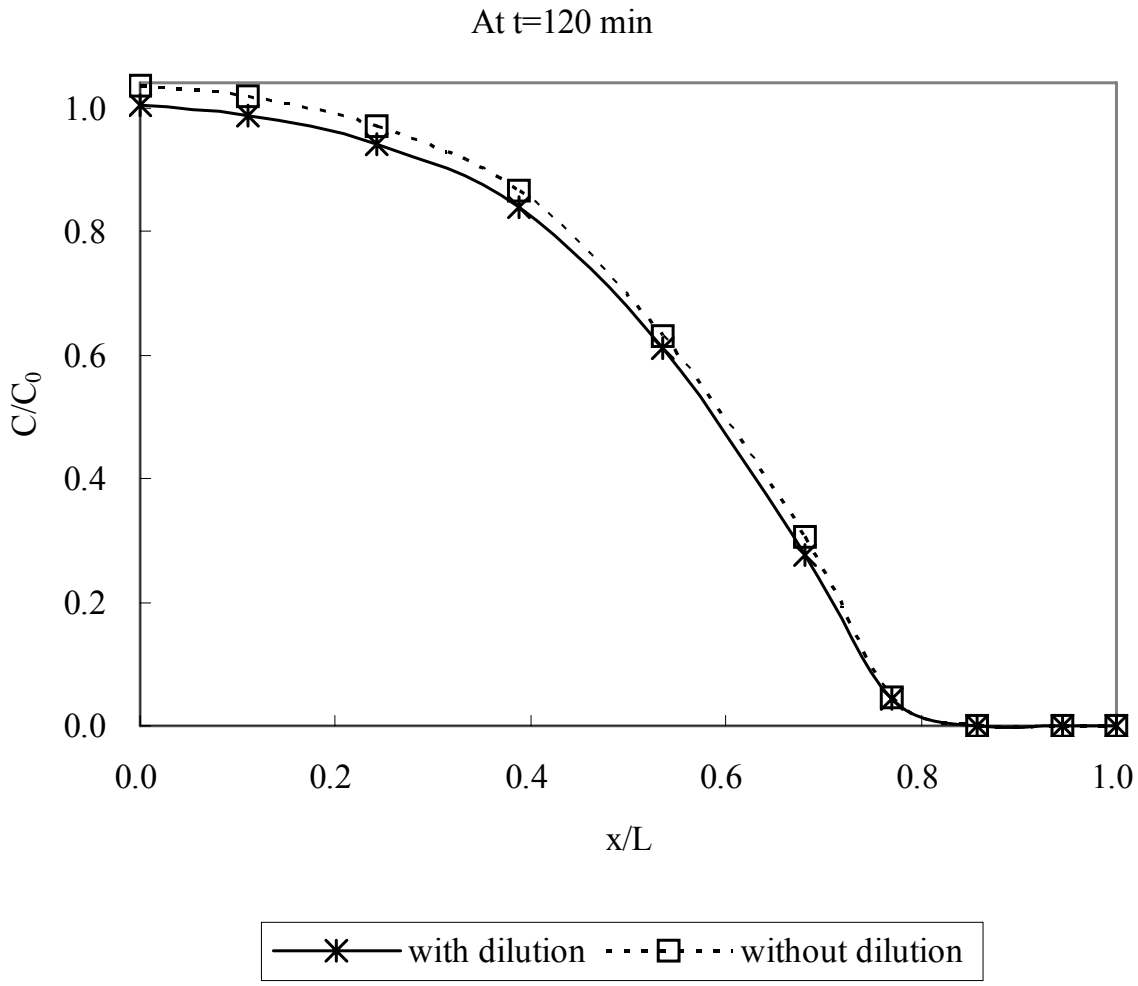

Figure 4.19 Contaminant Distribution subject to Dilution and Mixing (DF=29.39).

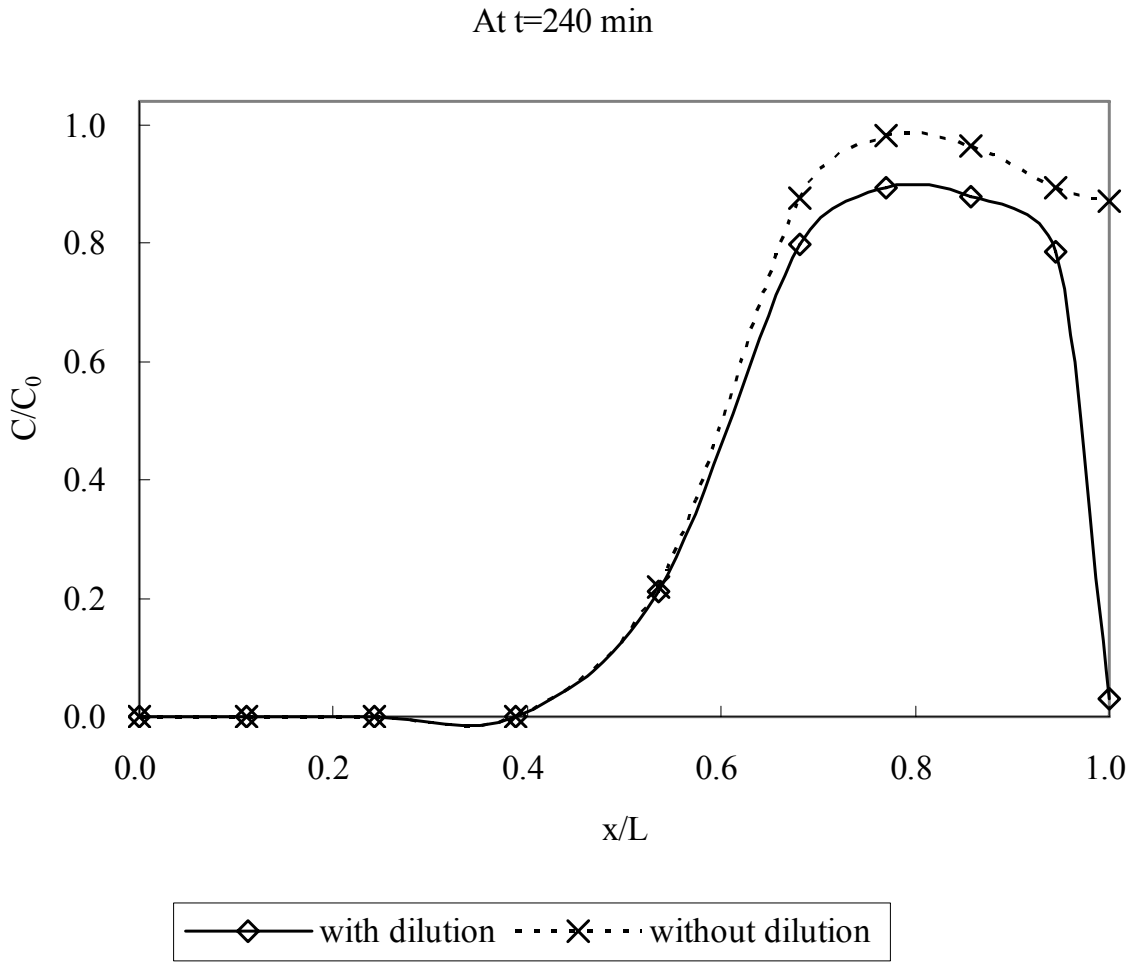

Figure 4.19 Contaminant Distribution subject to Dilution and Mixing (DF=29.39) (Continued).

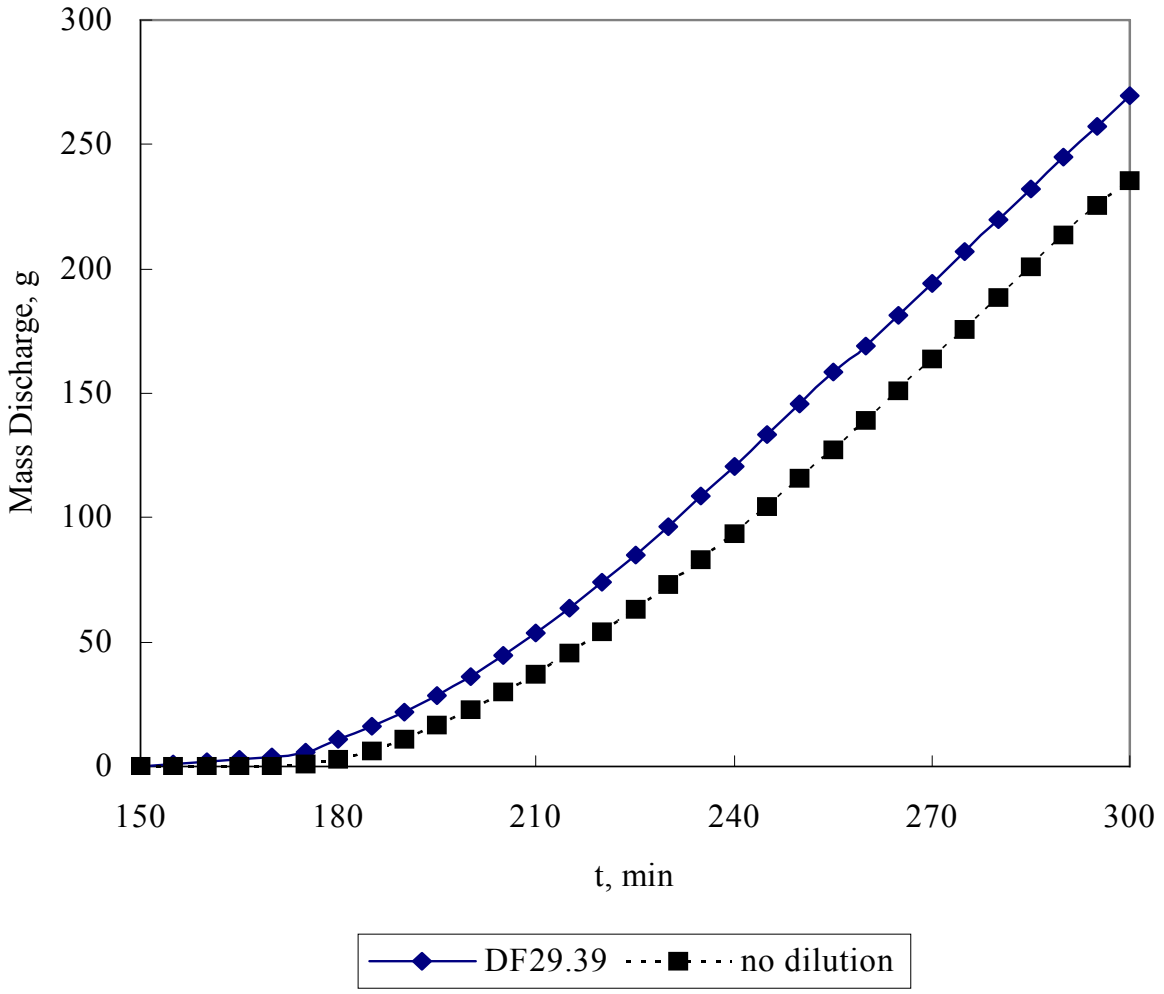

Figure 4.20 Contaminant Discharge Accelerated by Dilution and Mixing.

As discussed in the literature review, net groundwater discharge is only of small magnitude compared with the large volume of coastal water (Li et al., 1999). This can be represented by a large dilution factor, which can be of a range much larger than the dilution factors considered in the experiment. Consequently, contaminant concentration in coastal water should even be much less than the level indicated in the experiment, such that a zero-concentration approximation (first-type boundary condition) is reasonable for the coastal boundary.

4.2.3 Results of Unconfined-Condition Experiments

The unconfined-condition experiments are conducted to simulate the unconfined groundwater flow and contaminant transport subject to tidal fluctuations. A schematic representation of the experiment setup is illustrated in Figure 4.21.

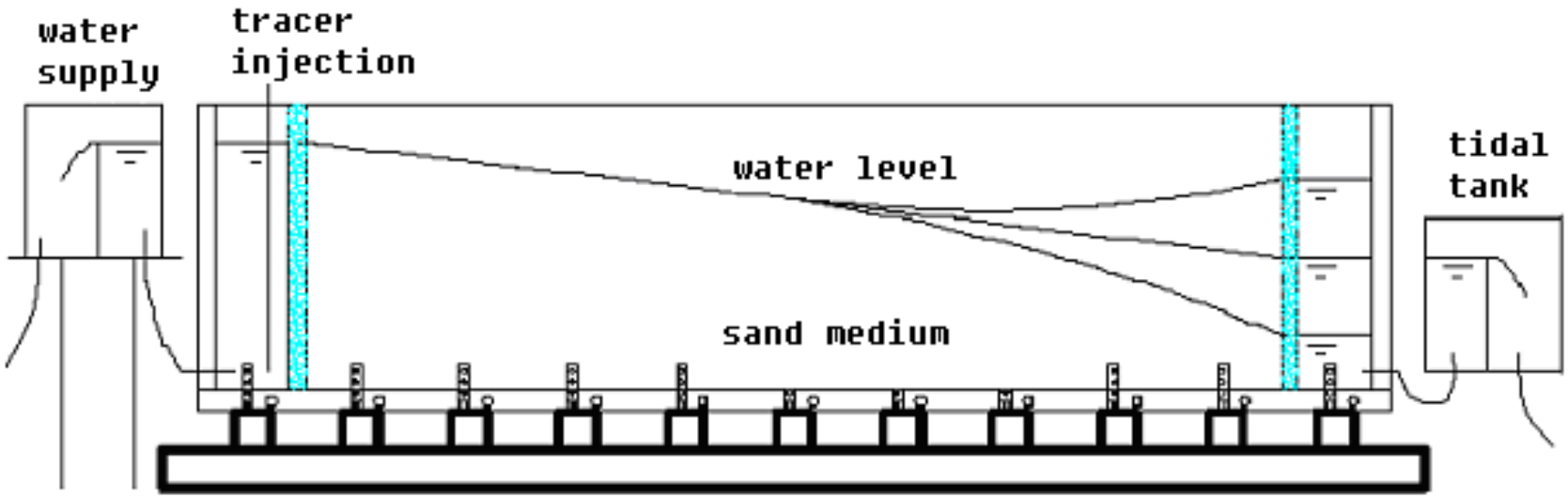

Figure 4.21 Unconfined-Condition Experiments.

Subject to experimental limitations, the hydraulic gradient, tidal amplitude, and dilution factor are subject to the constraint of each other. As a result, the parameter values for these experiments and the case numbers assigned to them are listed in Table 4.2 (page 88). Case B16/18 is the baseline case without tides and dilution, simulating the second-type boundary condition and is a comparison with the baseline used by this study to study the tidal effect. Case B16X is the baseline chosen by this study simulating the first-type boundary condition. The first set of experiments is conducted with a tidal period of 5 minutes and tidal amplitudes of 20 cm (Case T16) and 10 cm (Case T18). The concentration distributions at different times for these two cases, compared to baseline Case B16X, are illustrated in Figure 4.22 and Figure 4.23, respectively.

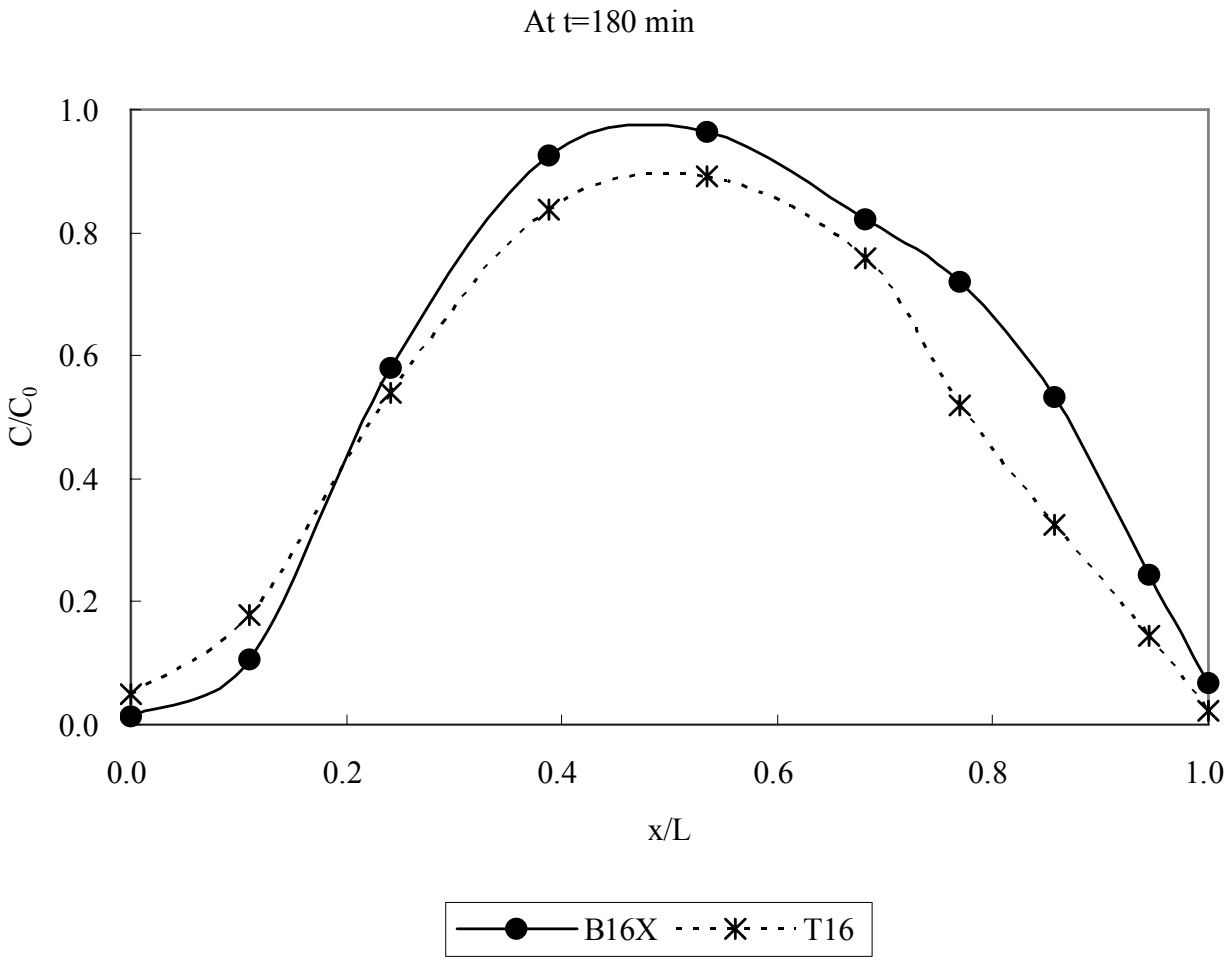

Figure 4.22 Contaminant Distribution for Case T16.

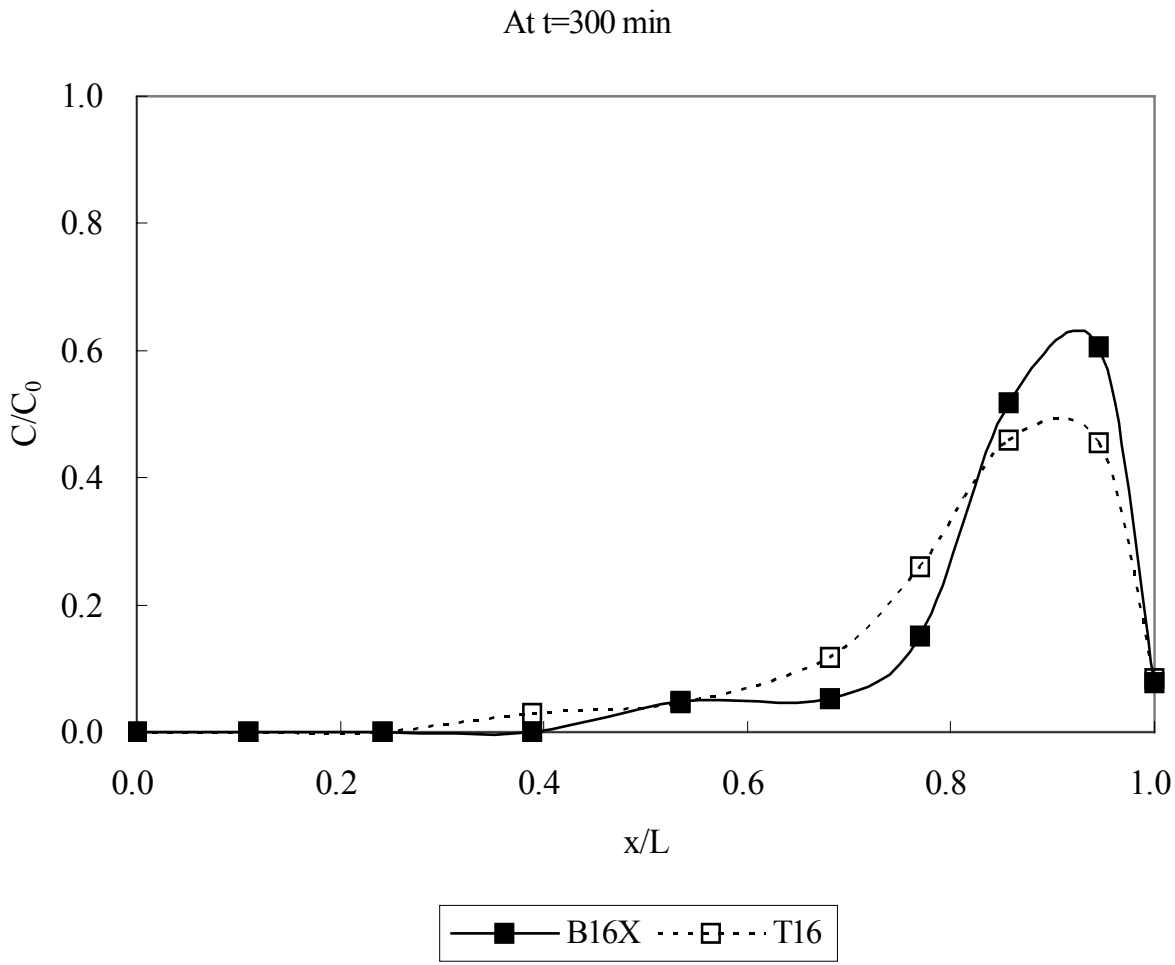

Figure 4.22 Contaminant Distribution for Case T16 (Continued).

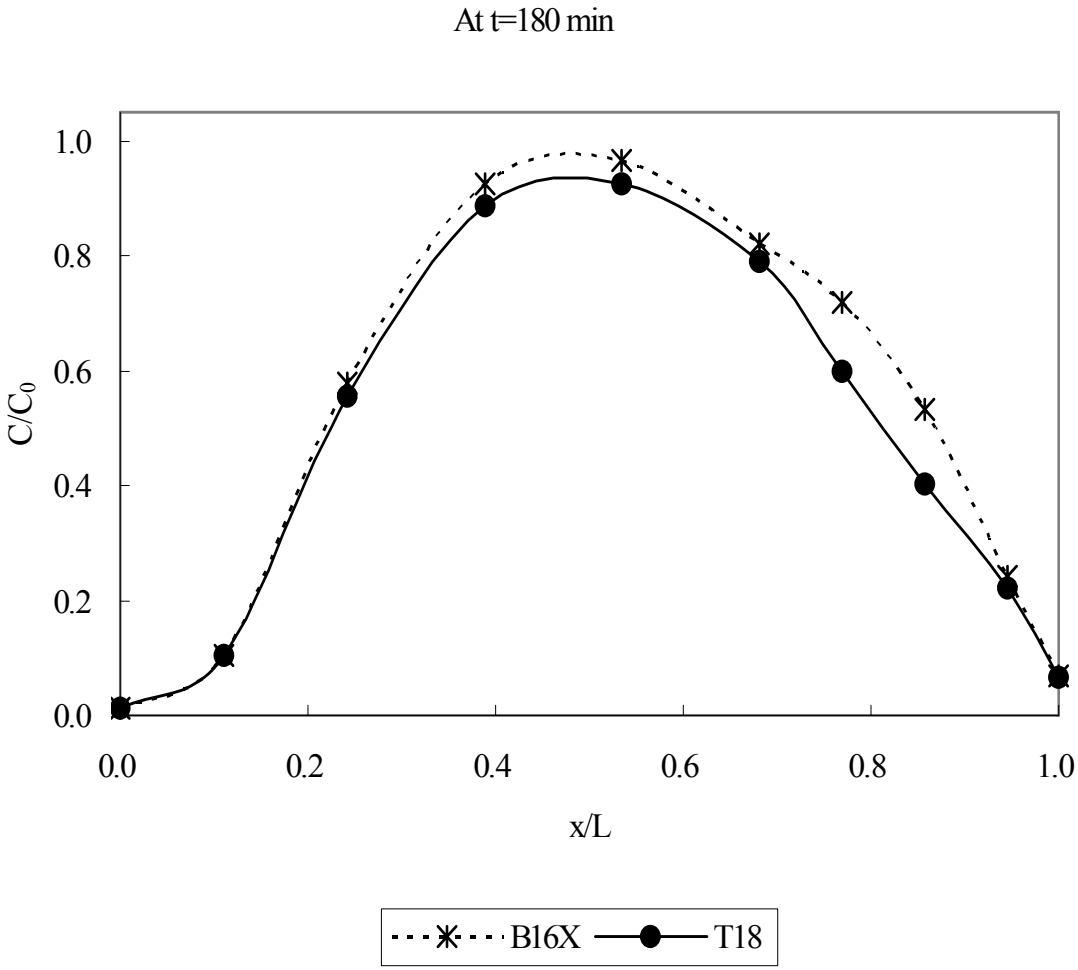

Figure 4.23 Contaminant Distribution for Case T18.

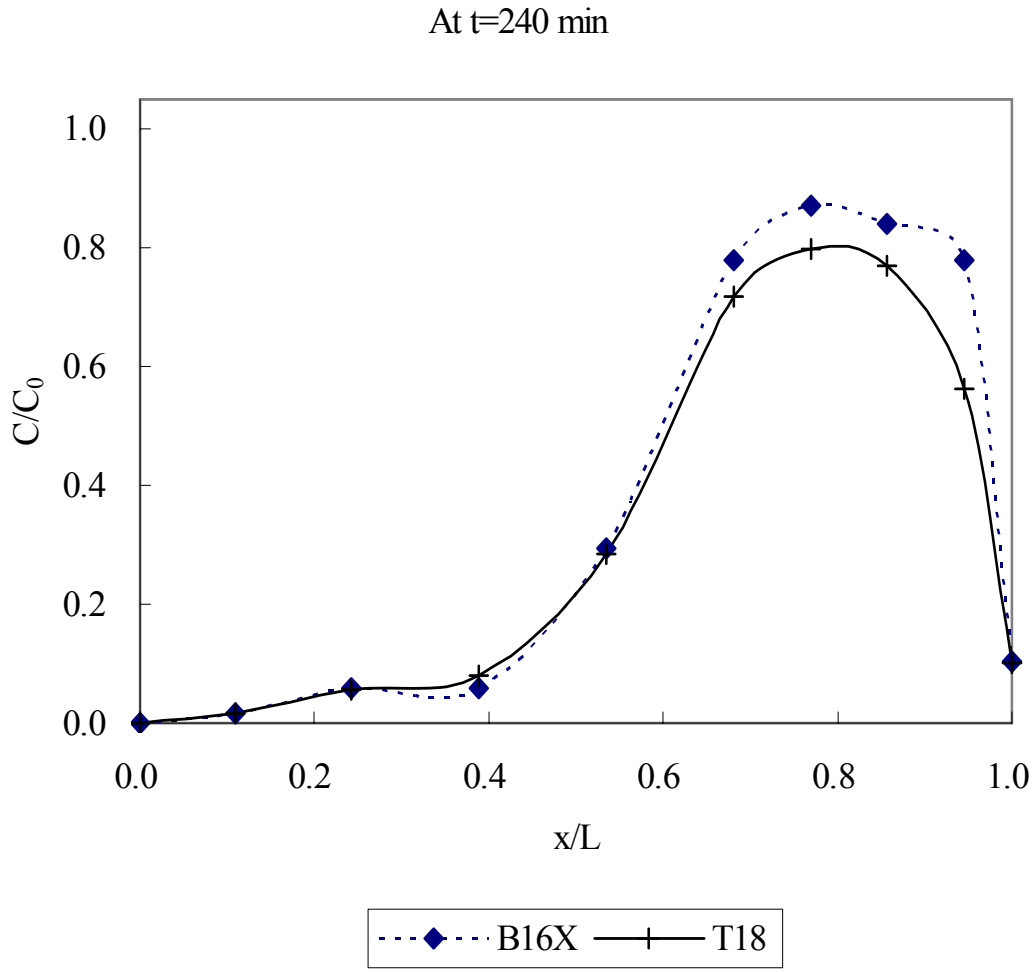

Figure 4.23 Contaminant Distribution for Case T18 (Continued).

These figures suggest that the tidal fluctuations have a slight to moderate influence on the contaminant transport: tidal activities cause the concentration to be slightly lowered compared to the counterpart experiment subject to no tidal fluctuations. The degree of the influence of the tides is approximately proportional to the tidal amplitude, i.e., the larger the tidal amplitude the greater the tidal influence. The tidal influence in these experiments is only slight with regard to the concentration distribution, while the tidal impact is slightly more significant with regard to the acceleration of the discharge caused by tidal activities for the case with relatively large tidal amplitude (20cm, Case T16). Figure 4.24 and Figure 4.25 compare the contaminant discharges for Case T16, Case T18, and the baseline without tides (Case B16X) as a function of time.

The slight influence of tidal fluctuations in the two cases above can be attributed to either the relatively small dilution factor or the relatively large tidal period. When the dilution factor is small, the contaminant concentration at the boundary would not be diluted to a very low level, so when the tide rises the contaminant would be pushed back into the aquifer sand medium, and would not dilute the contaminant concentration in the medium to the level that otherwise would be achieved with higher dilution at the boundary. That would cause the results not to show a significant tidal influence. On the other hand, different tidal periods would induce different frequencies at which the tidal water washes contaminant out of, and pushes fresh water into, the sand medium, and thus cause the tidal influences to deviate.

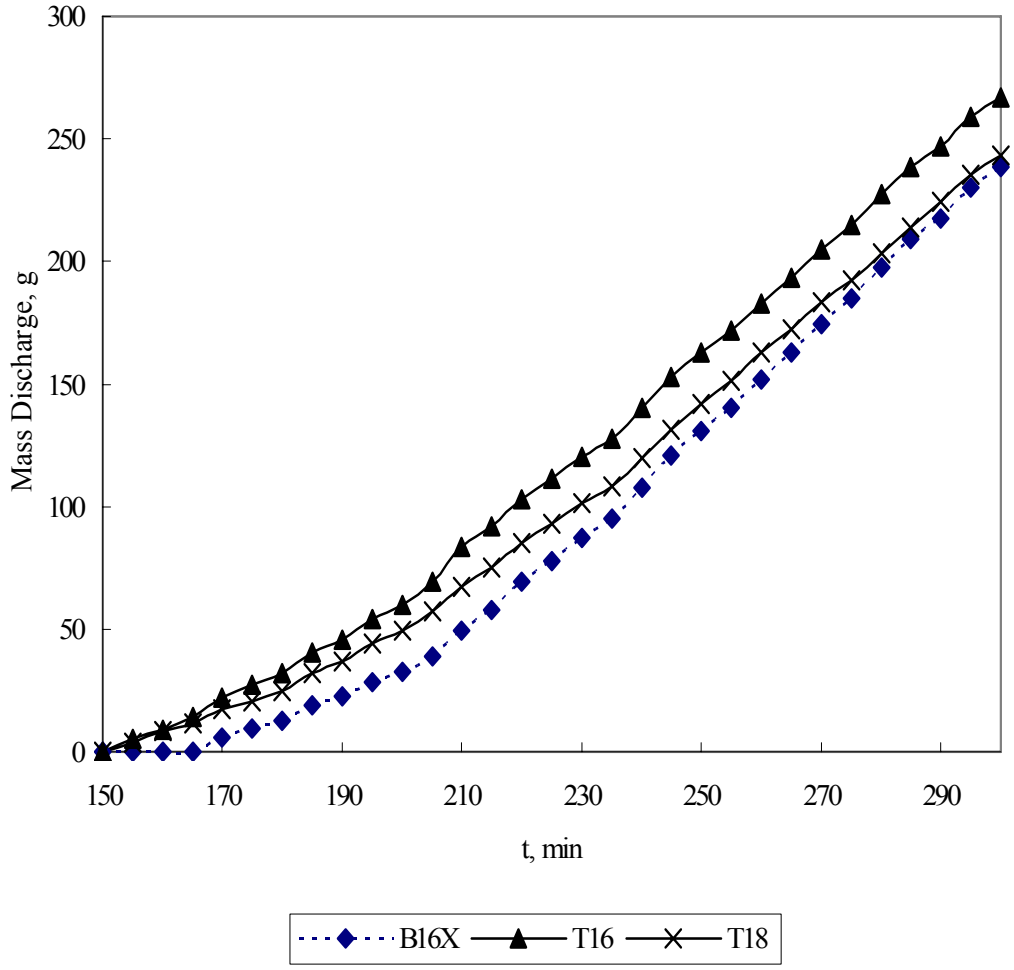

Figure 4.24 Contaminant Discharge Comparison.

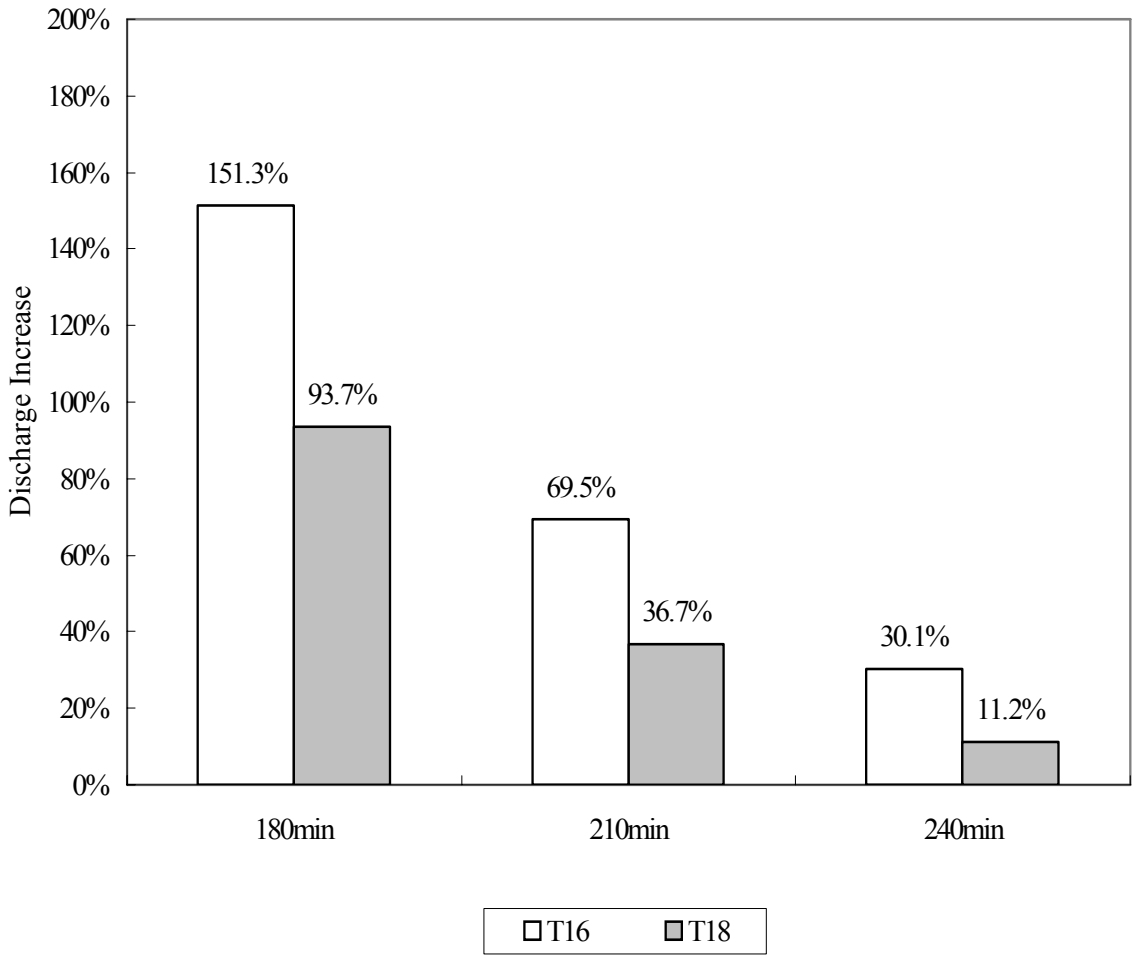

Figure 4.25 Contaminant Discharge Increase over the Baseline.

Due to experimental limitations, the dilution factor under the unconfined condition can not be raised while the tidal amplitude is kept constant. However, the tidal period can be adjusted within certain limits. Thus two more cases are studied: cases U2 and U3, with a tidal period of 2 minutes (see Table 4.2).

Figure 4.26 shows the contaminant concentration distribution for case U2. From the graph, it is observed that the reduced tidal period (or increased tidal wash frequency) leads the tidal effect to be larger than was observed in the previous two cases (T16 and T18). The effect can be seen better in Figure 4.27, which shows that the contaminant discharge is augmented by the tidal activities in case U2. The increased contaminant discharge is especially apparent during early times. As Figure 4.28 shows, contaminant discharge with tides is almost triple that in the case without tides at 180 minutes (case U2 increased 187% above the baseline case B16X), and it is almost double at 210 minutes (case U2 is 83% above the baseline case B16X). Even after 240 minutes, the discharge is still enhanced by 40% above the baseline. In addition, note that a lower tidal amplitude (case U3, 10 cm) results in a lower contaminant discharge compared to a higher tidal amplitude (case U3, 20 cm) at all three time intervals.

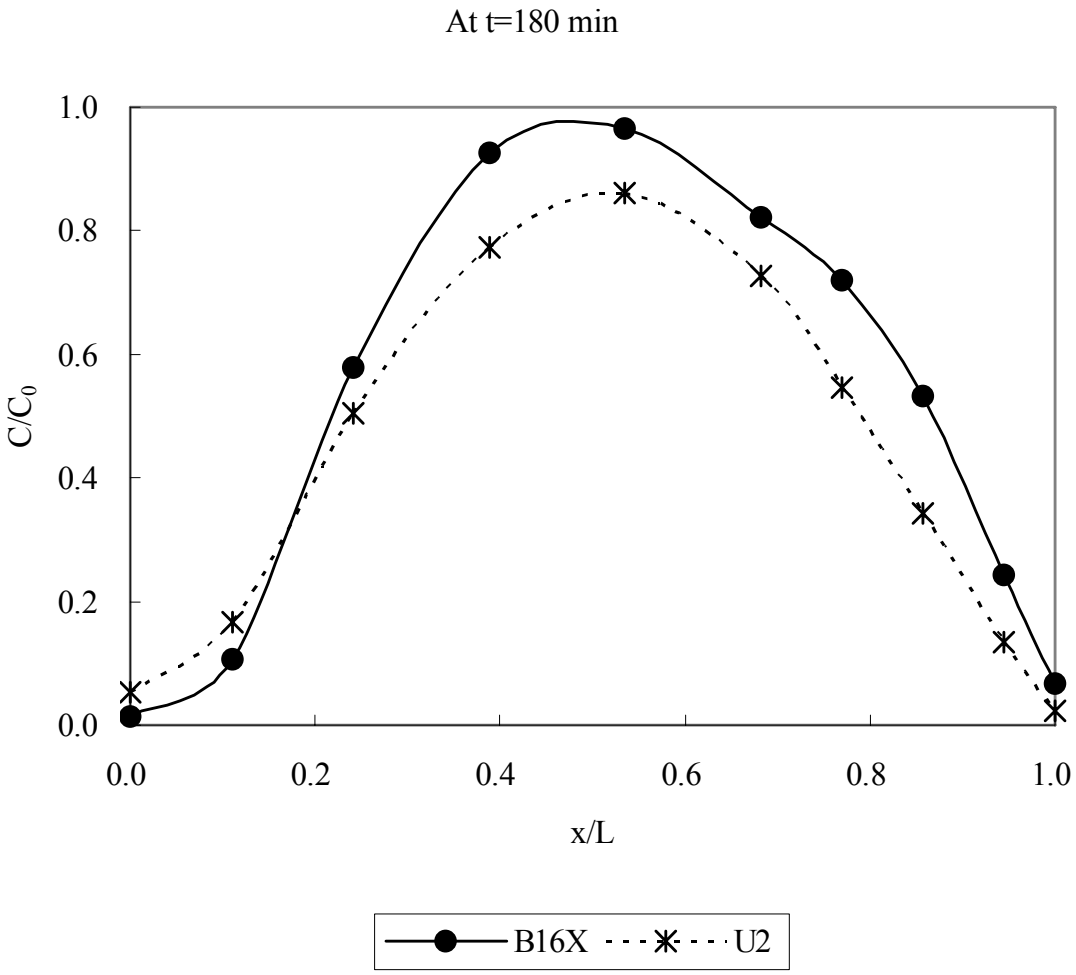

Figure 4.26 Contaminant Distribution for Case U2.

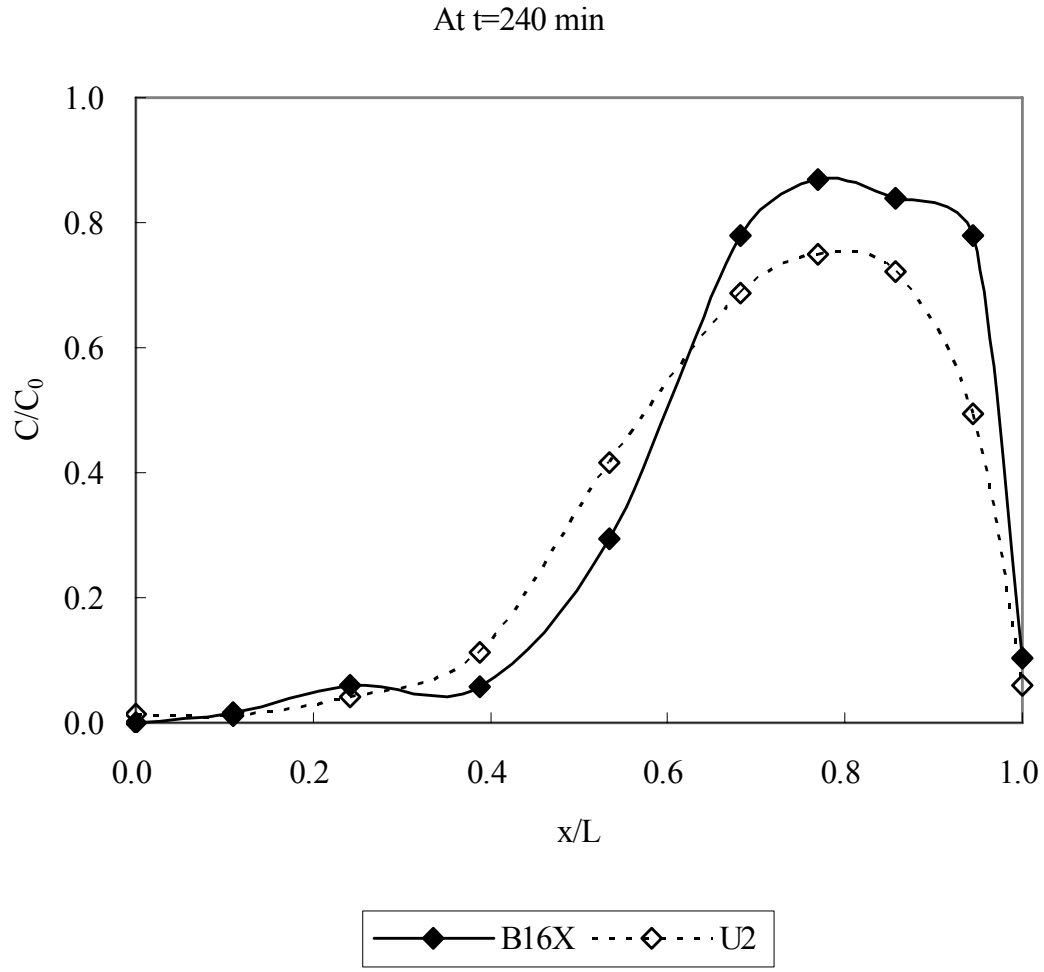

Figure 4.26 Contaminant Distribution for Case U2 (Continued).

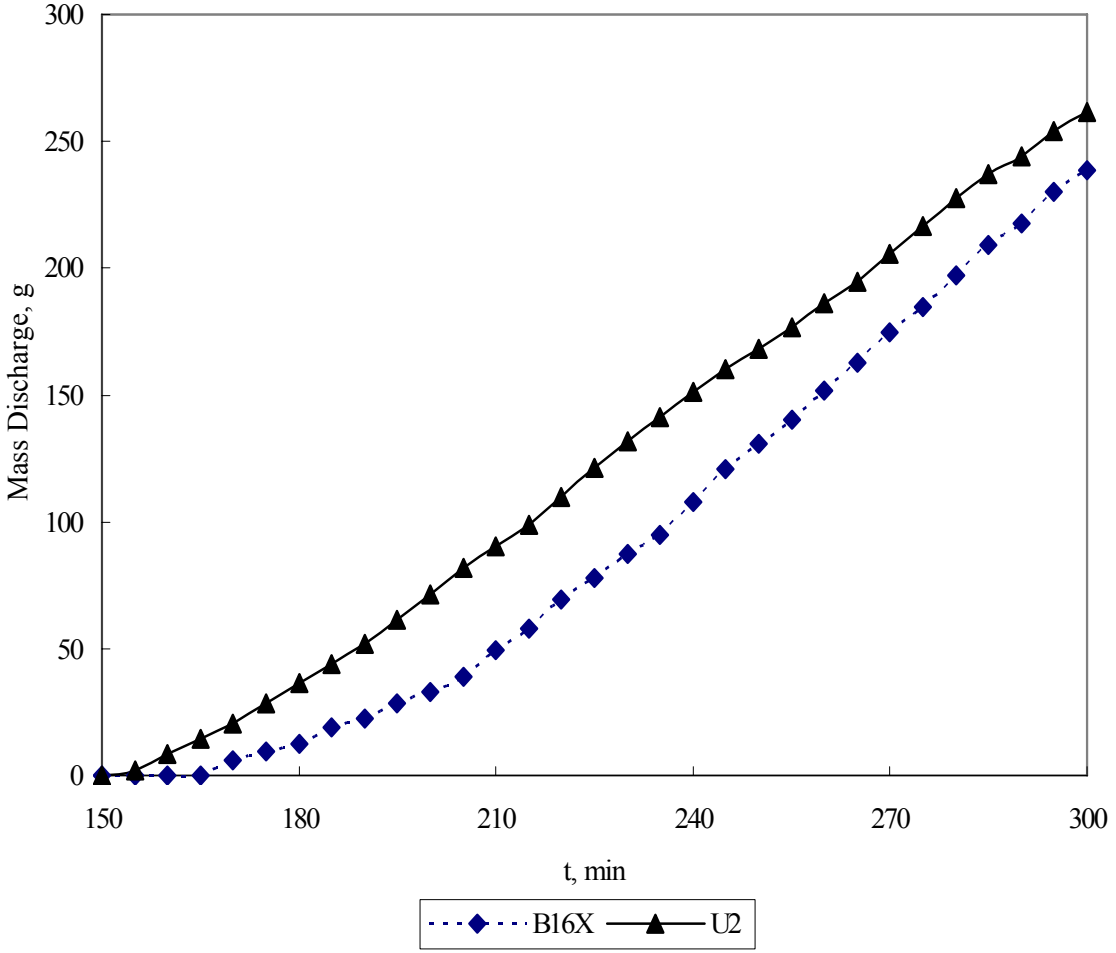

Figure 4.27 Contaminant Discharge Comparison.

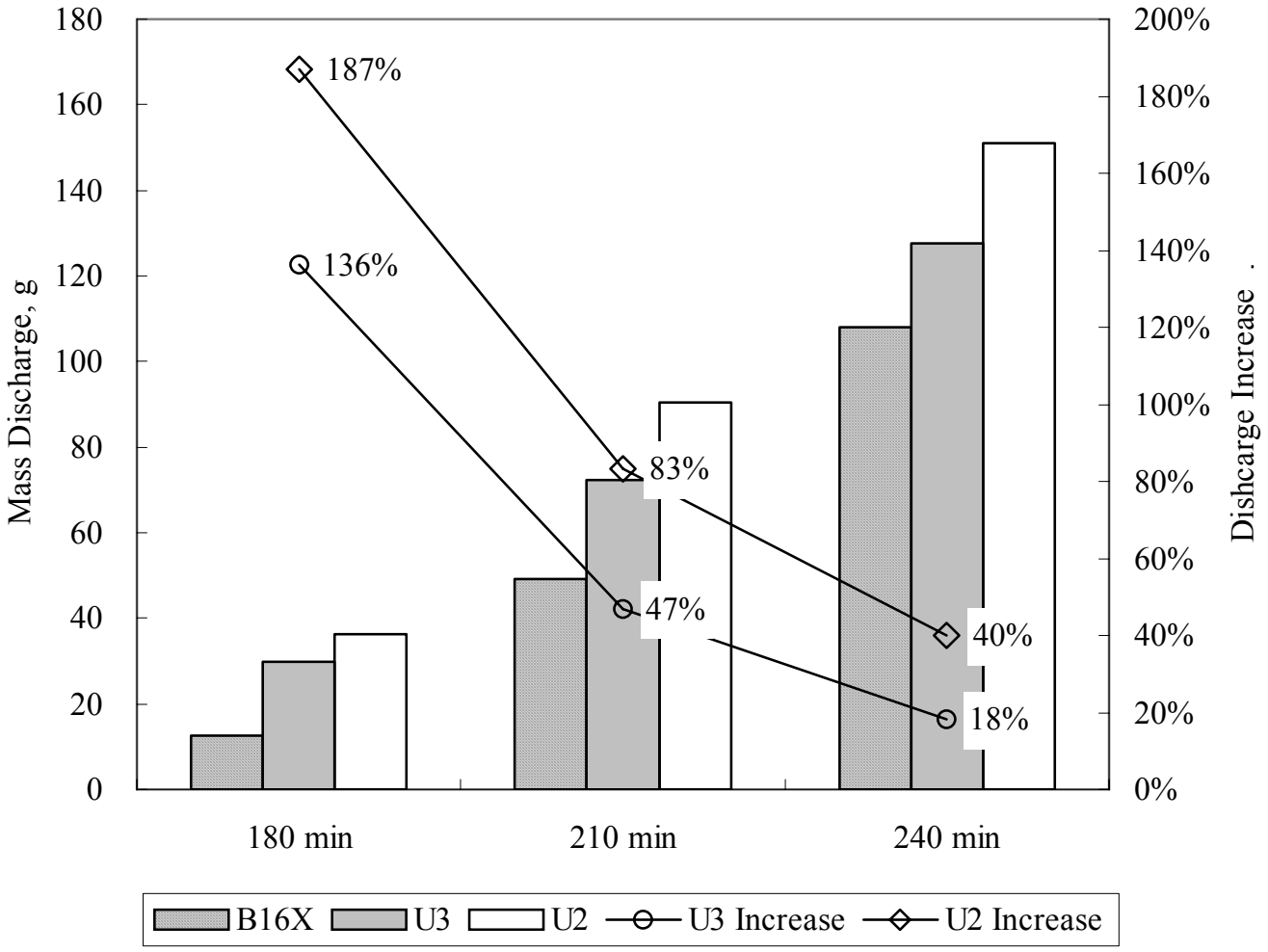

Figure 4.28 Contaminant Discharge Comparison.

Even with an increased tidal washing frequency or decreased tidal period, the influence by the tides is insignificant with a relatively small tidal amplitude.

Figure 4.29 gives the contaminant concentration distribution of case U3 compared to the baseline case B16X, and Figure 4.30 gives the contaminant discharge over time for case U3 compared to the baseline. From the discharge profiles, tidal fluctuations only slightly enhance the contaminant discharge, especially during the early time interval (Figure 4.30; case U3 increased 136% over the baseline case B16X at 180 minutes, but only 9-47% at the other times). However, this information regarding the impact of tides is consistent with the previous cases, and this can be important information which may help lead to conclusions later with regard to tidal effects.

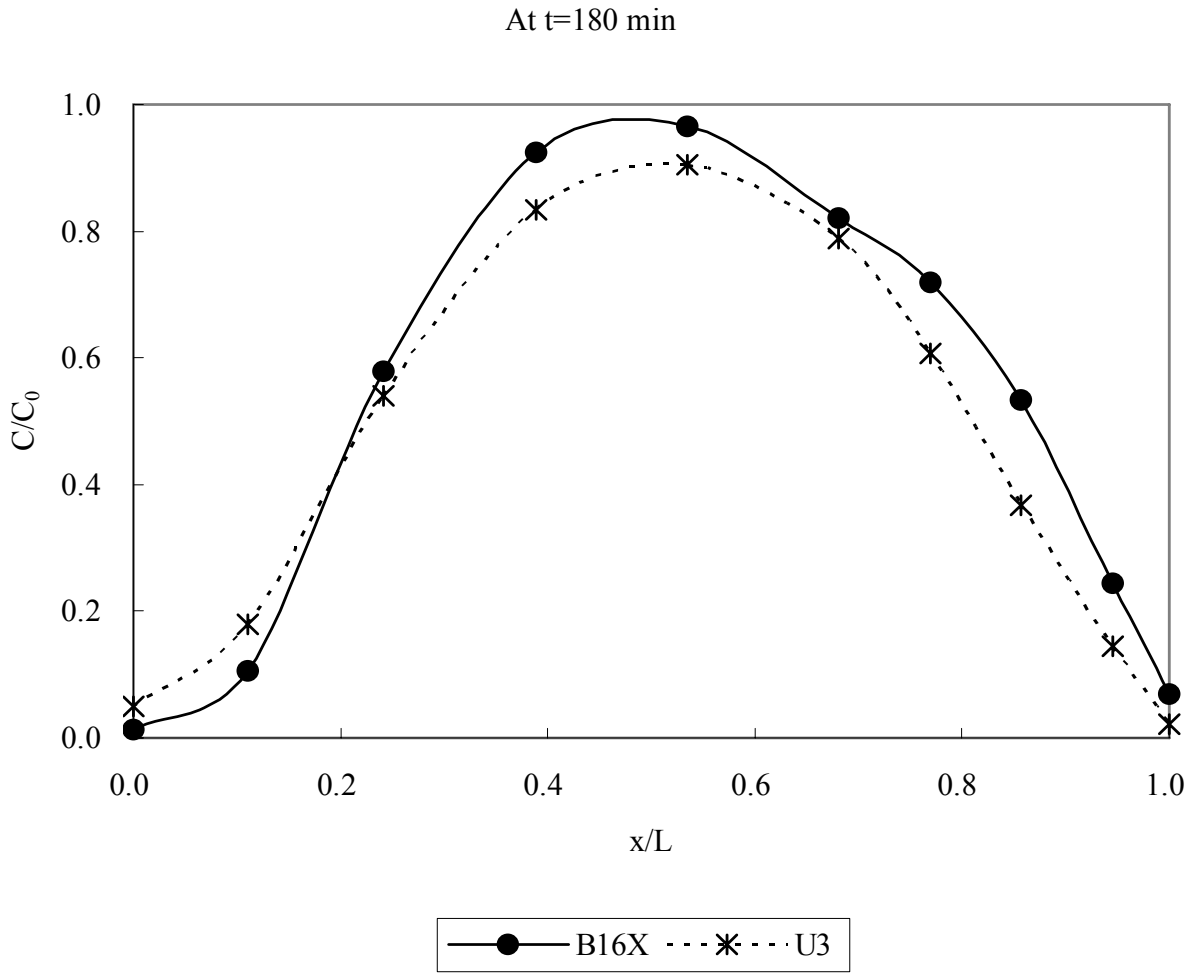

Figure 4.29 Contaminant Distribution for Case U3.

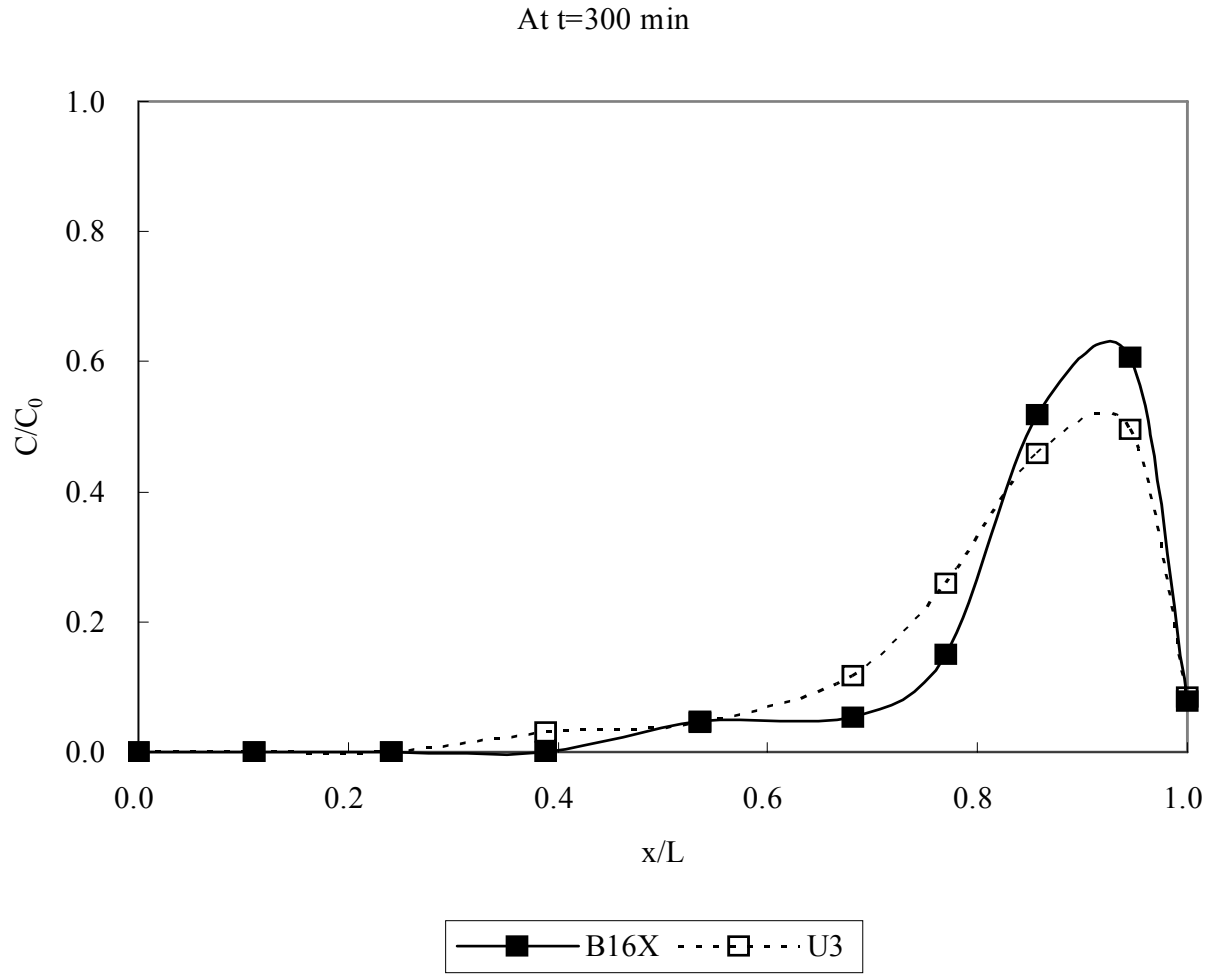

Figure 4.29 Contaminant Distribution for Case U3 (Continued).

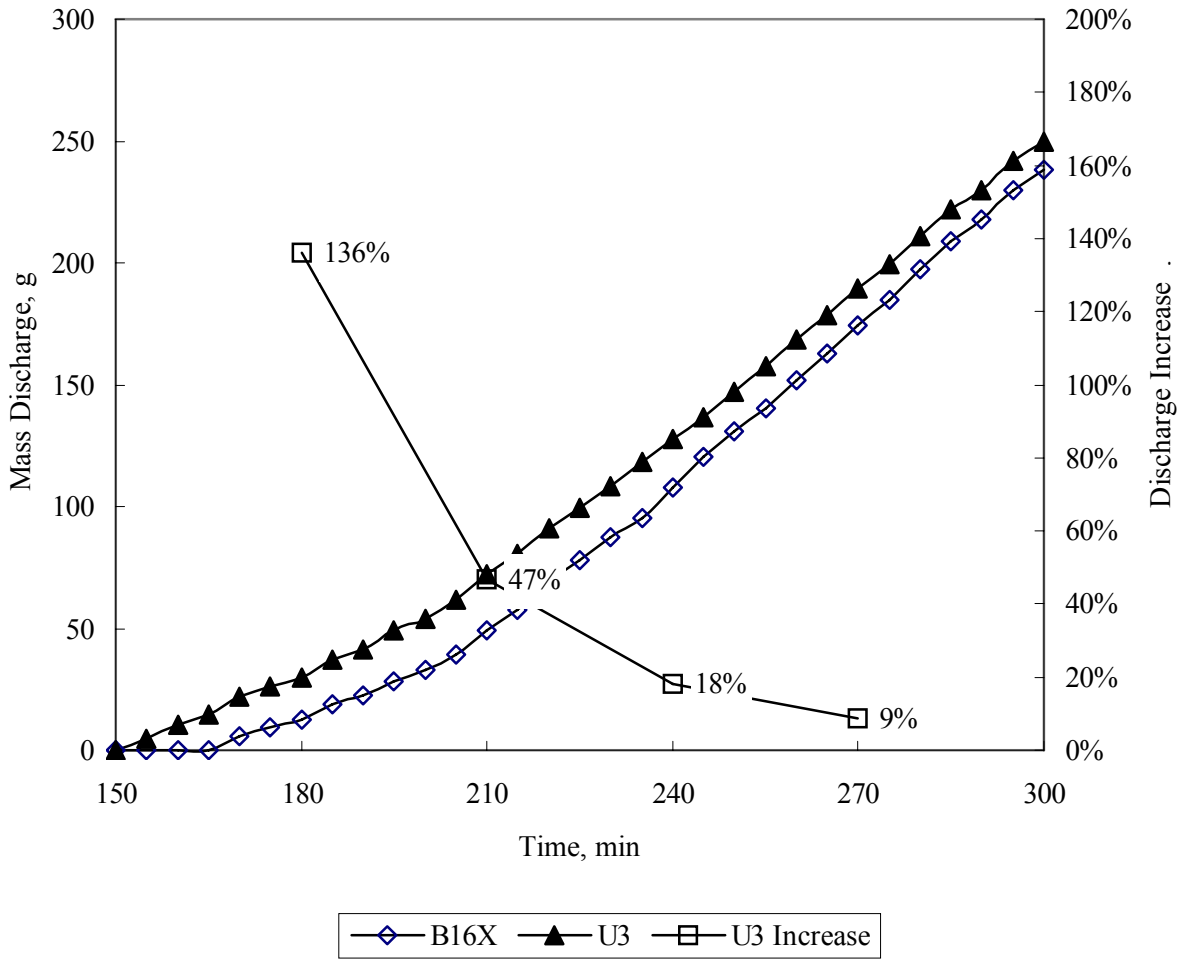

Figure 4.30 Contaminant Discharge Comparison.

4.2.4 Results of Confined-Condition Experiments

In the confined-condition experiments, the lid is added onto the tank and sealed by bolts and buffering rubber. Subsequently, the piezometric water level in the tank is raised above the top of the tank. Again, the hydraulic head at the influent chamber is set constant at five and a half feet above the bottom of the sand tank. The tidal tank is raised accordingly at the right end of the sand tank to reach the desired effluent water level. A schematic representation of the experiment is illustrated in Figure 4.31.

As mentioned in the previous section, due to experimental limitations, the hydraulic gradient, tidal amplitude, and dilution factor are subject to the constraint of each other. The rising of the hydraulic water level in the sand tank, however, allows a more flexible selection of experimental parameter values than in the unconfined-condition experiments. In the confined-condition experiments, considered are two hydraulic gradients of 0.1 and 0.05, two tidal amplitudes of 20 cm and 30 cm, and a smaller tidal period of 1 minute, in addition to the period of 5 minutes used earlier in the unconfined-condition experiments. The parameter values for the confined-condition experiments and the case numbers assigned to them are listed in Table 4.3 (page 88).

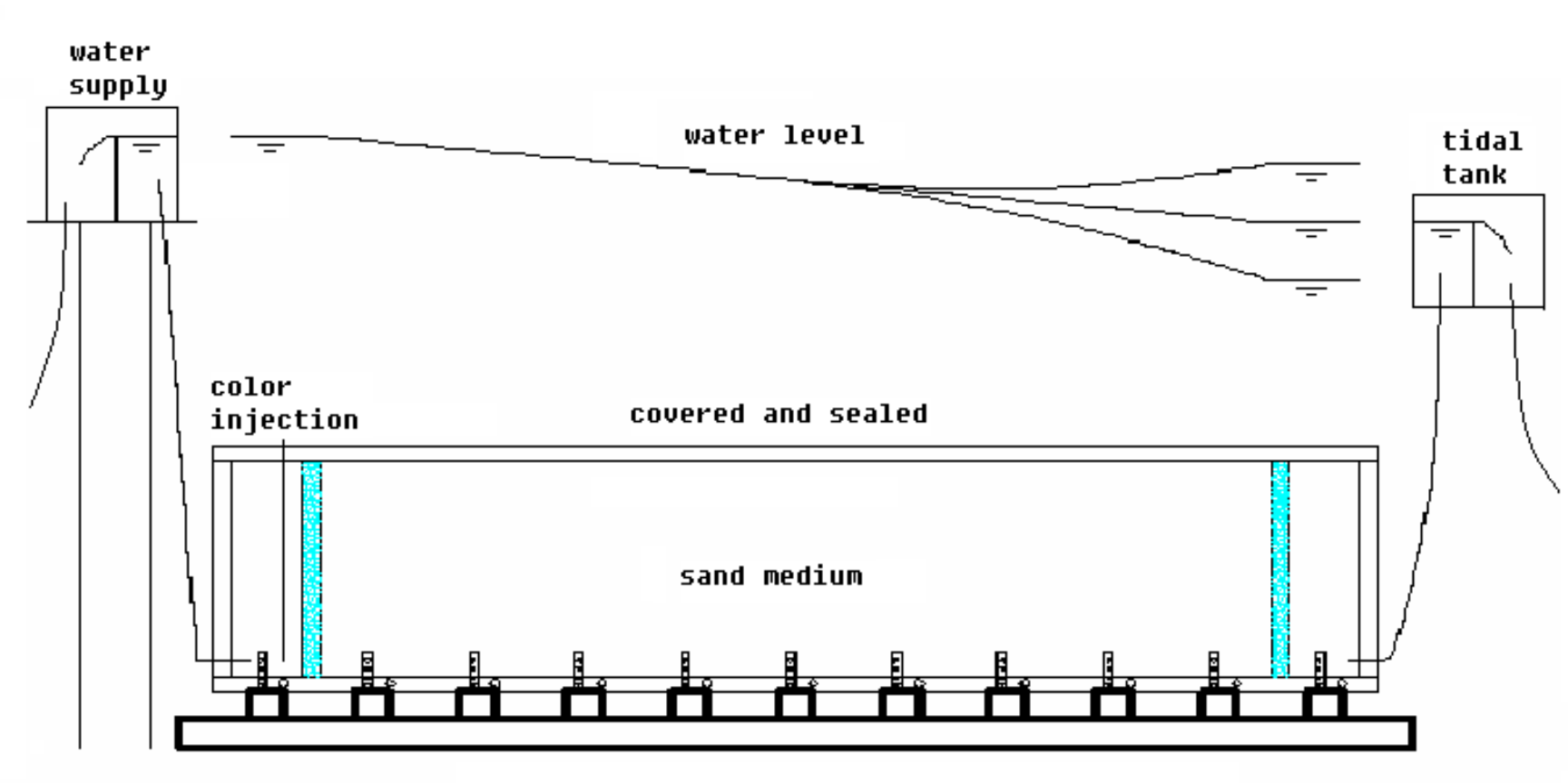

Figure 4.31 Confined-Condition Experiments.

The first set of experiments is conducted with a high hydraulic gradient of 0.1, with tidal periods of 5 minutes and one minute, and with tidal amplitudes of 20 cm and 30 cm, respectively. The second set of experiments is conducted with a lower hydraulic gradient of 0.05, and with similar tidal periods and tidal amplitudes. Case B19X and case B20X are the baseline cases chosen by this study simulating the first-type boundary condition. Case B19 and case B20 are baseline cases without tides and dilution, simulating second-type boundary condition (they are included as a comparison with the baseline chosen to study tidal effect, which is a point emphasized throughout this document).

The concentration distributions at different times for case T19 are illustrated in Figure 4.32 and compared to the baseline, case B19X. Under the confined condition, a combination of a high hydraulic gradient, relatively large tidal period, small dilution factor, and moderate tidal amplitude results in only a slight influence on the contaminant transport by tidal activities. As seen in Figure 4.33, a comparison of the contaminant discharge for case T19 and the baseline case without tide (B19X) leads to the same conclusion. Contaminant discharge in case T19 increases only 5-37% compared to the baseline case B19X.

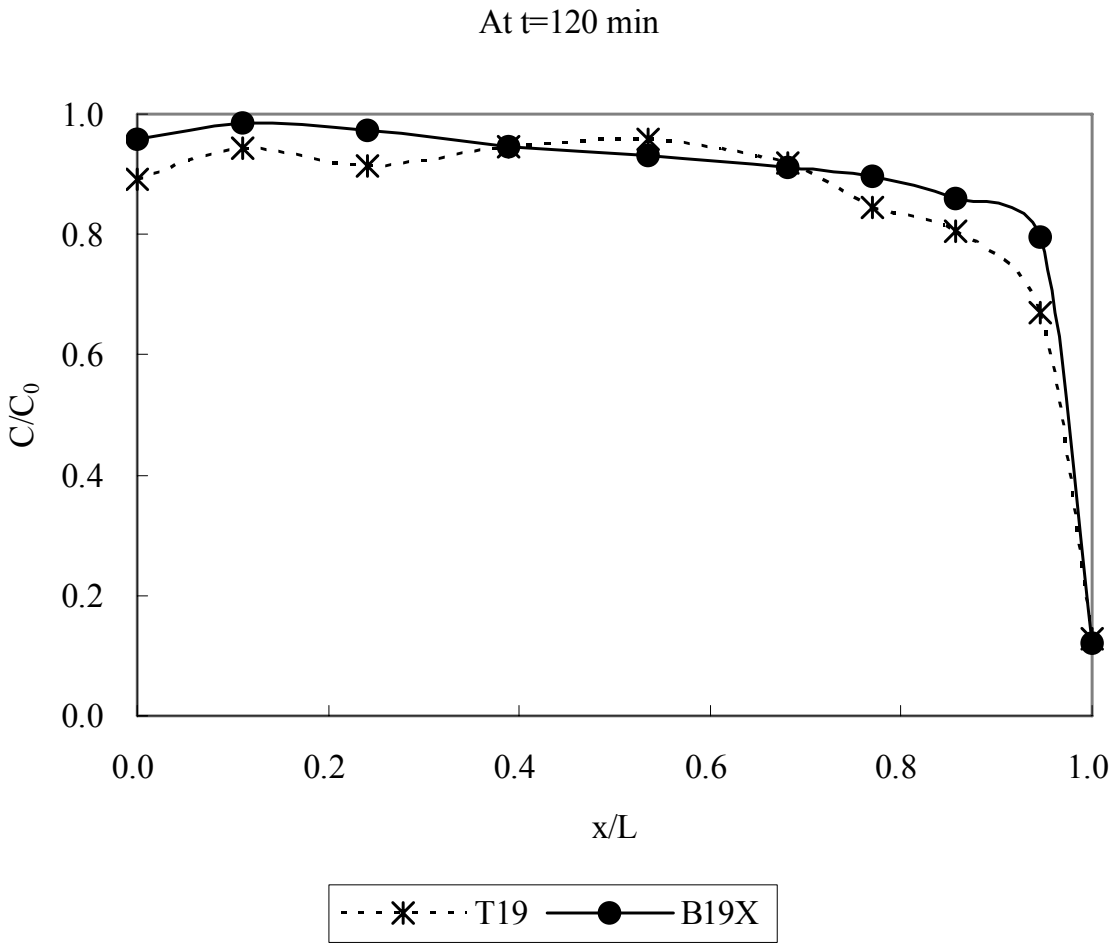

Figure 4.32 Contaminant Distribution for Case T19.

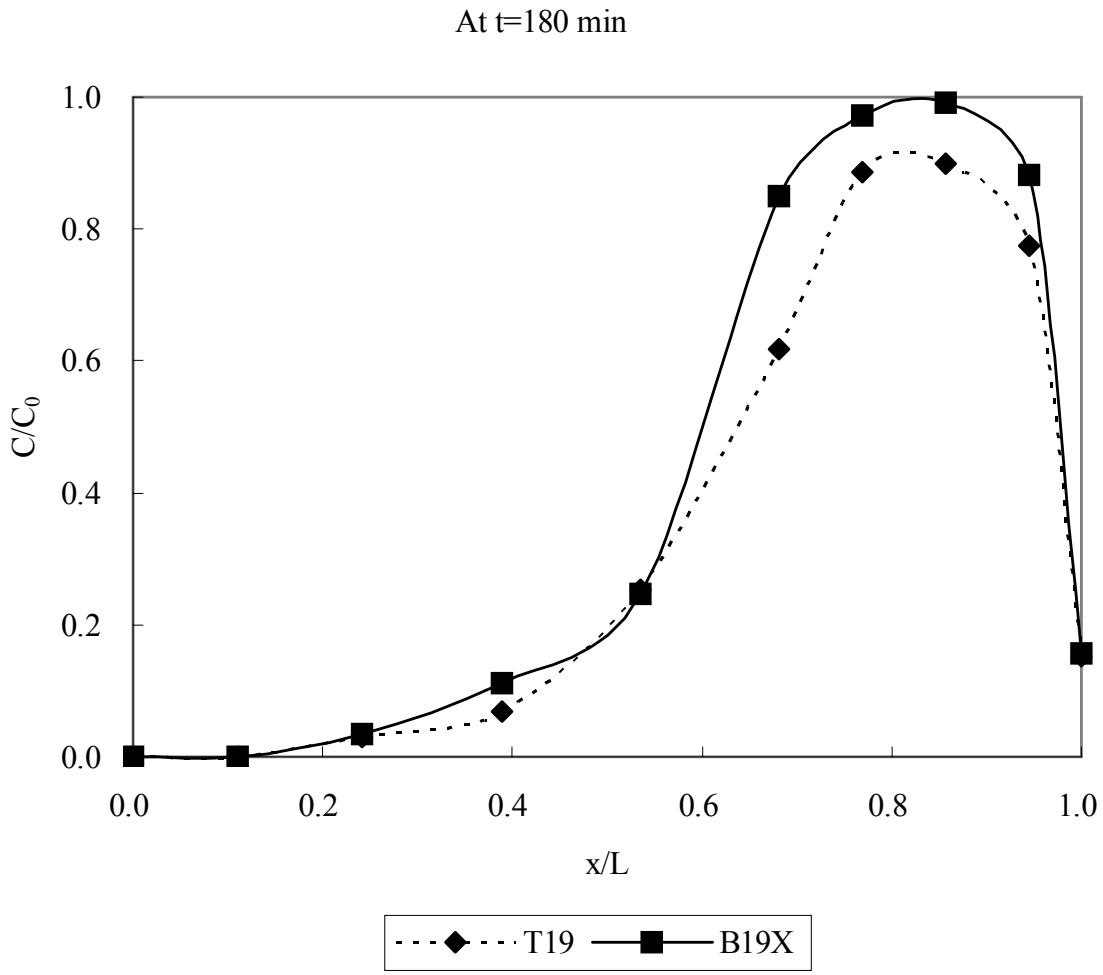

Figure 4.32 Contaminant Distribution for Case T19 (Continued).

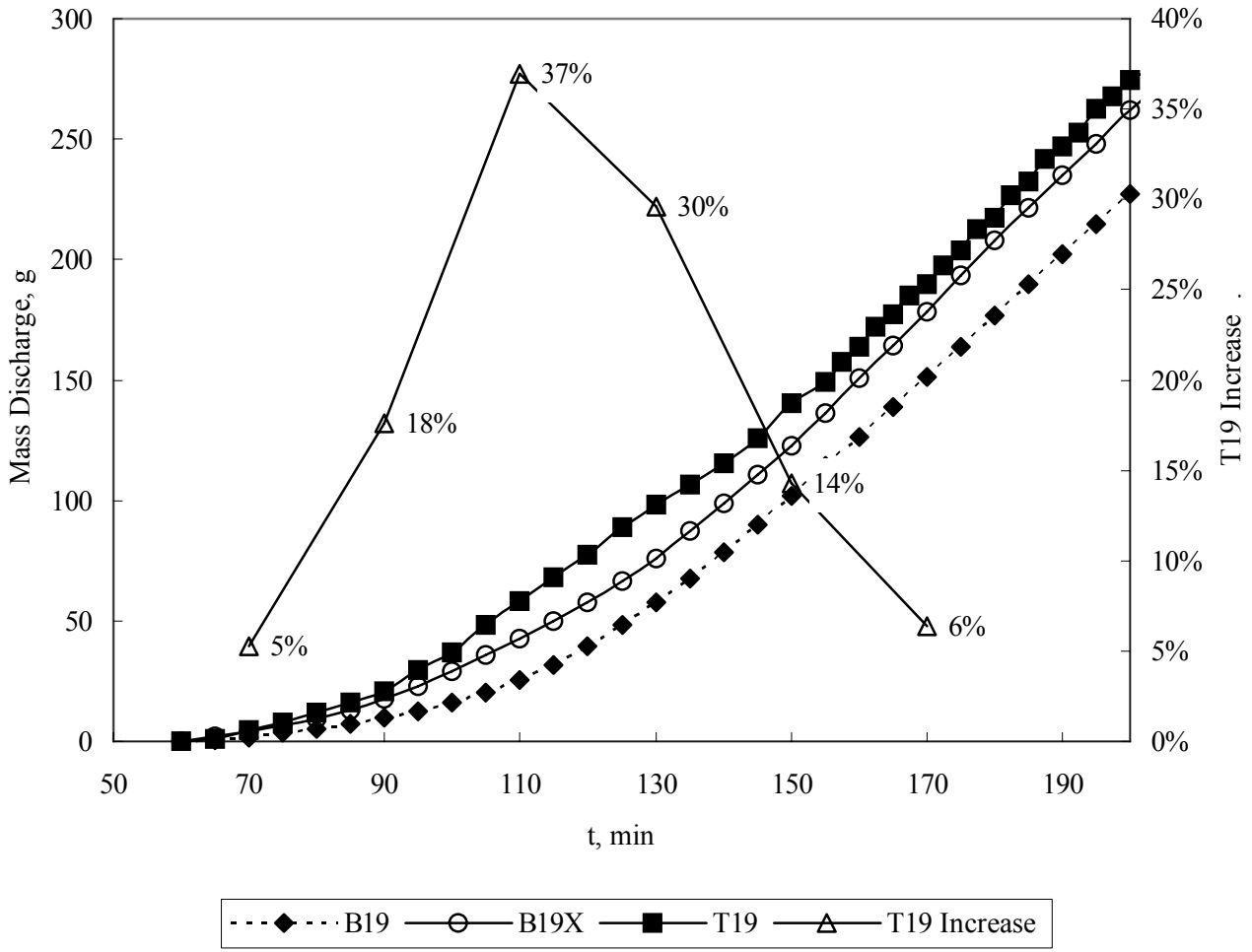

Figure 4.33 Contaminant Discharge Comparison.

It has been mentioned that the tidal influence is subject to tidal amplitude: the degree of the influence of the tides is approximately proportional to the tidal amplitude, i.e., the larger the tidal amplitude the more influential the tides. In addition, the tidal influence may also subject to tidal period. The study thus proceeds in two directions: one, reducing tidal period, and secondly, increasing tidal amplitude.

Case CON4 reduces the tidal period to one minute (from 5 minutes) while the tidal amplitude is kept the same as in case T19 (20 cm). Figure 4.34 gives the results regarding concentration distribution, and Figure 4.35 and Figure 4.36 give the results with regard to contaminant discharge. These results suggest that, with a reduced tidal period, the tidal influence is slightly augmented compared to case T19. Compared to the baseline condition, contaminant discharges are 5-55% higher in case CON4 (Figure 4.36). This effect is less significant compared to the results under the unconfined-condition experiments (refer to the discussion in the Section 4.2.3), where contaminant discharges were 11-151% higher than the baseline for case T16 (see Figure 4.25).

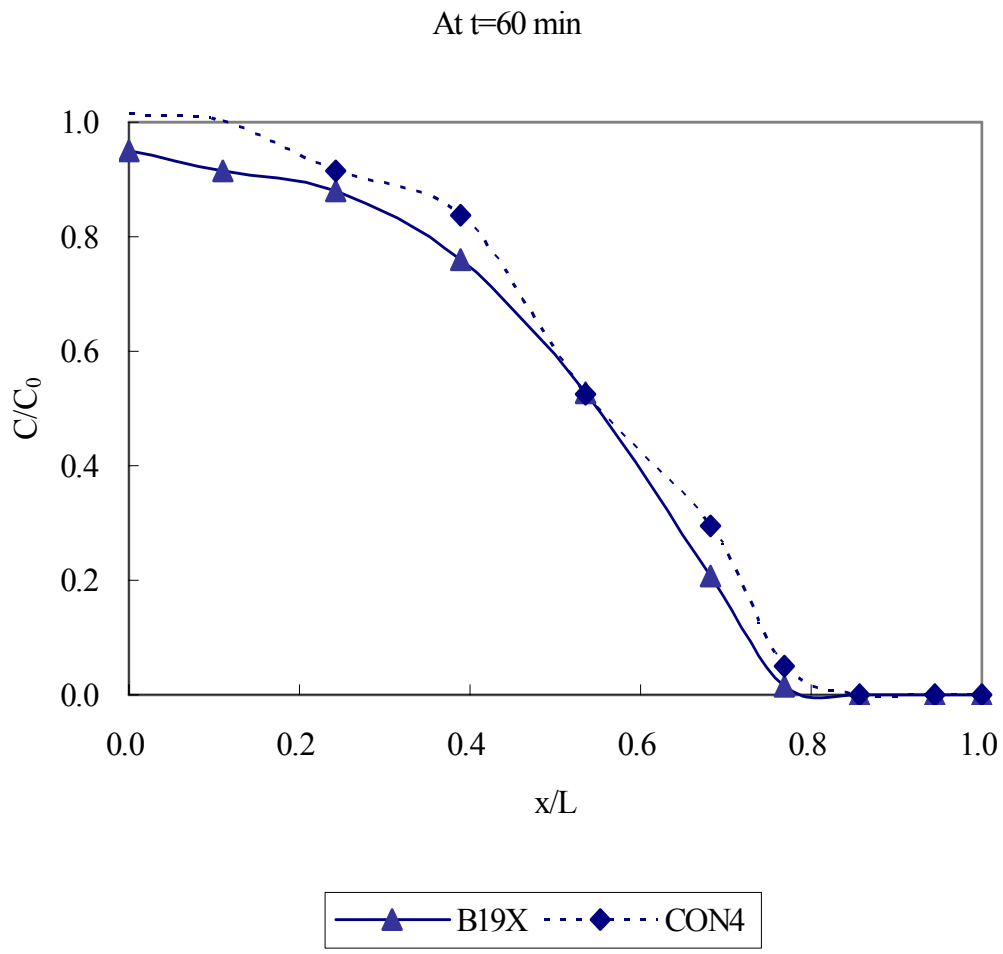

Figure 4.34 Contaminant Distribution for Case CON4.

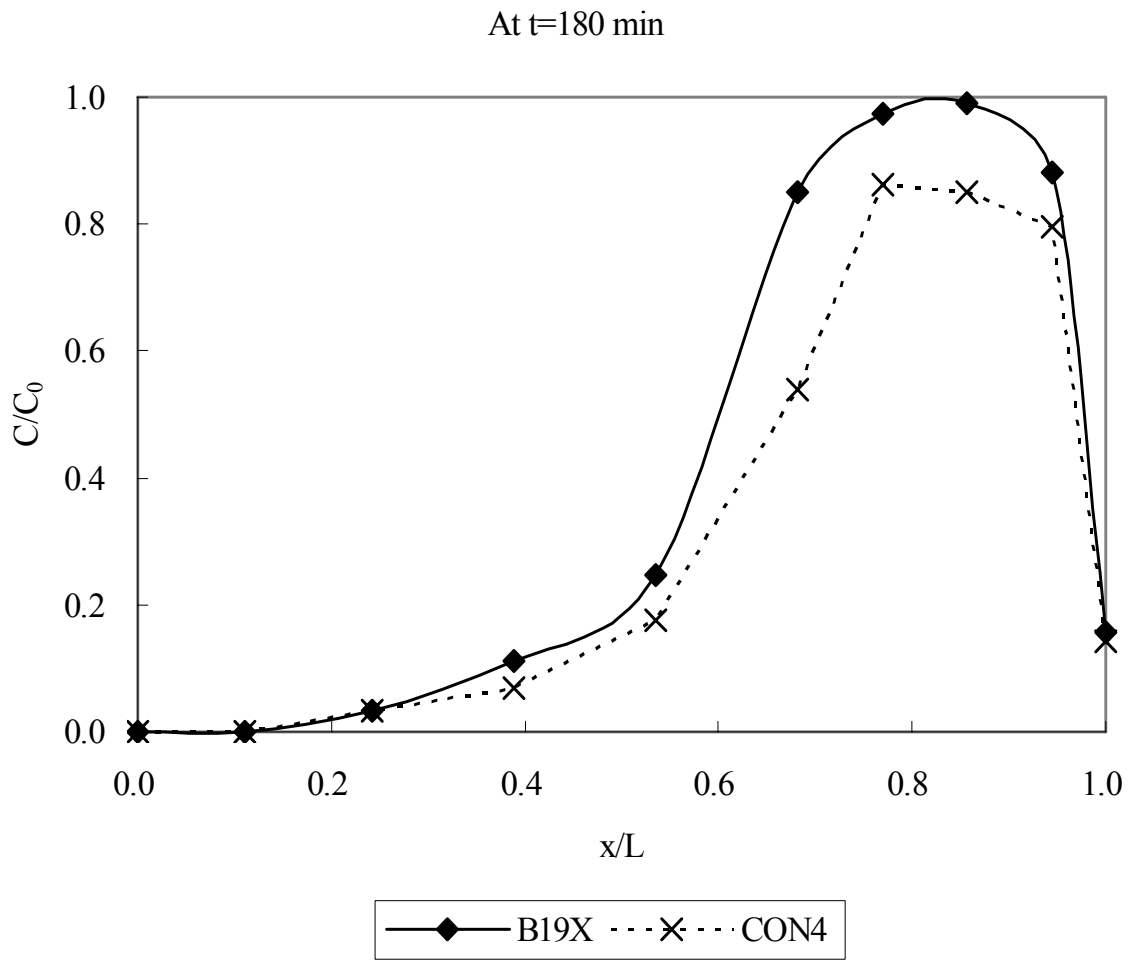

Figure 4.34 Contaminant Distribution for Case CON4 (Continued).

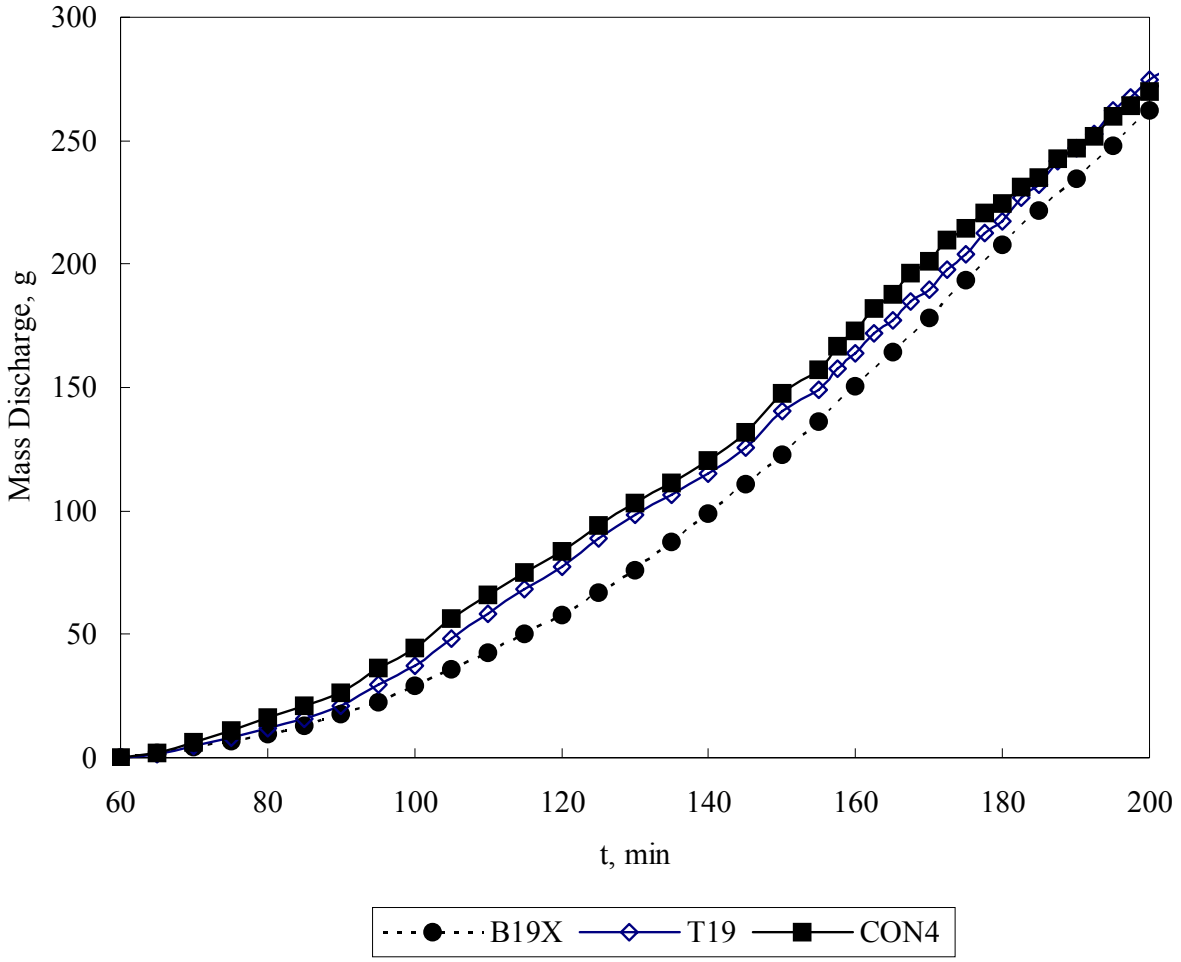

Figure 4.35 Contaminant Discharge Comparison.

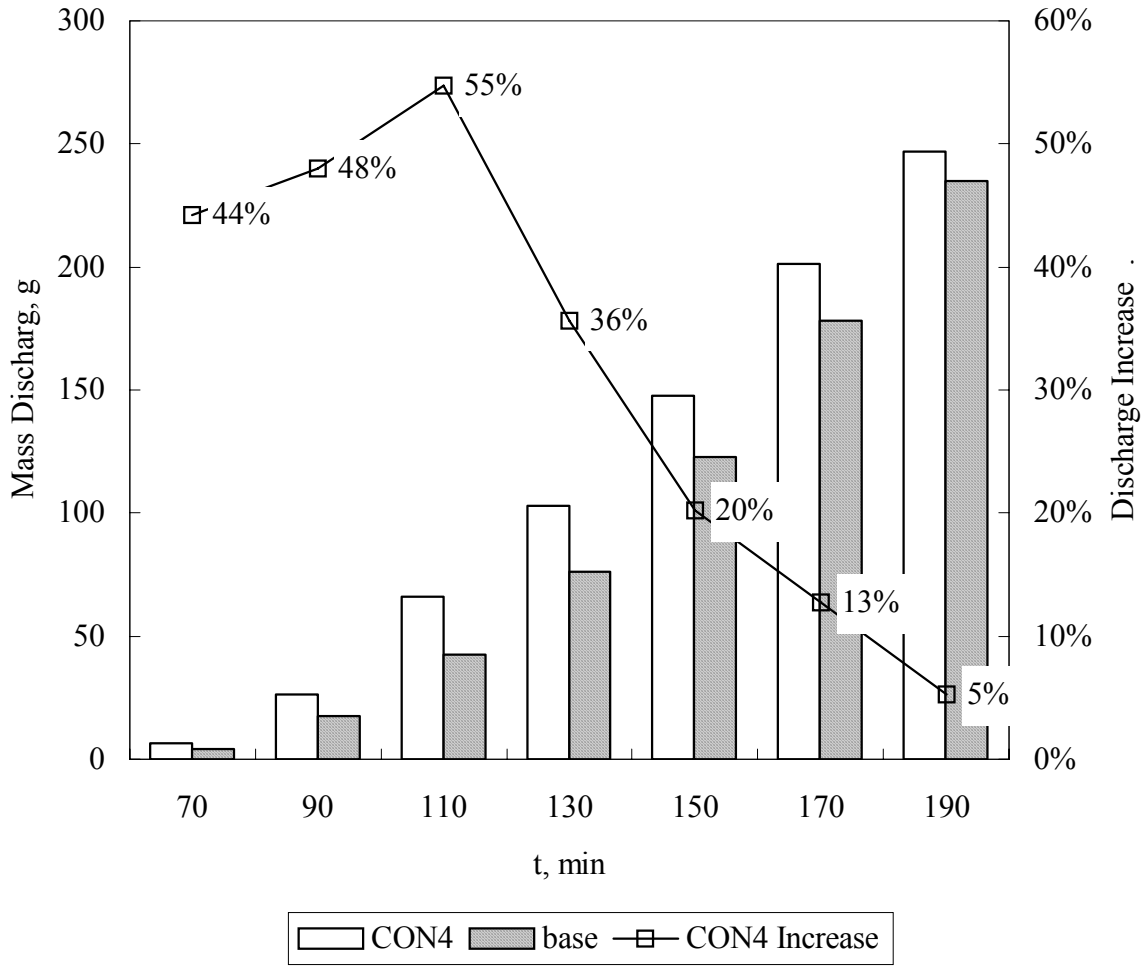

Figure 4.36 Contaminant Discharge Comparison.

Case CON3 further increases the tidal amplitude to 30 cm, from the 20 cm used in case CON4. Figure 4.37 through Figure 4.39 show the results of the concentration distributions and contaminant mass discharge. Consistent with the aforementioned trend that the larger the tidal amplitude, the more tidal impact, the tidal activities in case CON3 further reduce the concentration in the area near the boundary and enhance the contaminant discharge. As a result, the total effect of the reduced tidal period and increased tidal amplitude becomes dramatic compared to the baseline, case B19X. Note that the significant effect is manifest especially during the early time of discharge as shown on the discharge curves (see Figure 4.38). Figure 4.39 further indicates that the discharge is accelerated by 68% at 90 minutes, 64% at 120 minutes, and 34% at 150 minutes compared to the baseline case B19X. In addition, Figure 4.39 shows the combined effect on contaminant discharge of the decreased tidal period (1 minute) and increased tidal amplitude (30 cm) in case CON3 compared to case T19 (5 minutes and 20 cm, respectively).

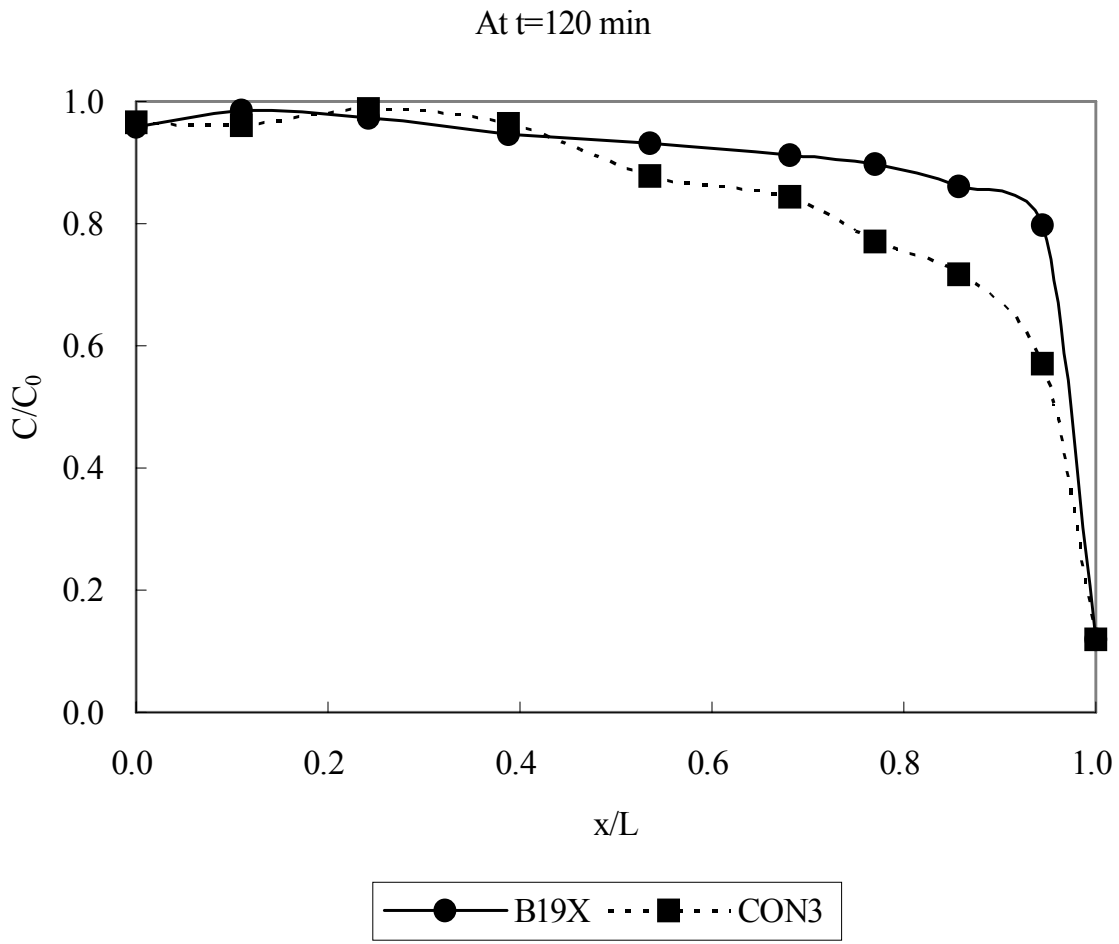

Figure 4.37 Contaminant Distribution for Case CON3.

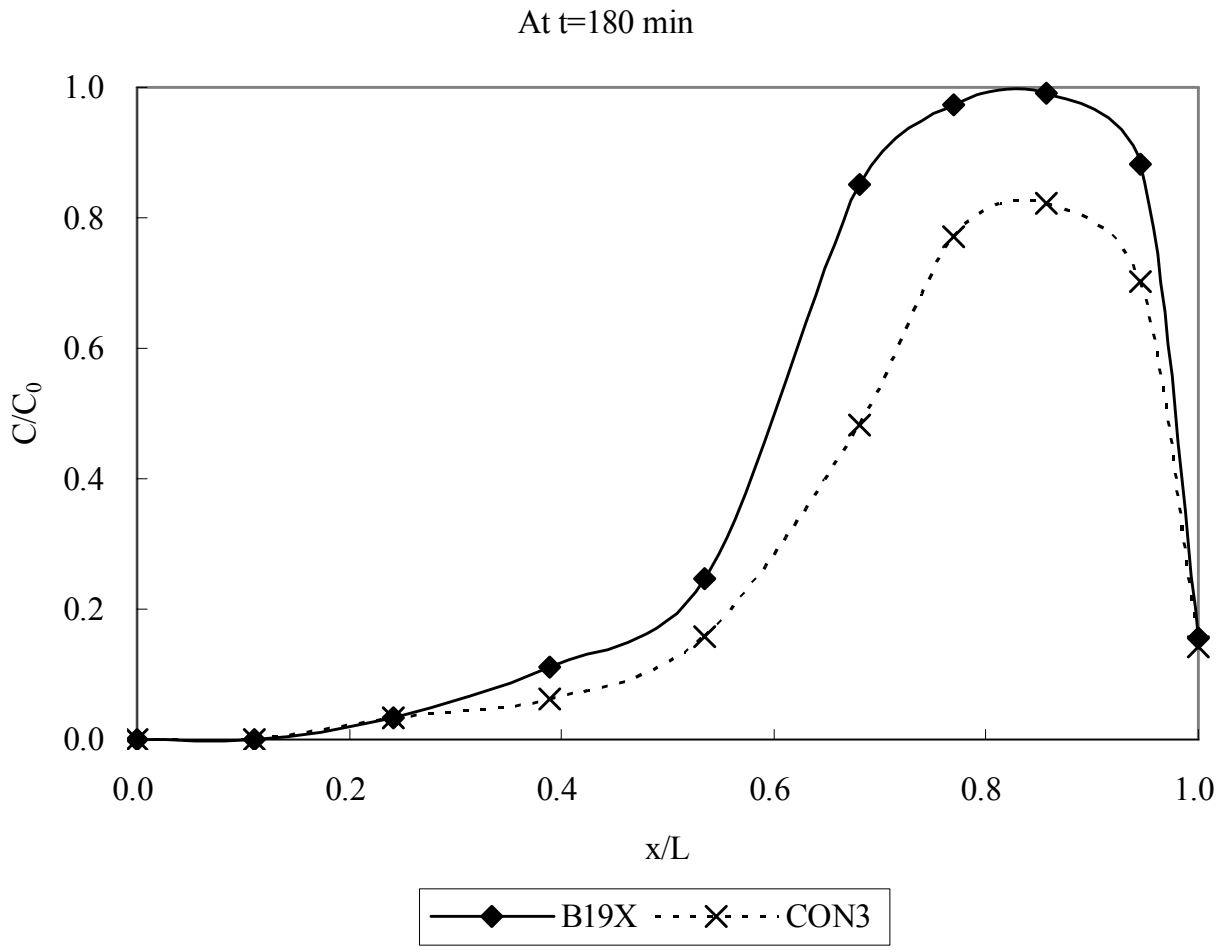

Figure 4.37 Contaminant Distribution for Case CON3 (Continued).

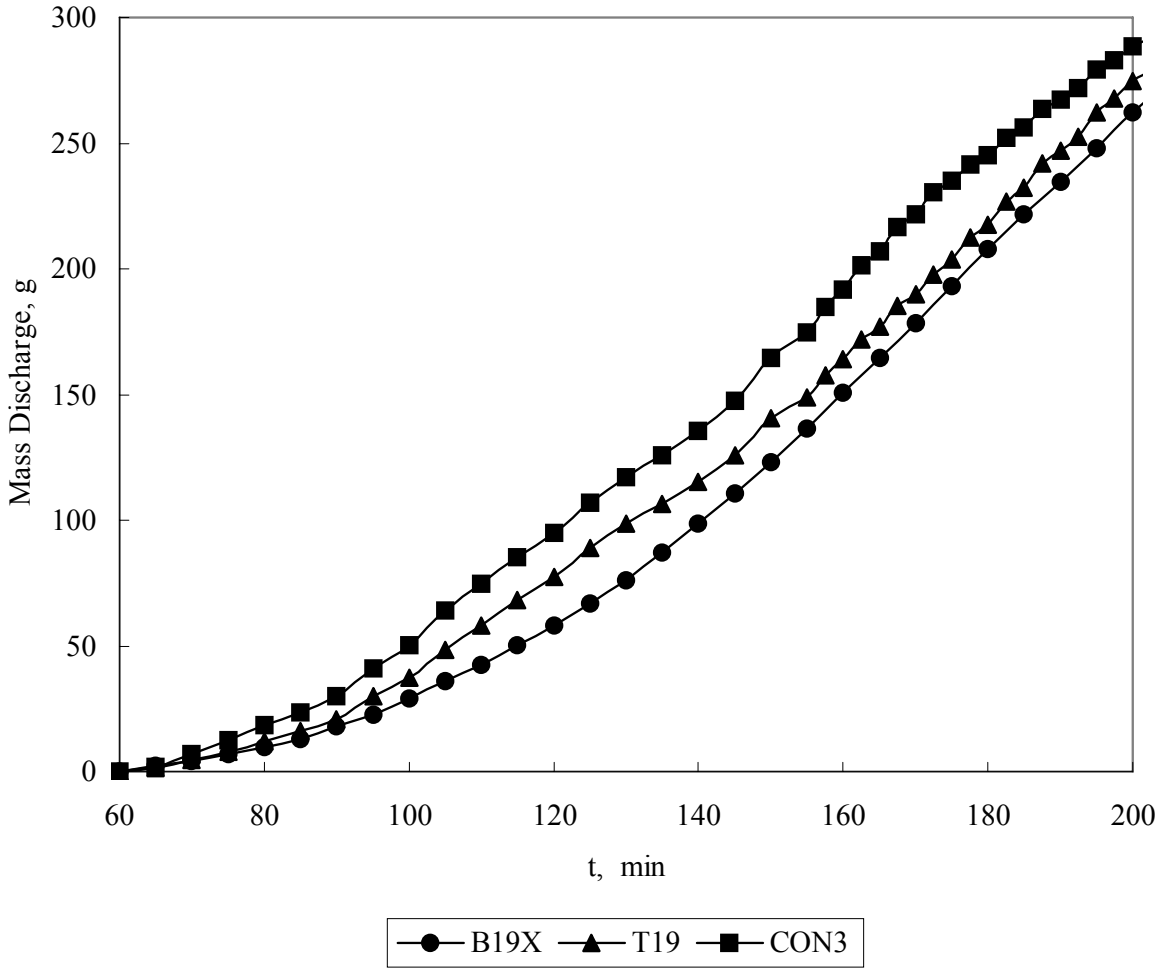

Figure 4.38 Contaminant Discharge Comparison.

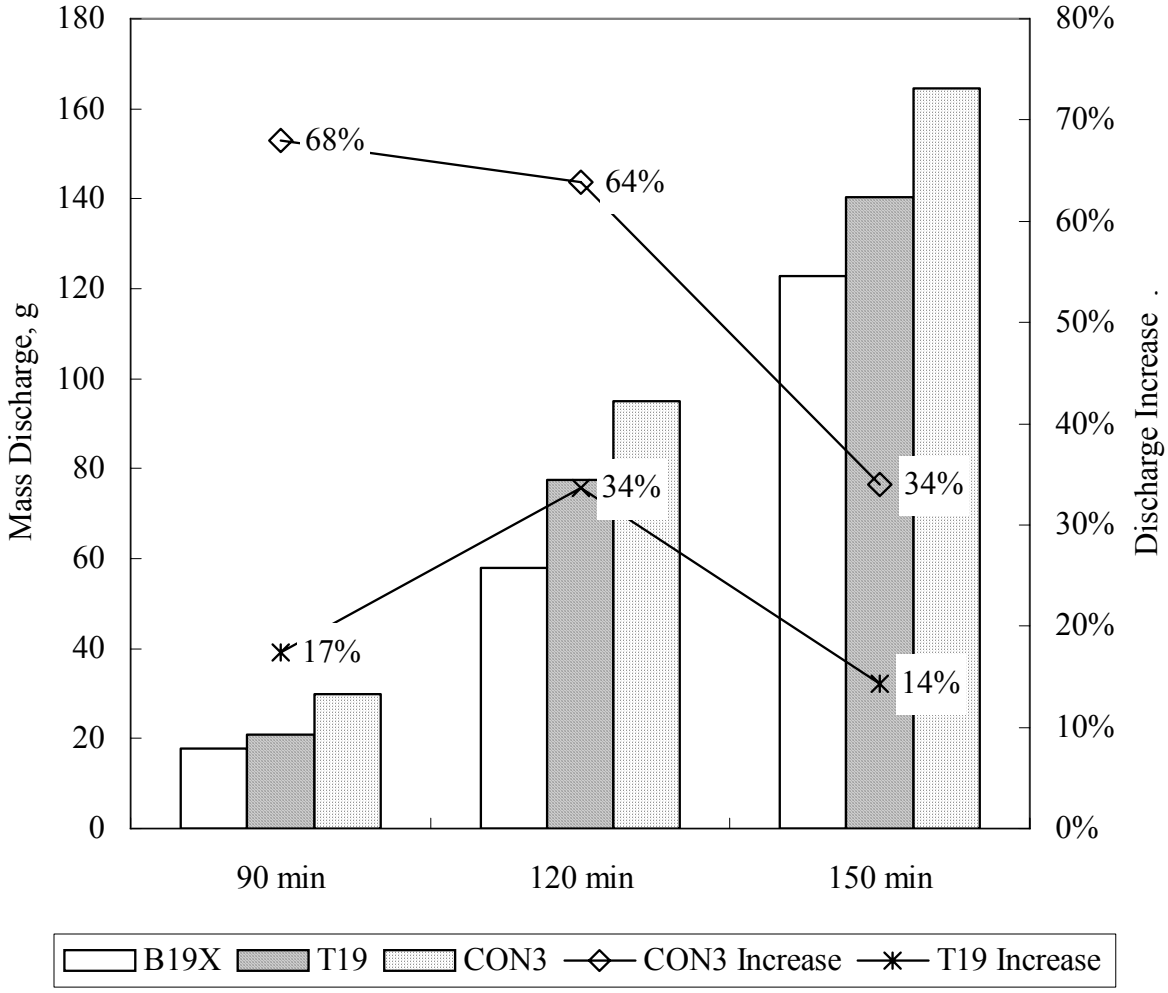

Figure 4.39 Contaminant Discharge Comparison.

The cases discussed so far are under the condition of a relatively high hydraulic gradient, in which case the groundwater flow velocity is large. The relatively insignificant tidal influence in most of these cases can be attributed to the large flow velocity, which means a large convection component of contaminant transport. When the flow velocity rises to certain level, contaminant transport would be dominated by convection over dispersion, which would consequently dwarf the tidal effect which is represented more by dispersion as the cause of local flow heterogeneity.

Next, the results are presented with the hydraulic gradient decreased from 0.1 to 0.05. The baseline cases (B20 and B20X) and the cases with tides under this condition (T20, CON1, and CON2) are as listed in Table 4.3.

First considered is a tidal period of 5 minutes and a tidal amplitudes of 20 cm, case T20. The concentration distributions at different times for case T20 are illustrated in Figure 4.40 and are compared to the baseline case B20X.

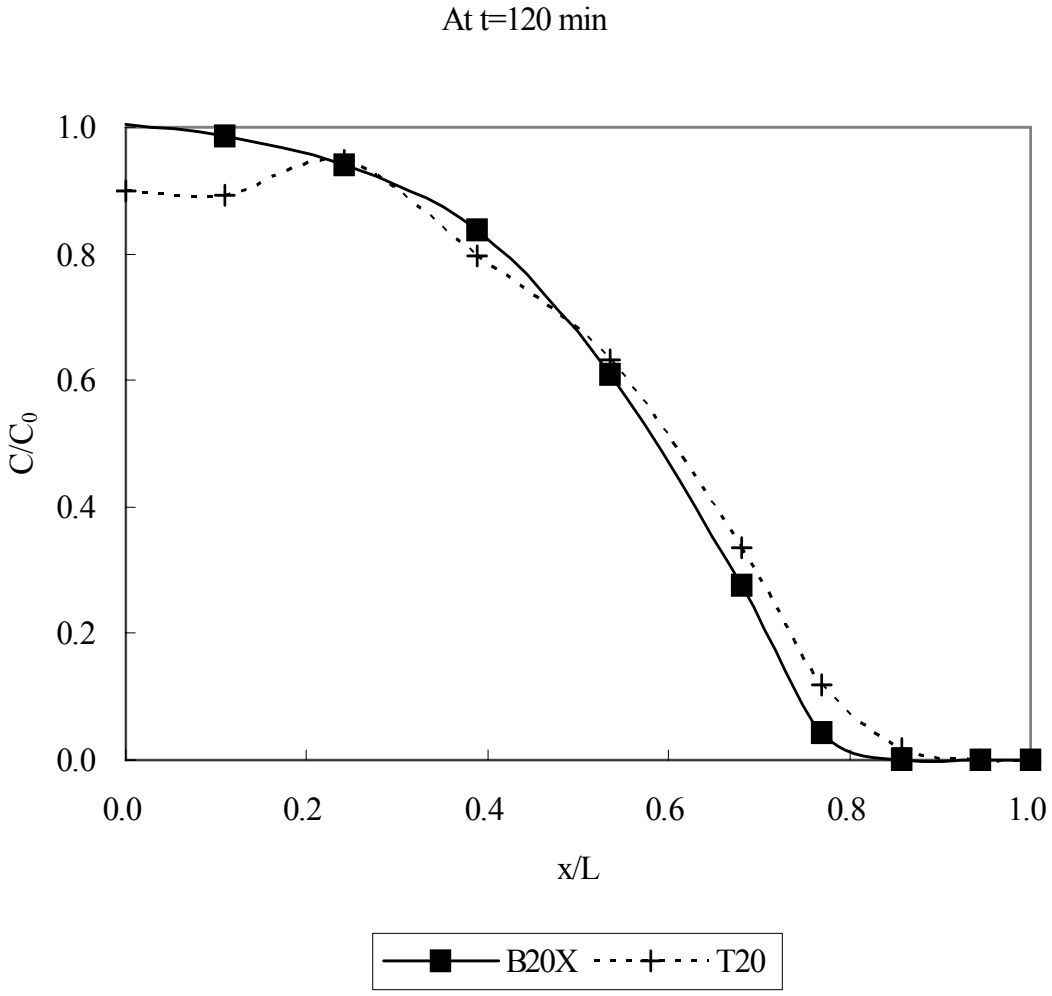

Figure 4.40 Contaminant Distribution for Case T20.

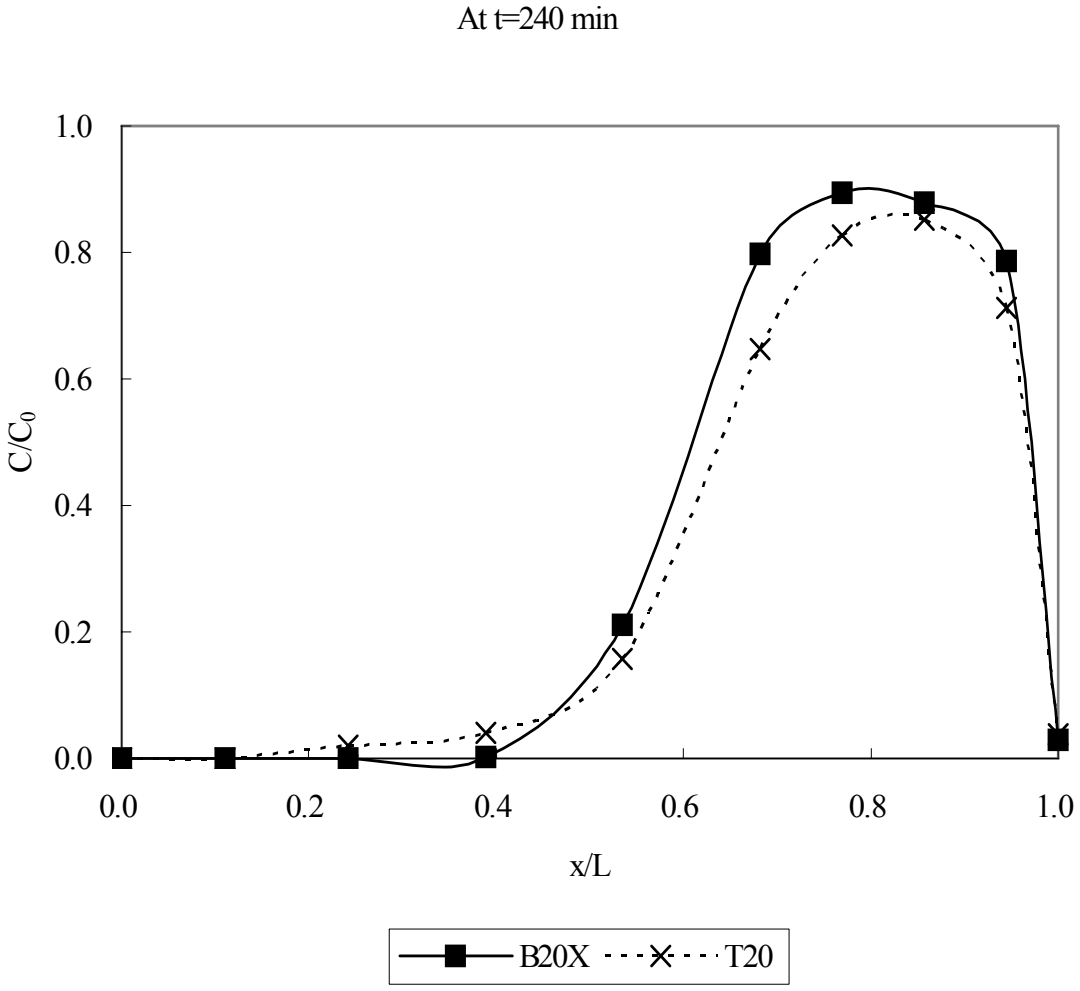

Figure 4.40 Contaminant Distribution for Case T20 (Continued).

Two points are worth noting here. One, the dilution factor considered here is increased dramatically (to 29.39) because of less experimental constraints, and this is believed to be more comparable to the coastal boundary condition. As a result, the contaminant concentration at the boundary is diluted to such a low level that it can be considered to be insignificant and ignored (thus complying with the first-type boundary condition specifying a zero-concentration). The other point is that the first-type boundary condition (case B20X) and the second-type boundary condition (case B20) do result in noticeable differences in contaminant transport as evidenced by the discharge curves in Figure 4.41. Because of the baseline used, i.e., case B20X, under the confined condition, the relatively large tidal period and moderate tidal amplitude lead to a slight influence on the contaminant transport by tidal activities (refer to Figure 4.40 and Figure 4.41).

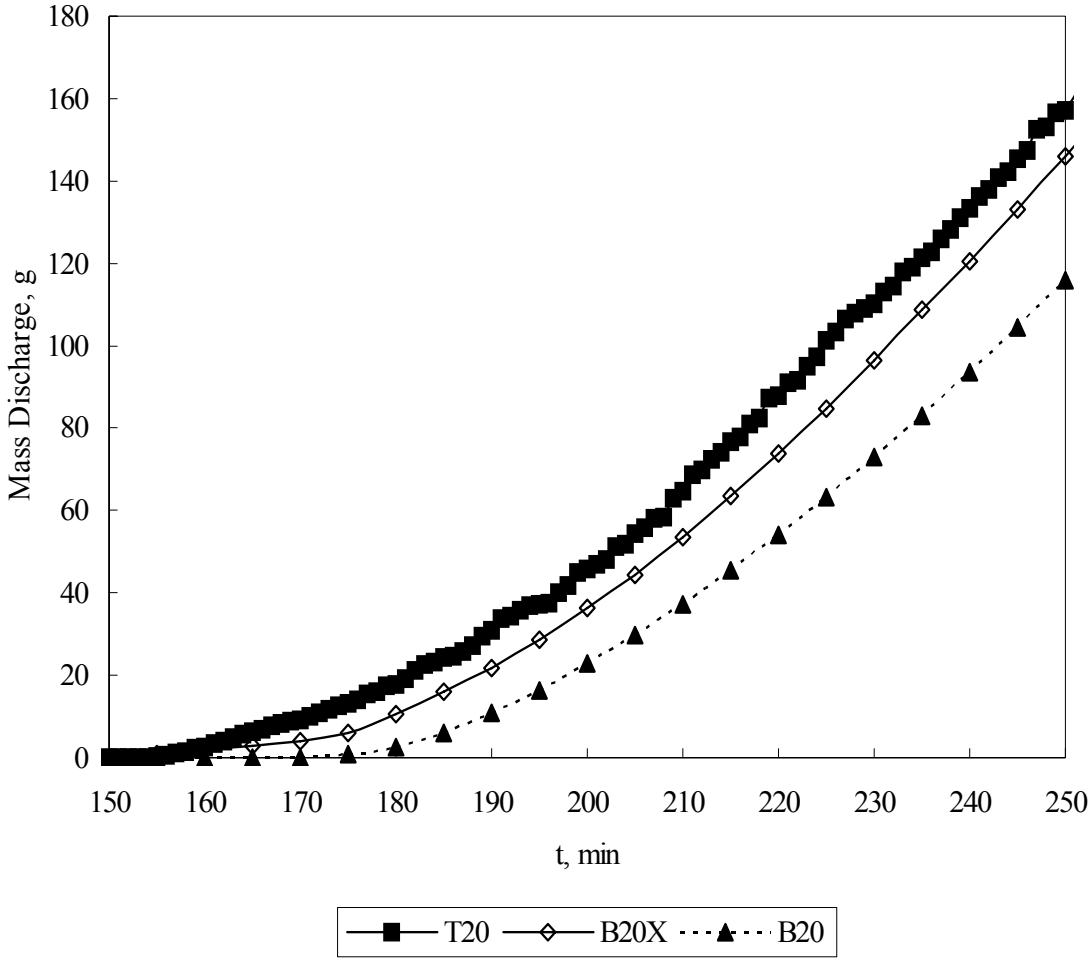

Figure 4.41 Contaminant Discharge Comparison.

Case CON2 reduces the tidal period to one minute while the tidal amplitude is kept the same as in case T20 (20 cm). Figure 4.42 gives the results regarding concentration distribution and Figure 4.43 and Figure 4.44 with regard to contaminant discharge. These results suggest that, similarly as under the condition of a hydraulic gradient of 0.1 (cases T19 and CON4), the tidal influence is slightly augmented when the tidal period is reduced. However, the absolute tidal effect as compared with case B20X is noticeable as indicated by Figure 4.43. In addition, Figure 4.44 shows that contaminant discharge is increased 16-156% in case CON2 over the baseline case B20X, but this increase is smaller (11-65%) in case T20 with the longer tidal period of 5 minutes.

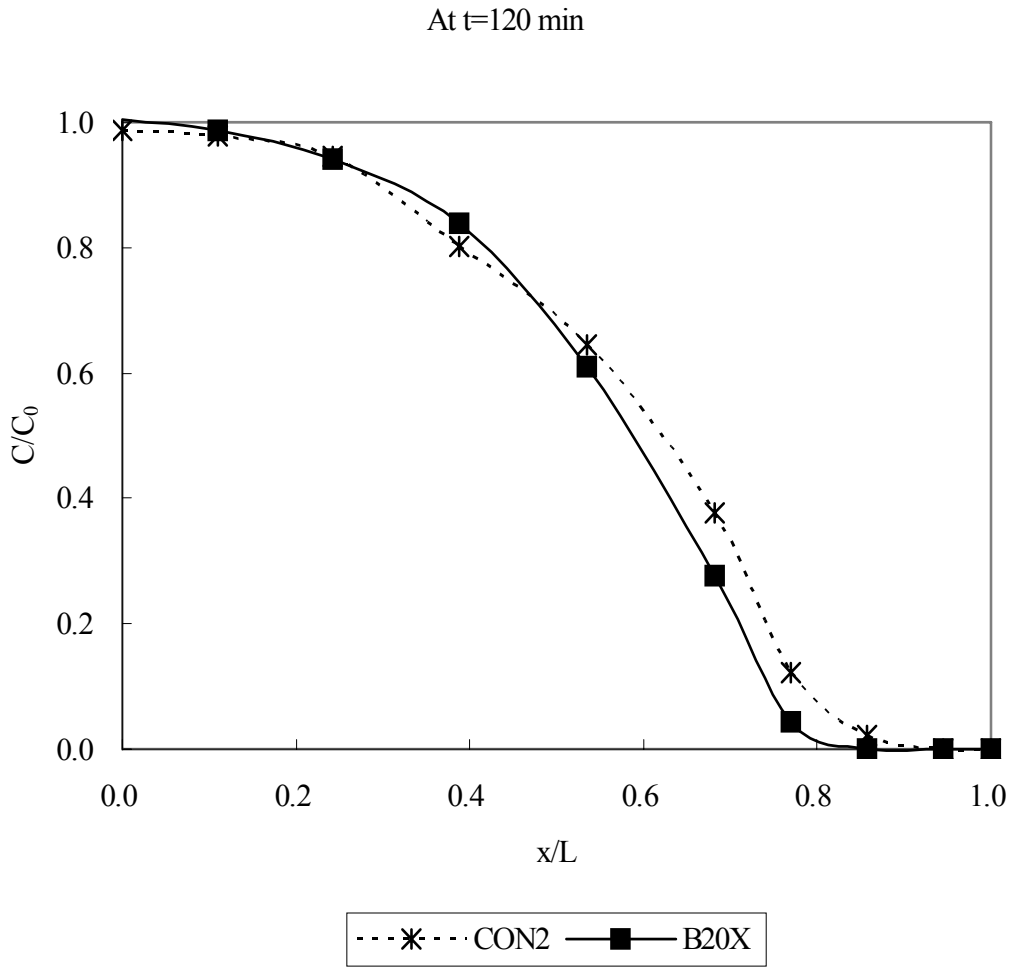

Figure 4.42 Contaminant Distribution for Case CON2.

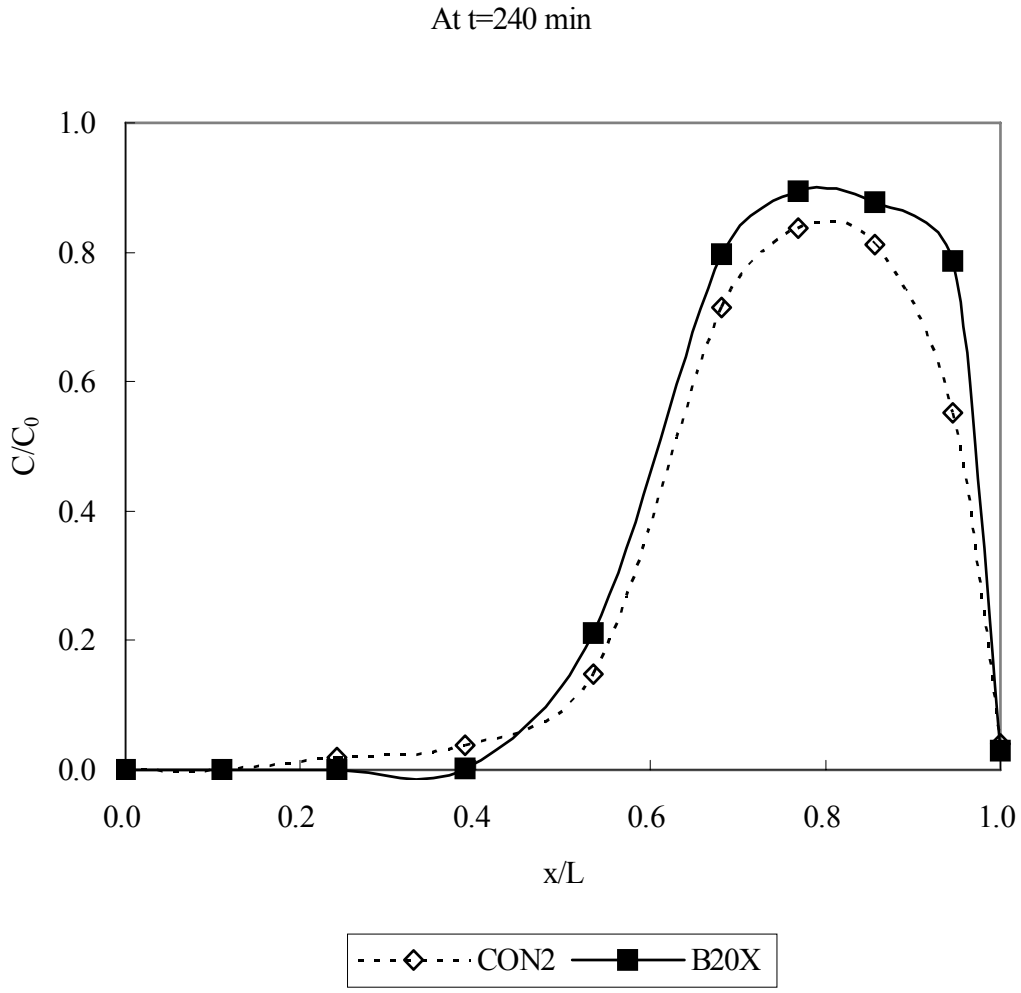

Figure 4.42 Contaminant Distribution for Case CON2 (Continued).

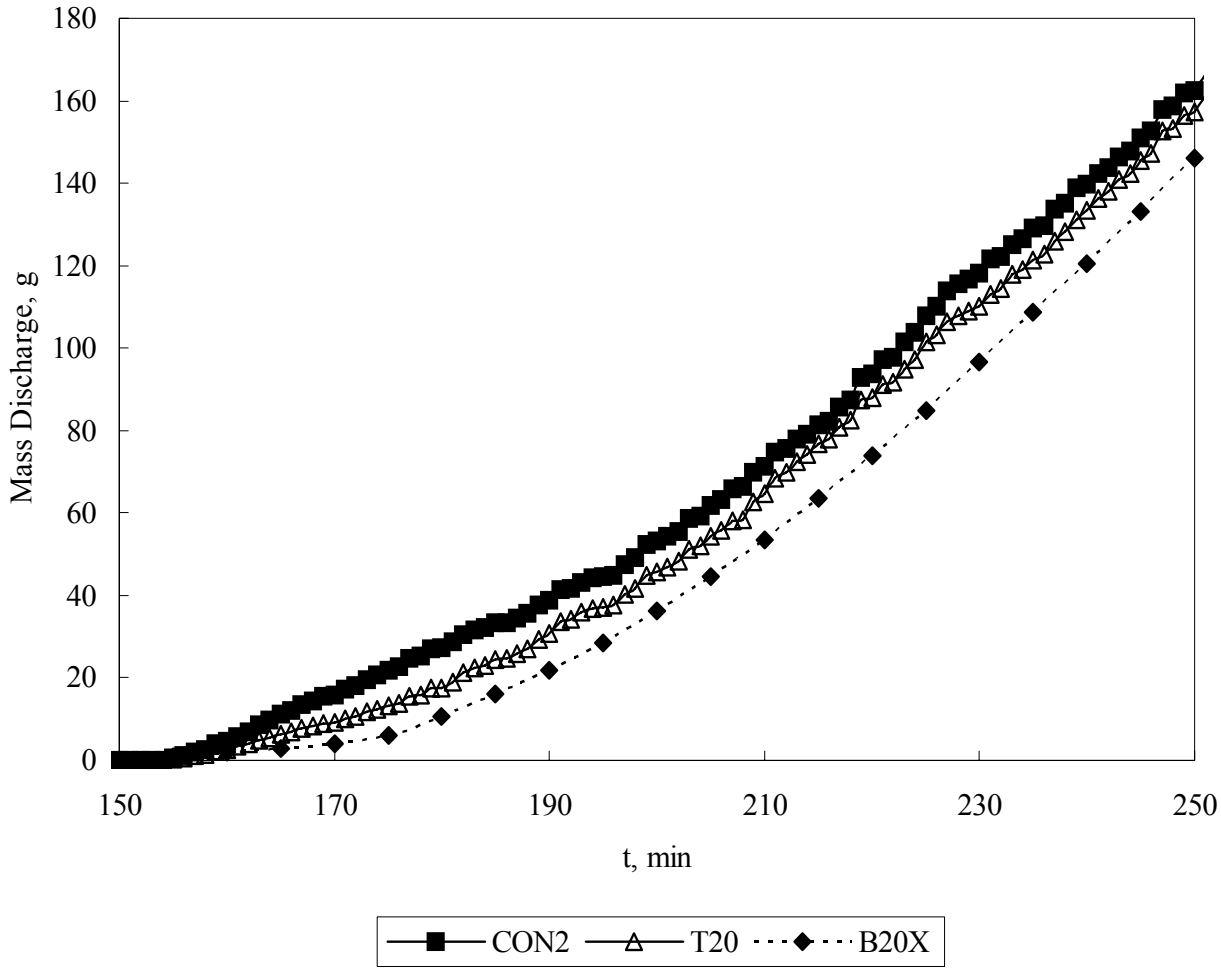

Figure 4.43 Contaminant Discharge Comparison.

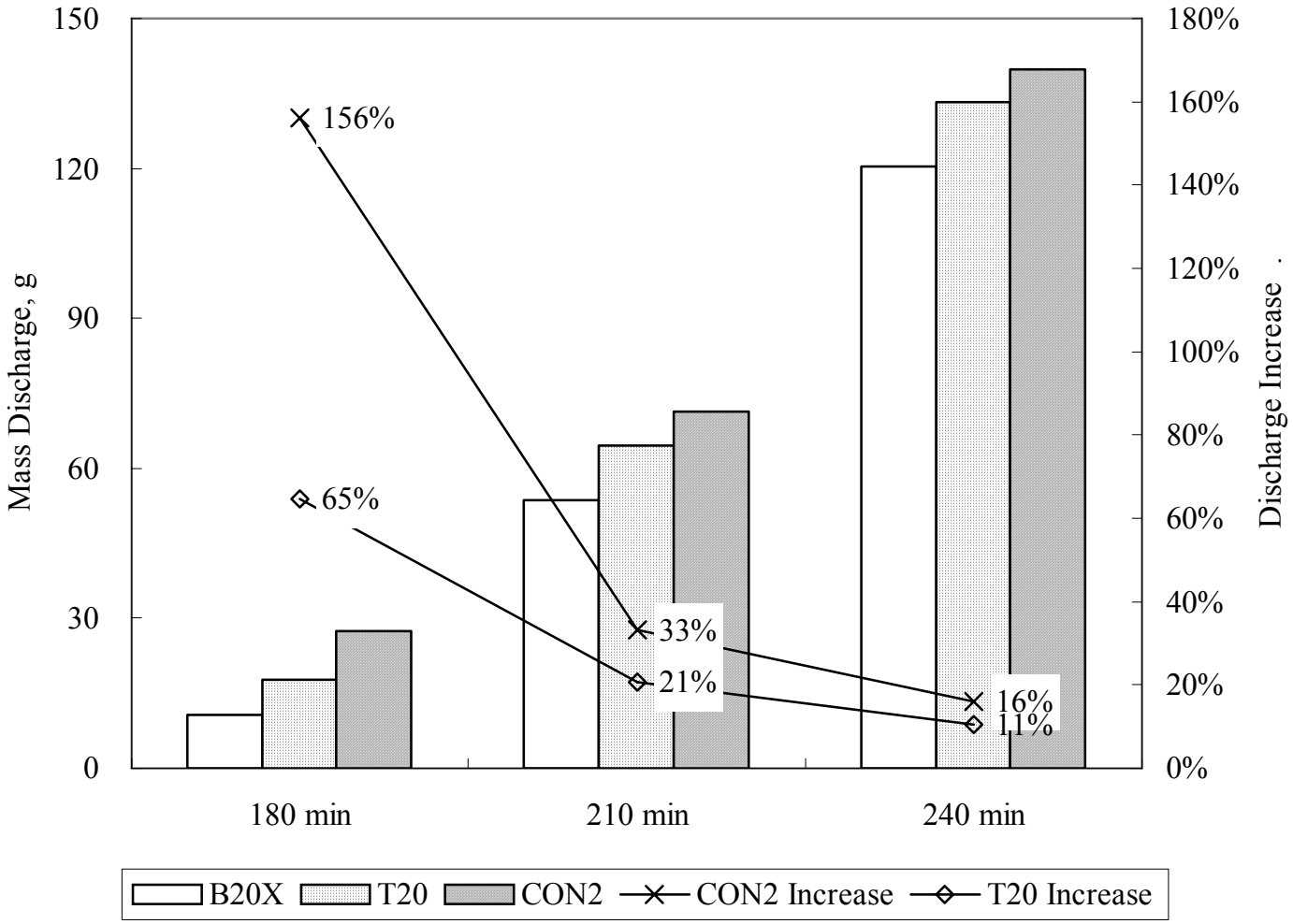

Figure 4.44 Contaminant Discharge Comparison.

Case CON1 further increases the tidal amplitude from 20 cm (in cases T20 and CON2) to 30 cm. Figure 4.45 and Figure 4.46 show the results of the concentration distribution and discharge for this case. Consistent with the aforementioned trend that the larger the tidal amplitude, the greater the tidal impact, tidal activities further reduce the concentration in the area near the boundary and enhance the contaminant discharge. As a result, the total effect of the reduced tidal period and increased tidal amplitude becomes dramatic compared to the baseline, case B20X, as well as compared to cases T20 and CON2 (see Figure 4.46). Note that the significant effect is manifest especially during the early time of discharge as shown on the discharge curves (see Figure 4.46). Figure 4.47 shows from another perspective that the discharge is enhanced by 295% at 180 minutes, 94% at 210 minutes, and 44% at 240 minutes over the baseline in case CON1. In addition, the contaminant discharge in case CON1 is greater than that in case T20 (with a small tidal amplitude of 20 cm and a longer tidal period of 5 minutes).

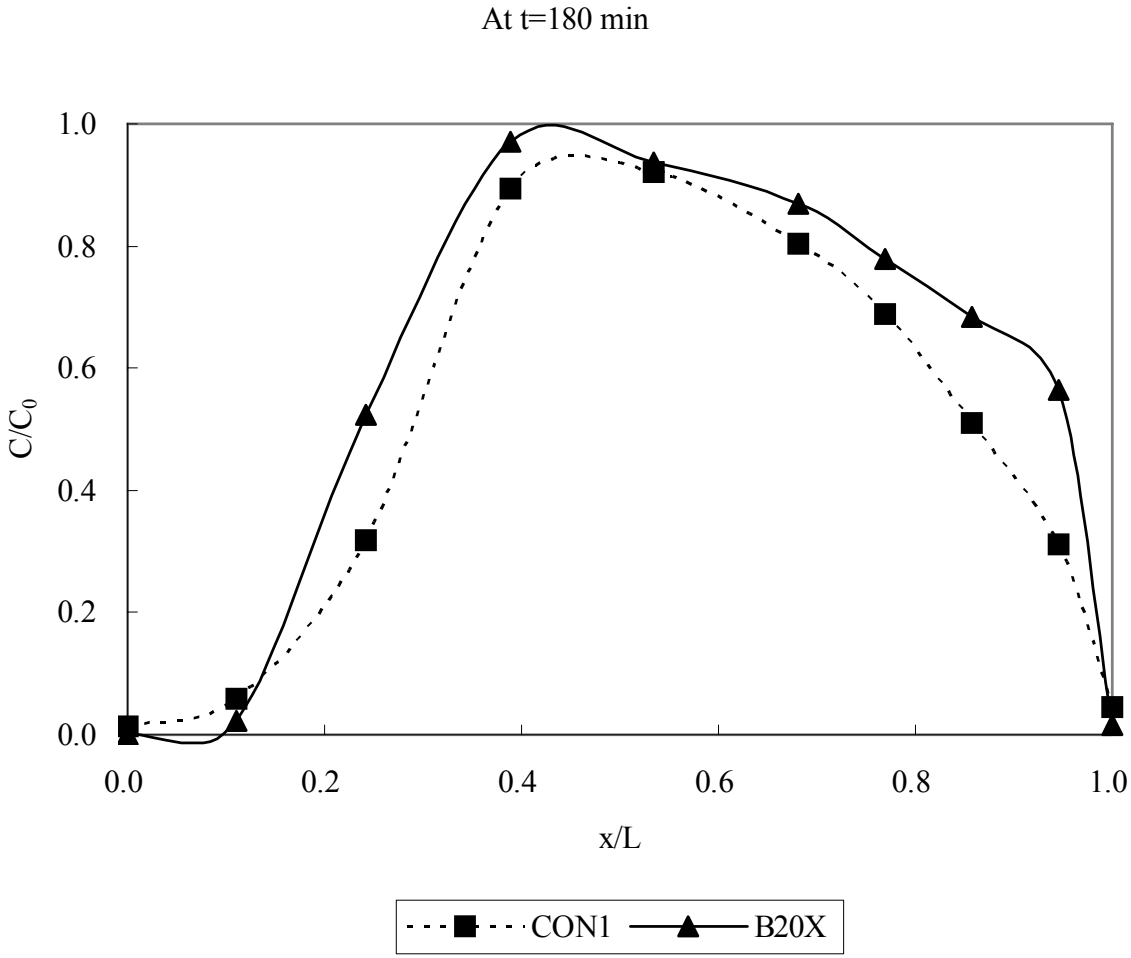

Figure 4.45 Contaminant Distribution for Case CON1.

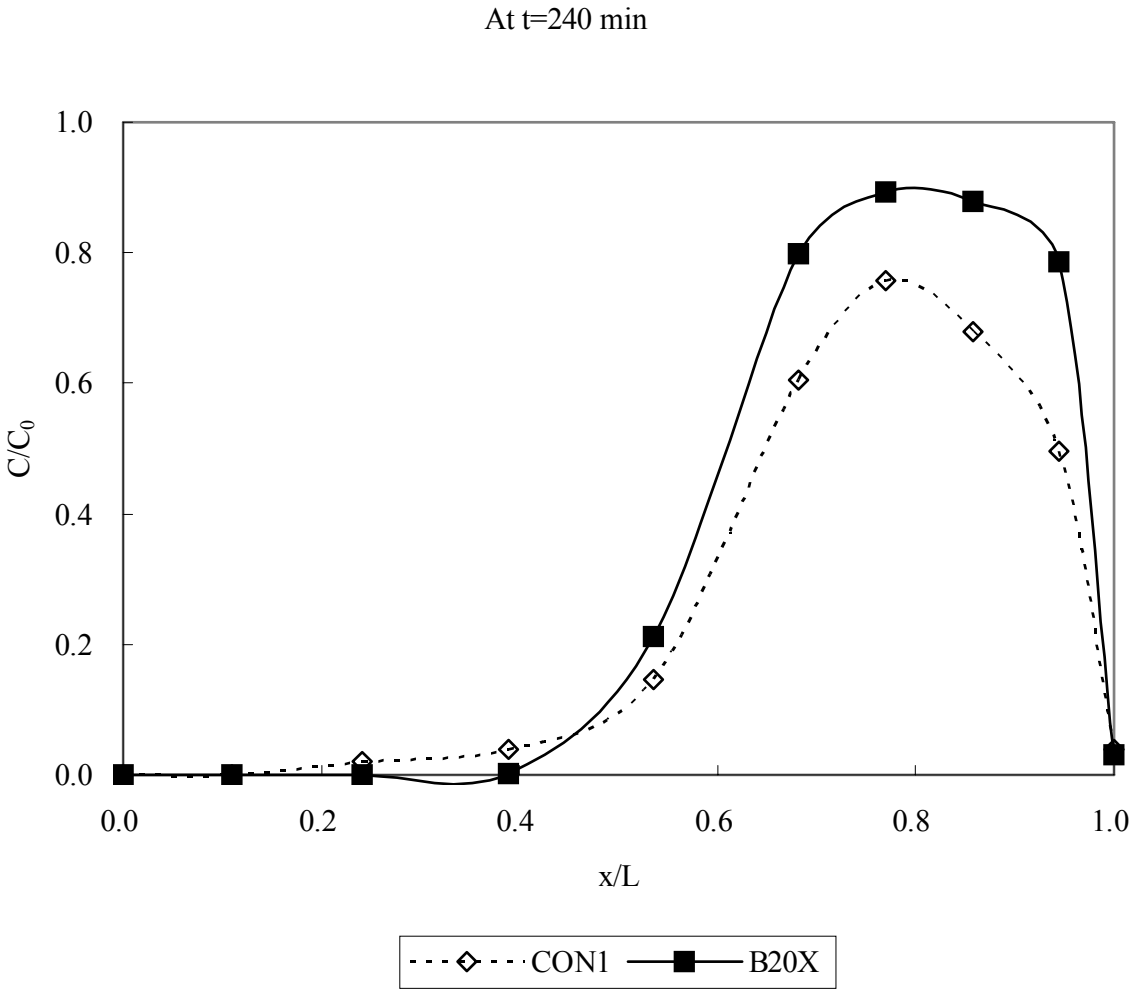

Figure 4.45 Contaminant Distribution for Case CON1 (Continued).

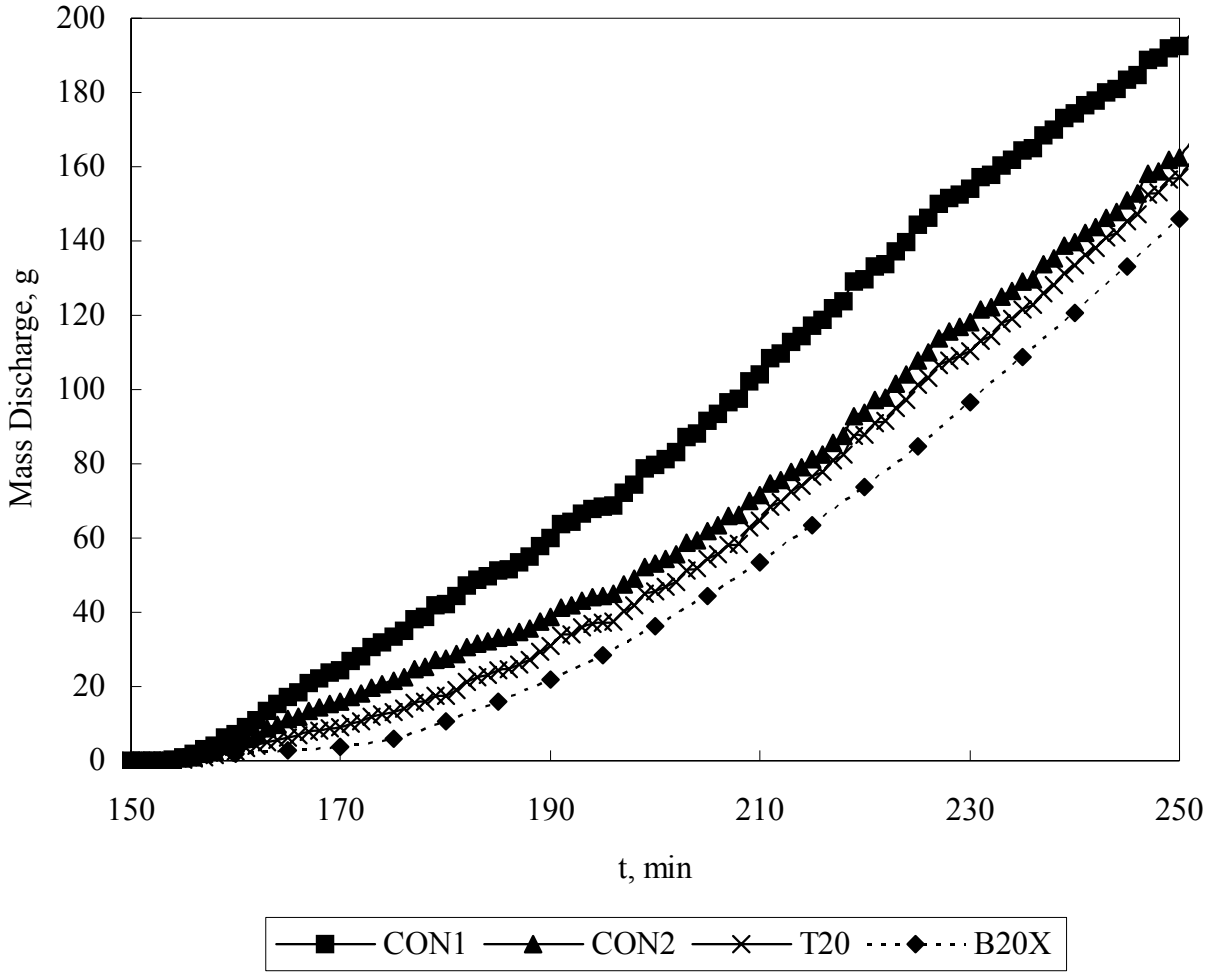

Figure 4.46 Contaminant Discharge Comparison.

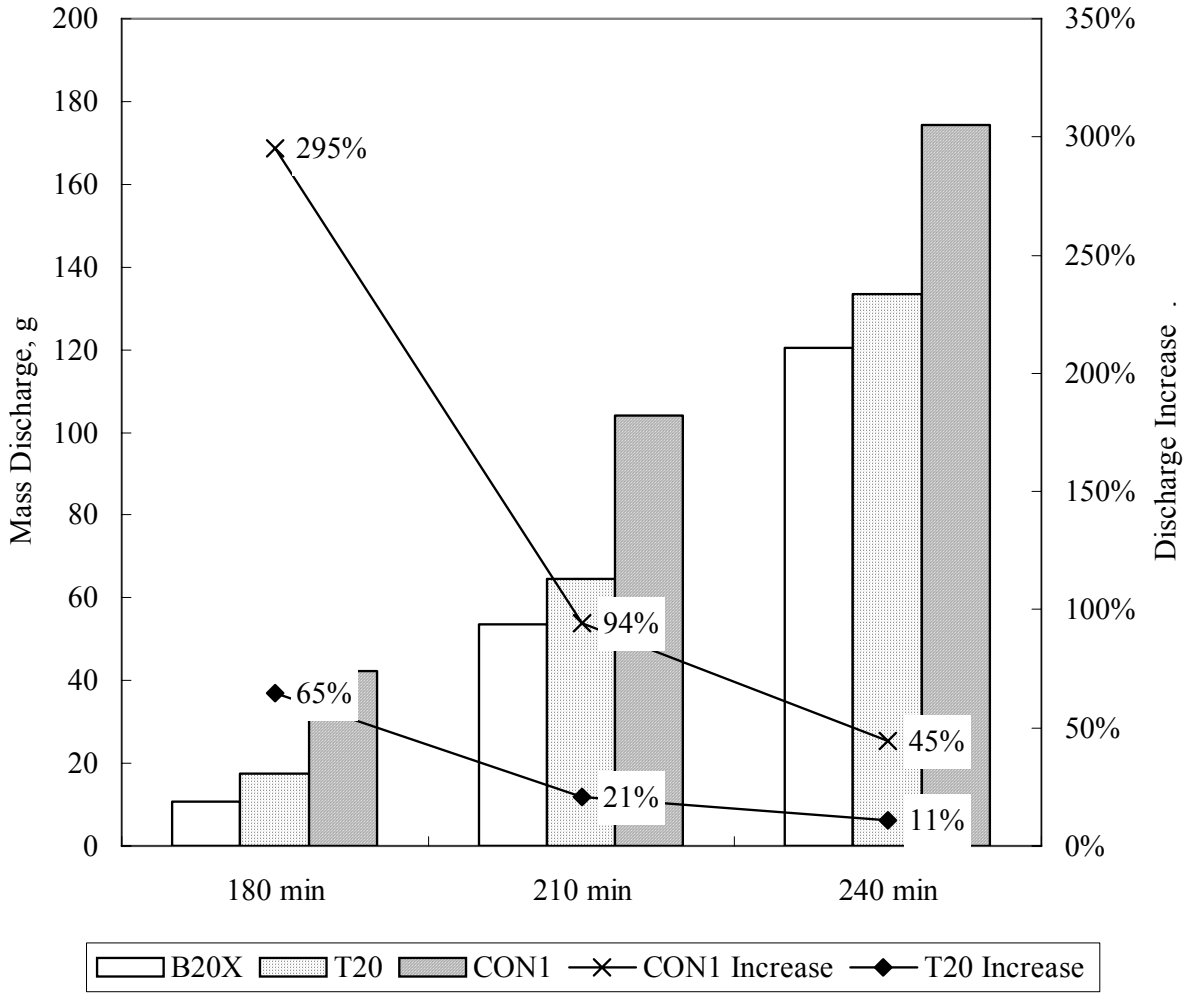

Figure 4.47 Contaminant Discharge Comparison.

4.3 Summary of Experimental Study

In the experimental study of tidal impact on contaminant transport in coastal aquifers, considered are both unconfined aquifer cases through unconfined-condition experiments and confined aquifer cases through confined-condition experiments. Tidal fluctuations are considered by varying the tidal period and tidal amplitude. The significance of the tidal influence is also evaluated under conditions of variable hydraulic gradients and dilution factors at the boundary.

4.3.1 Summary of Experimental Results

Due to the limitations and constraints of the experimental facility in the unconfined-condition experiments, a moderate dilution factor and hydraulic gradient are used. As a result, only a slight to moderate tidal influence is observed as a whole in the unconfined-condition experiments, except for case U2 in which a more significant impact resulted from a lowered tidal period and moderate tidal amplitude. These limitations and constraints, however, are avoided in the confined-condition experiments because the raised water level allowed more flexibility in choosing a larger range of parameter values. This leads to a more significant tidal impact observed in some of the cases under the confined condition experiments.

The impact on contaminant transport by the coastal boundary condition and the tides observed in the experimental study can be summarized in the following conclusions.

1. The coastal boundary condition is more correctly represented by the first-type boundary condition than by the second-type boundary condition. The experimental results with a large dilution factor are very consistent with the first-type boundary condition, and this large dilution factor is deemed a reasonable simplification and representation of the coastal water boundary. With different boundary conditions, i.e., no dilution or high dilution, contaminant concentration

distribution and discharge show noticeable differences. These differences would have given a biased perspective with regard to the tidal effect if the case under the second-type boundary condition or with no dilution had been selected as the baseline condition in the experiments.

2. The tidal effect can be important – resulting in an increase in the mass of contaminants discharged - under certain conditions: a combination of low flow velocity, high dilution at the boundary, moderate to large tidal amplitude, and low tidal period. Tidal influence is manifested more in the discharge profiles under various conditions, especially during the early stage in time after the contaminant begins to discharge. The enhancement in discharge may be tripled during very early time periods, doubled some time later, and can be increased over 40% even after a prolonged time since the initial discharge begins.

3. The importance of the tidal effect is influenced by the tidal amplitude: the tidal effect increases with tidal amplitude but the magnitude of this increase is influenced by other factors (hydraulic gradient, tidal period, and degree of dilution). In the unconfined-condition experiment, only with a relatively large tidal amplitude, i.e., over 20 cm, may the tidal effect be noticeable.

4. The importance of the tidal effect is also influenced by the tidal period and dilution in the boundary water. Tidal period affects the frequency at which tidal water washes into and out of the aquifer. Dilution, on the other hand, affects the contaminant concentration in the boundary water. With a higher dilution, tidal water would push cleaner water into the aquifer when the tidal water rises, and would enhance the diffusion of contaminant when the tidal water falls. The tidal effect would have been more dramatic in the open-tank experiments if the dilution factor and tidal frequency could have been increased more as was done in the confined-condition experiments.

5. The significance of the tidal effect is also subject to the hydraulic gradient. Groundwater flow velocity, and thus the speed at which the contaminant is transported, is directly related to the average regional hydraulic gradient. A large flow velocity means a large convection component of contaminant transport. When the flow velocity rises to certain level, contaminant transport would be overwhelmingly dominated by convection over dispersion, which would consequently overshadow the tidal effect, which resembles dispersion in the way it causes local flow heterogeneity.

6. Tidal fluctuations can have variable impacts on contaminant transport in unconfined and confined aquifers. Under unconfined conditions, the tidal impact is slightly more dramatic than under confined conditions with similar tidal parameters. Under even slightly more stringent conditions in the unconfined case (see case U2 in Figure 4.28), for example, contaminant discharge with tides is increased by 187% at 180 minutes, 83% at 210 minutes, and 40% at 240 minutes. But under similar conditions in the confined case (see case CON2 in Figure 4.44),

the contaminant discharge enhanced by 156% at 180 minutes, 33% at 210 minutes, and 16% at 240 minutes.

4.3.2 Application of Experimental Results

As discussed in Section 4.1.1 of this text, the experimental model is set up to be similar to the prototype according to the scale listed in Table 4.1. This means that whatever results are gained in the experiments can be used to interpret what happens in the prototype (field conditions) so long as the field conditions fall within the range of values for the prototype outlined in Table 4.1.

As an example, in the confined-condition experiment case CON2, the parameters considered include a hydraulic gradient of 0.05, tidal amplitude of 20 cm, and tidal period of 1 minute. In that case, it is found that the contaminant discharge increase due to tidal fluctuations is 156% and 33% at time 180 minutes and 210 minutes, respectively (refer to Figure 4.44). By similarity, these results apply to the field conditions calculated in Table 4.6. Specifically, this means that in an aquifer system of 1200 feet long and 30 feet deep, tidal fluctuations with a 2-foot amplitude would lead to a 156% discharge increase after 125 days and a 33% increase after 146 days. Similar explanations apply to other aquifer and experimental conditions.

Table 4.6 Interpretation of Experimental Results

Parameters	Prototype (typical value)	Scale	Model value
Aquifer Length, ft	1200	λ_h=0.01	12
Aquifer Thickness, ft	30	λ_v=0.1	3
Hydraulic Gradient	0.005	i_s= 10 (λ_v/λ_h)	0.05
Flow Velocity, ft/d	5	V_s=10 (K_s i_s)	50
Tidal Period, hr	12	T_s=0.001 (λ_h/ V_s)	1 min
Tidal Amplitude, m	2	λ_v=0.1	0.2
Time, day	125	T_s=0.001 (λ_h/ V_s)	180 min
Time, day	146	T_s=0.001 (λ_h/ V_s)	210 min

CHAPTER 5

NUMERICAL STUDY

Equation Chapter 5 Section 1In the previous chapter, experimental results are presented demonstrating the impact on contaminant transport by tidal fluctuations. Experimental study also verifies that the coastal boundary condition may be better represented by the first-type boundary condition than by the second-type boundary condition. This chapter presents the numerical results with regard to tidal influence. The numerical study takes advantage of its strong capability of simulating groundwater flow and contaminant transport under conditions which can otherwise not be achieved in the experimental study due to certain restrictions. In this chapter, tidal fluctuations are studied in two aspects: their impact on hydraulic heads and on contaminant transport. The tidal effect is also evaluated by comparing its significance under various conditions of varying flow velocity, retardation, decay, aquifer dimension, and aquifer confining status.

5.1 Tide Induced Groundwater Table Fluctuations

It has been mentioned in the LITERATURE REVIEW that there are inconsistencies about how far inland from the coastline the tide influences water table fluctuations in unconfined aquifers, and that there is also a significant difference in the potential influence area between confined and unconfined aquifers. In this section, these topics are discussed in further detail using the numerical solution developed in Chapter 3.

In this study, attention is given to the situation whereby the water table fluctuations induced by tides are negligible compared to aquifer thickness, thus equation (3.5) derived in Chapter 3 applies for both confined and unconfined aquifers, that is,

$$h = h_0 - i_r\left(L - x\right) + Ae^{-\beta(L-x)}\sin\left(\omega t - \beta\left(L - x\right)\right) \tag{5.1}$$

where $\beta = \sqrt{\pi S / \delta T}$.

This solution shows that the tidal oscillations remain sinusoidal with a time lag and exponential decrease in amplitude (tidal efficiency factor) with distance from the coastline (Erskine, 1992).

$$\text{Tidal Efficiency Factor} = e^{-(L-x)\sqrt{\pi S / \delta T}} \tag{5.2}$$

Notice that the difference between the confined aquifer and the unconfined aquifer with regard to equation (5.1) is the storage coefficient, S, assuming that all the other conditions are the same. For the confined aquifer, S is the storativity, while for the unconfined aquifer, S represents specific yield. Since the specific yield of an unconfined aquifer is generally several orders of magnitude greater than the storativity of a confined aquifer, it is anticipated that the tidal effect would be different.

Consistent with the conditions used for baseline selection in Chapter 3, the conditions used for the evaluation of tidal influence on groundwater flow and contaminant transport are in the typical ranges of parameter values which are commonly encountered in coastal aquifers around the world. The basic values for the parameters considered in this study are listed in Table 5.1, and some of the parameter values will be changed such that their impact can be evaluated.

Table 5.1 Parameter Values Used in the Evaluation of Tidal Influence

Parameter Name	Unconfined Aquifer	Confined Aquifer
Tidal Period, hour	12.5	12.5
Tidal Amplitude, m	1.0	1.0
Specific Yield / Storativity	0.15	0.005
Porosity	0.3	0.3
Hydraulic Conductivity, m/day	15	15
Average Regional Hydraulic Gradient, m/m	0.01	0.01
Contaminant Release Concentration, kg/m^3	1.0	1.0
Contaminant Release Duration, year	1.0	1.0
Dispersivity, m	10	10
Retardation Factor	1.0	1.0
Decay Constant, day^{-1}	0	0
Aquifer Thickness, m	10	10
Aquifer Length, m	100	100
Coastline Length, m	100	100

The storativity of a confined aquifer and the specific yield of an unconfined aquifer are chosen to be 0.005 and 0.15, respectively. All these are representative values for medium sand (Todd, 1980). And the coastline length of 100 meters is used as a base for the calculation of total contaminant mass discharge and for convenient comparison of tidal influence on contaminant discharge under various conditions. As a result, the constant contaminant release of one year is equivalent to a total release of 1825 kg contaminant over a hundred meter coastline.

Figure 5.1 shows the trend of tidal efficiency factor changes over distance from the coastline. It is demonstrated that the tidal amplitude is damped quickly in an unconfined aquifer as it goes inland, while the confined aquifer tends to have a much smaller capability to damp the tidal fluctuations. If it is further assumed that wherever the tidal efficiency factor is greater than 5%, the tide-induced water level fluctuations are significant, then the distance whereby tides have a significant effect on water level is dramatically different between unconfined and confined aquifers. And note that this

distance in confined aquifer is about 230 meters inland, which is about six times greater than that in an unconfined aquifer, i.e., about 40 meters. These results are consistent with Serfes (1991), Erskine (1991), and White and Robert (1994), but are not consistent with Li et al (2000) and Lanyon et al. (1982).

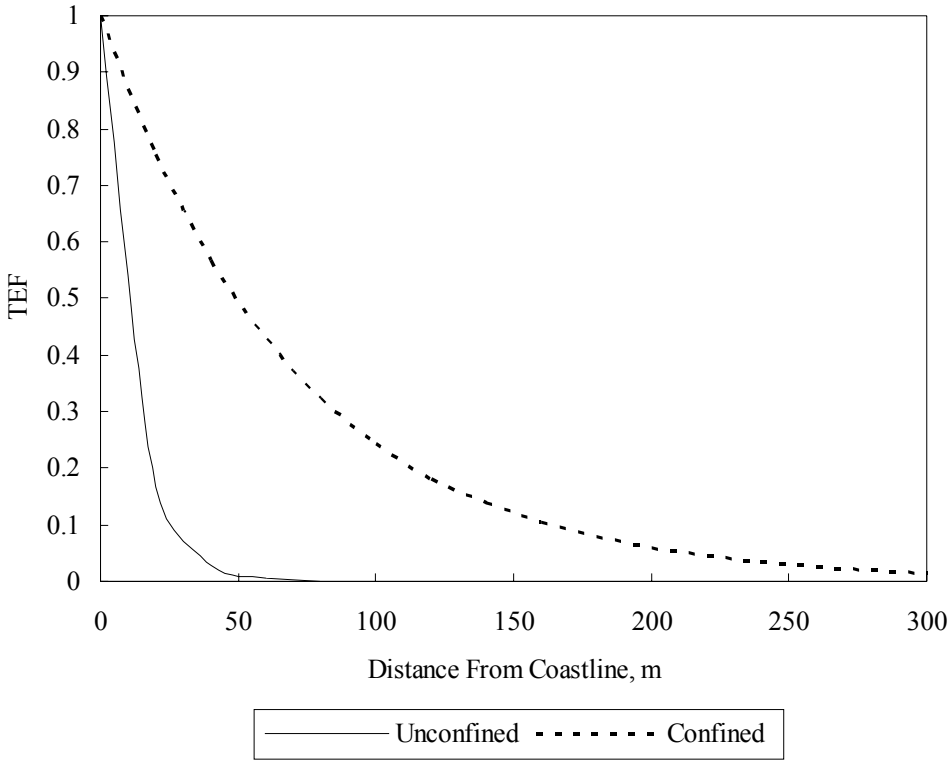

Figure 5.1 Tidal Efficiency Factor under Confined and Unconfined Conditions.

5.2 Tide Induced Contaminant Transport Fluctuations

From the previous section it is shown that a dramatic difference in the tidal effect on hydraulic heads resulted from the confined condition compared with the unconfined condition in terms of potential impact area, i.e., the affected distance inland from the coastline. But what about the tidal effect on contaminant transport in these two

situations? Would tides influence contaminant transport the same way as they affect hydraulic heads? Or would it be just the reverse? These questions, in addition to the tidal influence under all sorts of other conditions, are analyzed in this section.

With the same conditions used in the previous section, the contaminant distribution along the aquifers at different points in time is illustrated in Figure 5.2. From the concentration profiles it is observed that the tidal effect on contaminant transport is much more dramatic in an unconfined aquifer than that in a confined aquifer, which is unexpectedly the opposite of its effect on hydraulic head fluctuations. At some point in time (approximately 200 days), the distance from the coastline affected by tides is of the same magnitude for both the confined aquifer and the unconfined aquifer, while at the other times shown, this distance is slightly larger for the unconfined case. Also notice that this distance is consistent with what is observed in the previous section for an unconfined aquifer, i.e., about 60 meters, but surprisingly, this distance is more than an order of magnitude smaller than the potential effect distance regarding hydraulic head fluctuations for an confined aquifer.

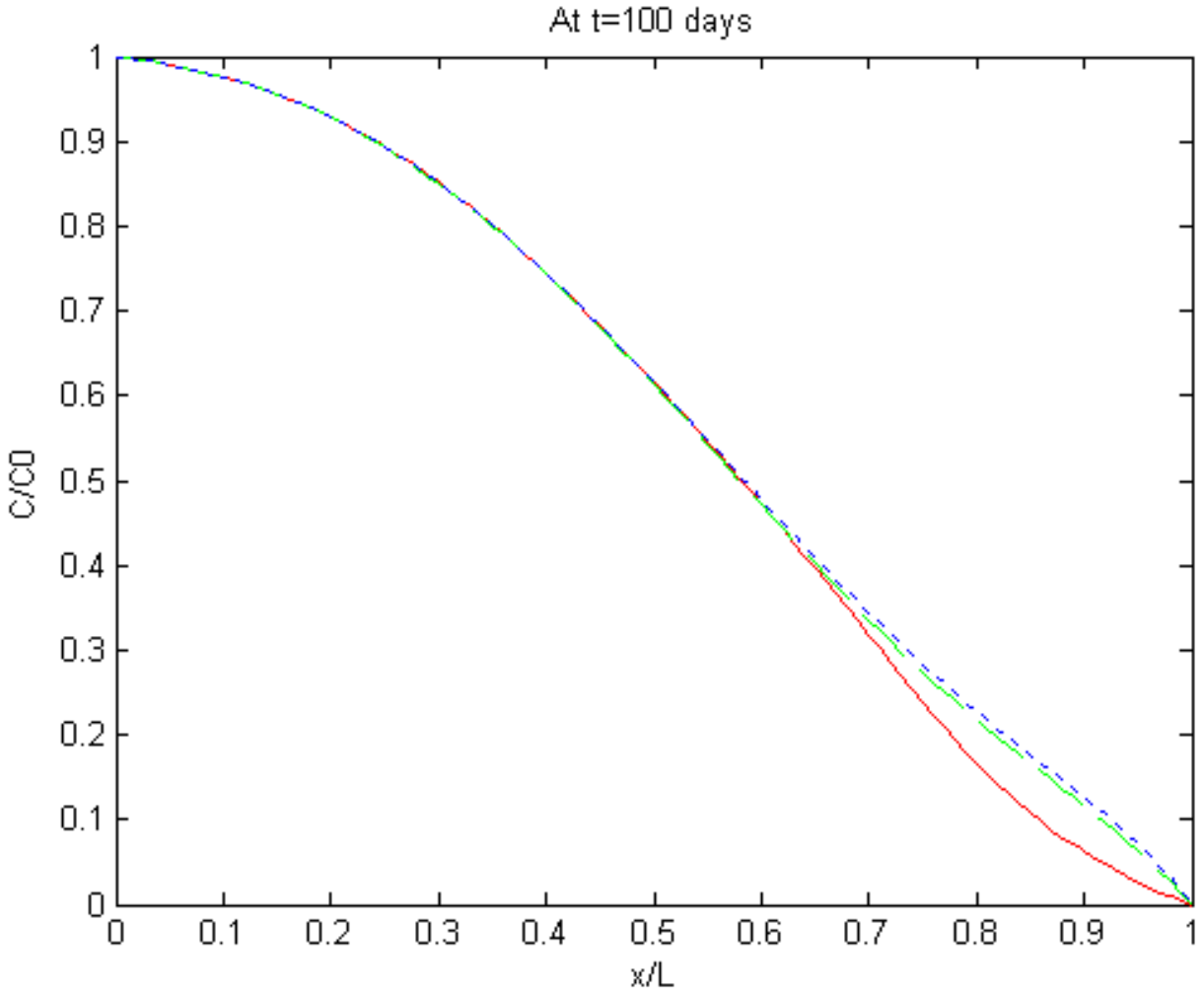

Legend: Dot-Baseline (without tidal effect), Dash-Confined, Solid-Unconfined

Figure 5.2 Tidal Effect on Contaminant Distribution in Confined versus Unconfined Aquifers.

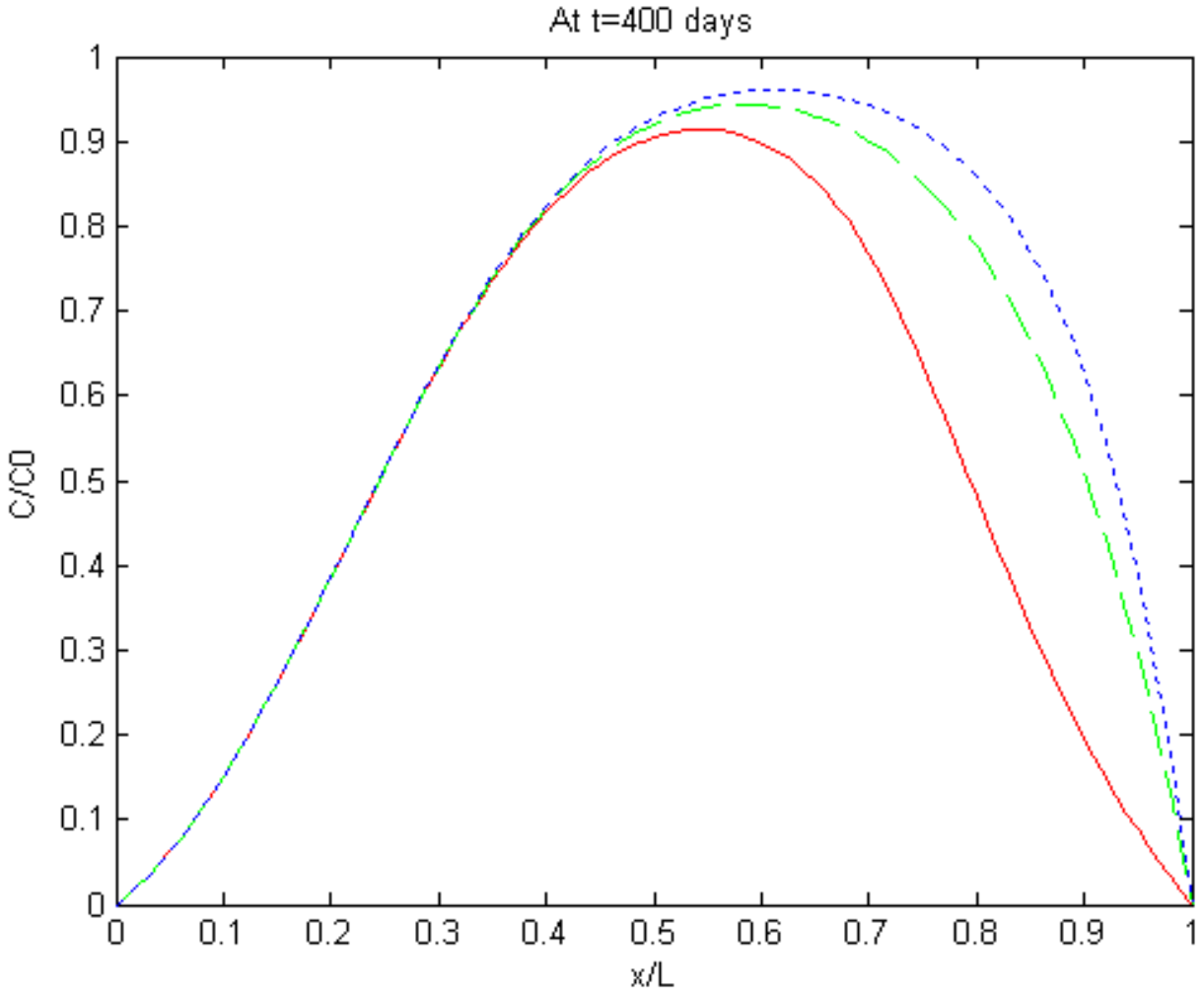

Legend: Dot-Baseline, Dash-Confined, Solid-Unconfined

Figure 5.2 Tidal Effect on Contaminant Distribution in Confined versus Unconfined Aquifers (Continued).

Next, the tidal effect on contaminant mass discharge is compared for the confined and unconfined cases. The contaminant mass discharge for the different cases at different points in time is shown in Figure 5.3.

Two important observations are worth mentioning. One, tidal fluctuations have a significant impact on mass discharge, especially under unconfined condition and during the early stages since the initial discharge starts. After 100 days since the contaminant release begins, for example, mass discharge for the unconfined case is more than doubled (110%) over the baseline (60.1 kg versus 28.6 kg), while it is enhanced by 25.8% for the confined case. After 200 days, mass discharge for the unconfined case is still augmented by over 30%. The other important observation is that, consistent with the effect on concentration distribution, the tidal impact on mass discharge is more significant in the unconfined case than in the confined case. After 200 days, for instance, mass discharge for the unconfined case is increased by 31%, in contrast to an increase of only 8% over the baseline for the confined case; after 300 days, these numbers are 13% for the unconfined case and 3.4% for the confined case.

Finally, note that under both the confined and unconfined conditions, the increase in contaminant mass discharge over the baseline condition decreases as time after the initial discharge increases, particularly in the confined case.

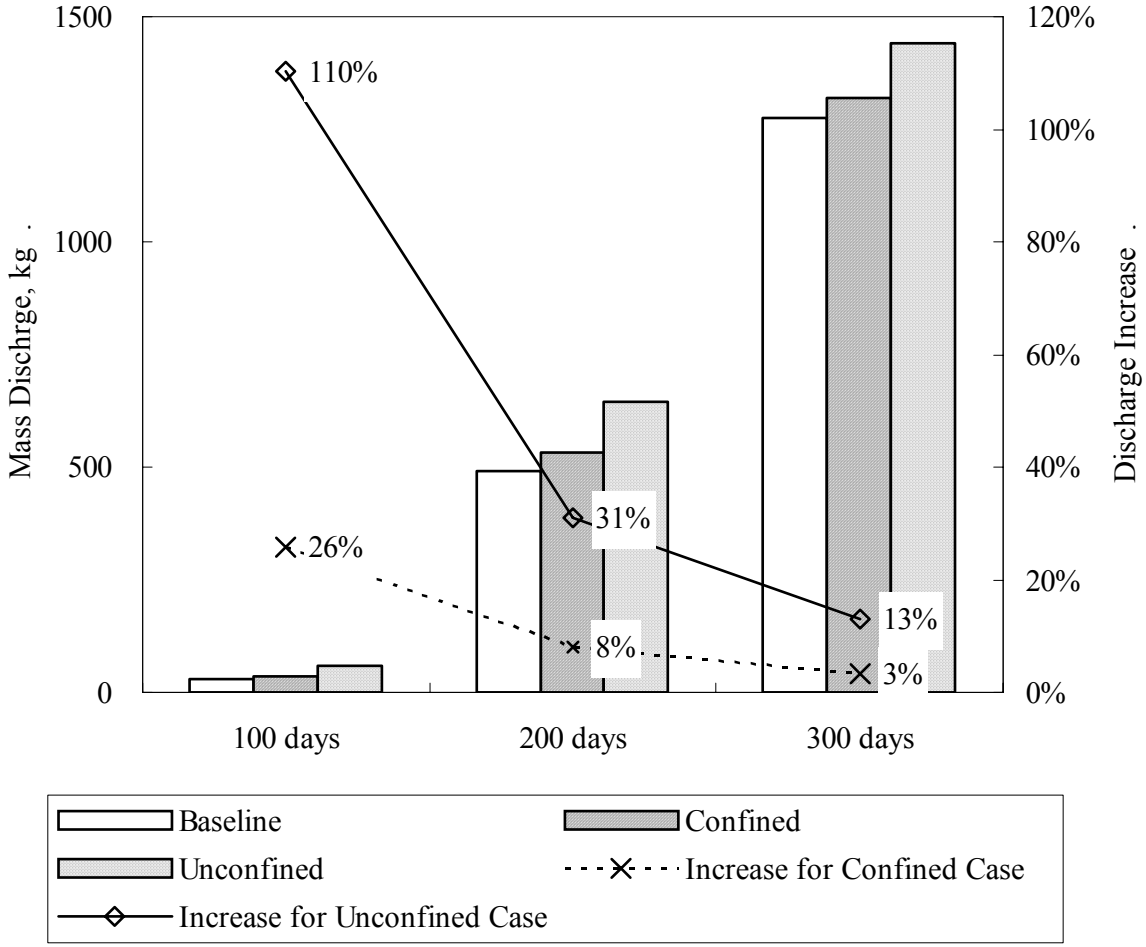

Figure 5.3 Tidal Effect on Contaminant Discharge under Confined versus Unconfined Conditions.

5.3 Tidal Influence under Unconfined Condition

This section presents the tidal influence on contaminant transport under the unconfined condition. It is worth redefining the parameters that are used for a convenient comparison of the results. These parameters are:

$$T = Vt/L, \text{ and } Z = x/L \tag{5.3}$$

Here, T is the number of displaced pore volumes, and Z the reduced distance (van Genuchten and Alves, 1982). These parameters are used as the temporal and spatial dimensions unless otherwise specified.

5.3.1 Effect by Tidal Amplitude

Tidal amplitude changes with locations on the earth and with time at different points during the day, month, and year due to particular relation between the sun, earth, and moon (Ippen, 1966). Compared here is how fluctuations in contaminant transport respond to tidal amplitude change. Table 5.2 lists the cases and assigned parameter values used for the evaluation for tidal effect.

Table 5.2 Cases Assigned in Evaluation of Tidal Effect

Case No.	N1 (Baseline)	N2	N3	N4
Tidal Amplitude, m	0.0	0.5	1.0	2.0

Figure 5.4 illustrates the contaminant concentration distribution at different points in time. It demonstrates the consistent influence by tidal fluctuations in a region extending as far as approximately 60% of the aquifer length from the coastline, which is equivalent to 60 meters. The results lead to the same conclusion as in experimental study: the significance of tidal influence is approximately proportional to the tidal amplitude.

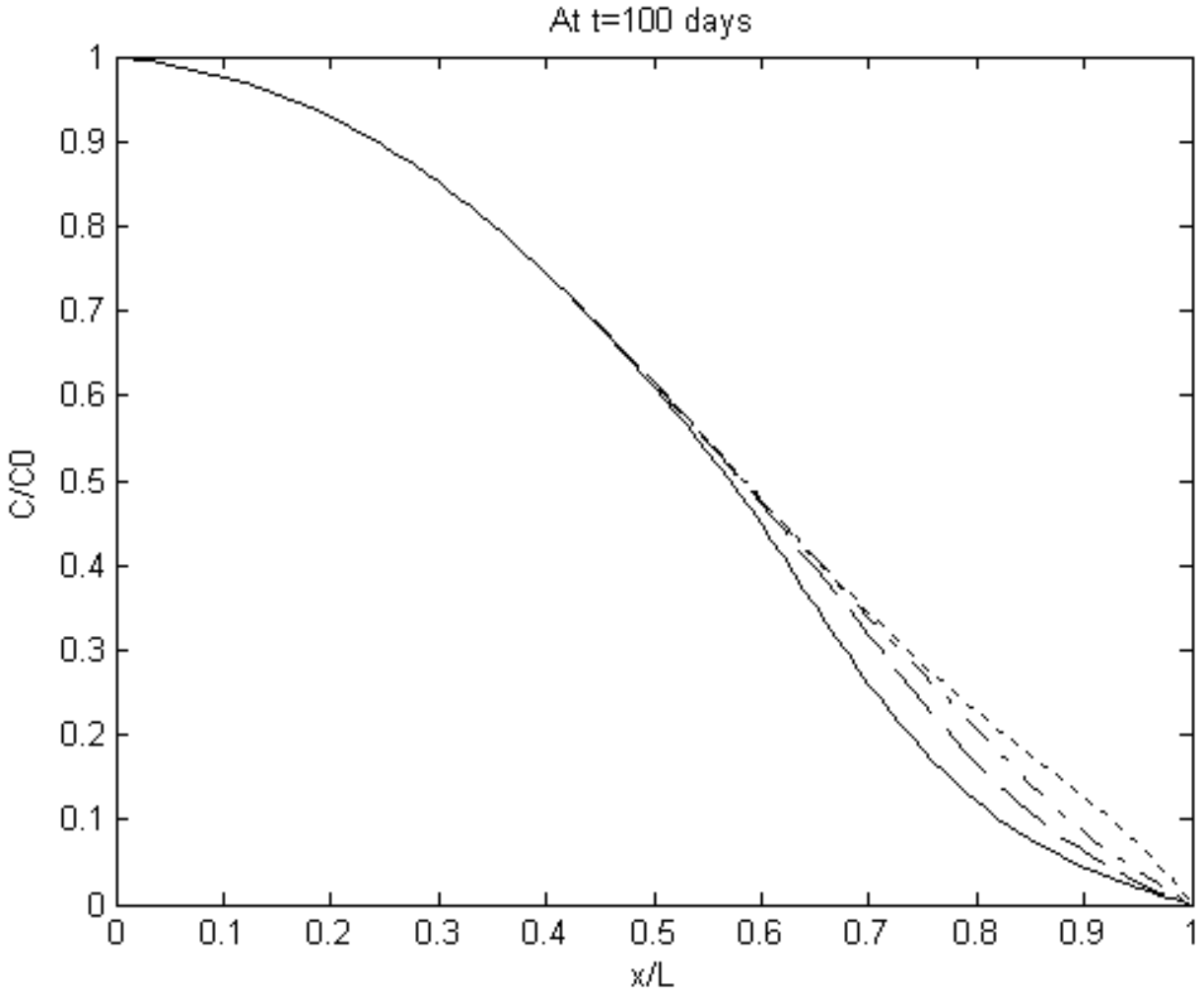

Legend: Dot-N1 (Baseline), Dash-N2, Dash Dot-N3, and Solid-N4

Figure 5.4 Tidal Effect on Contaminant Distribution.

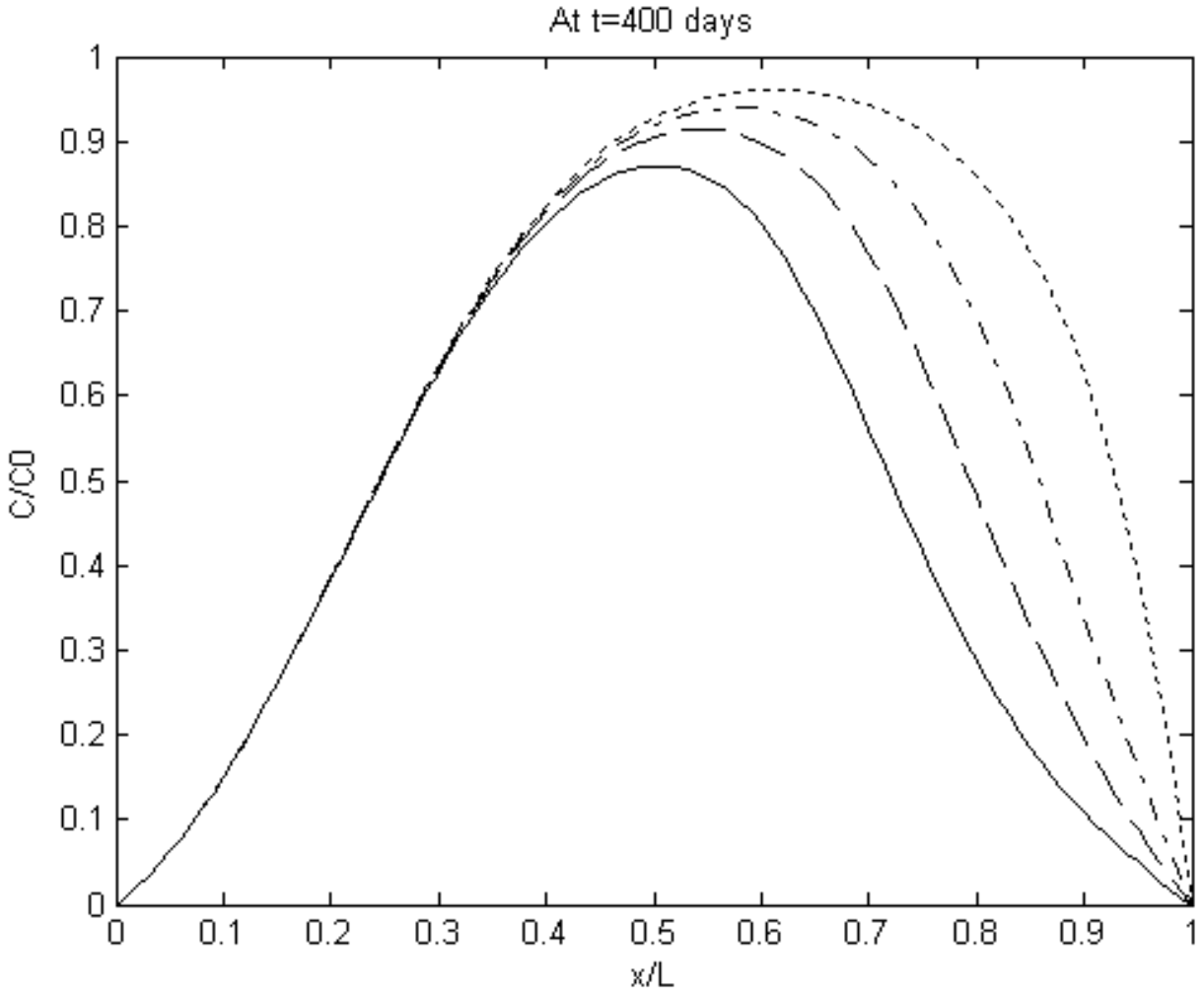

Legend: Dot-N1 (Baseline), Dash-N2, Dash Dot-N3, and Solid-N4

Figure 5.4 Tidal Effect on Contaminant Distribution (Continued).

Again assuming constant contaminant release for a period of one year, with a total discharge of 1825 kg over a hundred meter coastline, Figure 5.5 shows the contaminant discharge subject to different tidal amplitudes. It is demonstrated again that mass discharge is dramatically influenced by the magnitude of the tides. The mass discharge increase over the baseline (no tide, case N1) is also approximately proportional to the magnitude of the tidal amplitude. Doubling the tidal amplitude from 0.5 m (case N2) to 1.0 m (case N3) to 2.0 m (case N4), for example, the increase in mass discharge over the baseline after 100 days goes from 50% to 110% to 207% (see Figure 5.5); after 200 days these numbers are 16%, 31%, and 50%, respectively, and after 300 days, 7%, 13%, and 20%, respectively (see Figure 5.5).

Finally, also note that the increase in contaminant mass discharge over the baseline condition decreases as time after the initial discharge increases.

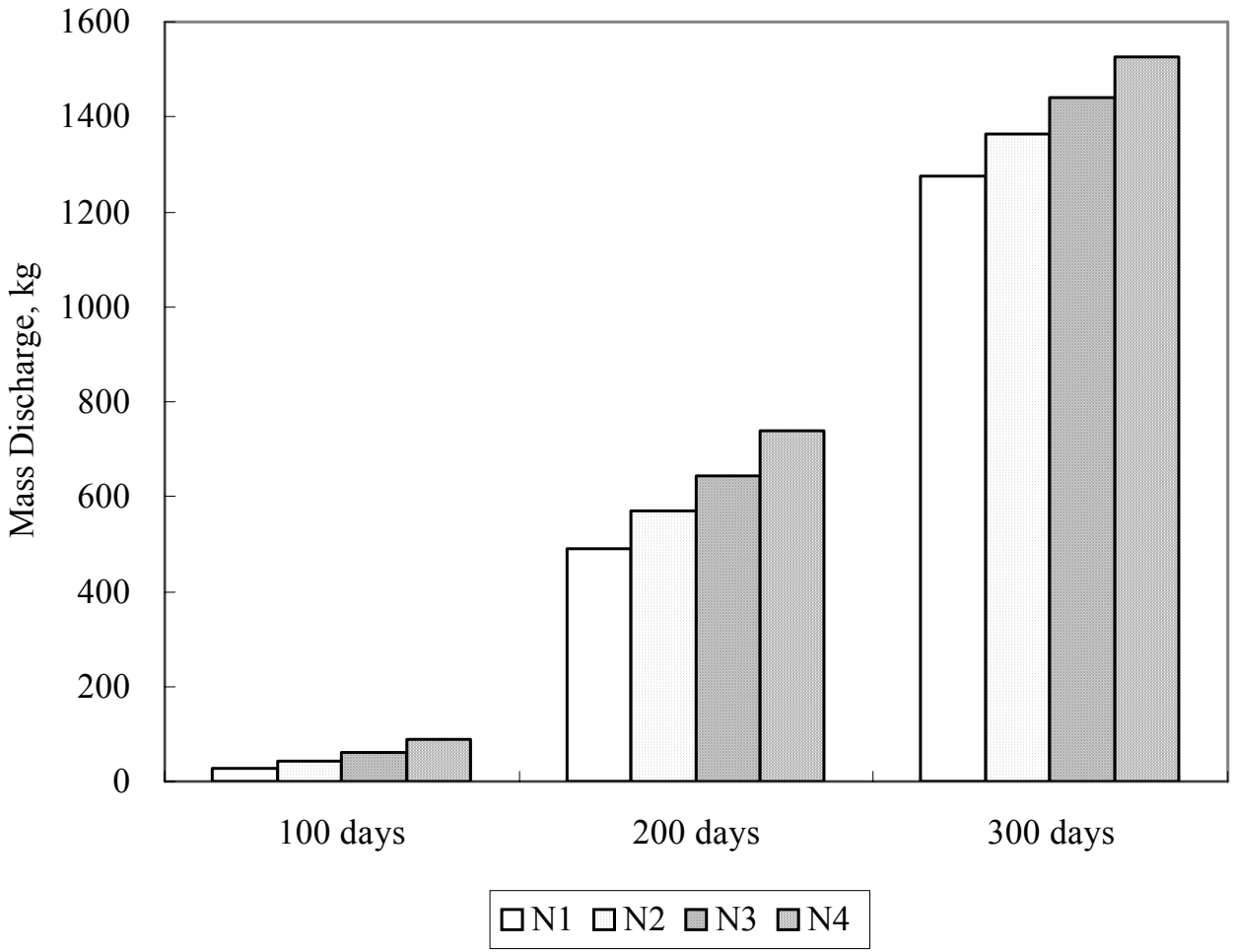

Figure 5.5 Contaminant Discharge subject to Different Tidal Amplitudes.

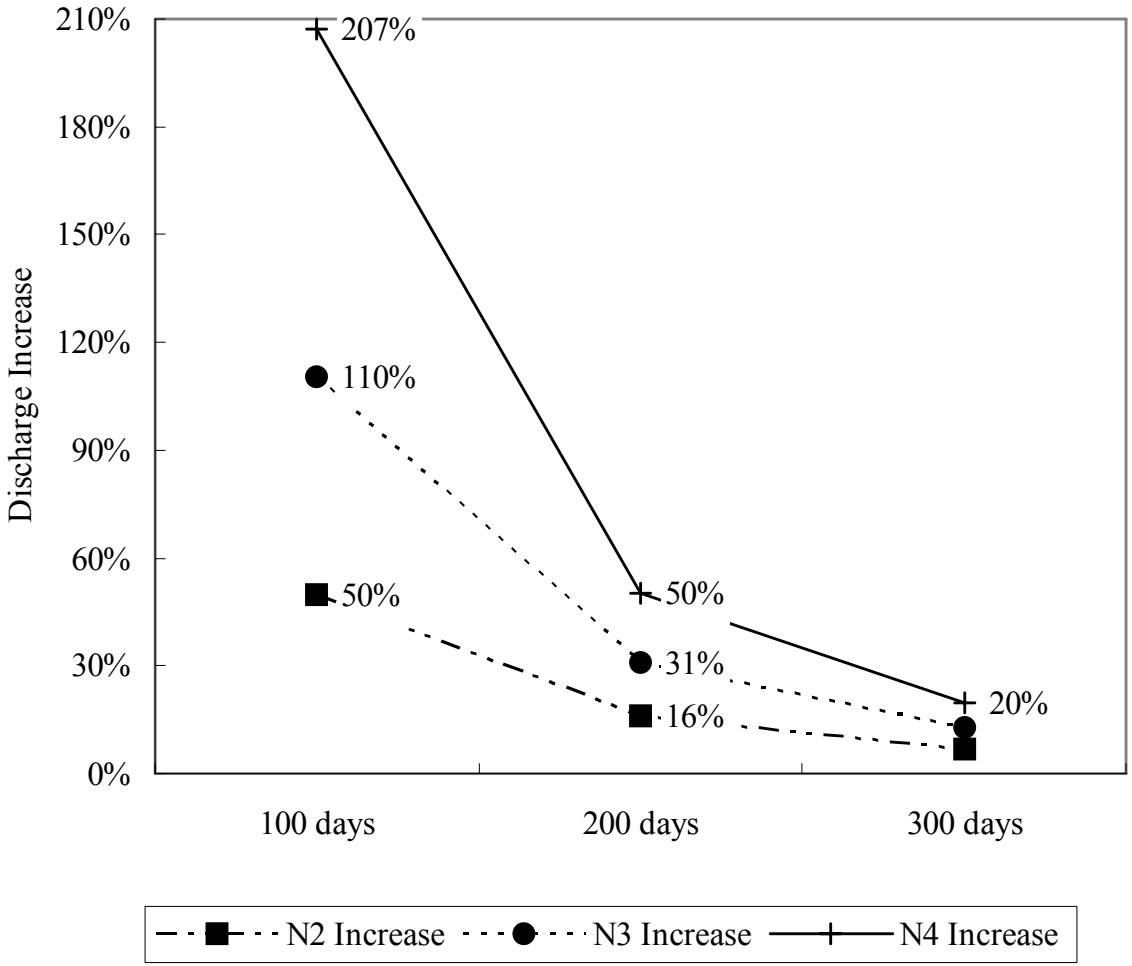

Figure 5.5 Contaminant Discharge subject to Different Tidal Amplitudes (Continued).

5.3.2 Tidal Effect with Different Flow Velocity

It is first evaluated in this section how flow velocity affects contaminant transport without including tidal fluctuations. The parameter values used and cases assigned for this purpose are listed in Table 5.3.

Table 5.3 Cases Assigned in Evaluation of Flow Velocity

Case No.	C_0 kg/m^3	V_x m/day	t_0 year	α_x m	D_x m^2/day	λ day^{-1}	R_f /	L m
B1	1.0	0.05	1	20	1.0	0.0	1.0	500
B2	1.0	0.2	1	20	4.0	0.0	1.0	500
B3	1.0	1.0	1	20	20	0.0	1.0	500

Obviously, flow velocity will affect the speed of contaminant transport since contaminant moves in the aquifer carried by groundwater flow. The smaller the flow velocity is, the slower the contaminant moves. Figure 5.6 demonstrates, as an example, how the contaminant concentration distribution profiles vary with flow velocity at different points in time.

The contaminant discharge, as shown in Figure 5.7, is also a function of velocity. Basically, the time for the contaminant discharge to reach 50% is approximately inversely proportional to the velocity by which the contaminant transports. That time is 25 years vs. 6.6 years vs. 1.75 years corresponding to the velocities of 0.05 m/d, 0.2 m/d and 1.0 m/d. It is worth noting that under the condition of very low flow velocity, contaminant transport can be very slow and it may take tens of years for the contaminant to reach the coastal boundary. It is under that condition, as will be demonstrated later, that tidal influence becomes especially important, causing the contaminant to discharge into the coastal water by a significant amount during the early years.

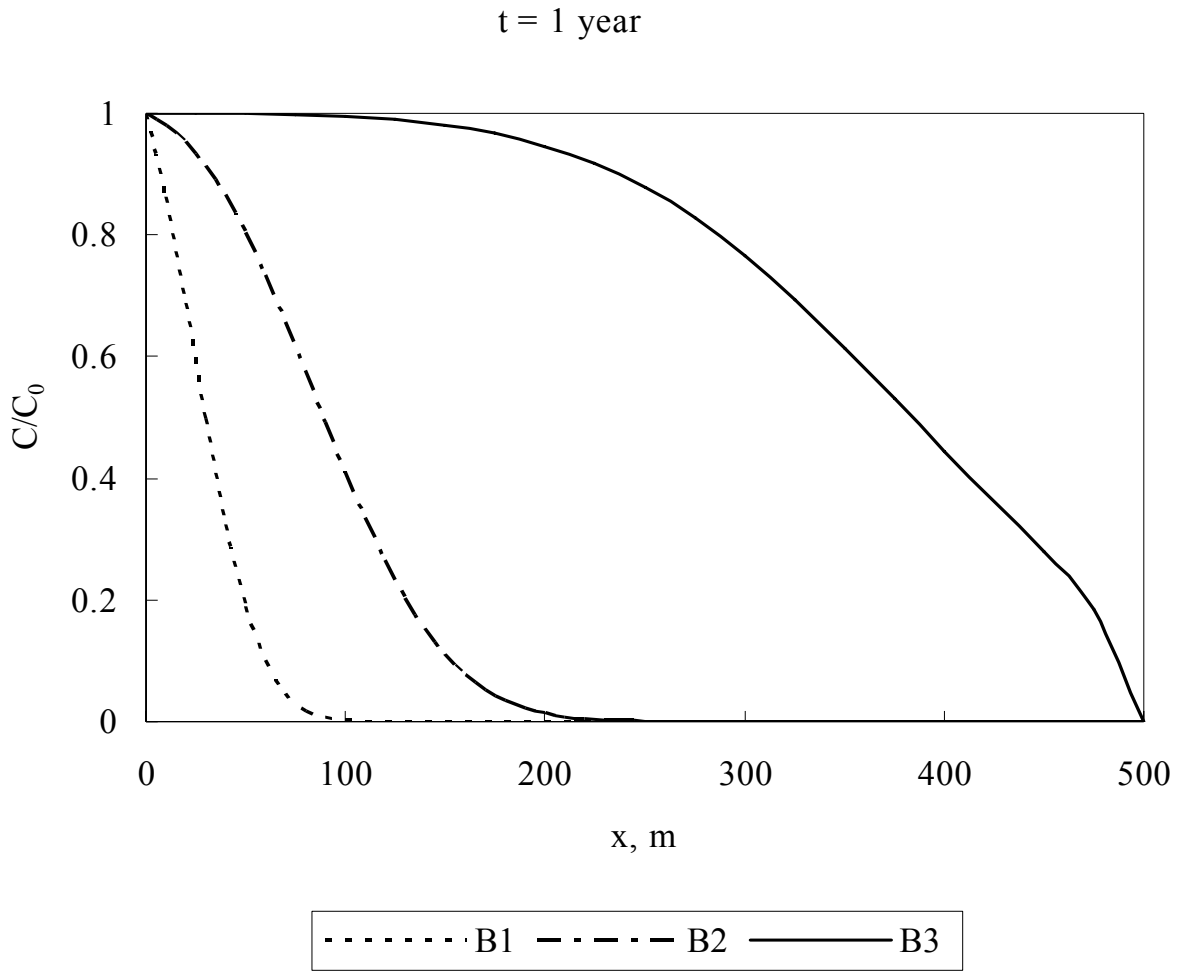

Figure 5.6 Evaluation of Velocity-Concentration Profiles.

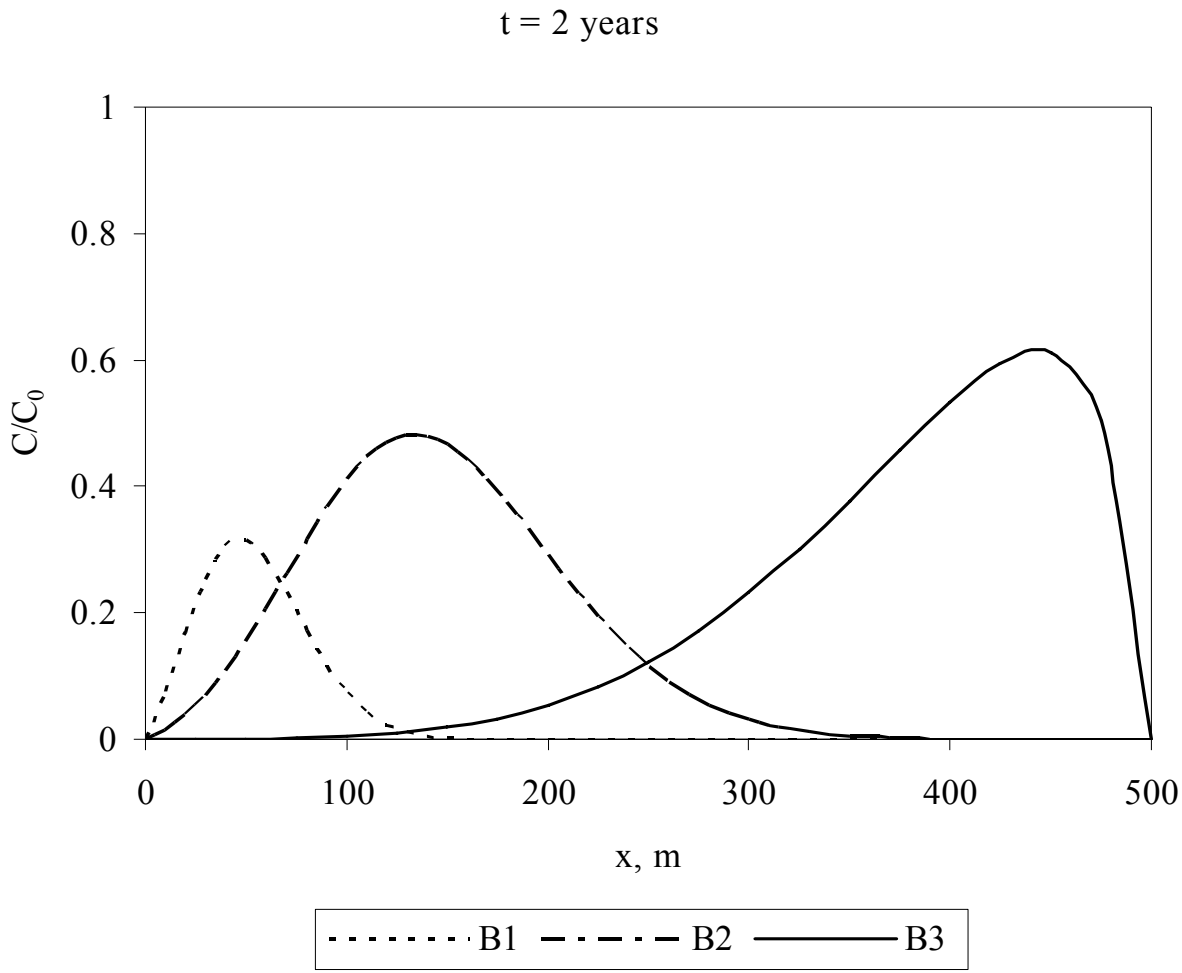

Figure 5.6 Evaluation of Velocity-Concentration Profiles (Continued).

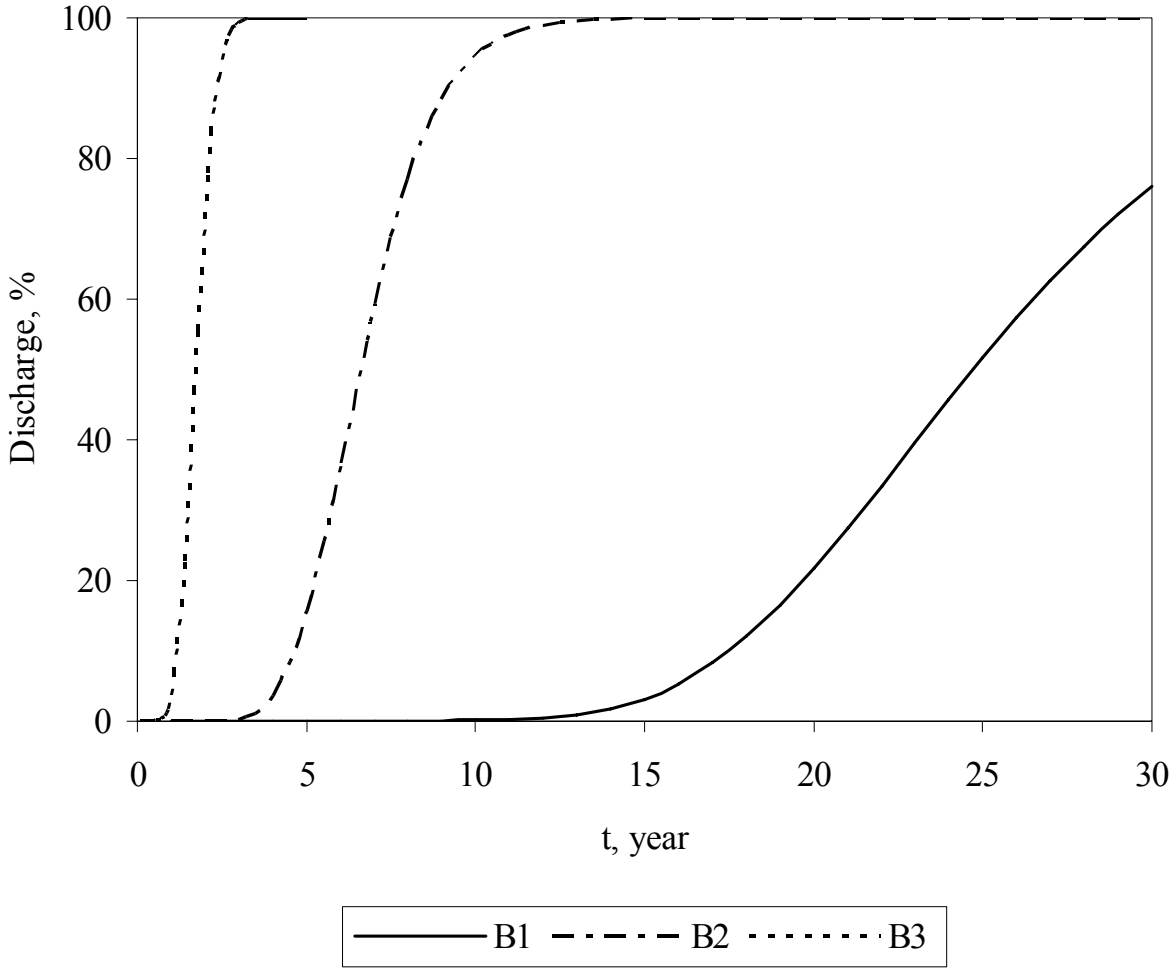

Figure 5.7 Evaluation of Velocity-Discharge Profiles.

Now that it has been analyzed how the contaminant transport relates to groundwater flow, it proceeds to include tidal fluctuations. Table 5.4 gives the cases and assigned values of flow velocity. The detailed conditions are summarized in Table 5.12.

Table 5.4 Cases Assigned in Evaluation of Tidal Effect

Case No.	N7	N3	N11
Flow Velocity, m/d	2.0	0.5	0.2

Figure 5.8 compares the contaminant concentration distribution at stage I (contaminant plume reaches approximately the middle of the aquifer).

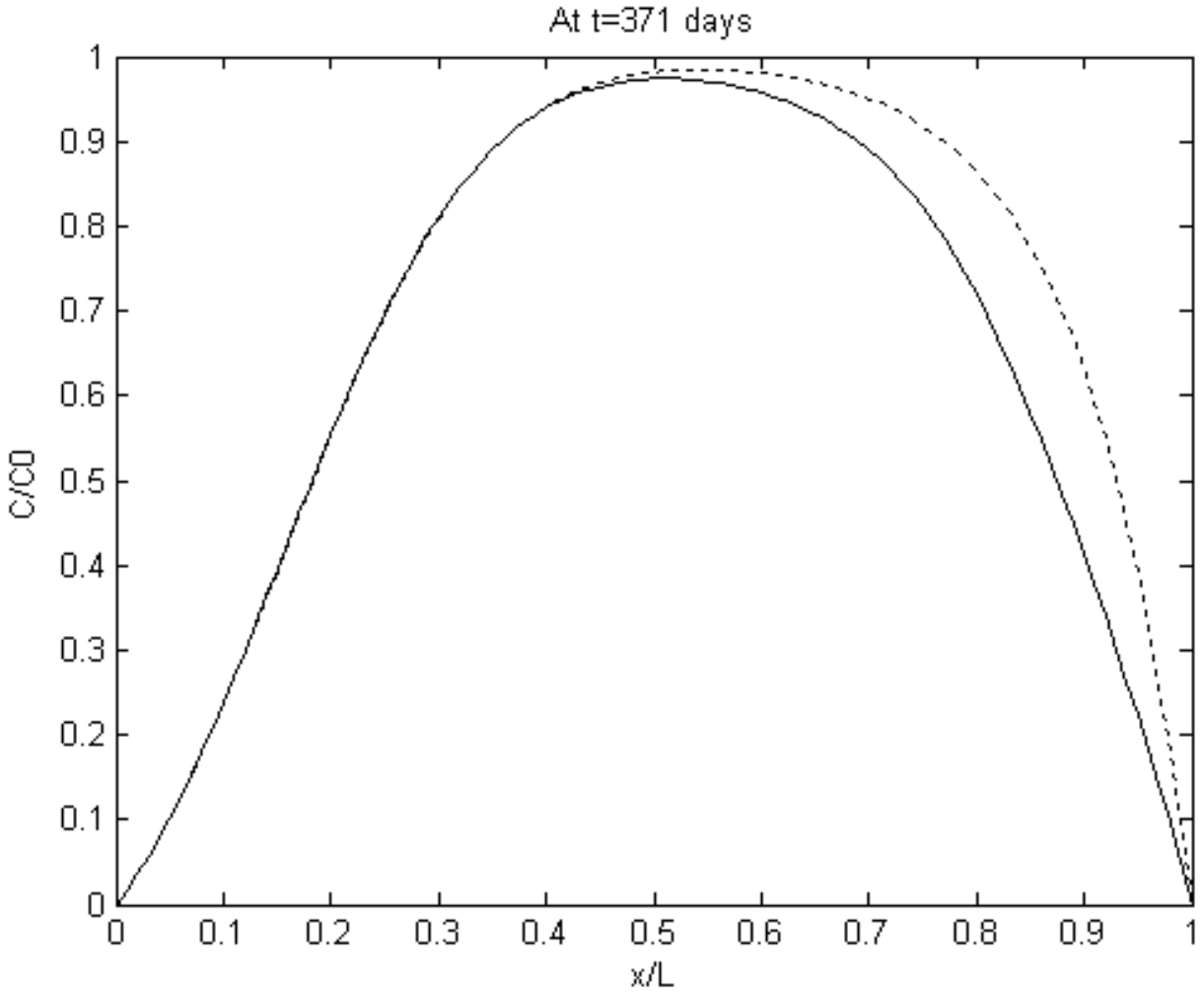

Legend: Solid-N7, Dot-Baseline (without tidal effect)

Figure 5.8 Comparison of Tidal Effect on Contaminant Distribution at Stage I.

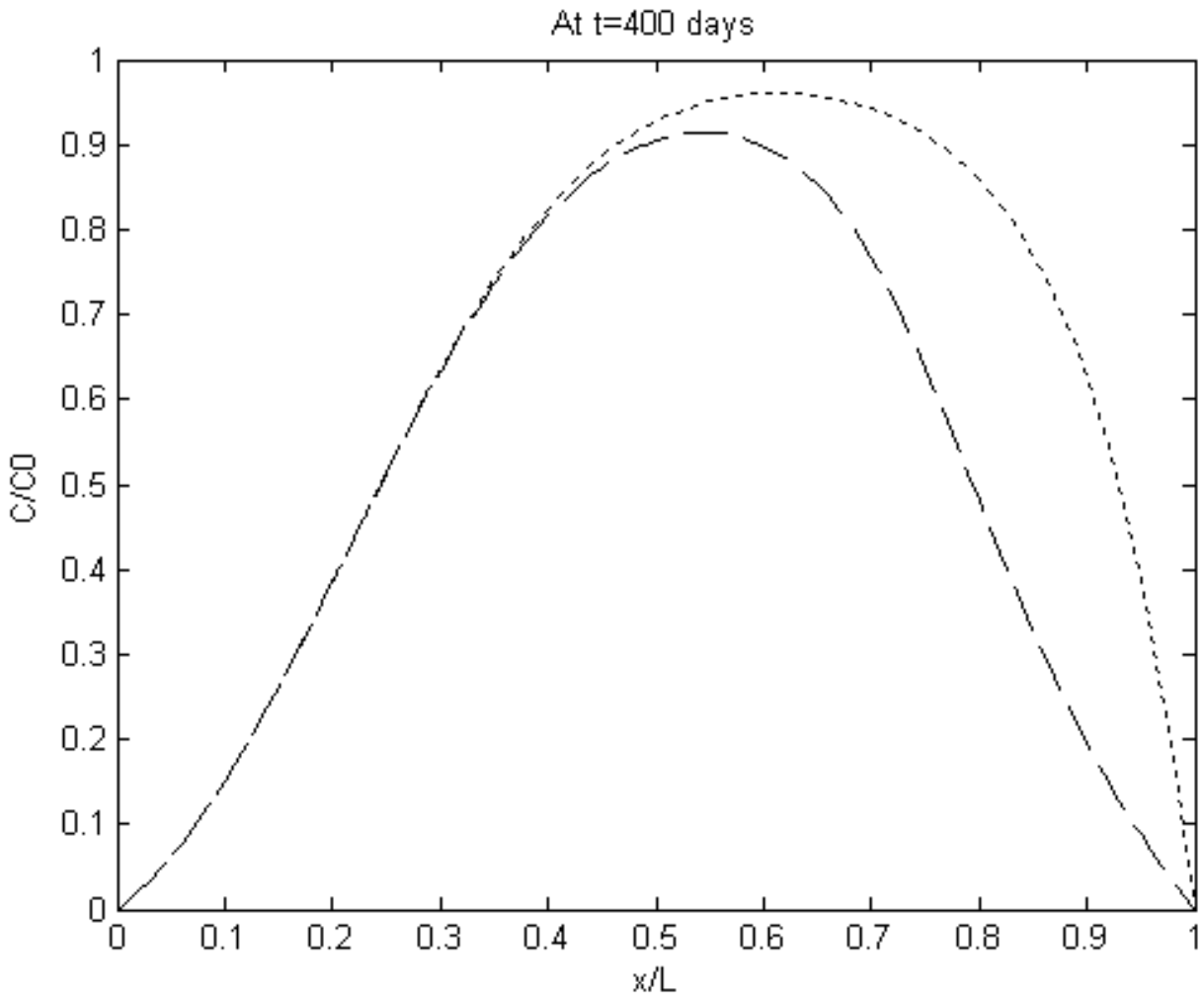

Legend: Dash-N3, Dot-Baseline

Figure 5.8 Comparison of Tidal Effect on Contaminant Distribution at Stage I (Continued).

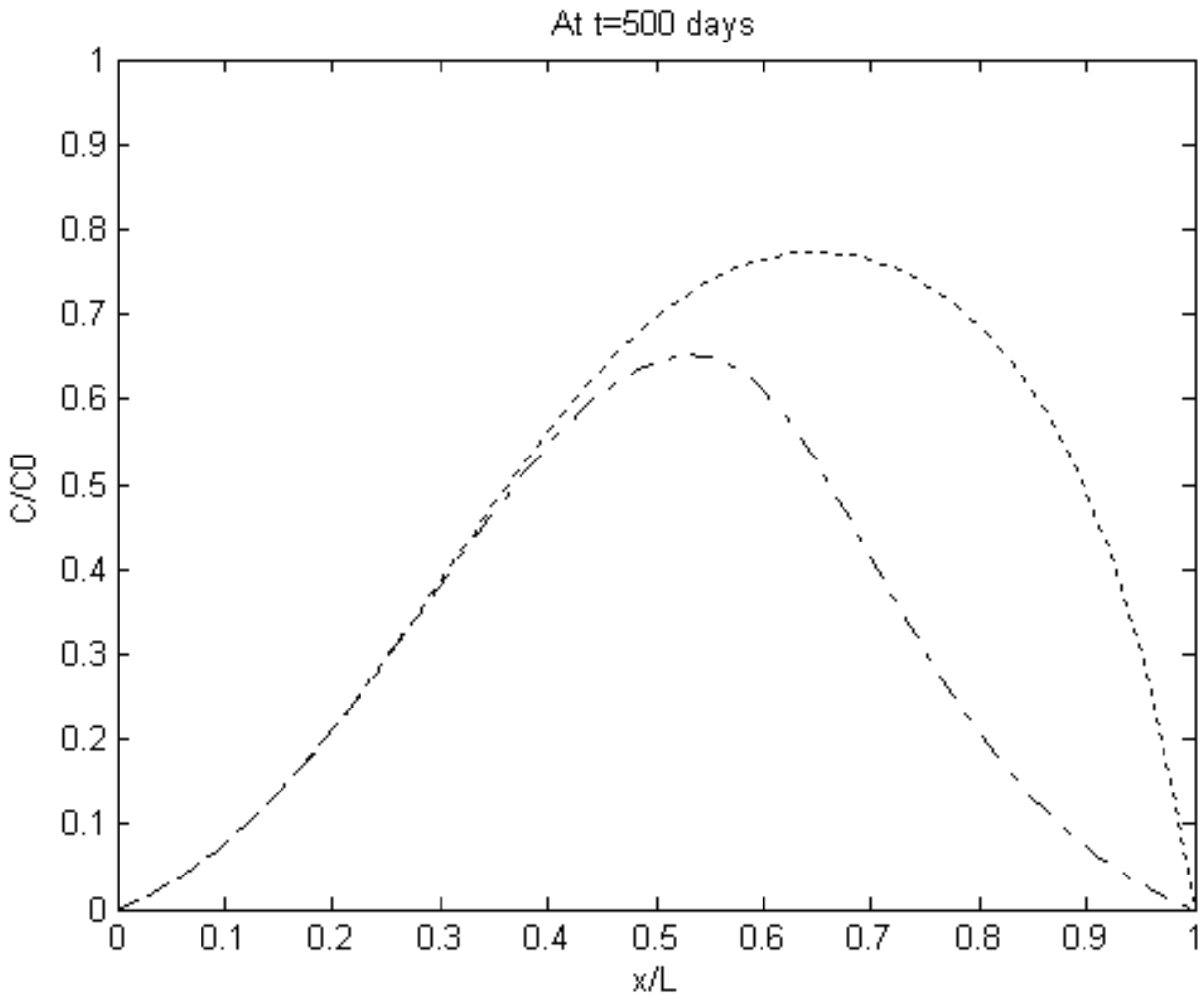

Legend: Dash-N11, Dot-Baseline

Figure 5.8 Comparison of Tidal Effect on Contaminant Distribution at Stage I (Continued).

Figure 5.9 compares the contaminant concentration distribution at stage II (contaminant plume reaches approximately the middle of the right half of the aquifer).

As shown in Figure 5.8 and Figure 5.9, the concentration distributions are compared for these cases at each stage when the contaminant plume reaches similar locations along the aquifer, though it takes a totally different time for the contaminant plume to reach that stage in each case. Observed in these cases is that the tidal influence is more significant under lower groundwater flow velocity.

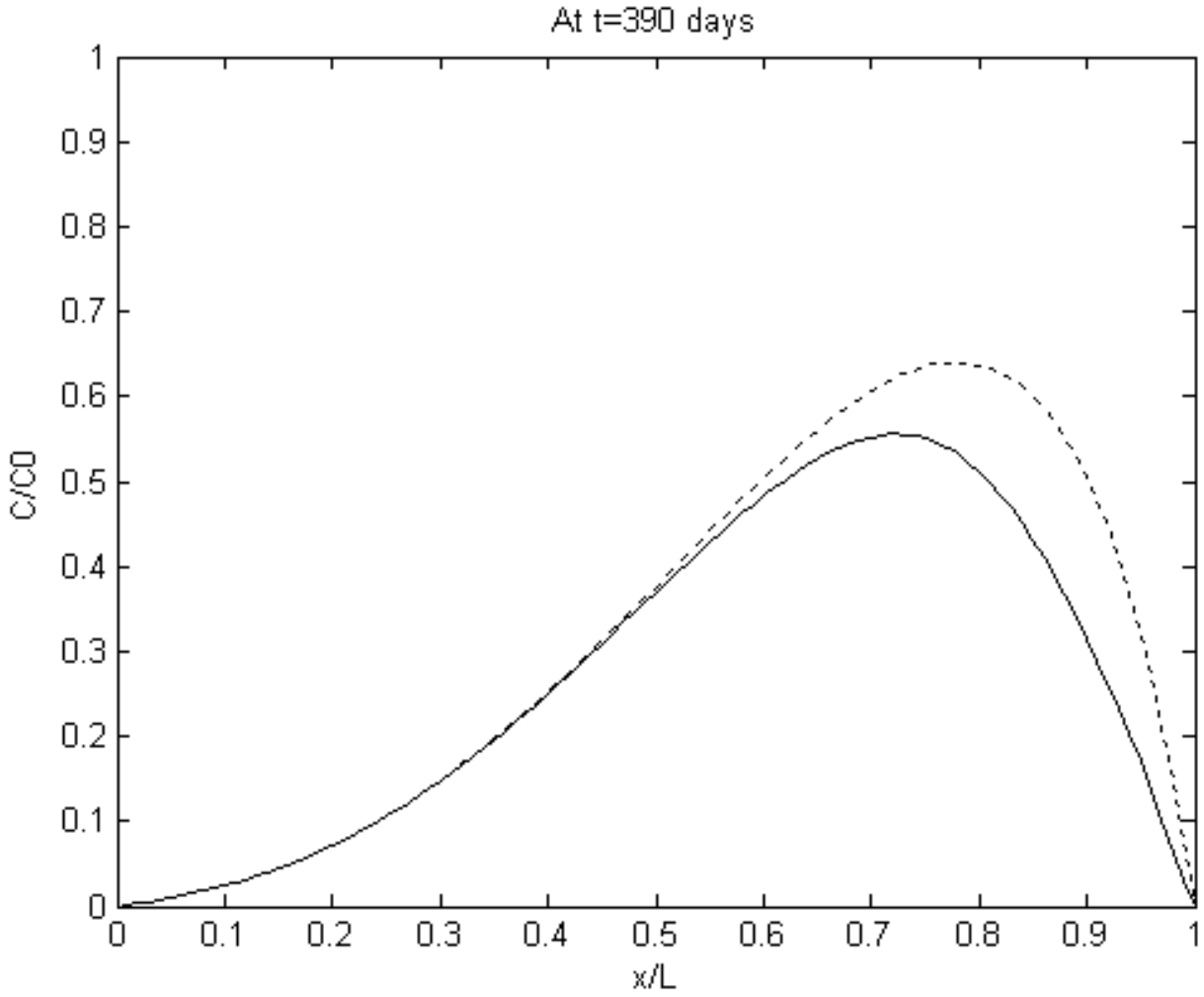

Legend: Solid-N7, Dot-Baseline

Figure 5.9 Comparison of Tidal Effect on Contaminant Distribution at Stage II.

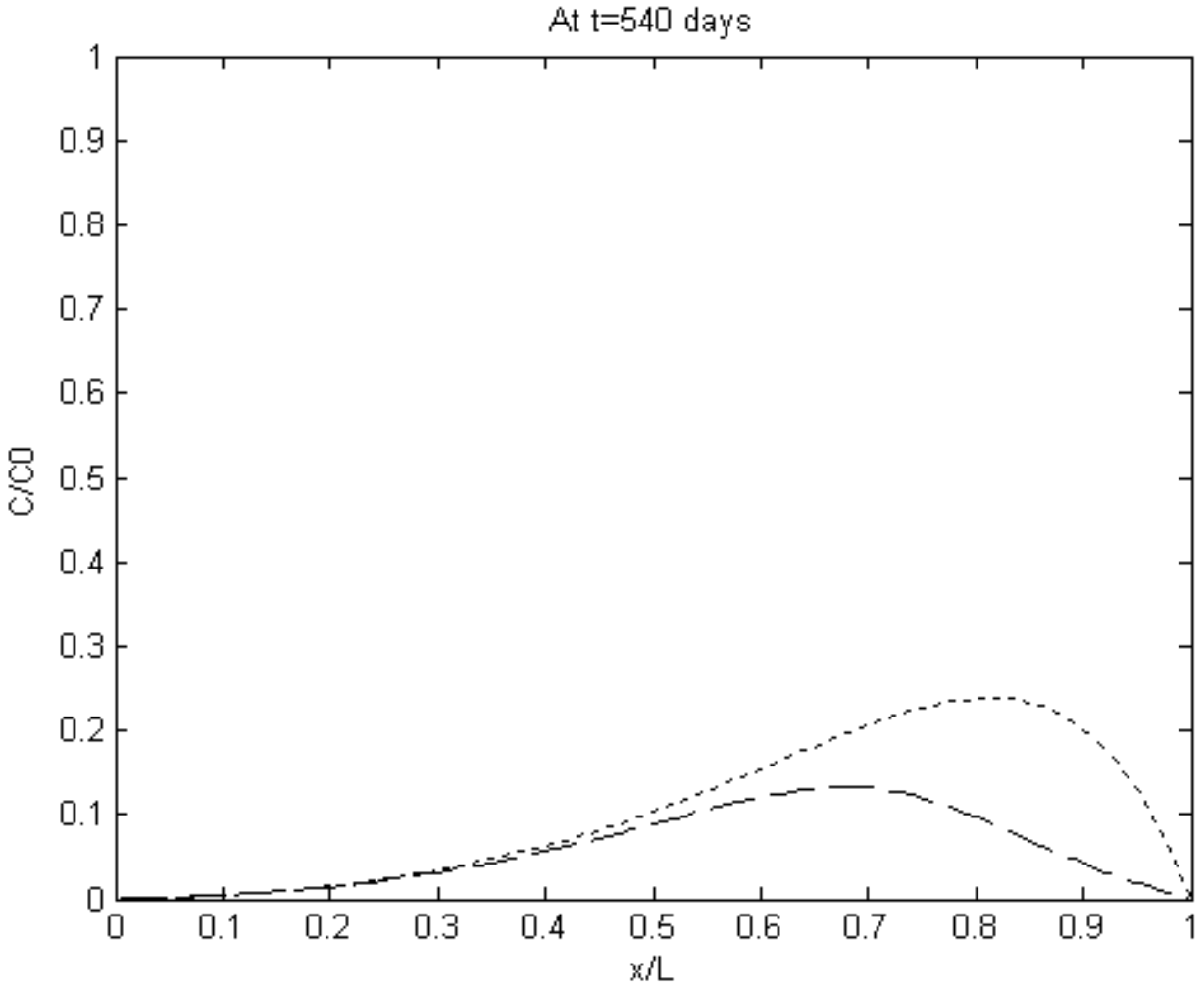

Legend: Dash-N3, Dot-Baseline

Figure 5.9 Comparison of Tidal Effect on Contaminant Distribution at Stage II (Continued).

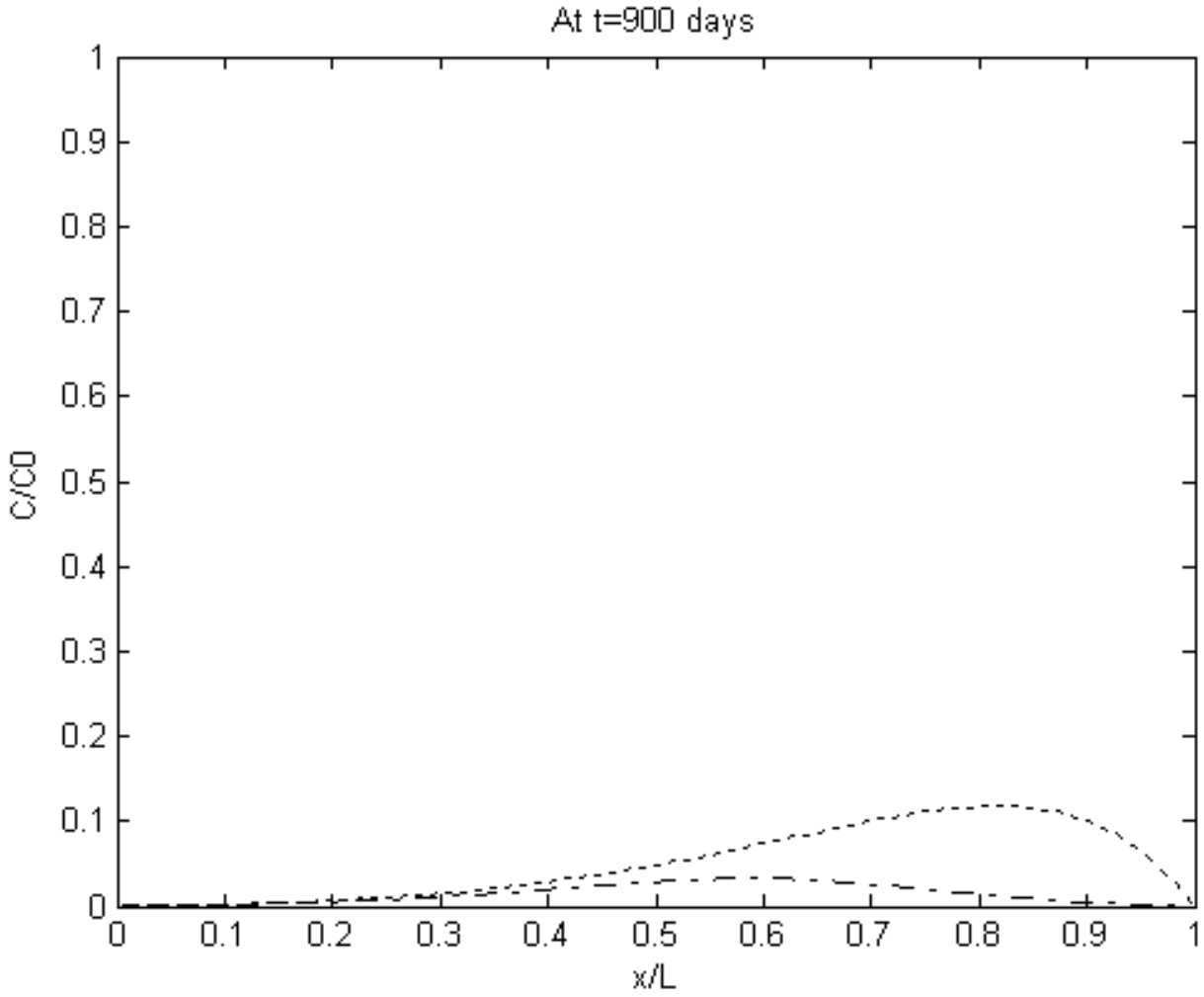

Legend: Dash-N11, Dot-Baseline

Figure 5.9 Comparison of Tidal Effect on Contaminant Distribution at Stage II (Continued).

Figure 5.10 and Figure 5.11 compare the contaminant discharge over time. This confirms the observation from the concentration distribution profiles. When the flow velocity is lowered to certain level, less than 0.5 m/d herein (cases N3 and N11), the tidal influence becomes significant. For example, at T=0.5, contaminant discharged with a flow velocity of 0.2 m/d (case N11) in increased 249% over the baseline, and with a flow velocity of 0.5 m/d (case N3) it is increased 110%. However, with a flow velocity of 2.0 m/d (case N7), the contaminant discharge is increased only 40% above the baseline. Finally, also note that the increase in contaminant mass discharge over the baseline condition decreases as time after the initial discharge increases irrespective of the flow velocity. Under such a condition, tidal fluctuations lead to dramatic concentration dilution in the regions adjacent to the coastline, and this region extends inland from the coastline approximately 60% of the aquifer dimension equivalent, to 60 meters.

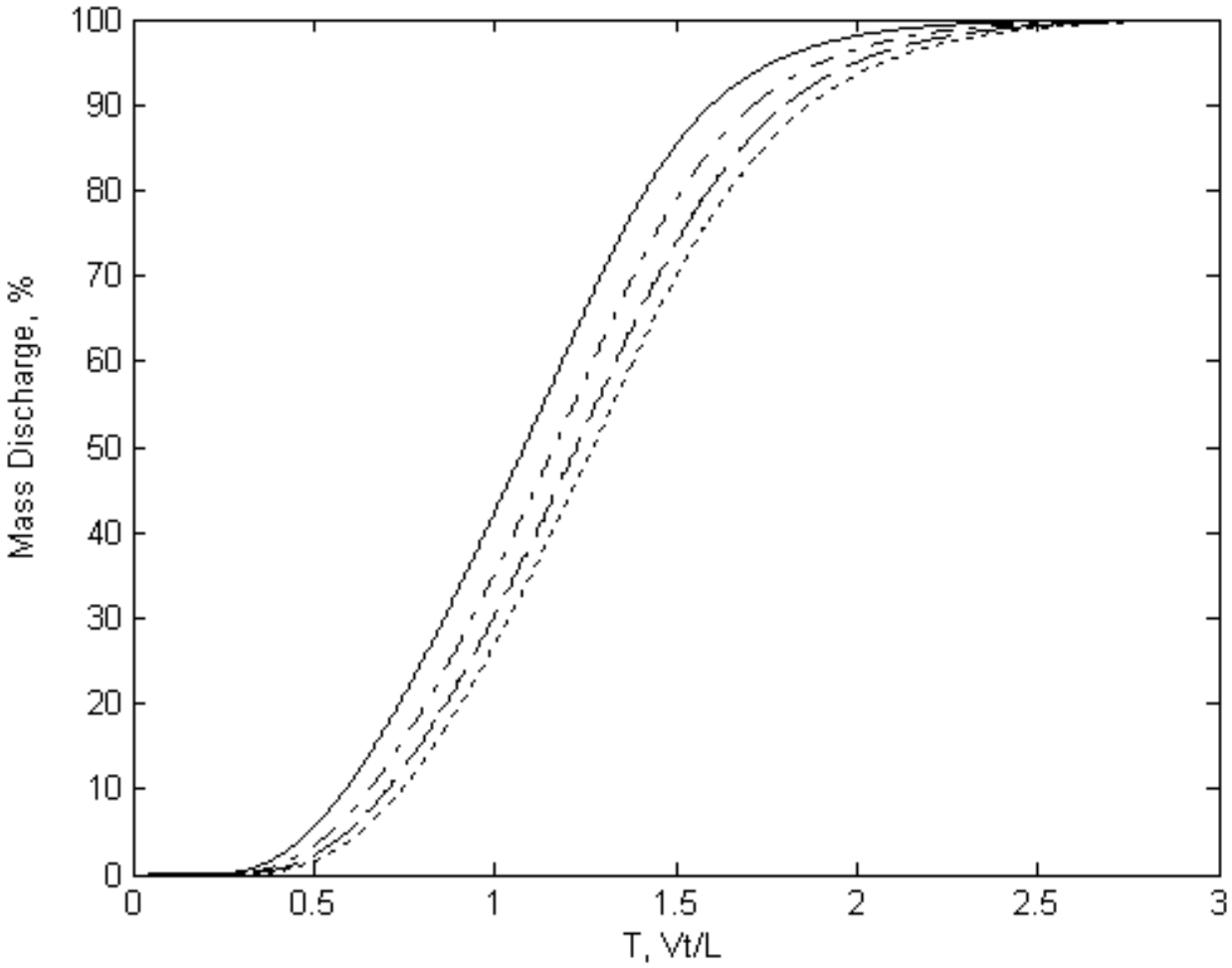

Legend: Dot-Baseline, Dash-N7, Dash Dot-N3, and Solid-N11

Figure 5.10 Tidal Effect on Contaminant Discharge subject to Different Flow Velocities.

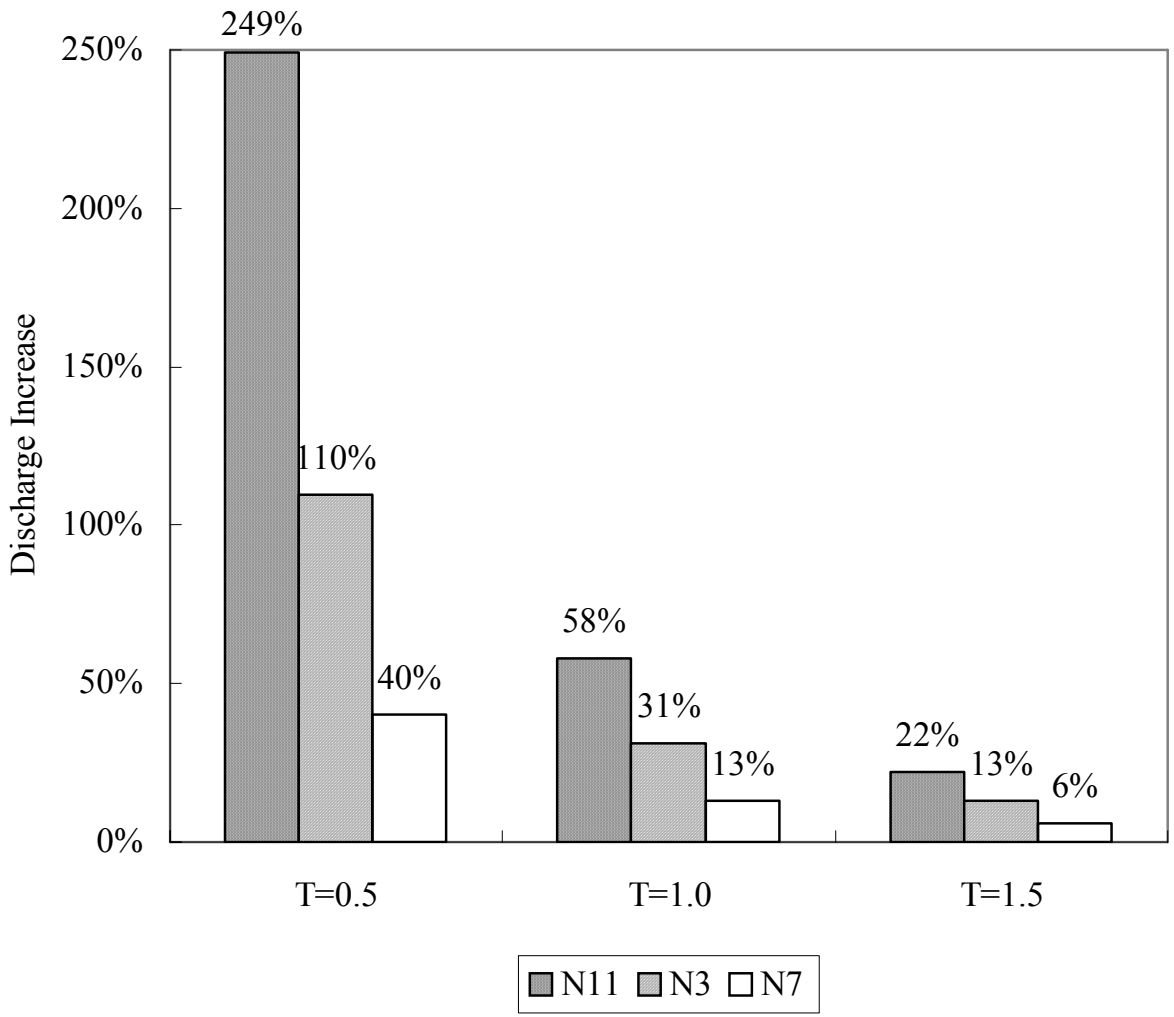

Figure 5.11 Tidal Effect on Contaminant Discharge subject to Different Flow Velocities.

5.3.3 Tidal Effect with Different Retardation

The effect of retardation factor on contaminant transport is similar to that of flow velocity even though the mechanisms are totally different. Retardation, as a result of equilibrium adsorption or ion exchange, merely serves to decrease the values of the transport parameters: dispersion (D) and contaminant transport velocity (V). Transport of contaminant subject to linear adsorption can be simulated in the same manner as a nonadsorbed contaminant using these scaled coefficients D/R_f and V/R_f (Domenico and Schwartz, 1997). Because the transport velocity of the adsorbed contaminant is reduced, the contaminant will arrive at a given spatial location later than a nonadsorbed contaminant. An evaluation of retardation effect is first conducted without considering tides, and the conditions considered are outlined in Table 5.5.

Table 5.5 Cases Assigned in Evaluation of Retardation Factor

Case No.	C_0 kg/m^3	V_x m/day	t_0 year	α_x m	D_x m^2/day	λ day^{-1}	[a]R_f /	L m
F1	1.0	1.0	1	20	20	0.0	1000	500
F2	1.0	1.0	1	20	20	0.0	100	500
F3	1.0	1.0	1	20	20	0.0	10	500
F4	1.0	1.0	1	20	20	0.0	1	500

[a] Values from top to bottom are corresponding to a partition factor of 428 ml/g, 42.4 ml/g, 3.86 ml/g, and zero, respectively.

Figure 5.12 gives the relationship between contaminant mass discharge and retardation factor. In the figure, very symmetrical discharge profiles are observed. From case F1 to F4, the retardation factor is increased approximately by an order of magnitude between two consecutive cases. The discharge profiles for case F1 to F4, then, shift accordingly from right to left by an order of magnitude on the logarithmic time scale.

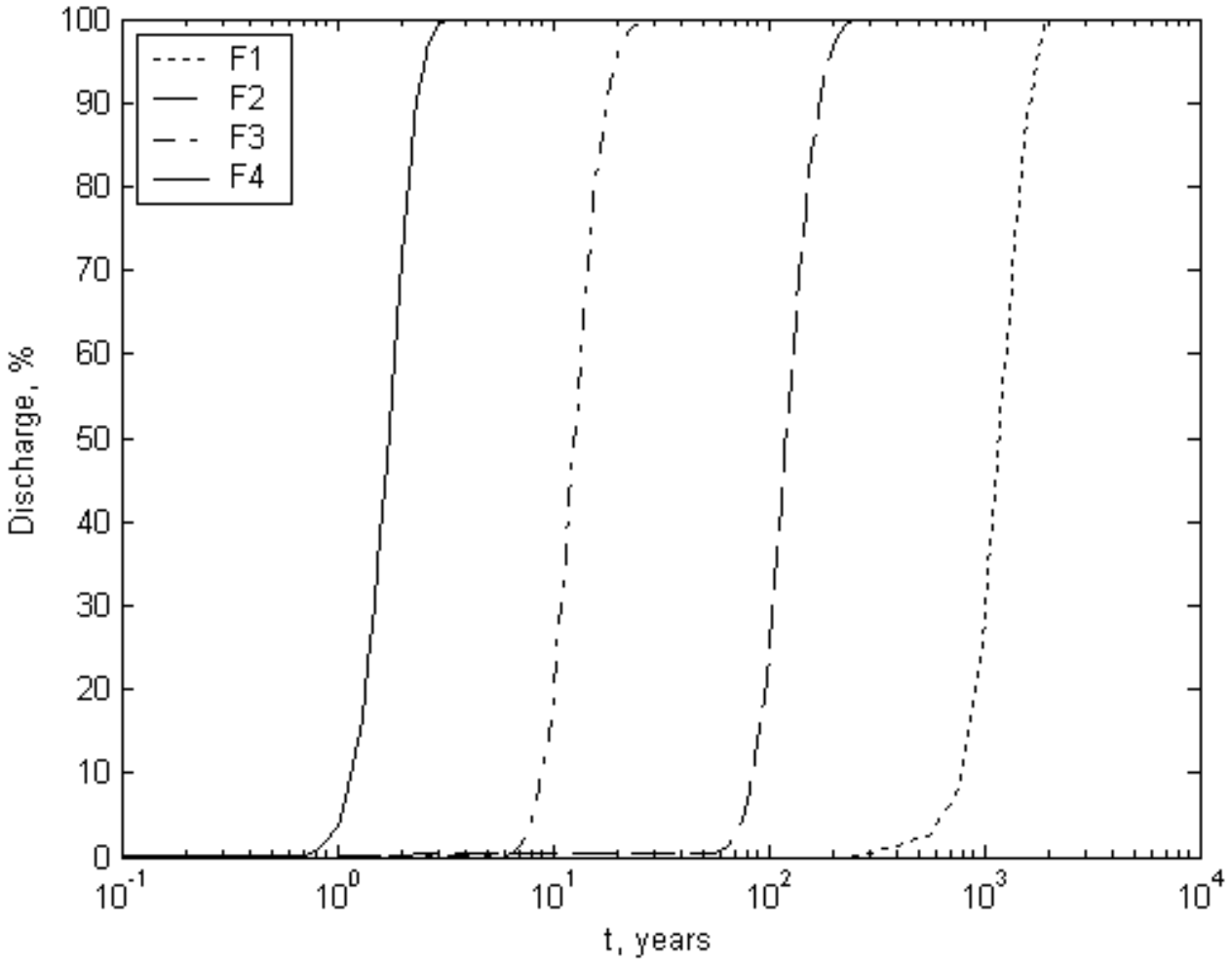

Figure 5.12 Retardation-Discharge Relation.

Next, the results are presented incorporating tidal fluctuations. Cases and assigned parameter values are listed in Table 5.6.

Table 5.6 Cases Assigned in Evaluation of Tidal Effect

Case No.	R1 Baseline	R1	R2 Baseline	R2
Retardation Factor	1.0	1.0	10.0	10.0
Tidal Amplitude, m	0	1.0	0	1.0

As shown in Figure 5.13, concentration distributions are compared for these cases at each stage when the contaminant plume reaches similar locations along the aquifer, even though it takes different times for the contaminant plume to reach that stage in each case. Observed in these cases is that concentration in the groundwater is significantly lowered with retardation due to adsorption of contaminant onto the aquifer soil matrix. As a result, tidal influence is more significant under lower retardation in terms of the absolute concentration reduced by tidal fluctuations.

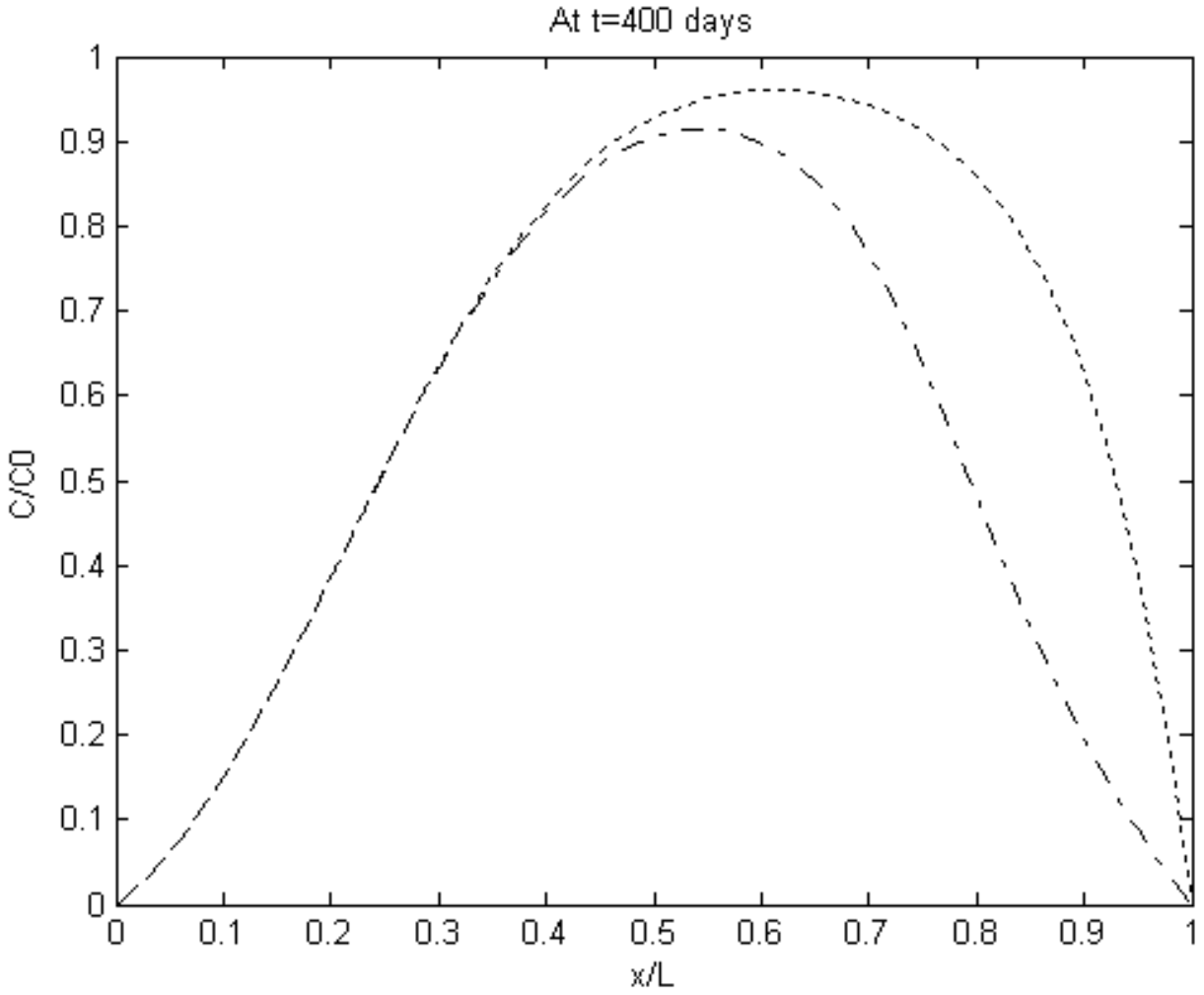

Legend: Dot-Baseline, Dash Dot-R1

Figure 5.13 Tidal Effect on Contaminant Distribution at Stage I.

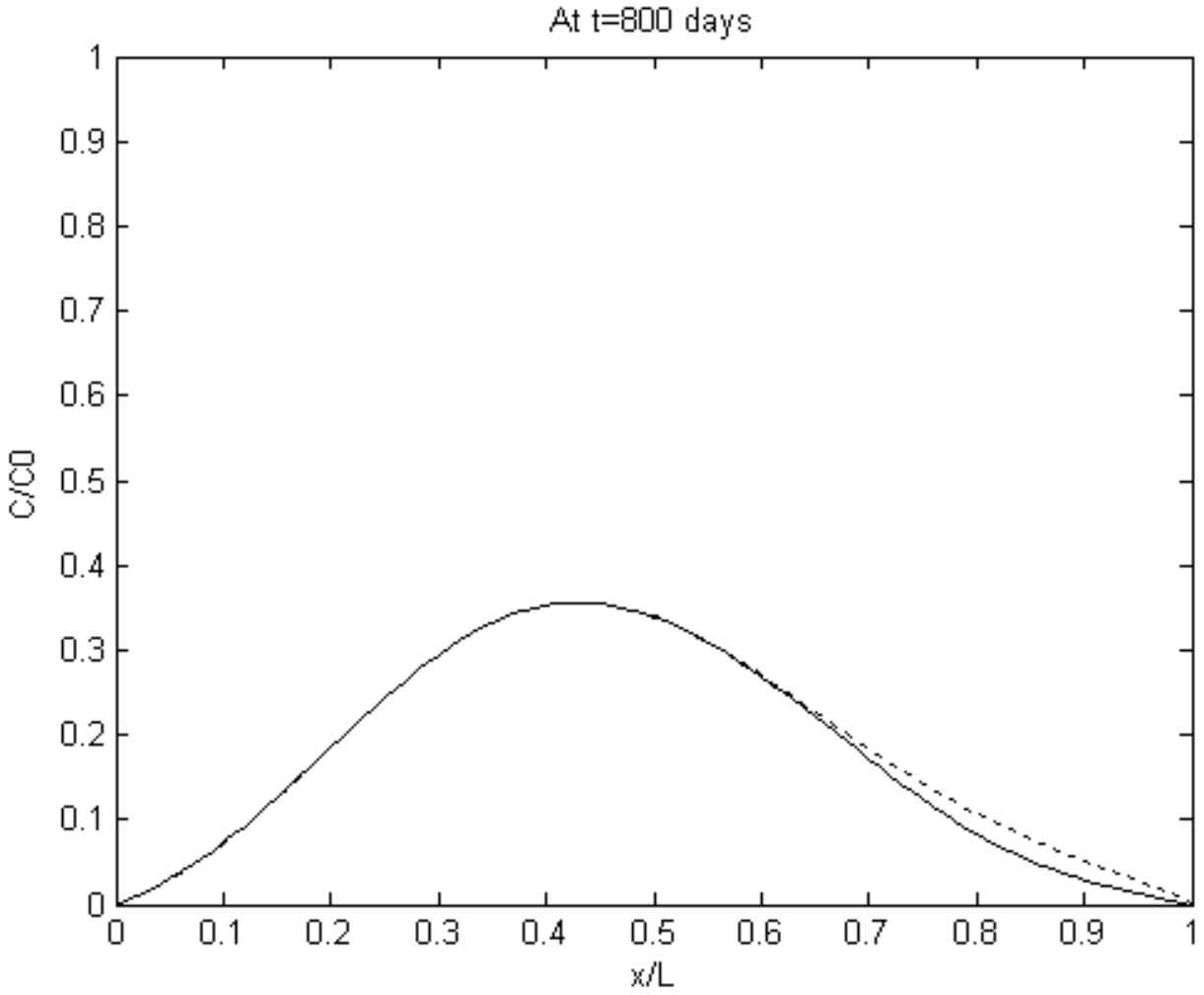

Legend: Dot-Baseline, Solid-R2

Figure 5.13 Tidal Effect on Contaminant Distribution at Stage I (Continued).

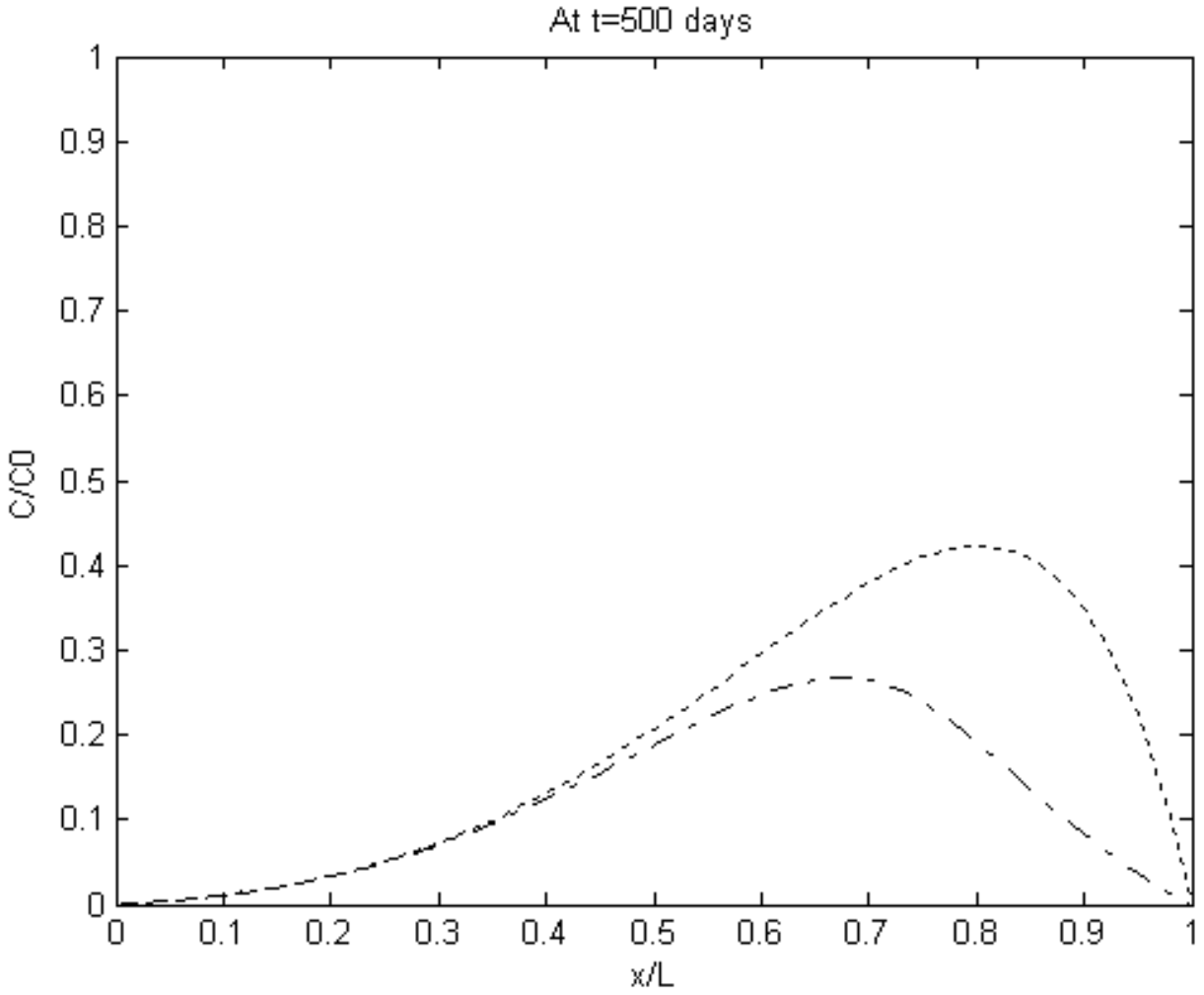

Legend: Dot-Baseline, Dash Dot-R1

Figure 5.13 Tidal Effect on Contaminant Distribution at Stage II (Continued).

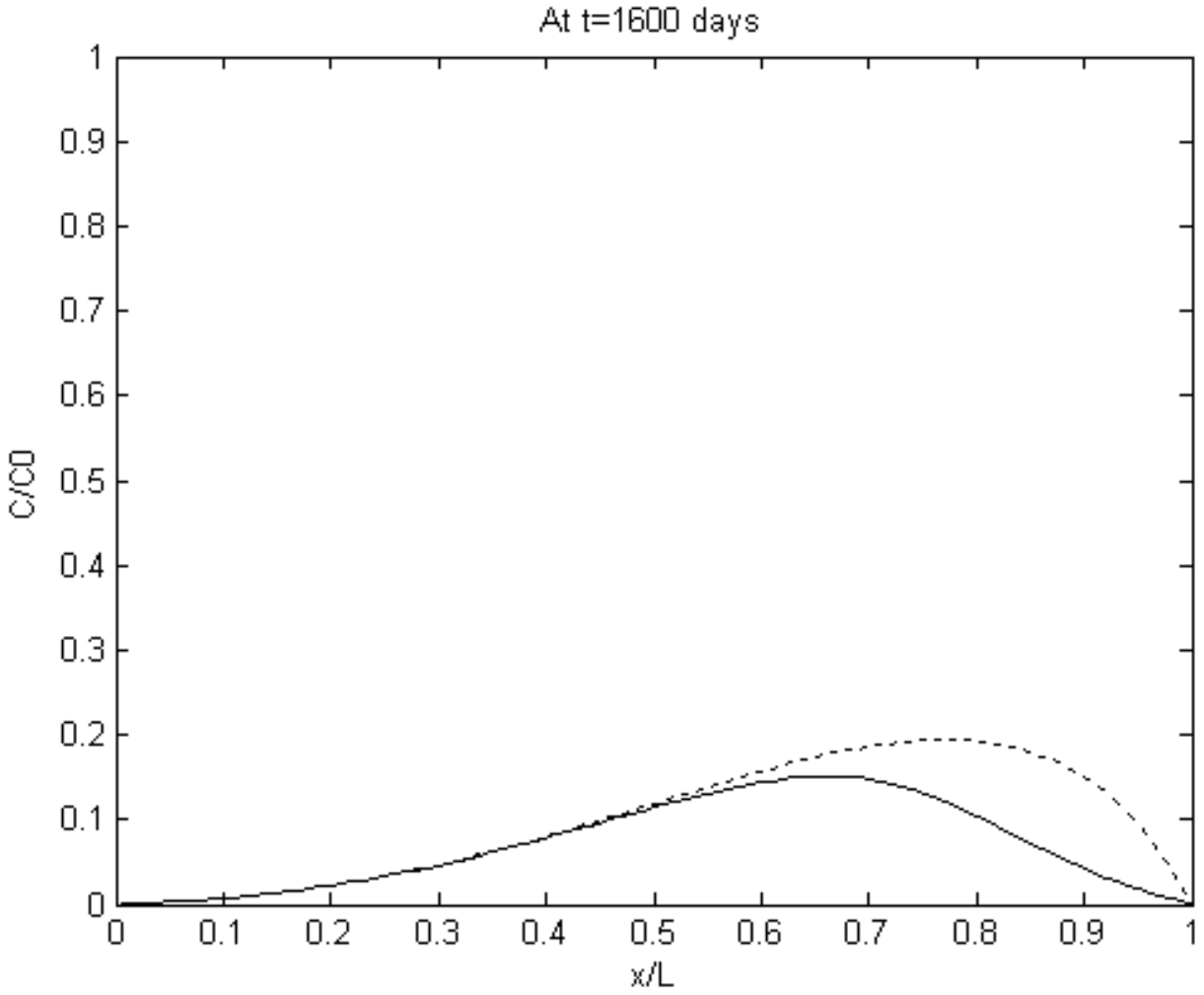

Legend: Dot-Baseline, Solid-R2

Figure 5.13 Tidal Effect on Contaminant Distribution at Stage II (Continued).

However, contaminant discharge is enhanced by tidal activities to a greater degree the larger the retardation factor; this is expected because the effects of varying retardation factors are similar to the situations subject to different flow velocities. Refer to Table 5.7 and Figure 5.14 for the time taken for the discharge to reach each level under different conditions. Generally, tides reduce the time needed for the discharge to reach a given level compared to the case without tides. However, higher retardation can result in a further reduction in this time. For example, to reach the level of 20% discharge of the total contaminant released into the aquifer, the time taken under the condition of no retardation (case R1) is decreased by 10%, while the time taken is decreased by 15% if a retardation factor of 10 is encountered (case R2). As mentioned earlier, this difference can be extraordinary if even larger retardation factors are dealt with. In those cases, while it takes tens of years for the contaminant to discharge even a small amount into coastal water if no tides are considered, a much larger amount of contaminant can be discharged in much less time if moderate to high tides are included.

Table 5.7 Time (T) for Contaminant to Reach Each Level of Discharge

Case No.	R1 Baseline	R1	% Time Reduced	R2 Baseline	R2	% Time Reduced
Discharge of 10%	0.74	0.65	12.2%	4.84	4.10	15.3%
Discharge of 20%	0.90	0.81	10.0%	5.68	4.83	15.0%
Discharge of 30%	1.04	0.94	9.6%	6.40	5.45	14.8%
Discharge of 40%	1.16	1.05	9.5%	7.08	6.06	14.4%

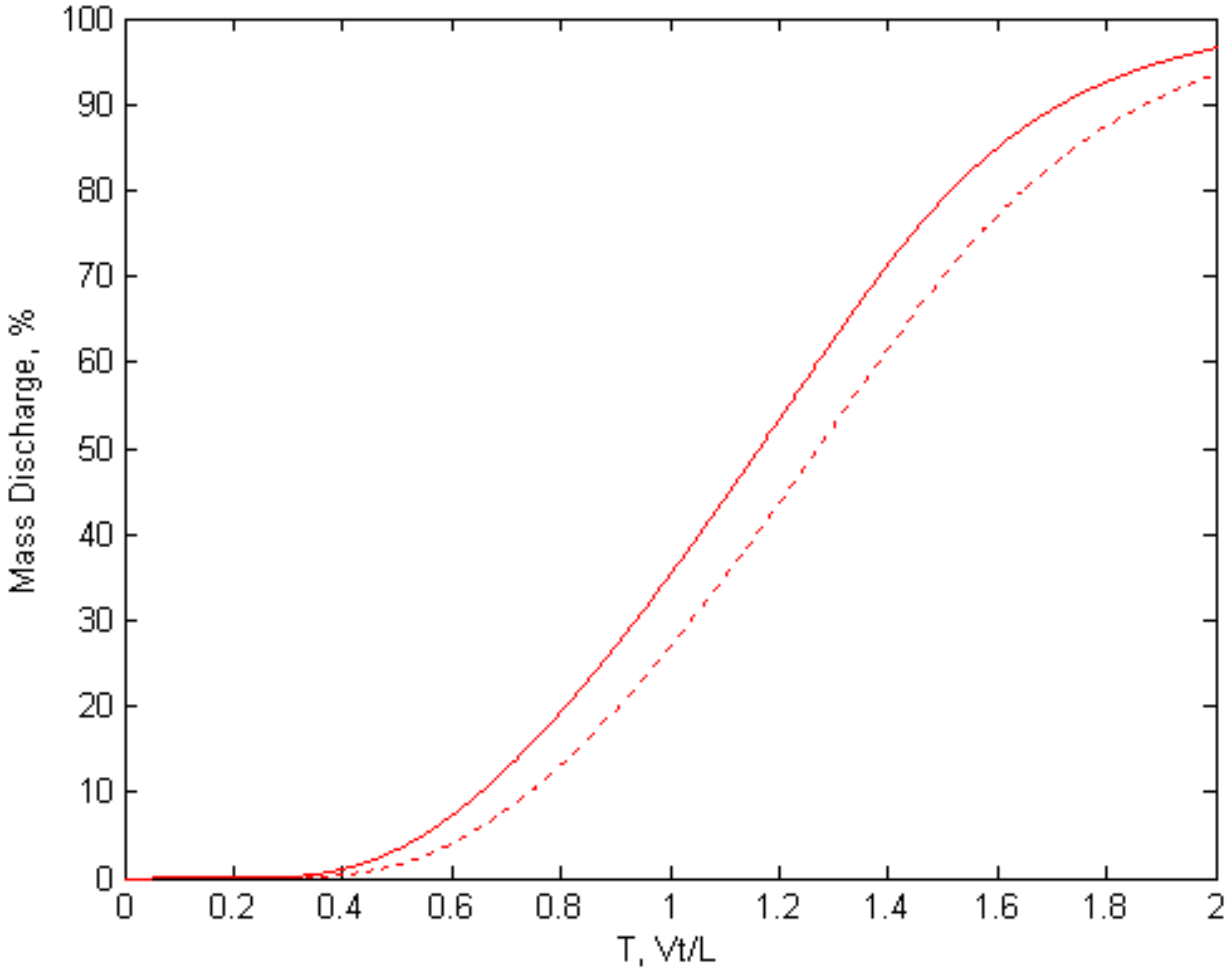

Legend: Dot-Baseline, Solid-R1

Figure 5.14 Tidal Effect on Contaminant Discharge subject to Different Retardation Factors.

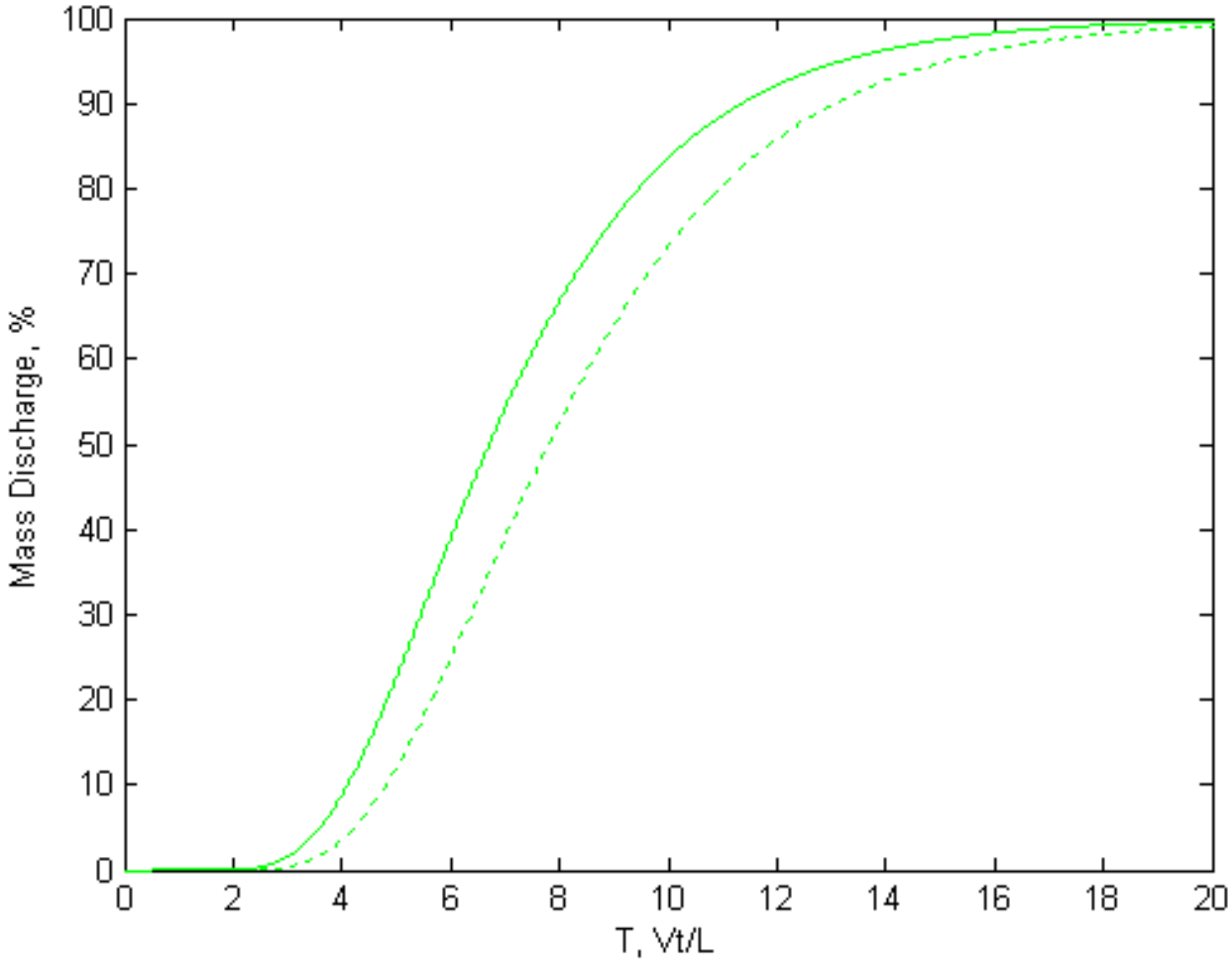

Legend: Dot-Baseline, Solid-R2

Figure 5.15: Tidal Effect on Contaminant Discharge subject to Different Retardation Factors.

5.3.4 Tidal Effect with Different Decay

The decay constant measures kinetic reactions, such as decay, chemical reactions, and biodegradation of the contaminant during the course of transport along an aquifer system. The degree and speed of mass decrease is a function of the decay constant, λ. The conditions considered are outlined in Table 5.8.

Table 5.8 Cases Assigned in Evaluation of Decay Constant

Case No.	C_0 kg/m^3	V_x m/day	t_0 year	α_x m	D_x m^2/day	[a] λ day^{-1}	R_f /	L m
E1	1.0	1.0	1	20	20	0.0	1.0	500
E2	1.0	1.0	1	20	20	2×10^{-5}	1.0	500
E3	1.0	1.0	1	20	20	2×10^{-4}	1.0	500
E4	1.0	1.0	1	20	20	2×10^{-3}	1.0	500
E5	1.0	1.0	1	20	20	2×10^{-2}	1.0	500

[a] Values from top to bottom are corresponding to a half-life of infinite, approximately 100 years, 10 years, 1 year, and 0.1 year, respectively.

Figure 5.16 compares the concentration distribution profiles for case E1 through E5 with different decay constants. It is observed that when the decay constant is less than 2×10^{-5} day^{-1}, no significant mass reduction occurs and the kinetic reaction can be neglected. When the decay constant is greater than 2×10^{-4} day^{-1}, each order of magnitude change in the decay constant would cause a significant change in the contaminant mass remaining in the system over time.

Figure 5.17 shows how mass discharge varies with the change in decay constant. As the decay constant goes up to certain degree, in case E5 for instance, the contaminant front may never reach the effluent boundary before it completely vanishes.

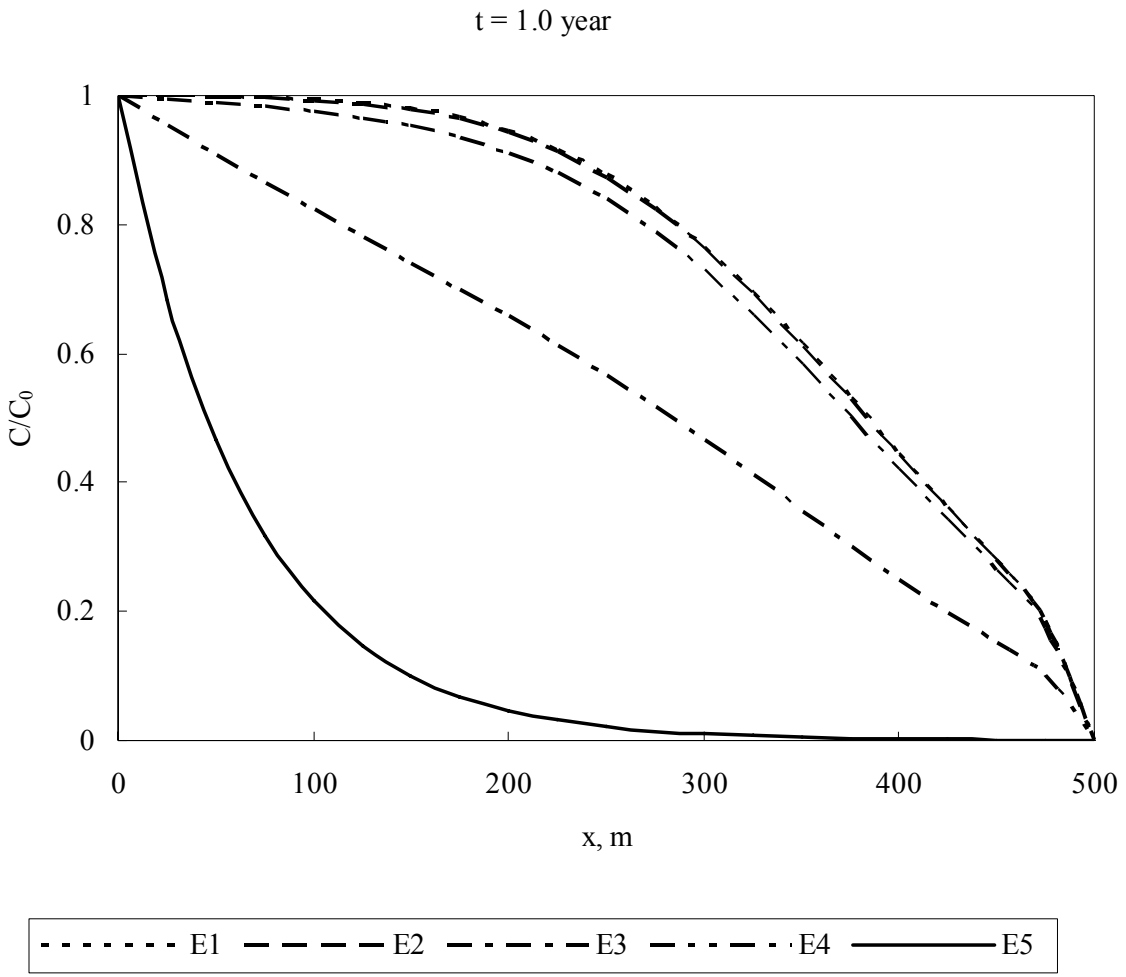

Figure 5.16 Evaluation of Decay-Concentration Distribution Relation.

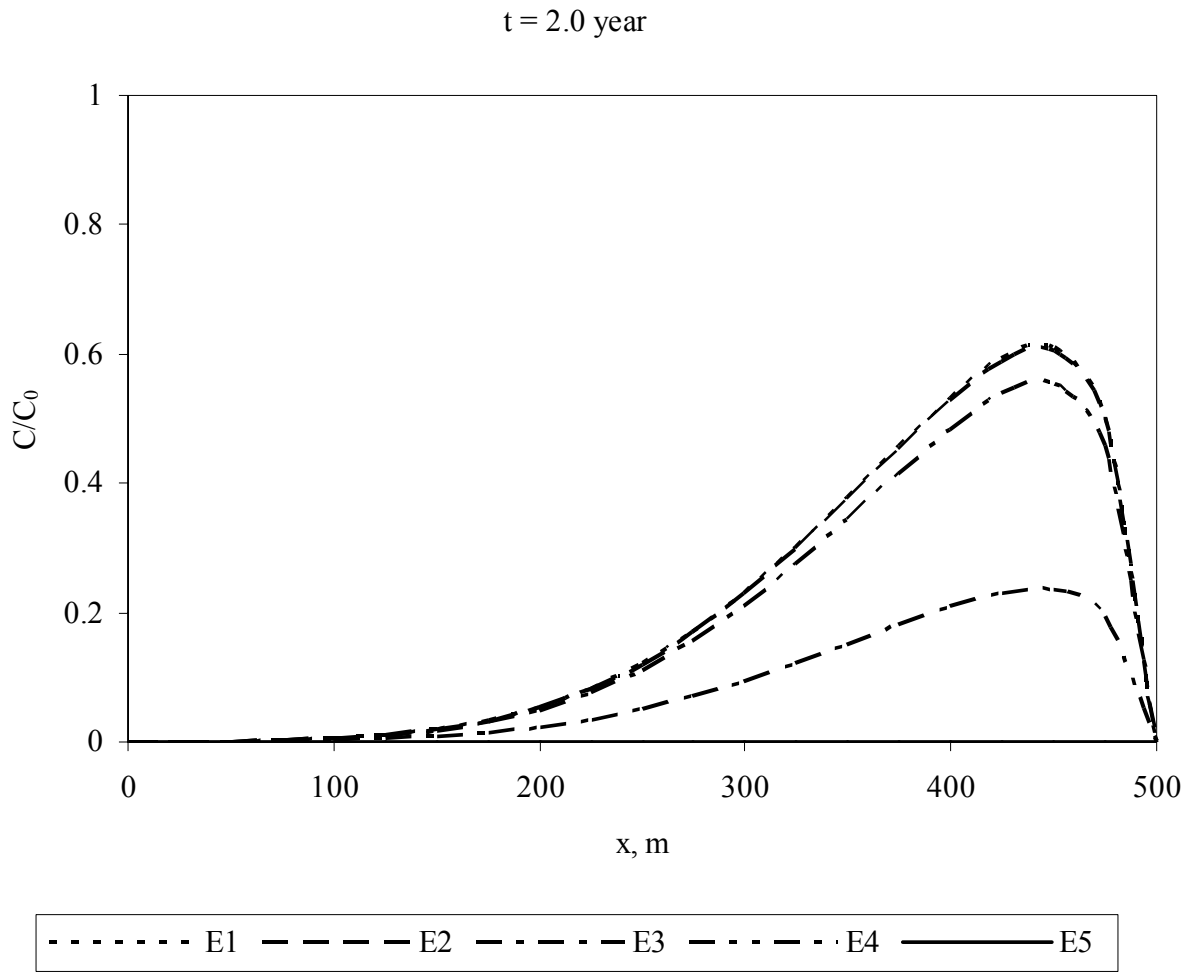

Figure 5.16 Evaluation of Decay-Concentration Distribution Relation (Continued).

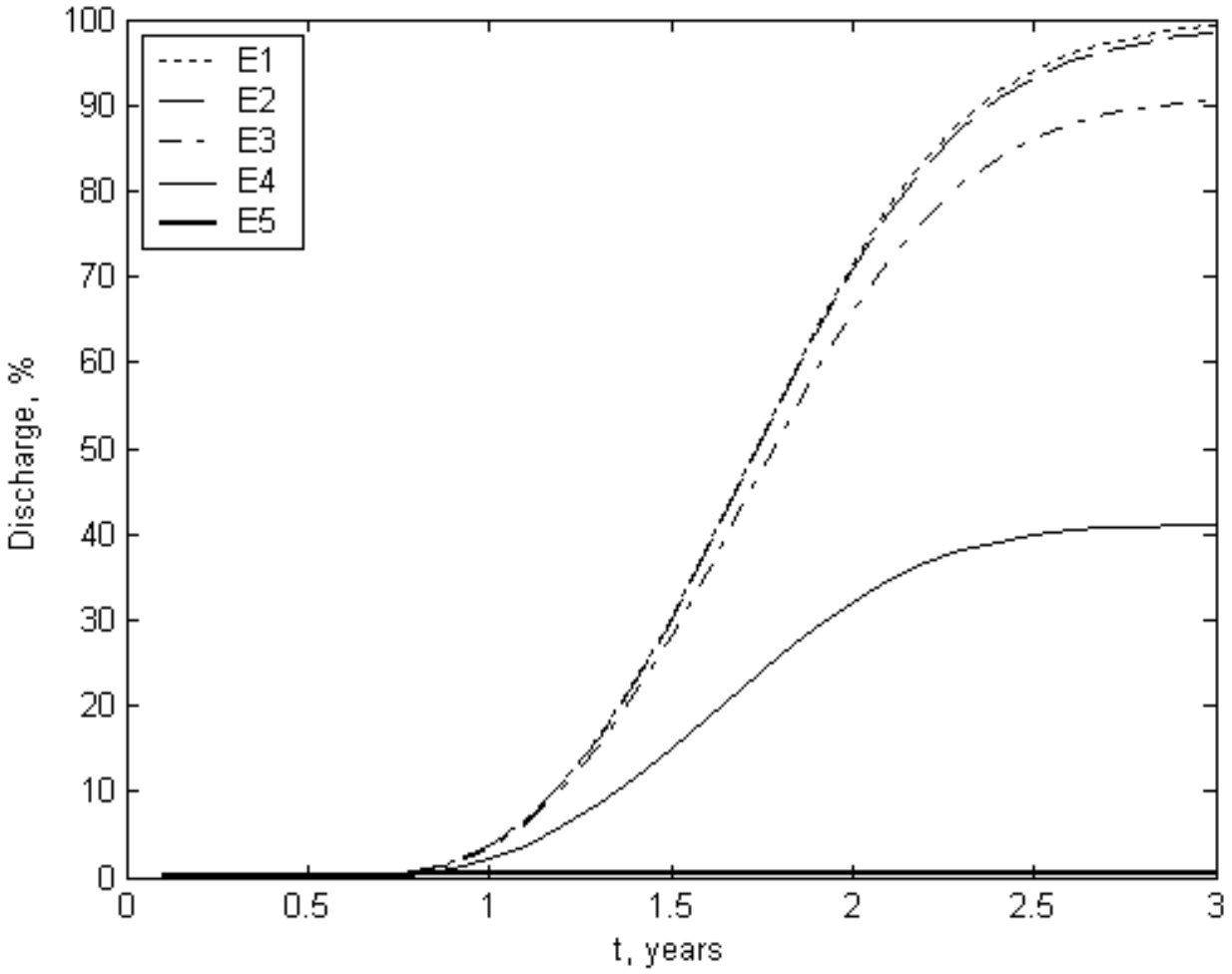

Figure 5.17 Evaluation of Decay-Discharge Relation.

The maximum contaminant discharge out of the system as a function of the decay constant can be approximated by formula (5.4) under the conditions adopted in this study (relations can be derived under other conditions in a similar manner).

$$\text{Maximum discharge} \approx 100e^{-350\lambda} \tag{5.4}$$

This relationship is also shown graphically in Figure 5.18.

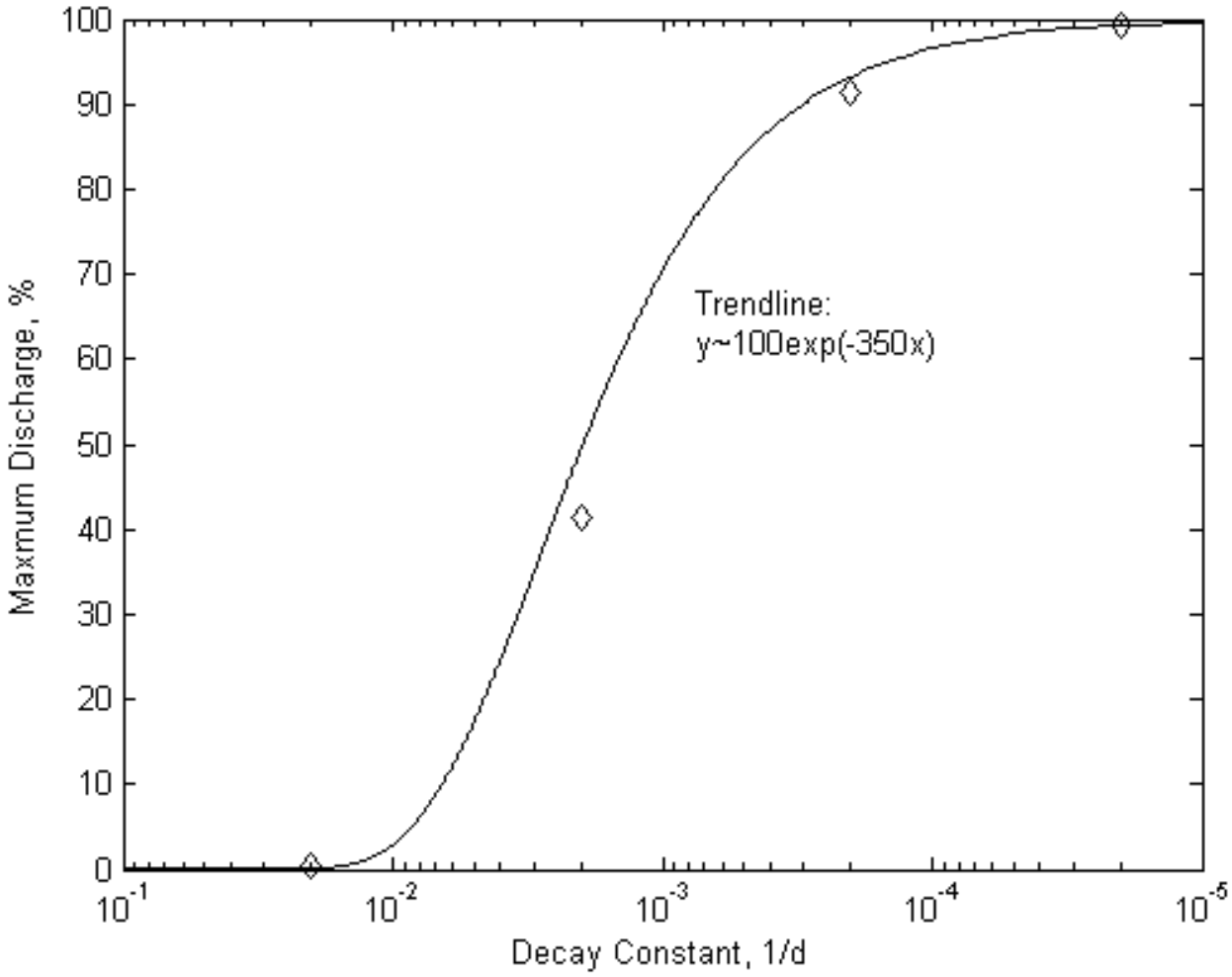

Figure 5.18 Decay Constant-Maximum Discharge Relationship.

Next the results are presented incorporating tidal fluctuations. Cases and assigned parameter values are listed in Table 5.9.

Table 5.9 Cases Assigned in Evaluation of Tidal Effect

Case No.	DC1 Baseline	DC1	DC2 Baseline	DC2	DC3 Baseline	DC3
Decay Constant, d^{-1}	0.0	0.0	2×10^{-4}	2×10^{-4}	2×10^{-3}	2×10^{-3}
Tidal Amplitude, m	0	1.0	0	1.0	0	1.0

Inclusion of tidal fluctuations leads to a significant concentration reduction in regions adjacent to the coastline (refer to Figure 5.19), which is consistent with the other cases studied earlier under other conditions. As discussed earlier, decay causes a concentration decrease. With different decay constants, however, tidal influence does not deviate noticeably from each other from the perspective of concentration distribution. A similar result is also observed in the contaminant discharge profiles as illustrated in Figure 5.20. There is an interesting point to make with regard to tidal influence under the condition of fast decay (or large decay constant). That is, tidal activities do lead to a slightly increased total contaminant discharge (refer to cases DC3 versus DC3 baseline). The difference can be attributable to the enhanced discharge by tides leading to less retention time in the aquifer and thus subject to less chance for decay to occur.

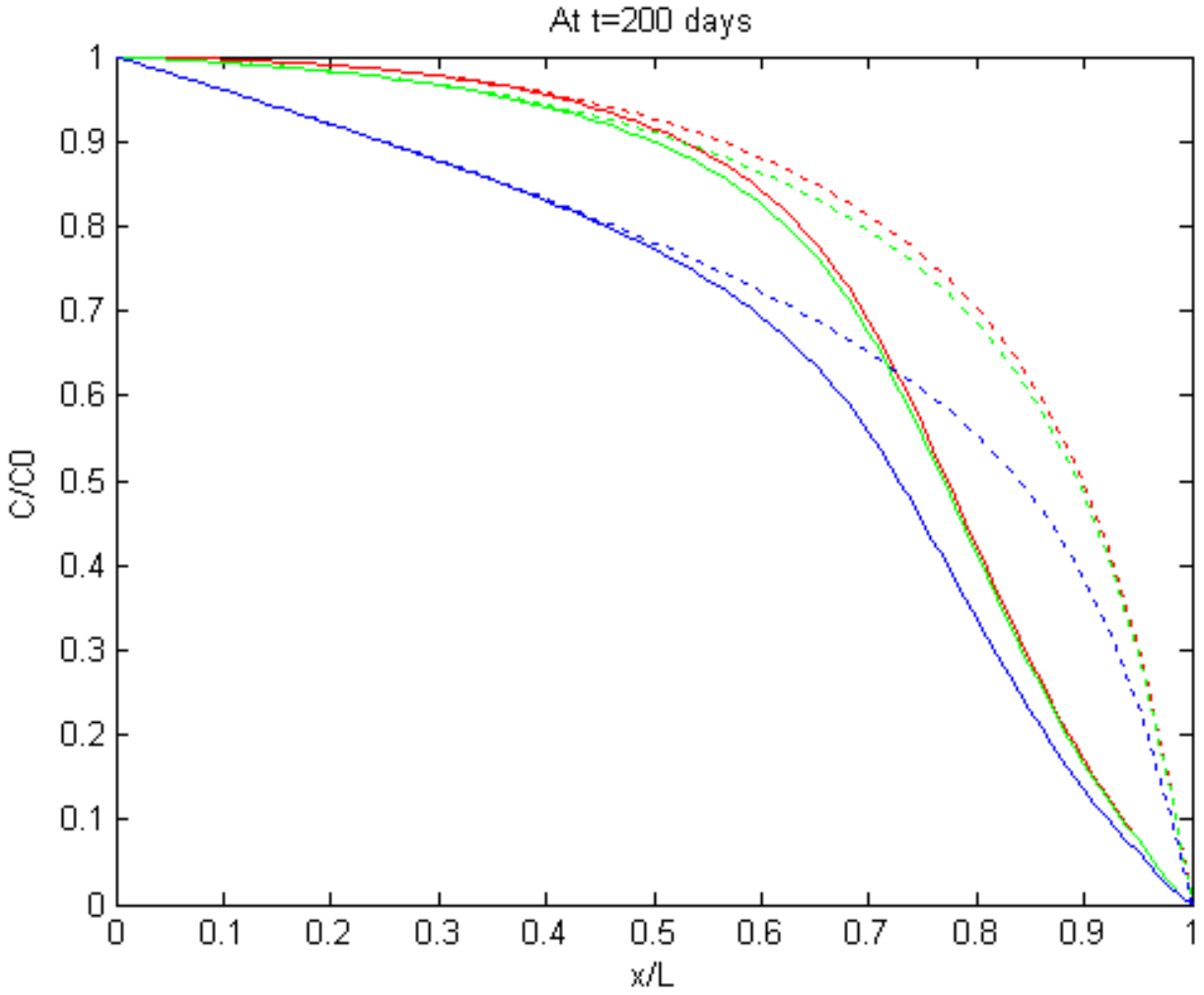

Legend: Dot-Baselines, Red Solid-DC1, Green Solid-DC2, and Blue Solid-DC3

Figure 5.19 Tidal Effect on Contaminant Distribution subject to Different Decay Constants.

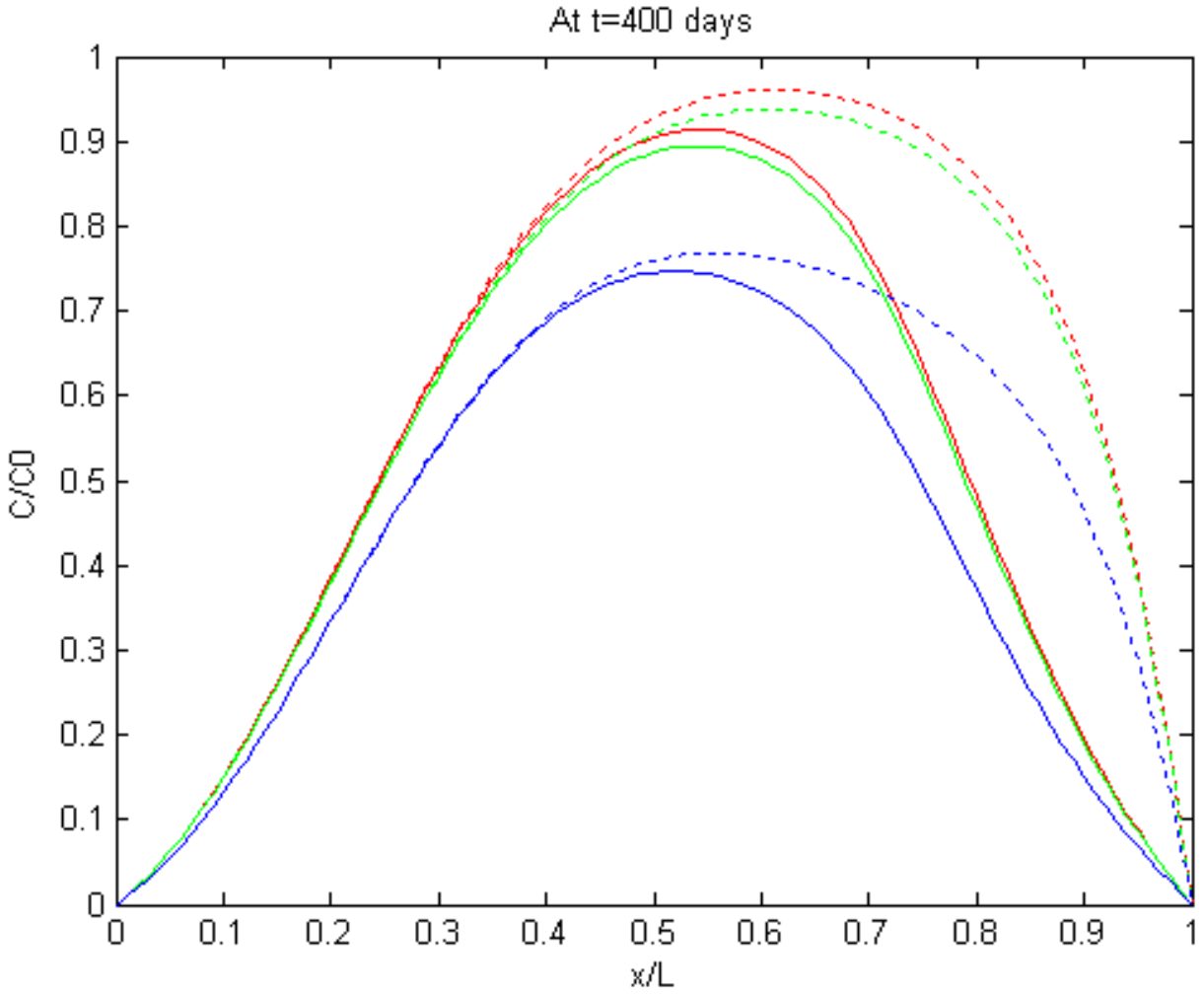

Legend: Dot-Baselines, Red Solid-DC1, Green Solid-DC2, and Blue Solid-DC3

Figure 5.19 Tidal Effect on Contaminant Distribution subject to Different Decay Constants (Continued).

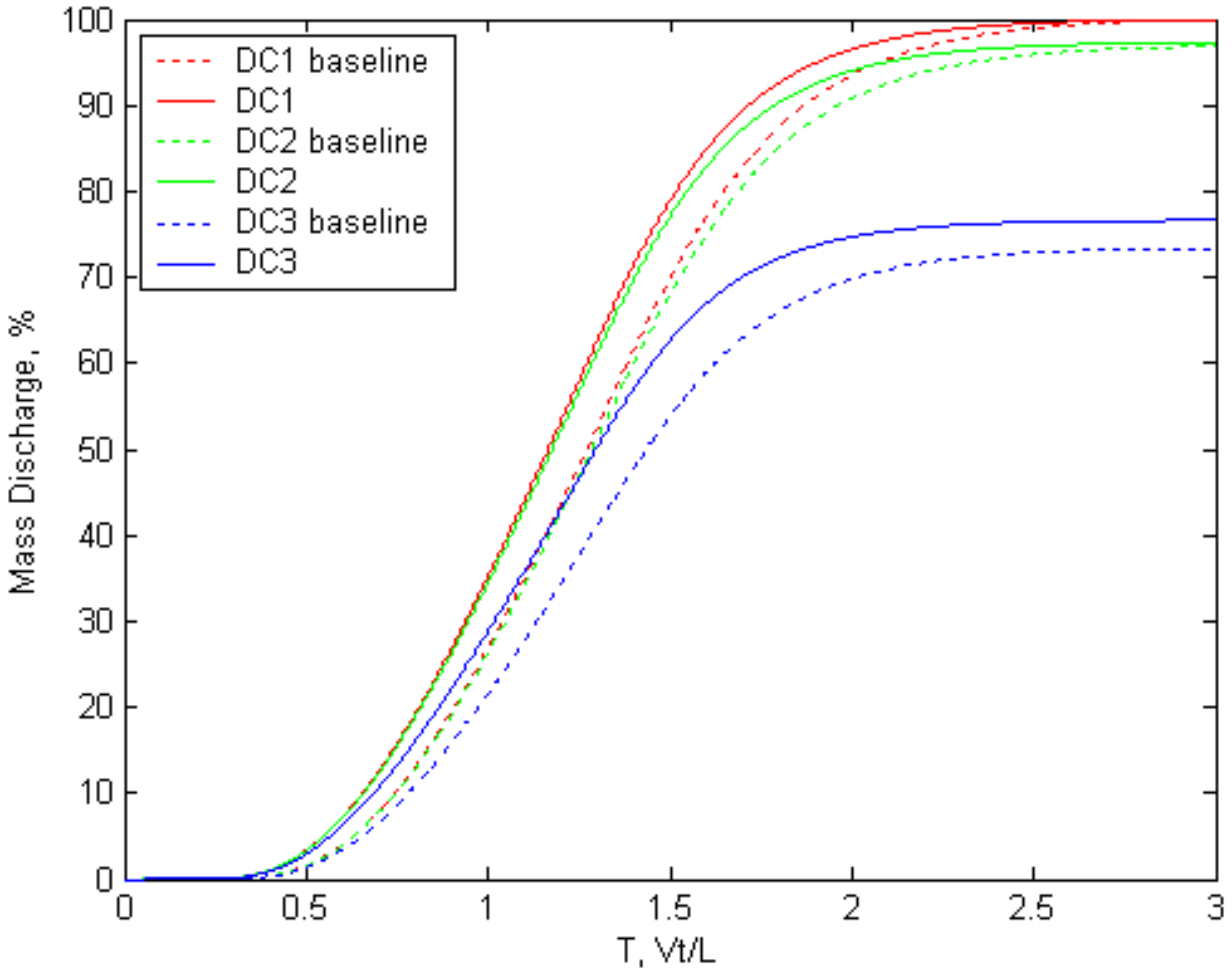

Figure 5.20 Tidal Effect on Contaminant Discharge subject to Different Decay Constants.

5.3.5 Tidal Effect with Different Aquifer Dimension

In this subsection, aquifer dimension is evaluated to see if tidal influence would be different under different situations in term of aquifer length. Since in the current study, the contaminant is assumed to be released at the inland end of the aquifer system, different aquifer dimensions mean different lengths of flow and transport paths from the point where the contaminant is released to the coastal boundary. Cases and assigned parameter values for this purpose are listed in Table 5.10.

Table 5.10 Cases Assigned in Evaluation of Tidal Effect

Case No.	DM1 Baseline	DM1	DM2 Baseline	DM2	DM3 Baseline	DM3
Aquifer Length, m	100	100	200	200	400	400
Tidal Amplitude, m	0	1.0	0	1.0	0	1.0

Figure 5.21 gives the concentration distribution profiles when the contaminant plume reaches the stage I (the contaminant plume reaches a location approximately 80 meters from the coastal boundary).

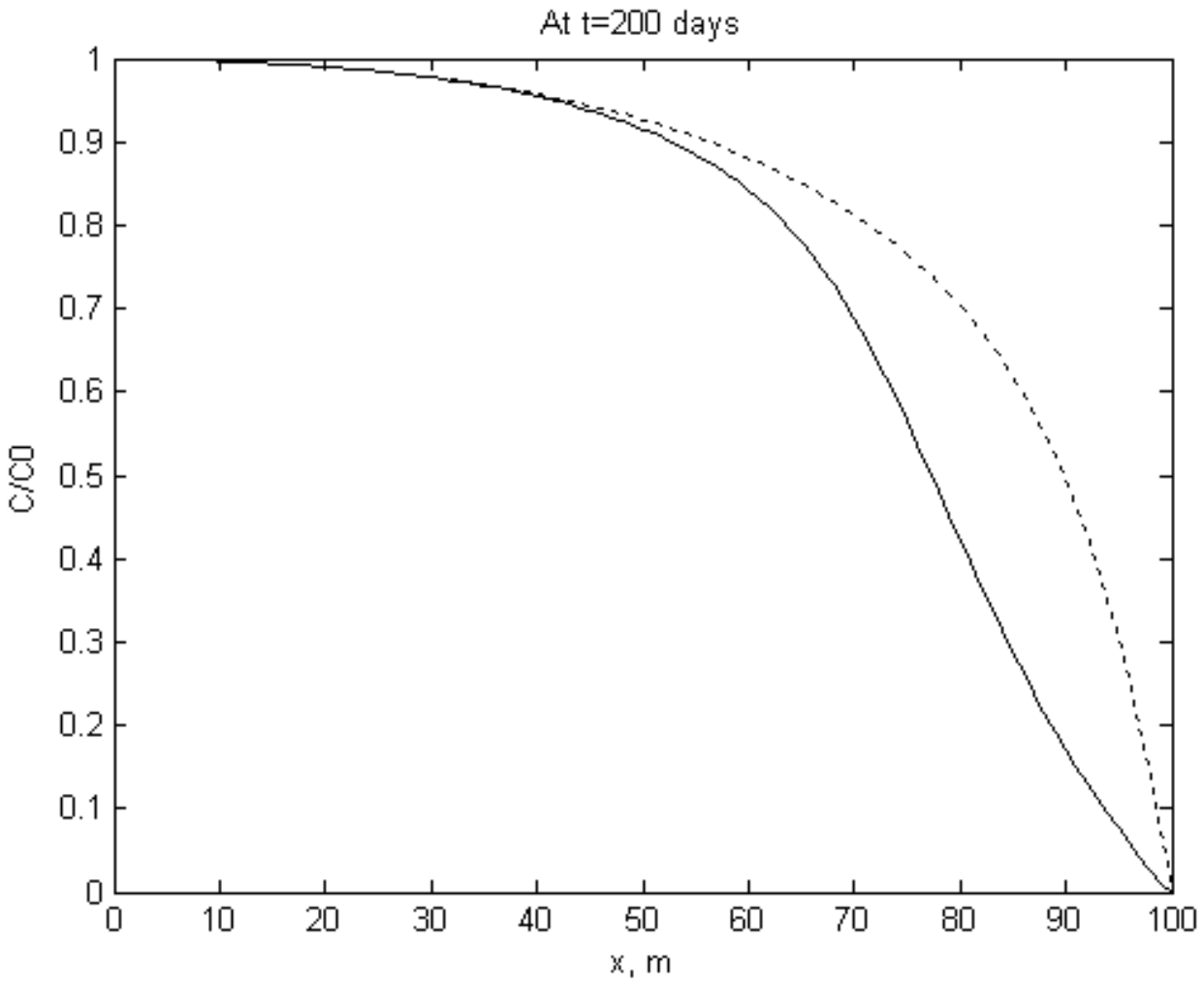

Legend: Solide-DM1, Dot-Baseline

Figure 5.21 Comparison of Tidal Effect on Contaminant Distribution at Stage I.

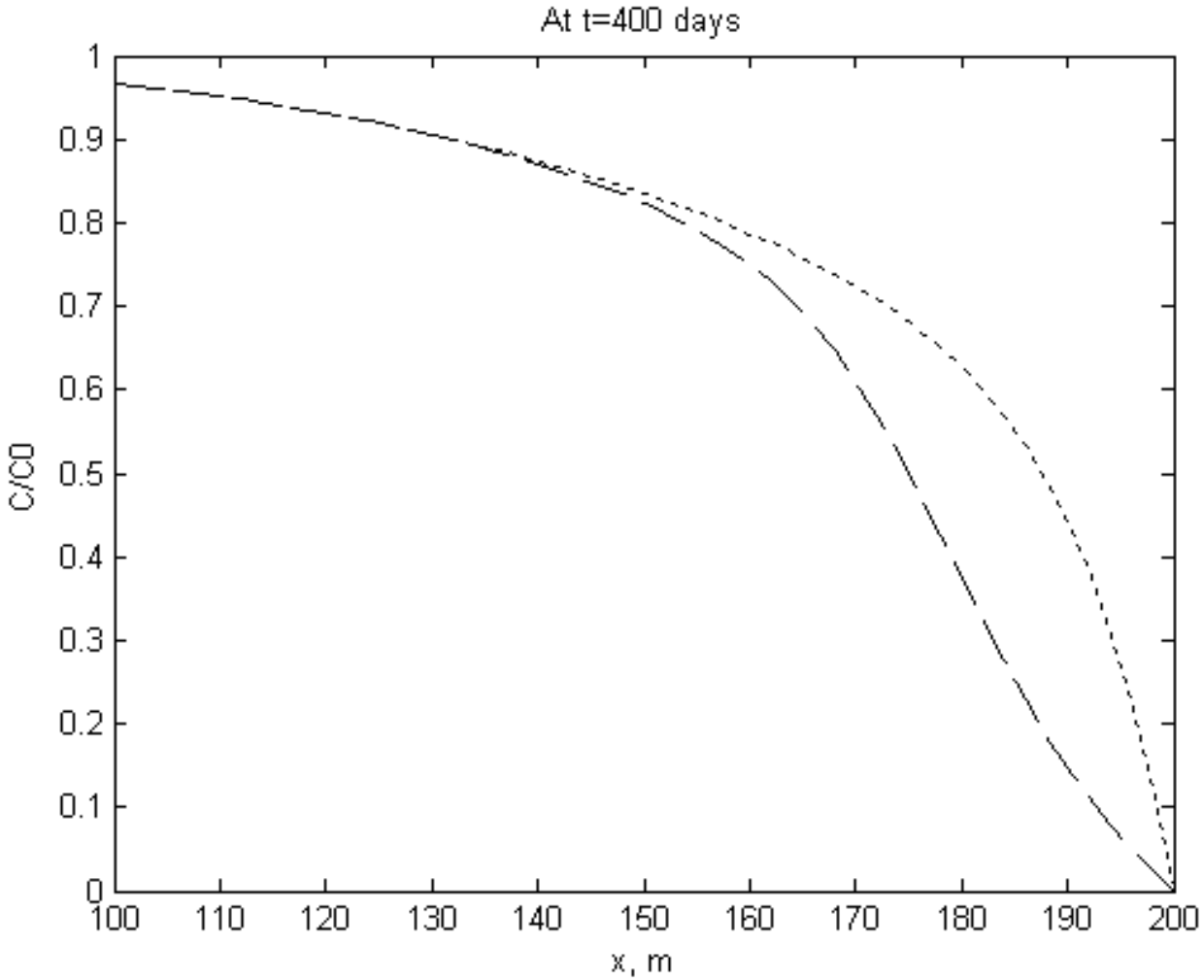

Legend: Dash-DM2, Dot-Baseline

Figure 5.21 Comparison of Tidal Effect on Contaminant Distribution at Stage I (Continued).

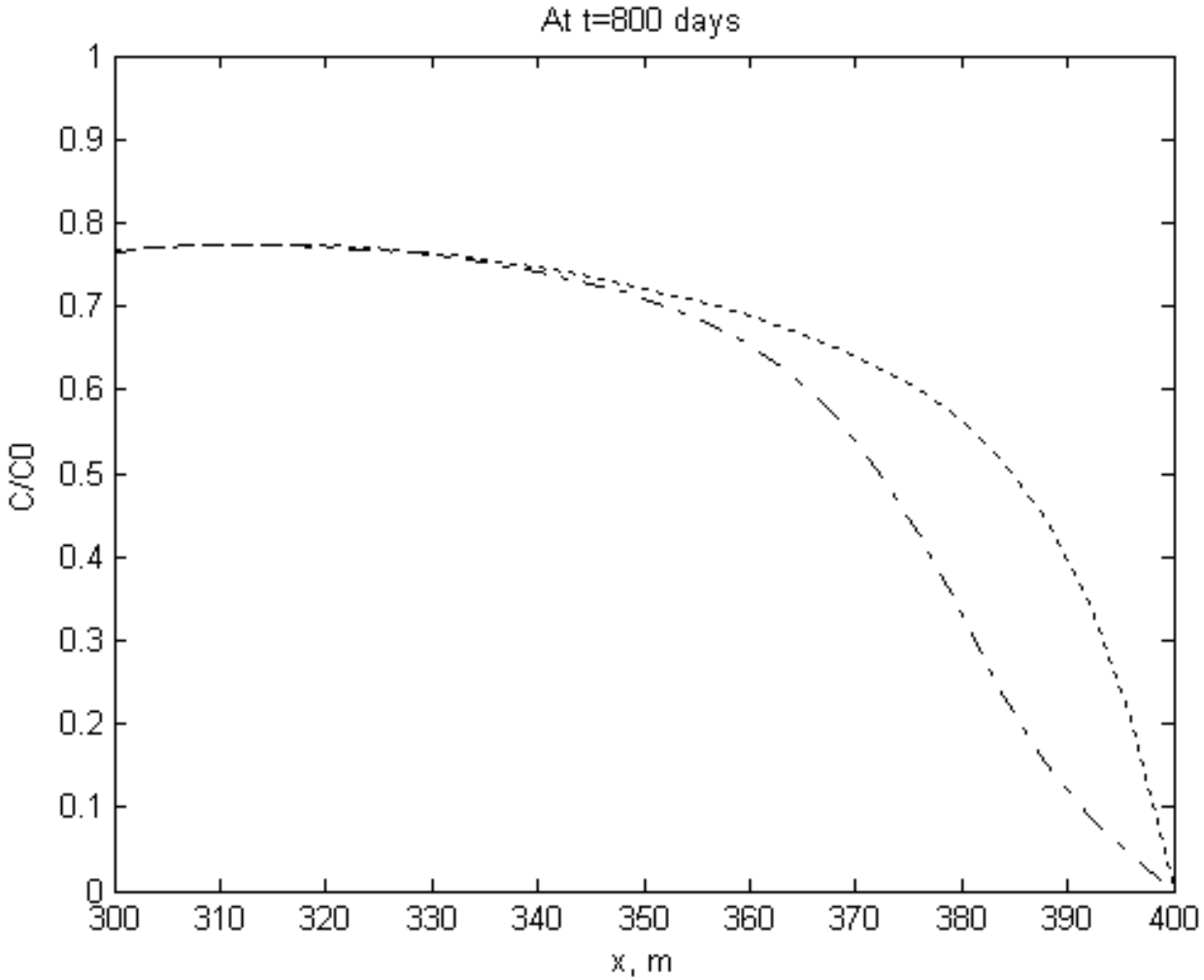

Legend: Dash Dot-DM3, Dot-Baseline

Figure 5.21 Comparison of Tidal Effect on Contaminant Distribution at Stage I (Continued).

Figure 5.22 gives the concentration distribution profiles when the contaminant plume reaches the stage II (the contaminant plume reaches a location approximately 40 meters from the coastal boundary).

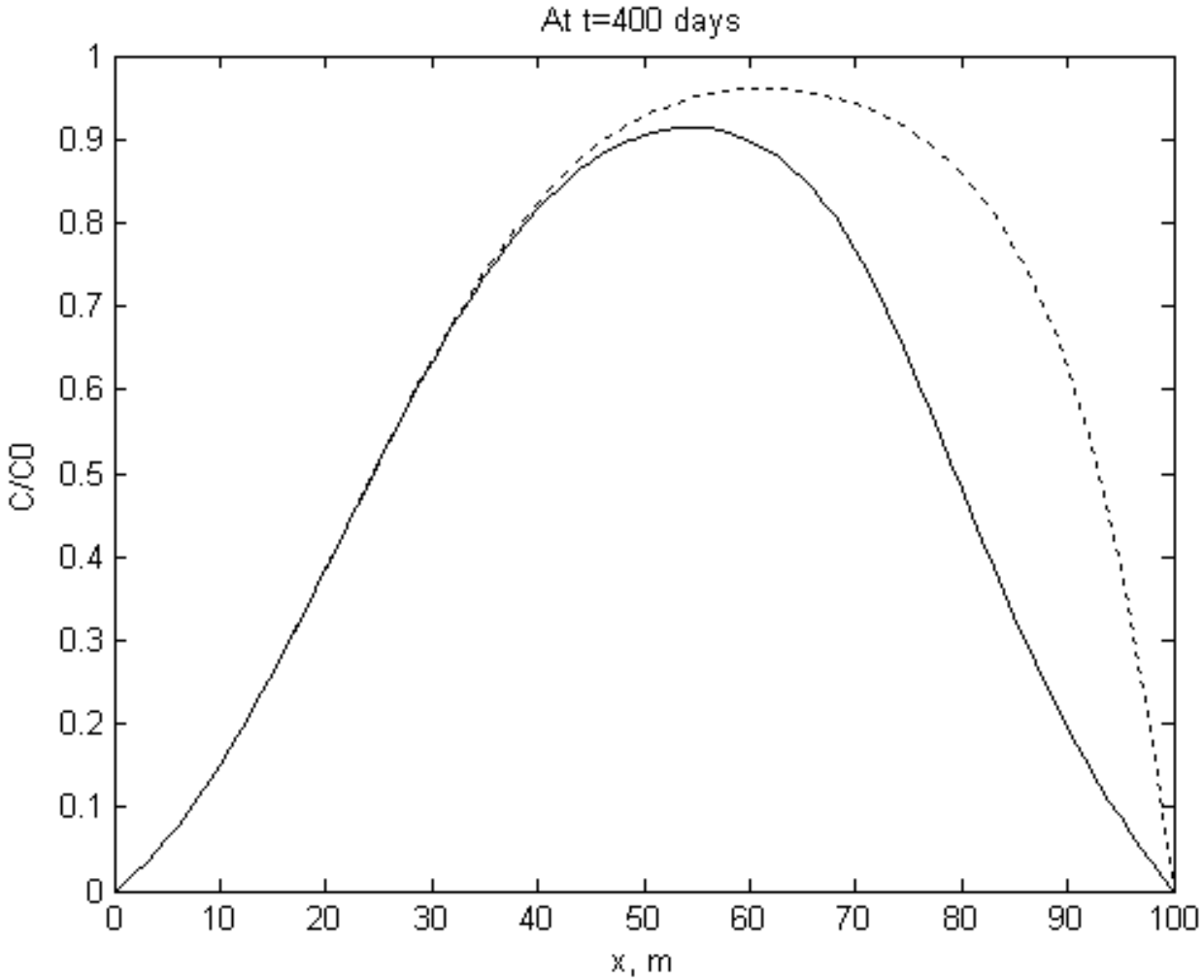

Legend: Solide-DM1, Dot-Baseline

Figure 5.22 Comparison of Tidal Effect on Contaminant Distribution at Stage II.

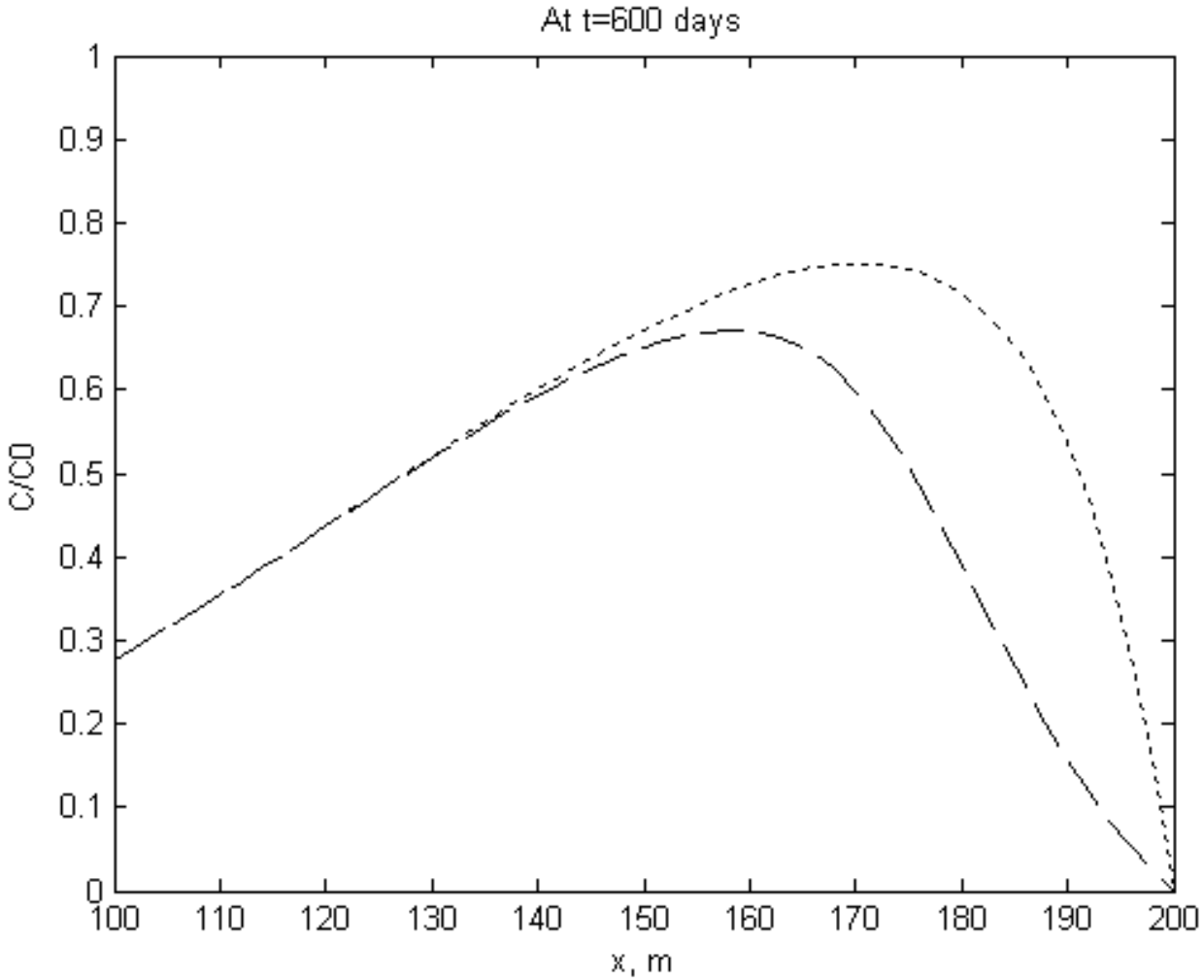

Legend: Dash-DM2, Dot-Baseline

Figure 5.22 Comparison of Tidal Effect on Contaminant Distribution at Stage II (Continued).

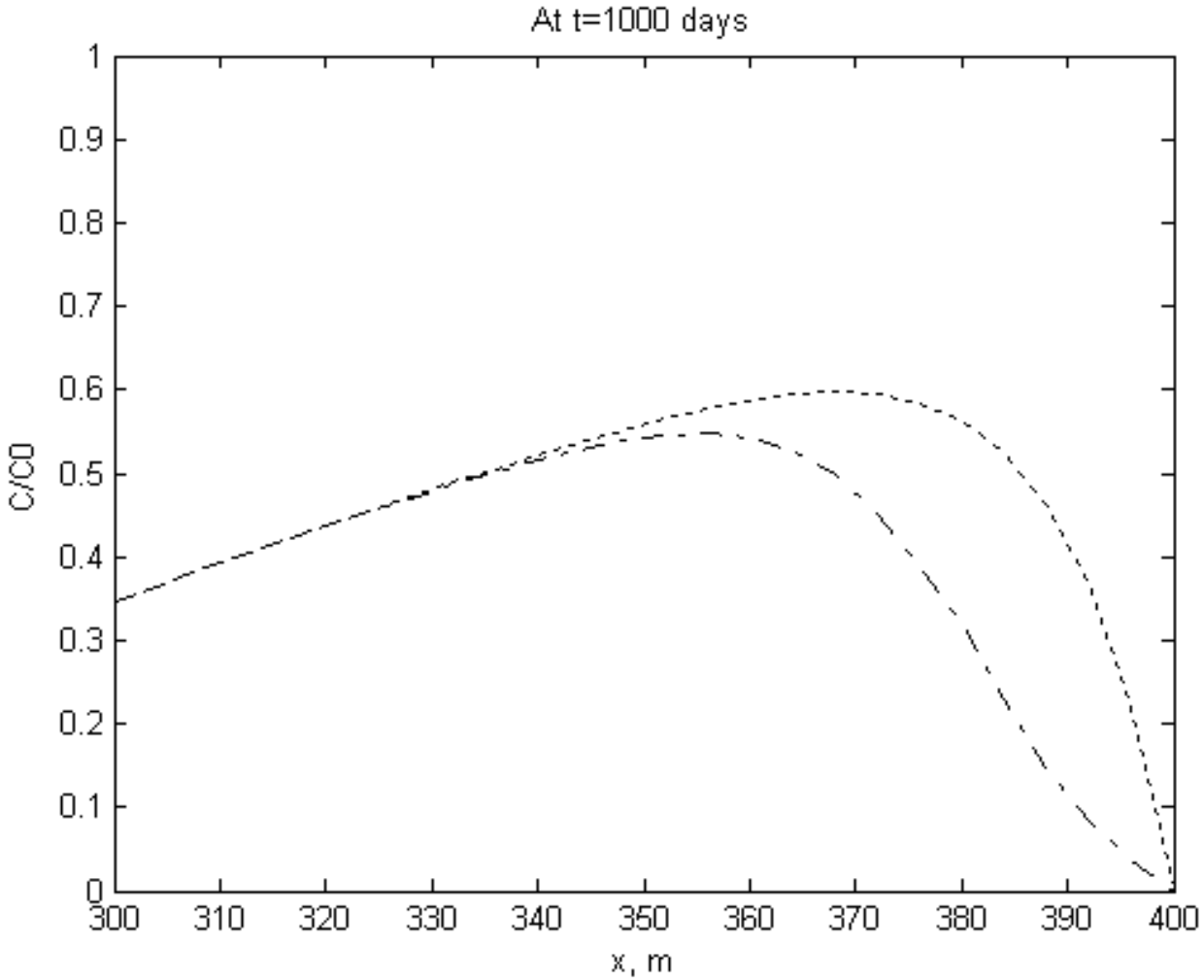

Legend: Dash Dot-DM3, Dot-Baseline

Figure 5.22 Comparison of Tidal Effect on Contaminant Distribution at Stage II (Continued).

As shown in Figure 5.21 and Figure 5.22, the concentration distributions are compared for these cases at each stage when the contaminant plume reaches similar locations relative to the coastline, though it takes a totally different time for the contaminant plume to reach that stage in each case. While the contaminant plume has a different shape at each stage for each case due to the different distance traveled, the tidal influence is almost identical in terms of the relative concentration reduced for these cases. On the other hand, the potential effect zone of the tides, or the location where the concentration deviates, is almost the same in these cases, and is approximately 60 meters from the coastline.

The aforementioned difference of tidal influence slightly deviates from the results regarding contaminant discharge as illustrated in Figure 5.23. With a longer aquifer domain, contaminant discharge is subject to slightly less tidal influence. This may be attributed to the lower contaminant concentration in the regions adjacent to the coastline when the contaminant plume reaches that point with a larger aquifer domain, which in turn results in relatively less effect by tides.

Notice again, that the discharge enhancement by tides can be significant during the early stages of discharge under any aquifer-dimension condition, as indicated in Figure 5.24 (87%-110% increase over the baseline at T=0.5), but this difference decreases as time since the start of contaminant discharge increases.

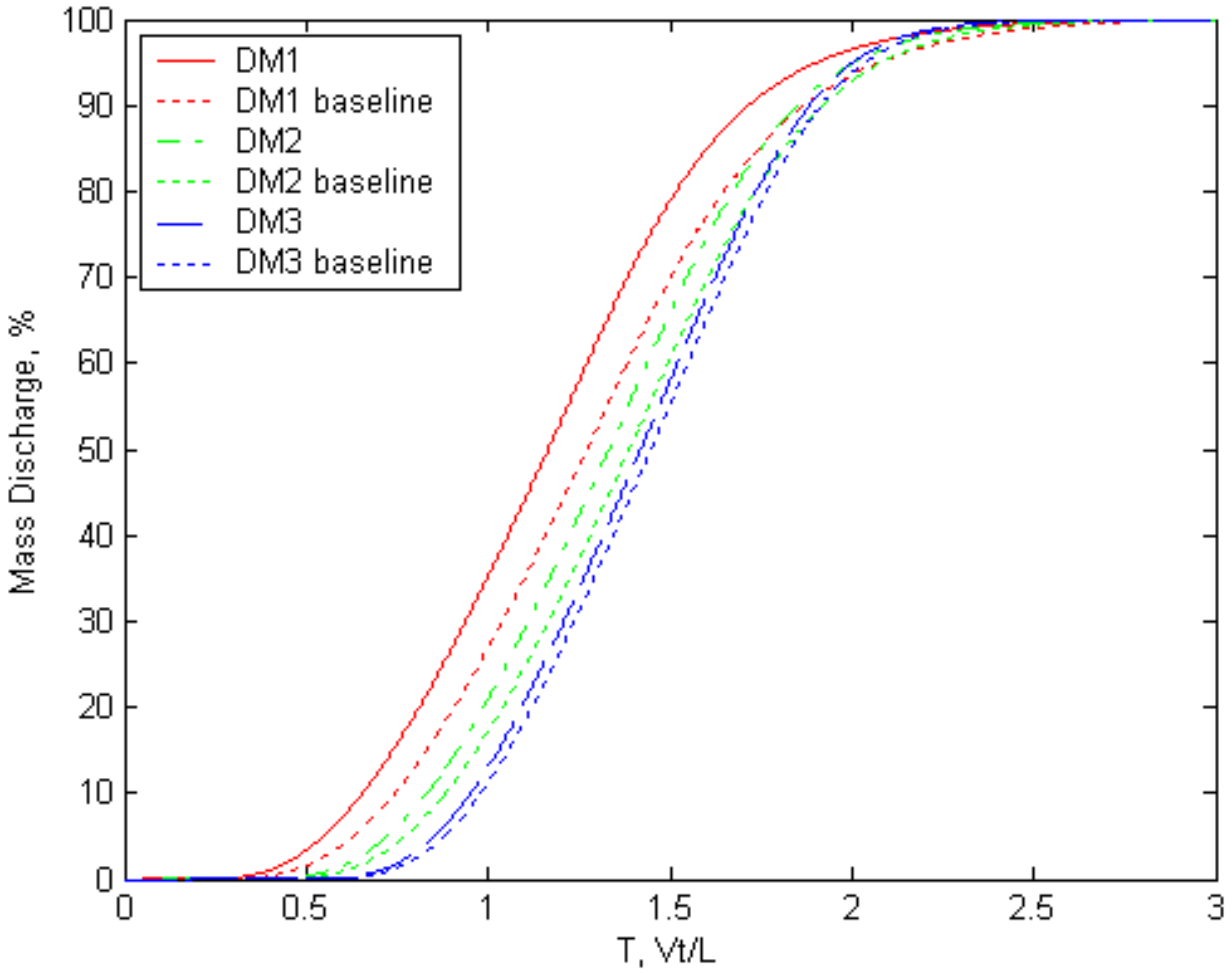

Figure 5.23 Tidal Effect on Contaminant Discharge subject to Different Aquifer Dimensions.

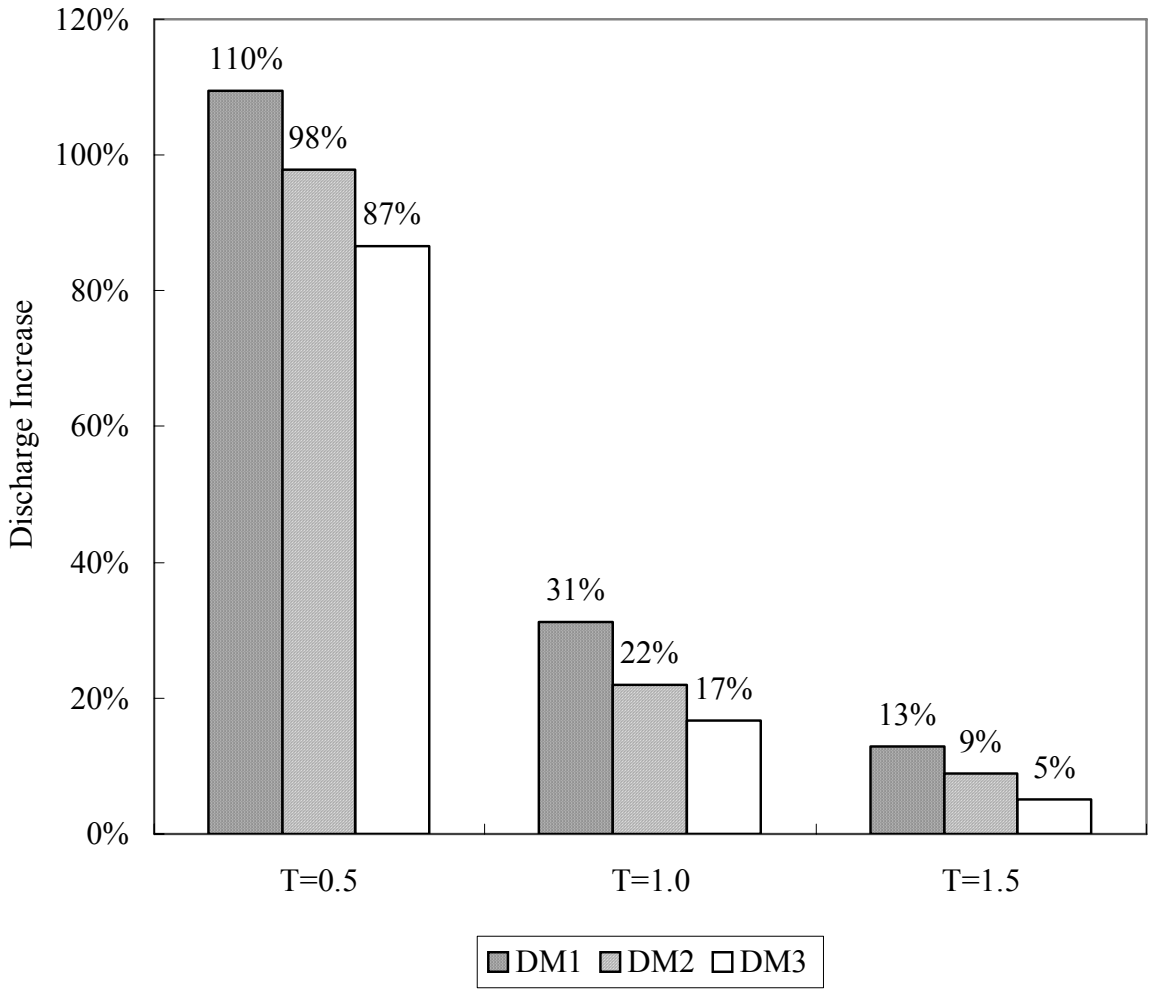

Figure 5.24 Tidal Effect on Contaminant Discharge subject to Different Aquifer Dimensions.

5.4 Tidal Influence under Confined Condition

It is mentioned early in Section 5.2 that the tidal influence is more significant under unconfined conditions than under confined conditions. To investigate if this is true under various situations where other aquifer and tide parameters are changed, a series of cases under confined conditions are studied and compared with those under unconfined conditions presented in the previous section. Table 5.11 lists all these cases considered. Note that the values with bold font in the table indicate the conditions which are favorable to tidal effect.

Table 5.11 Case Numbers Assigned in the Evaluation of Tidal Effect

Case No. Unconfined/Confined	Amplitude, m	Flow Velocity, m/d	Retardation	Decay, d^{-1}	Aquifer Length, m
N4/N16	**2.0**	0.5	1	0	100
N11/N23	1.0	**0.2**	1	0	100
R2/R6	1.0	0.5	**10**	0	100
DC3/DC6	1.0	0.5	1	$\mathbf{10^{-3}}$	100
DM3/DM6	1.0	0.5	1	0	**400**

The comparison of case N4 and N16 is illustrated in Figure 5.25, Figure 5.26, and Figure 5.27. A high tidal amplitude results in a significant impact on contaminant transport under both unconfined and confined conditions. Though the tide demonstrates a much stronger effect in the unconfined case, the potential effect zone in the confined case is greater than in the unconfined case, i.e., 80 meter versus 60 meters. As seen in Figure 5.27, at T=0.5 contaminant discharge is increased 206% compared to the baseline condition in the unconfined condition (case N4), while it is increased only 148% in the confined condition (case N16); similar differences are observed at T=1.0 and T=1.5.

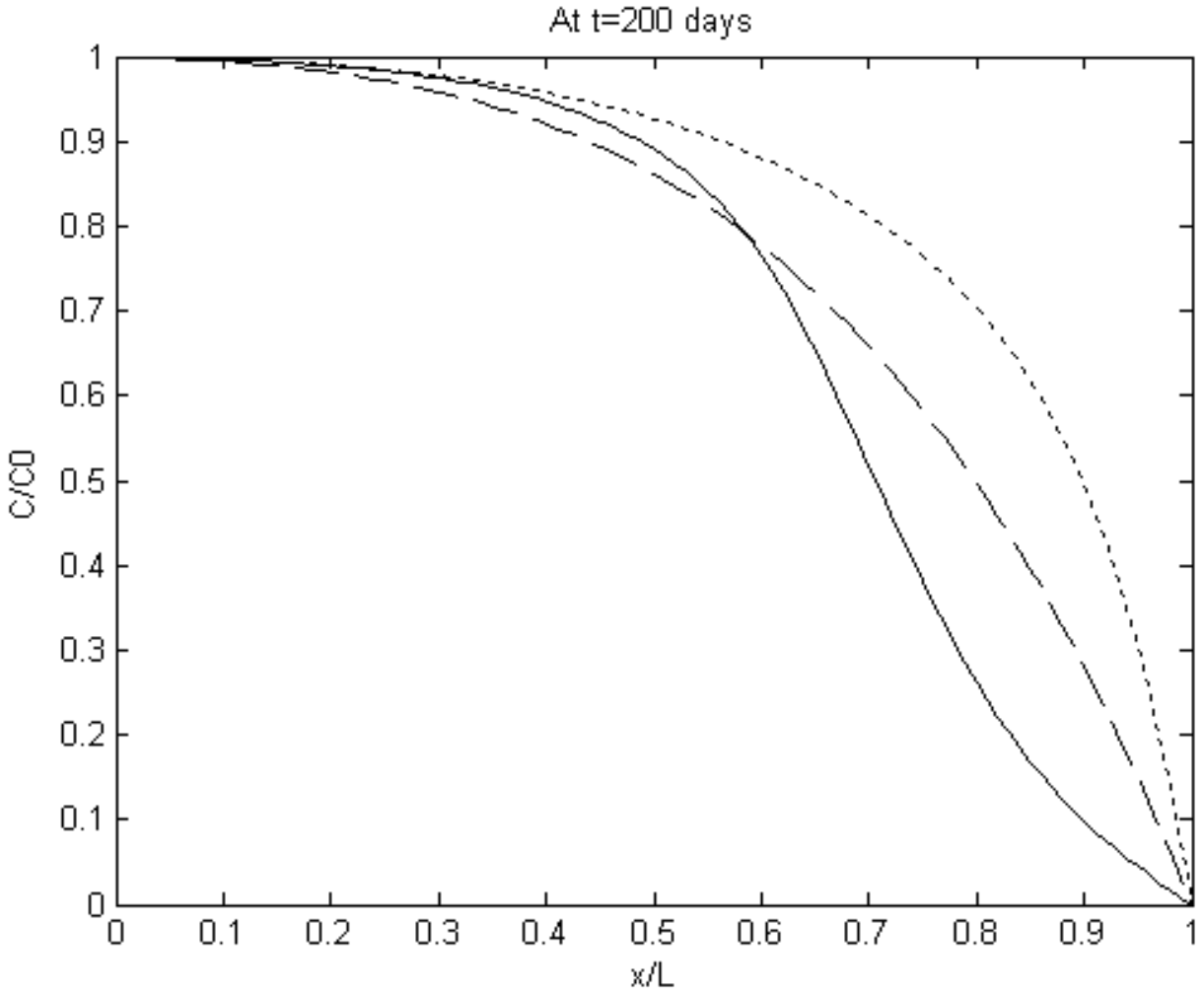

Legend: Dot-Baseline (without tidal effect), Solid-N4, and Dash-N16

Figure 5.25 Tidal Effect on Contaminant Distribution.

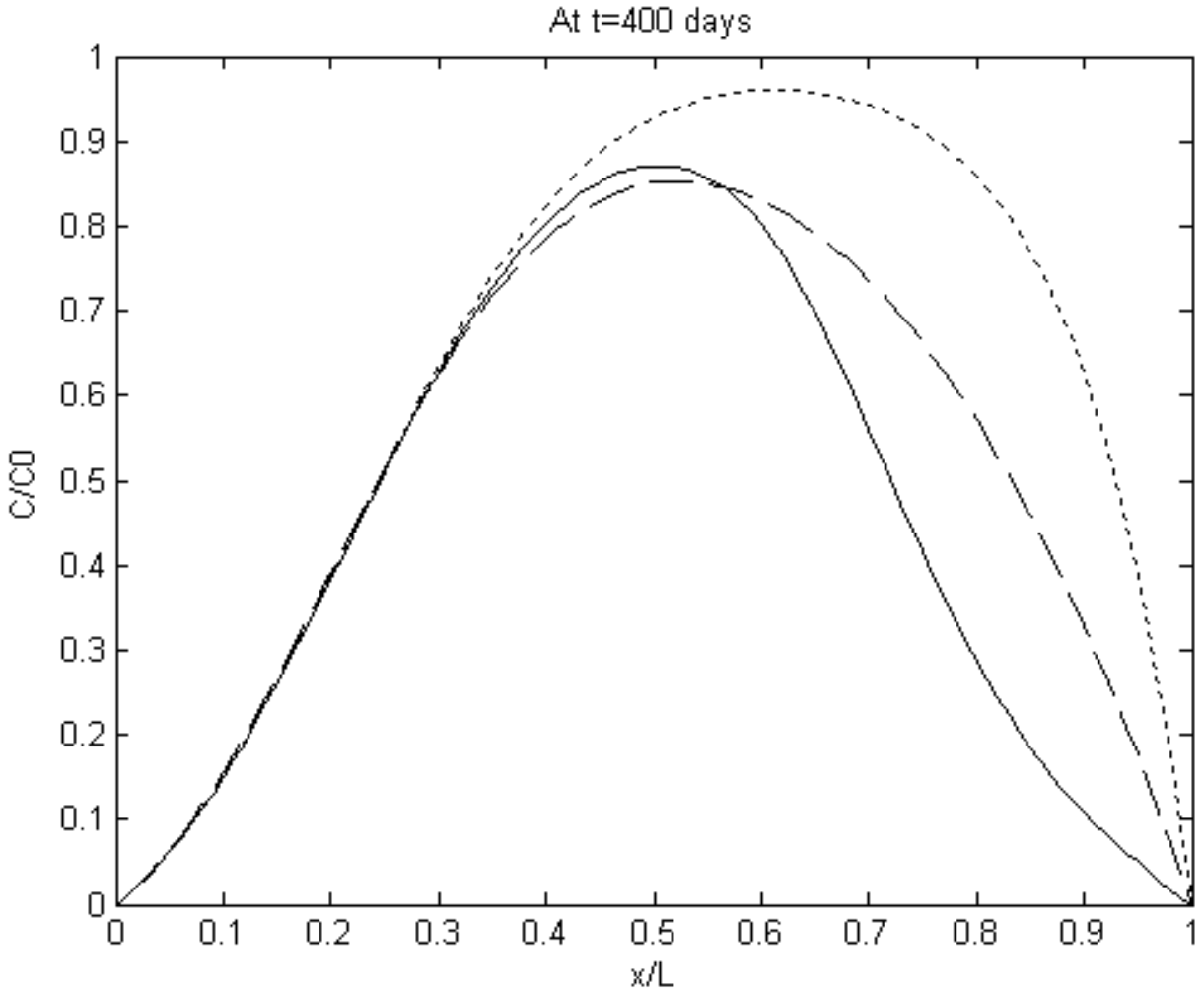

Legend: Dot-Baseline (without tidal effect), Solid-N4, and Dash-N16

Figure 5.25 Tidal Effect on Contaminant Distribution (Continued).

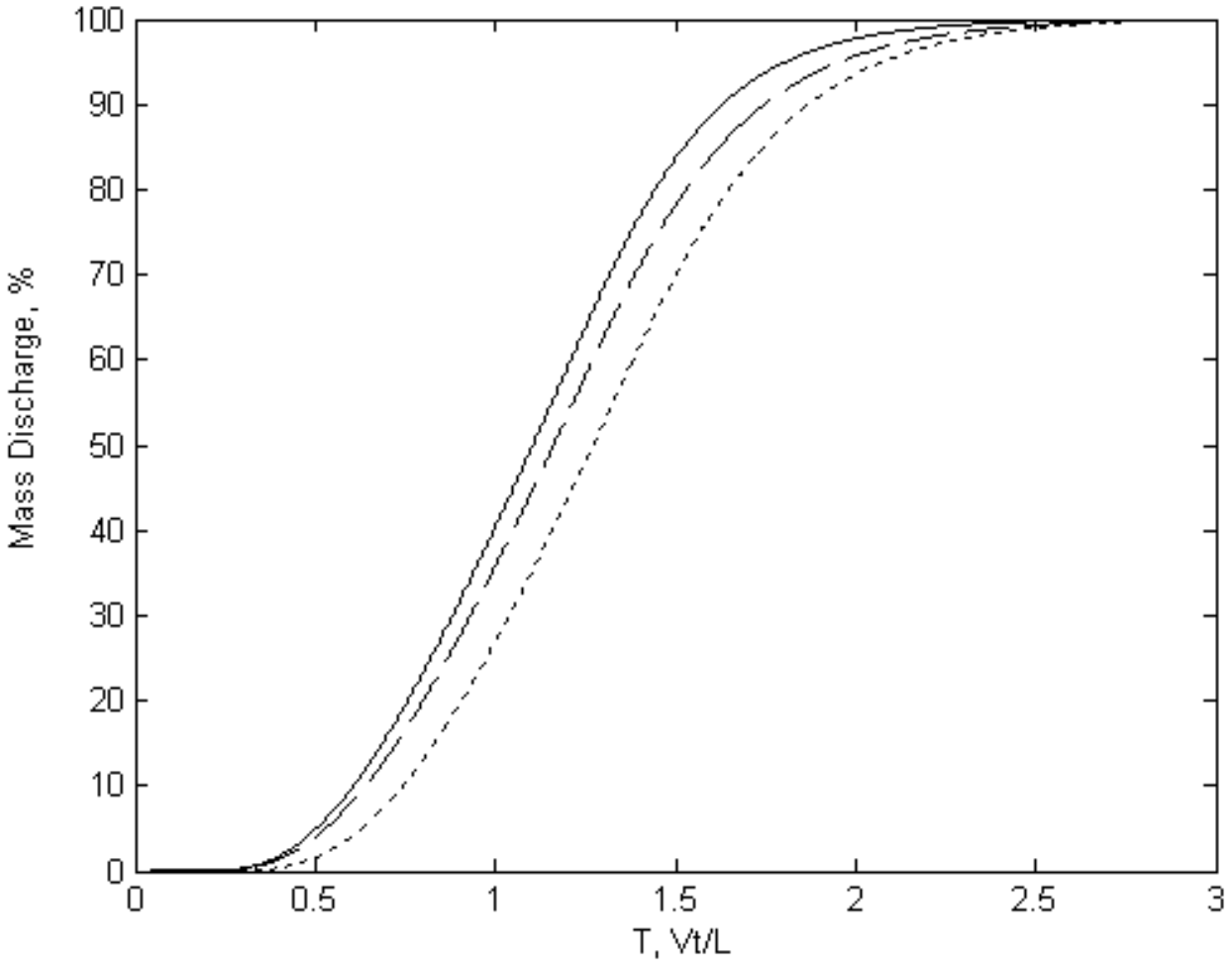

Legend: Dot-Baseline (without tidal effect), Solid-N4, and Dash-N16

Figure 5.26 Tidal Effect on Contaminant Discharge subject to Different Confining Status.

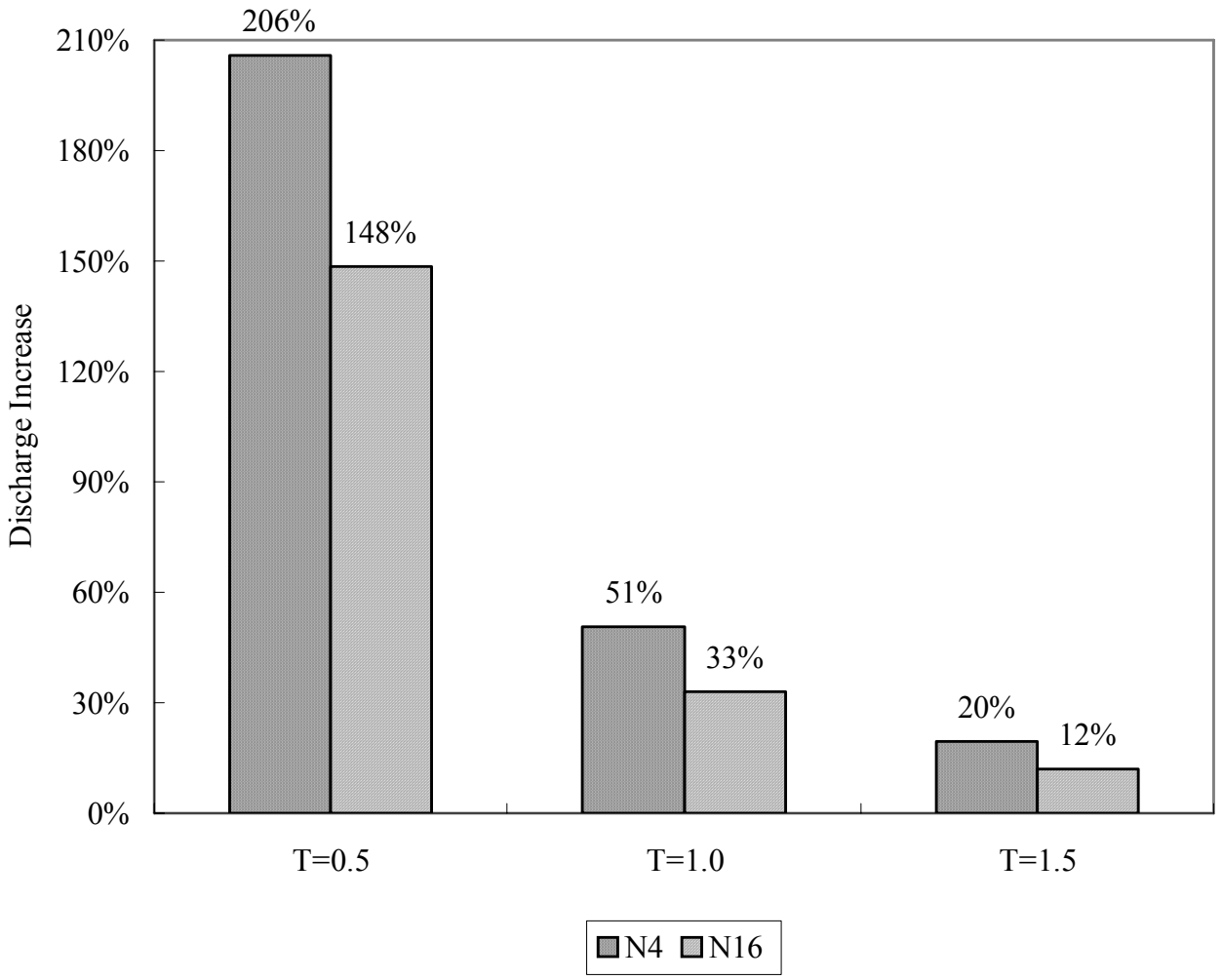

Figure 5.27 Tidal Effect on Contaminant Discharge subject to Different Confining Status.

The comparison of cases N11 and N23 is illustrated in Figure 5.28 through Figure 5.30. Tides show more significant impact under the unconfined condition (case N11) in terms of reduced concentration in areas adjacent to the coastal boundary. However, tidal impact reaches further inland under the confined condition (case N23). As a whole, tidal influence is slightly greater under the unconfined condition as demonstrated by the discharge curves. And as seen in Figure 5.30, the per cent increases in contaminant discharge over the baseline in the unconfined condition case are only 6-13% larger than those in the confined condition case.

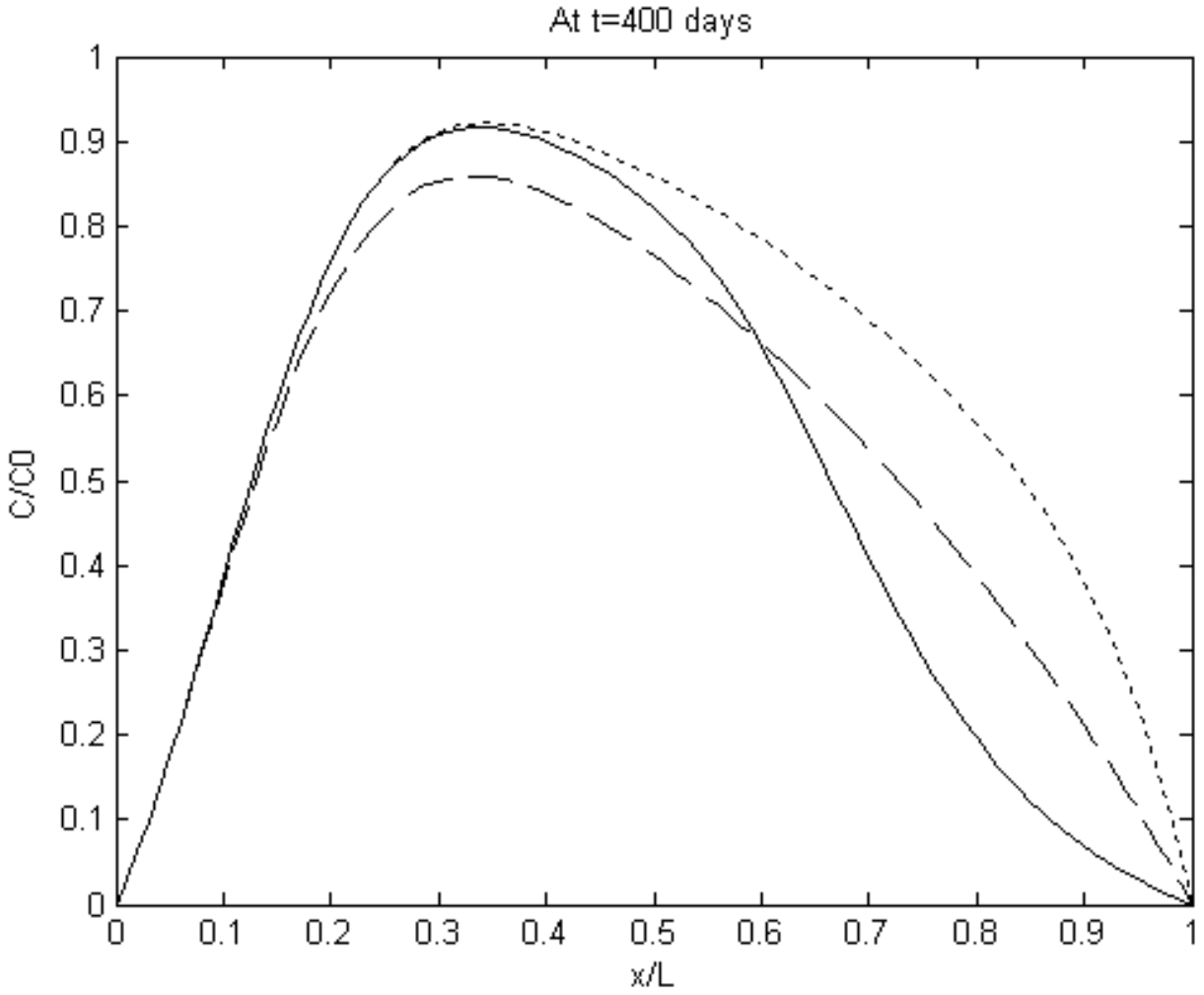

Legend: Dot-Baseline (without tidal effect), Solid-N11, and Dash-N23

Figure 5.28 Tidal Effect on Contaminant Distribution.

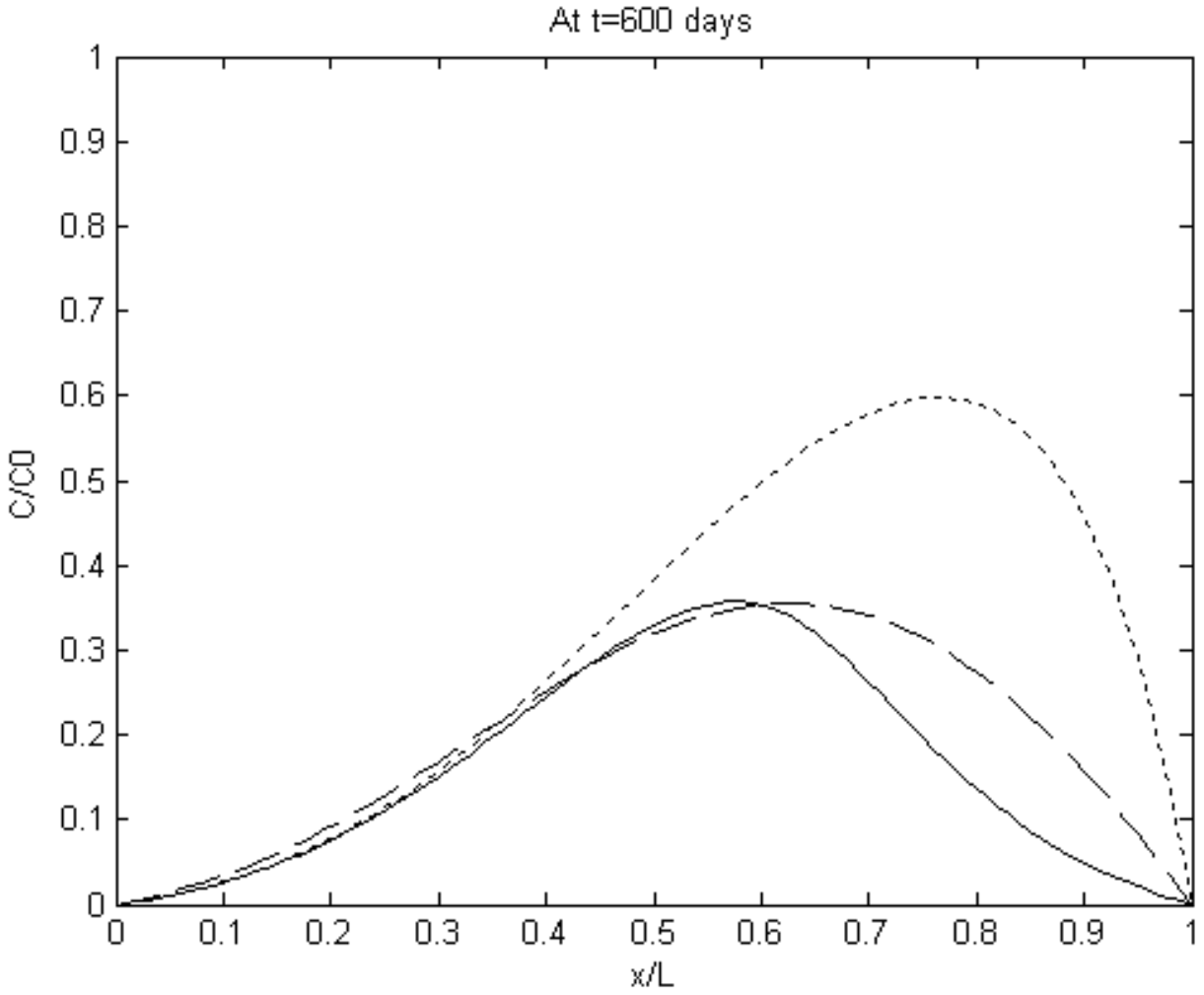

Legend: Dot-Baseline (without tidal effect), Solid-N11, and Dash-N23

Figure 5.28 Tidal Effect on Contaminant Distribution (Continued).

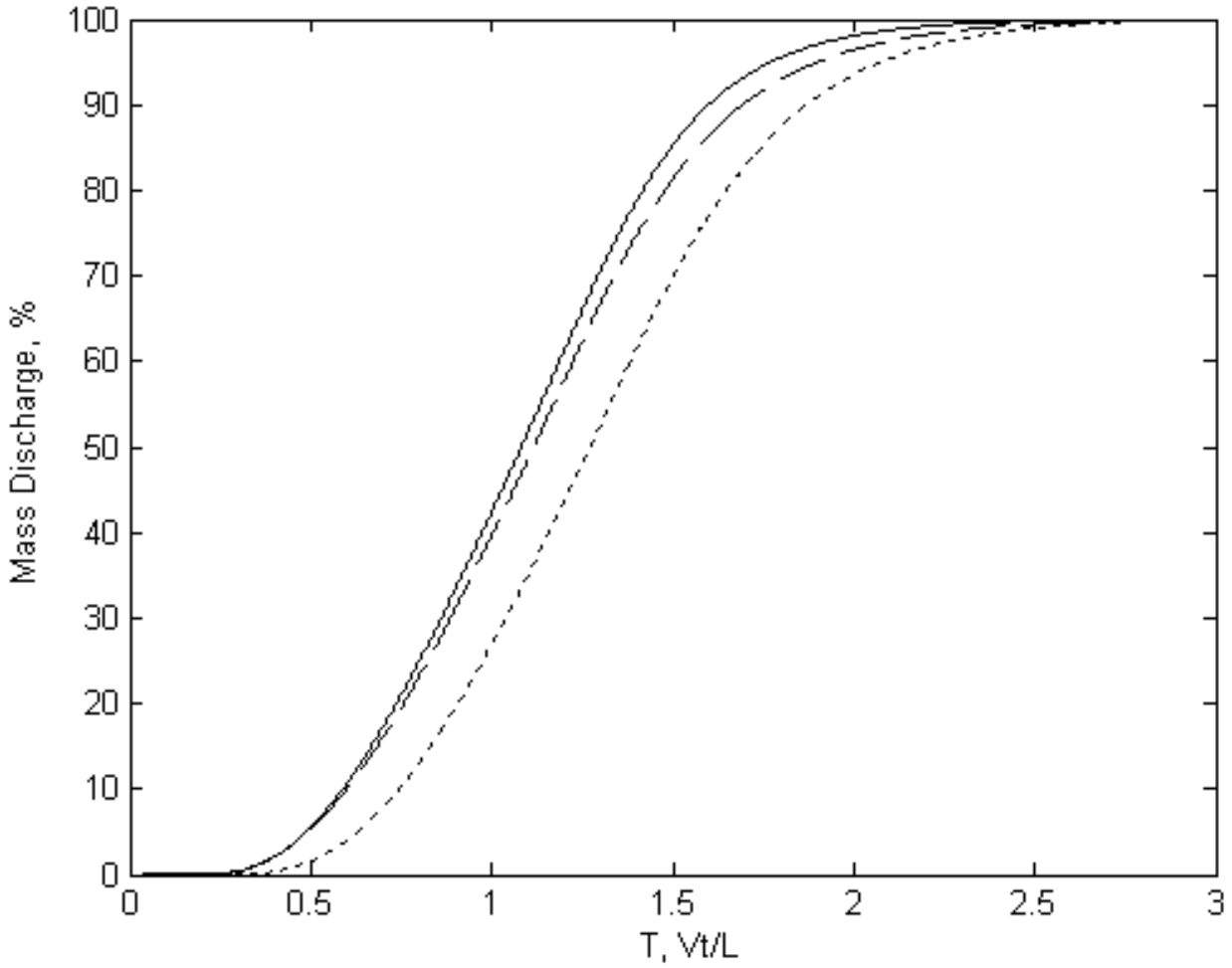

Legend: Dot-Baseline (without tidal effect), Solid-N11, and Dash-N23

Figure 5.29 Tidal Effect on Contaminant Discharge subject to Different Confining Status.

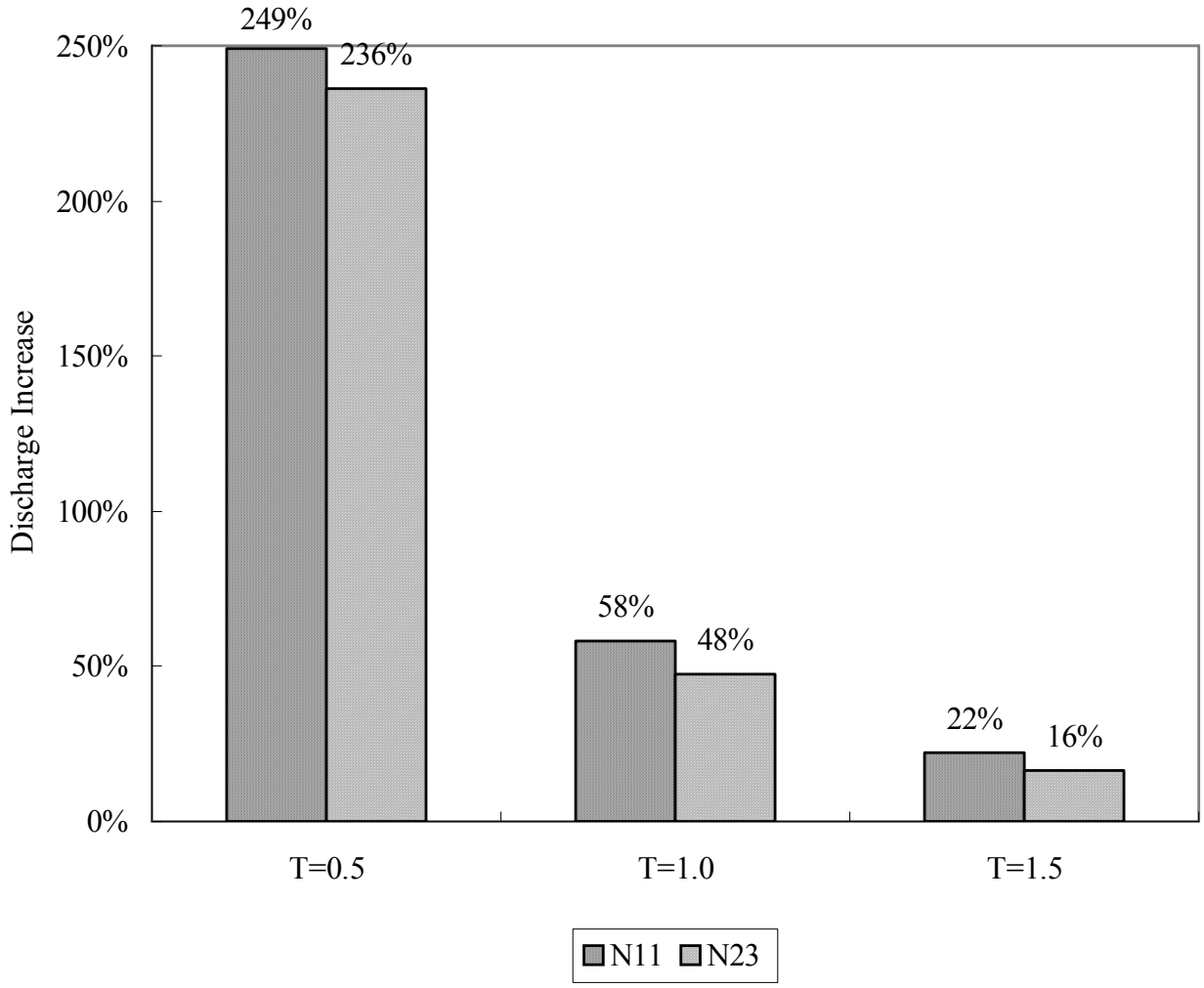

Figure 5.30 Tidal Effect on Contaminant Discharge subject to Different Confining Status.

The comparison of cases R2 and R6 is illustrated in Figure 5.31 through Figure 5.33. As was seen earlier in the unconfined cases, retardation can result in much lower contaminant concentration in groundwater, and thus lead to less tidal effect in terms of a reduced concentration in regions close to the coastal boundary. This is especially true in the confined situation, in which case tidal fluctuations induce negligible impact on contaminant transport, in contrast to significant effect on contaminant discharge observed in the unconfined situation. In Figure 5.33, the per cent increase in contaminant discharge over the baseline in the unconfined condition (case R2) is about 4 times that of the increase in the confined condition (case R6) at all three times presented.

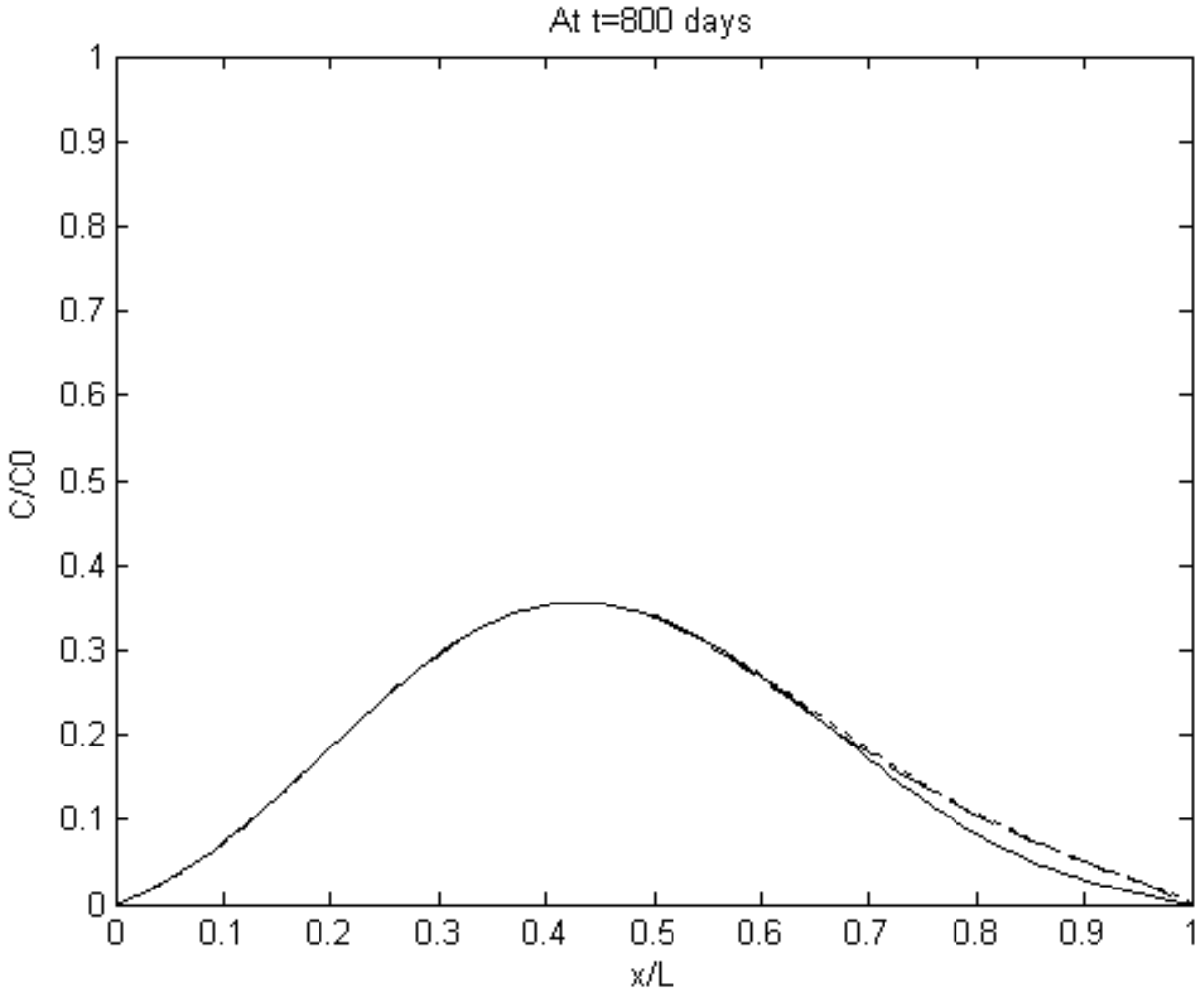

Legend: Dot-Baseline (without tidal effect), Solid-R2, and Dash-R6

Figure 5.31 Tidal Effect on Contaminant Distribution.

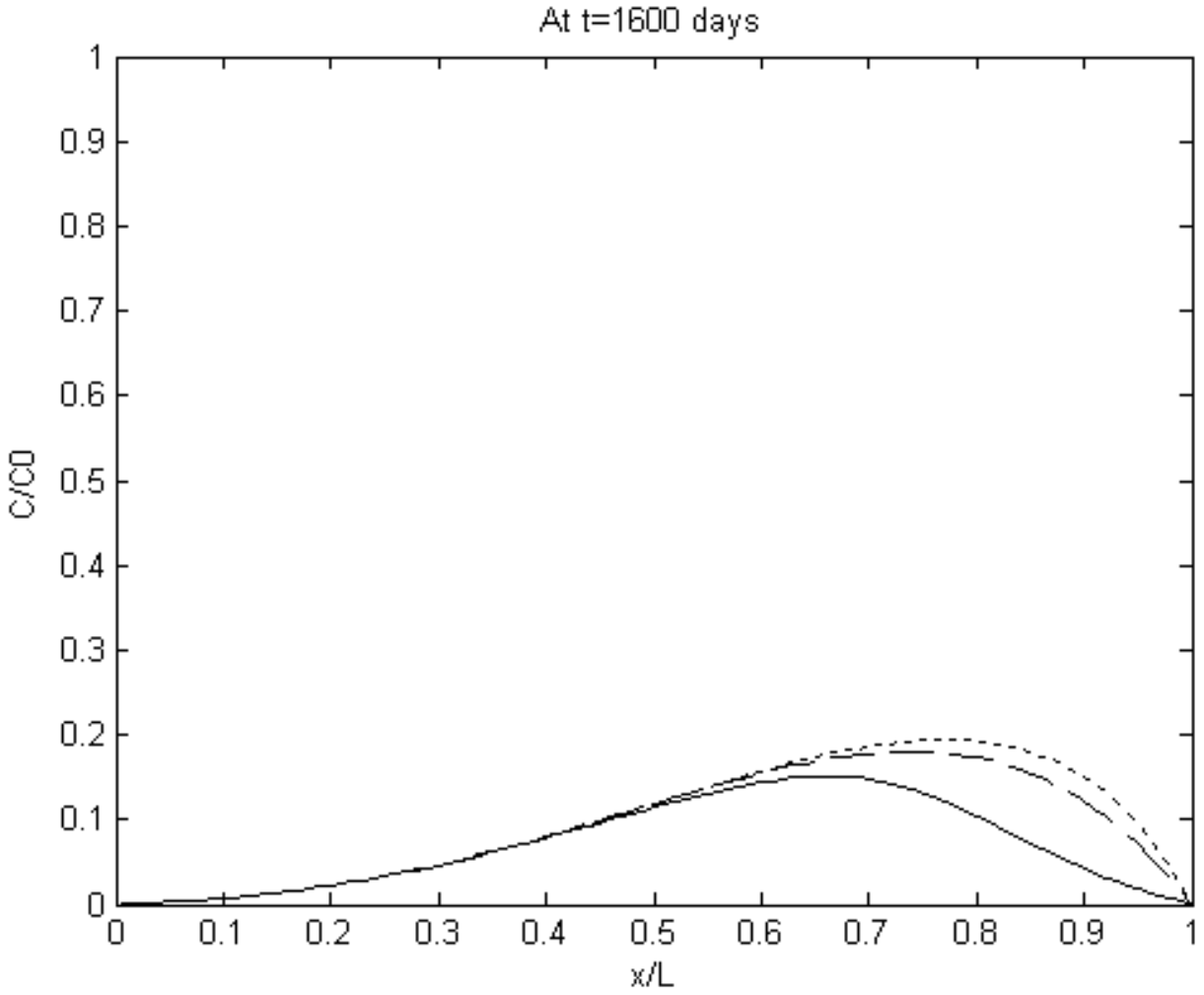

Legend: Dot-Baseline (without tidal effect), Solid-R2, and Dash-R6

Figure 5.31 Tidal Effect on Contaminant Distribution (Continued).

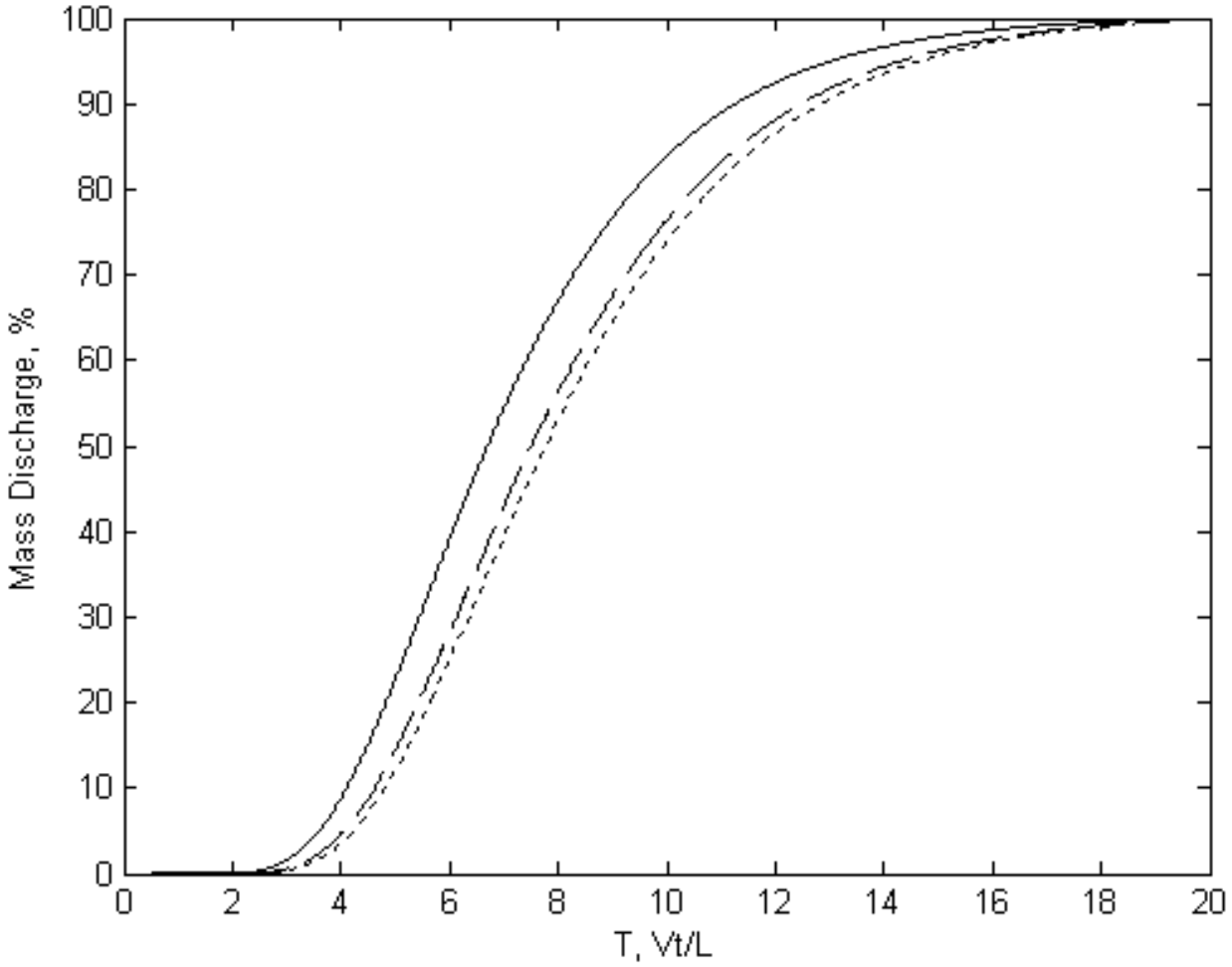

Legend: Dot-Baseline (without tidal effect), Solid-R2, and Dash-R6

Figure 5.32 Tidal Effect on Contaminant Discharge subject to Different Confining Status.

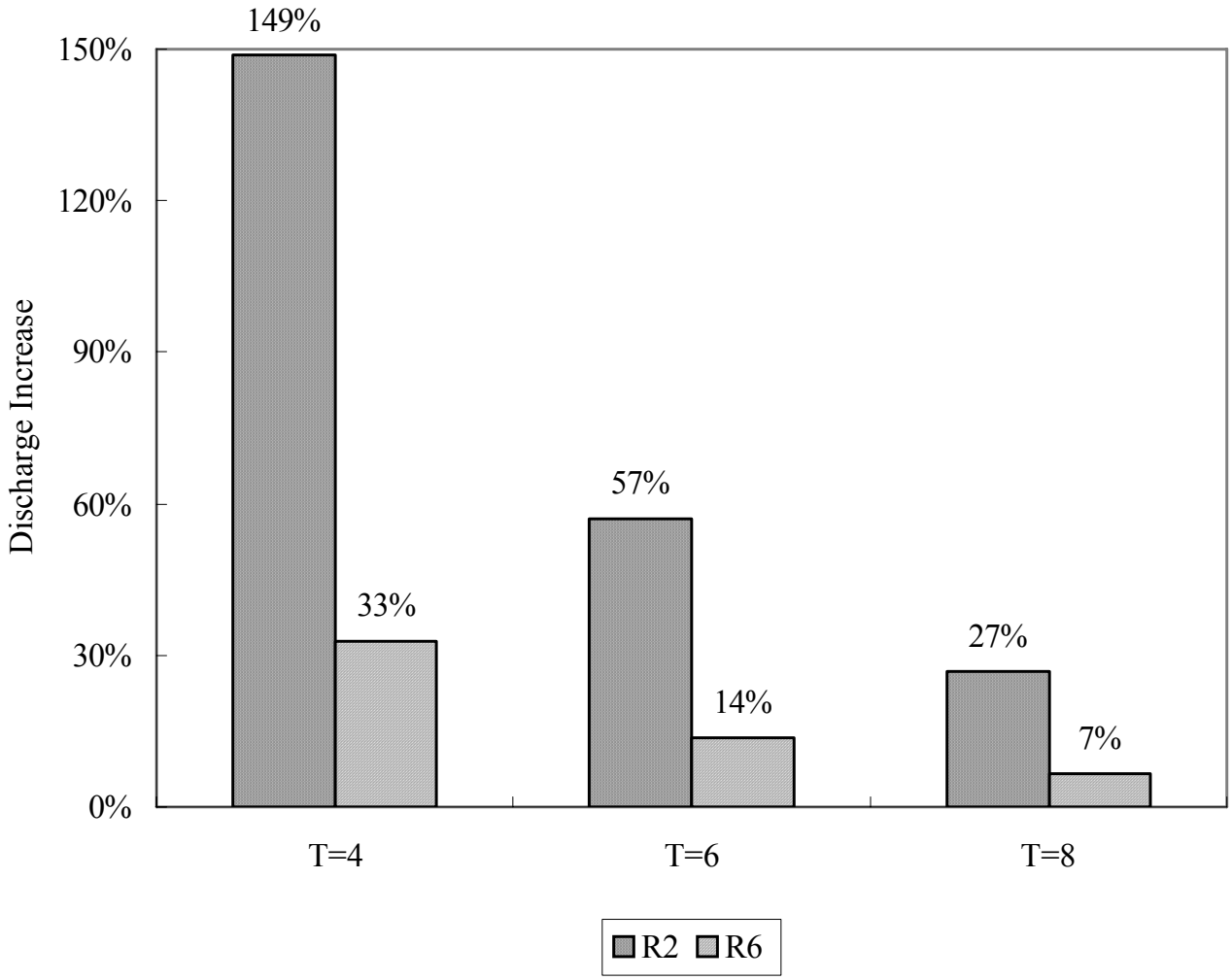

Figure 5.33 Tidal Effect on Contaminant Discharge subject to Different Confining Status.

The comparison of case DC3 and DC6, where the decay constant is varied, is illustrated in Figure 5.34 through Figure 5.36. Compared to the unconfined case (DC3), tidal activities have negligible impact on contaminant transport under the confined condition (case DC6). As seen in Figure 5.36, the per cent increase in contaminant discharge over the baseline in the confined condition is relatively low, and is only about one-fourth that of the per cent increase in the unconfined condition at all three times presented.

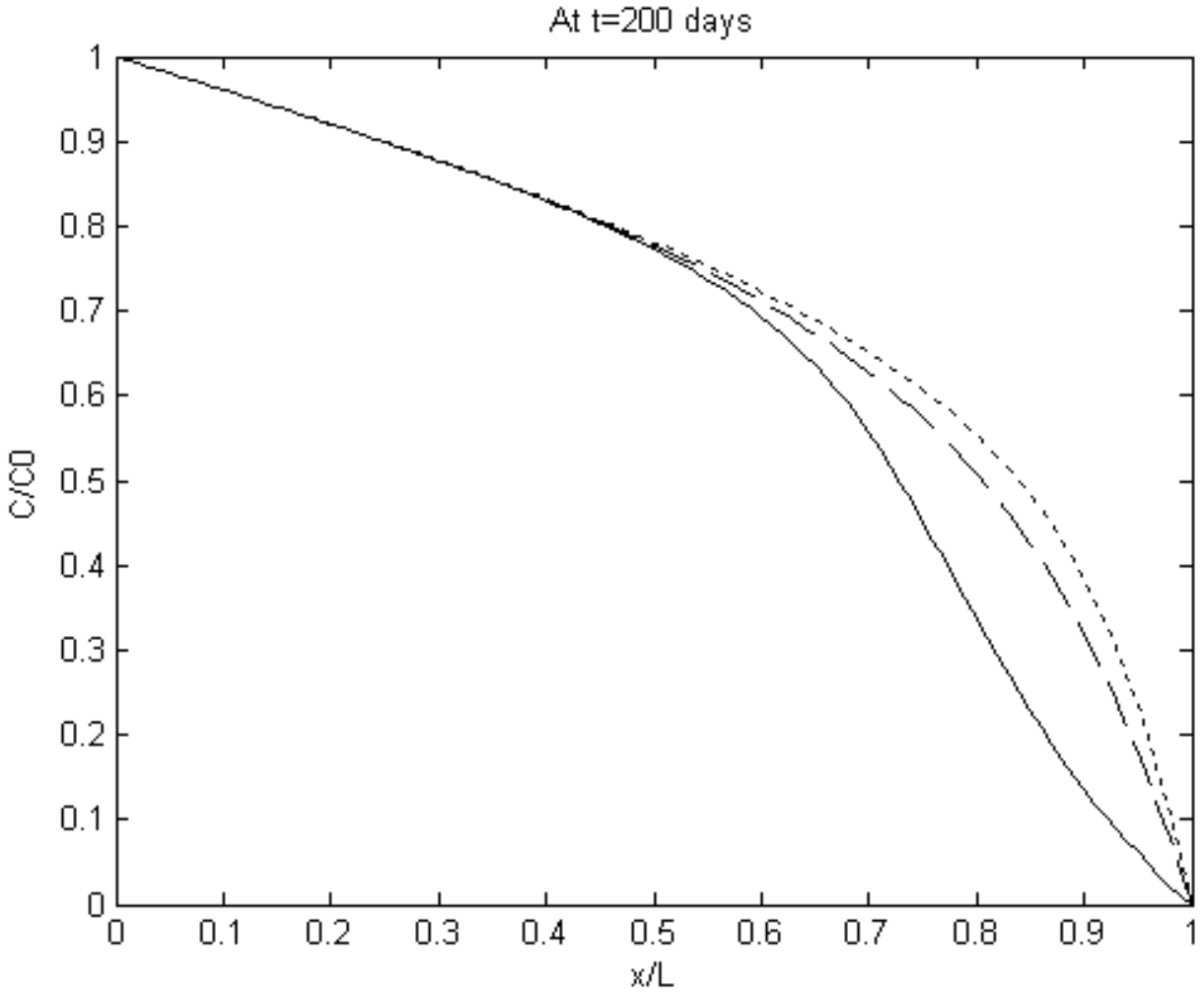

Legend: Dot-Baseline (without tidal effect), Solid-DC3, and Dash-DC6

Figure 5.34 Tidal Effect on Contaminant Distribution.

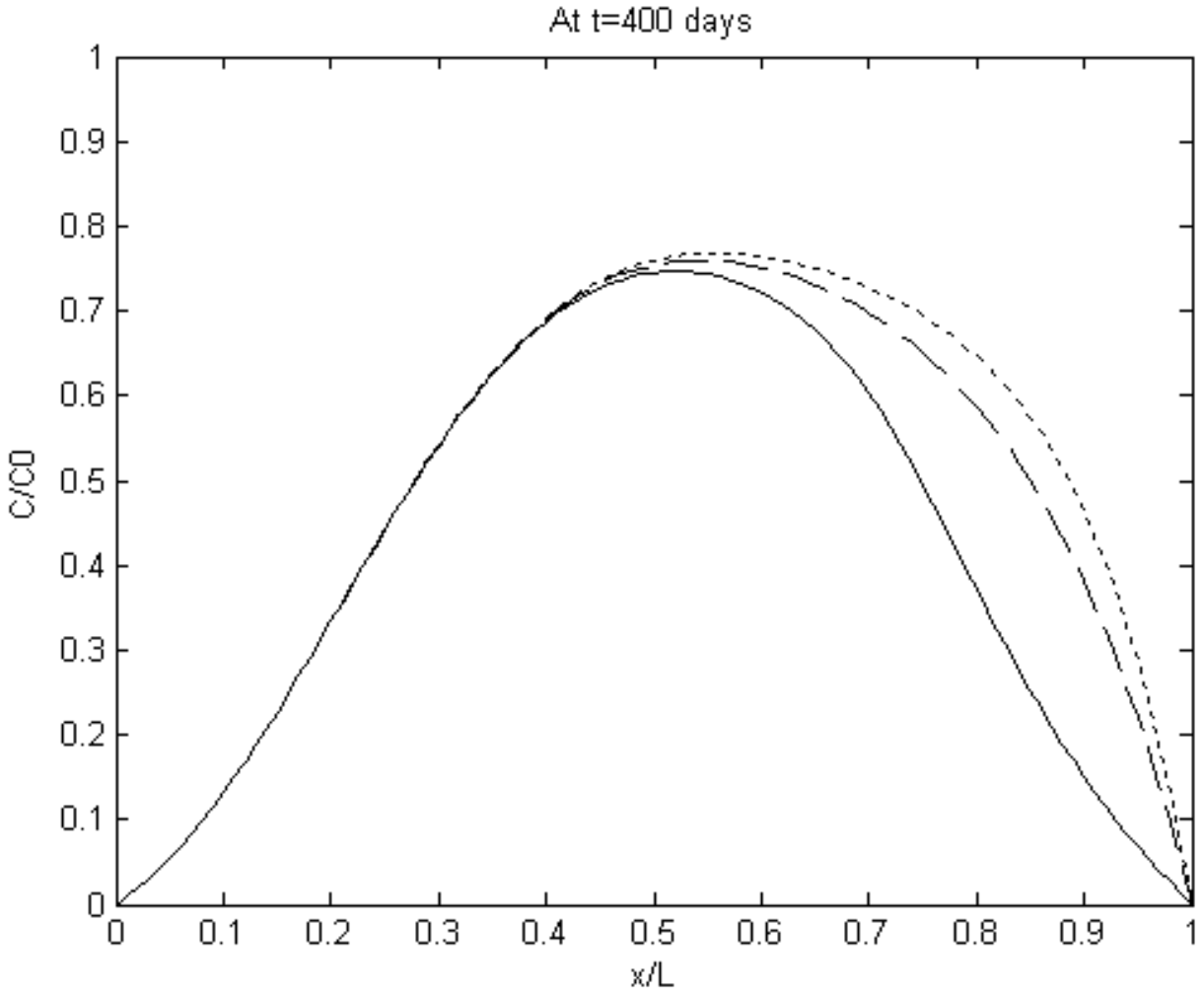

Legend: Dot-Baseline (without tidal effect), Solid-DC3, and Dash-DC6

Figure 5.34 Tidal Effect on Contaminant Distribution (Continued).

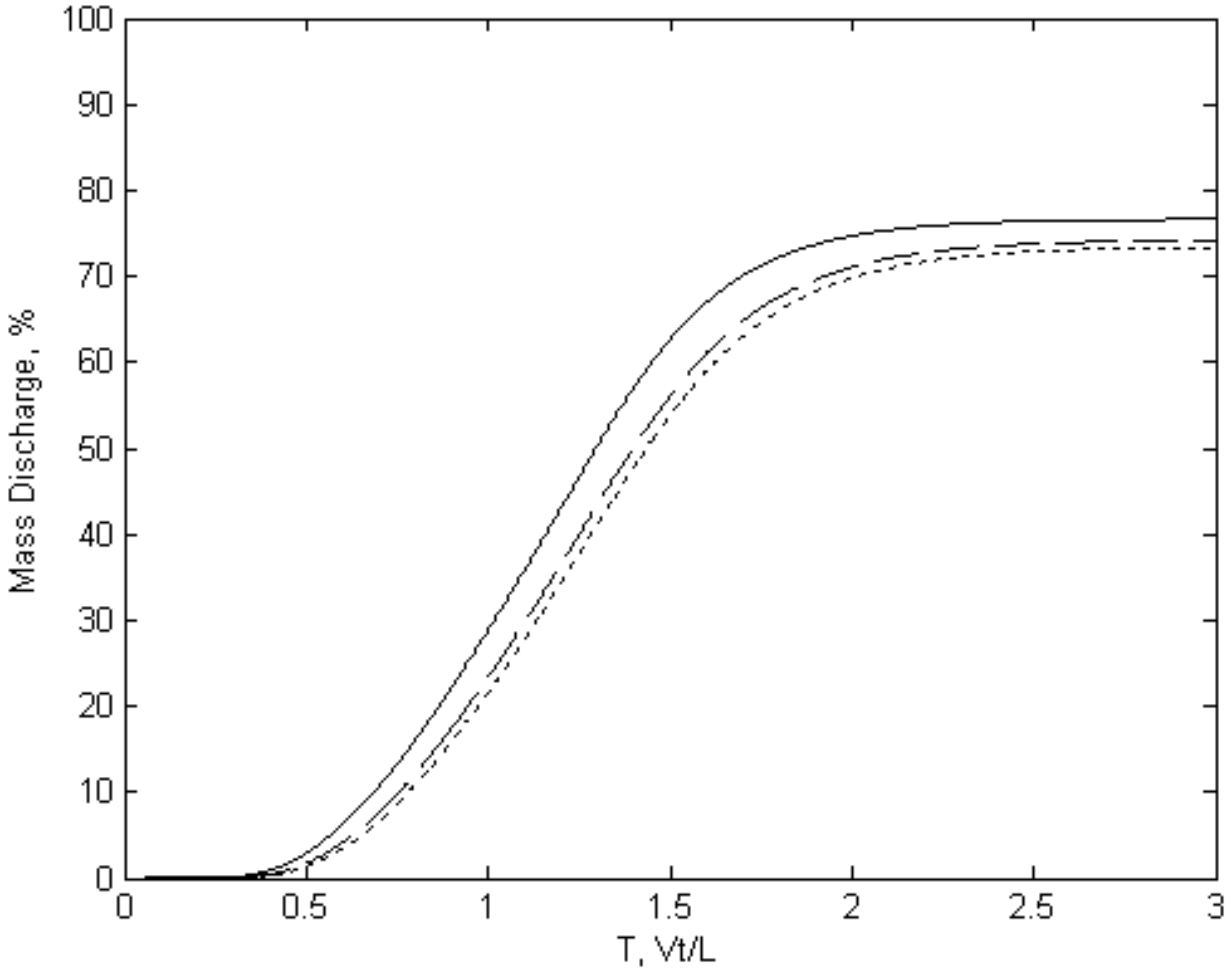

Legend: Dot-Baseline (without tidal effect), Solid-DC3, and Dash-DC6

Figure 5.35 Tidal Effect on Contaminant Discharge subject to Different Confining Status.

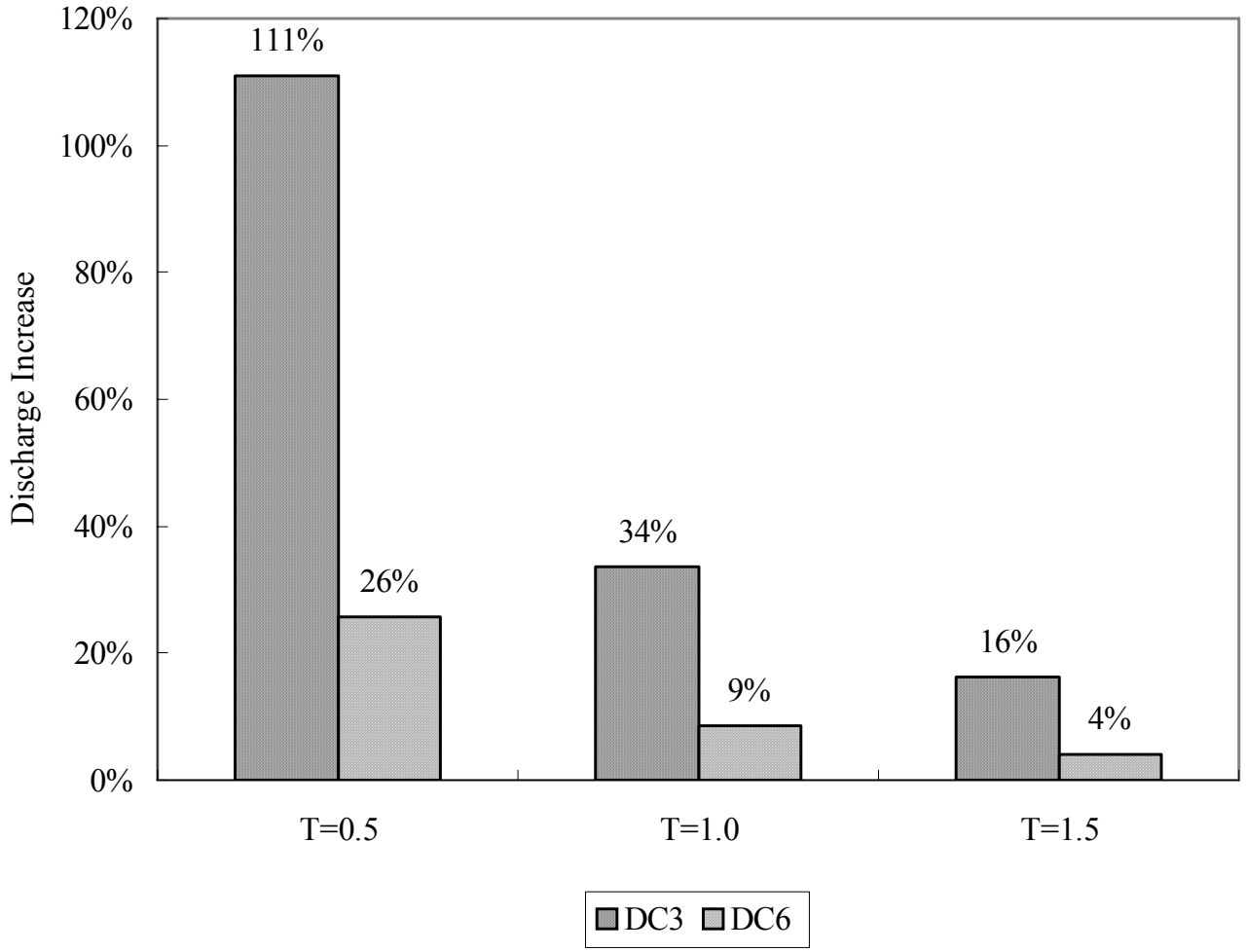

Figure 5.36 Tidal Effect on Contaminant Discharge subject to Different Confining Status.

The comparison of case DM3 and DM6, in which the aquifer length is varied, is illustrated in Figure 5.37 and Figure 5.39. Tides have a moderate impact on contaminant transport in the unconfined case, while the impact is again negligible in the confined case (see Figure 5.39, which shows only small increases in contaminant discharge over the baseline in both cases).

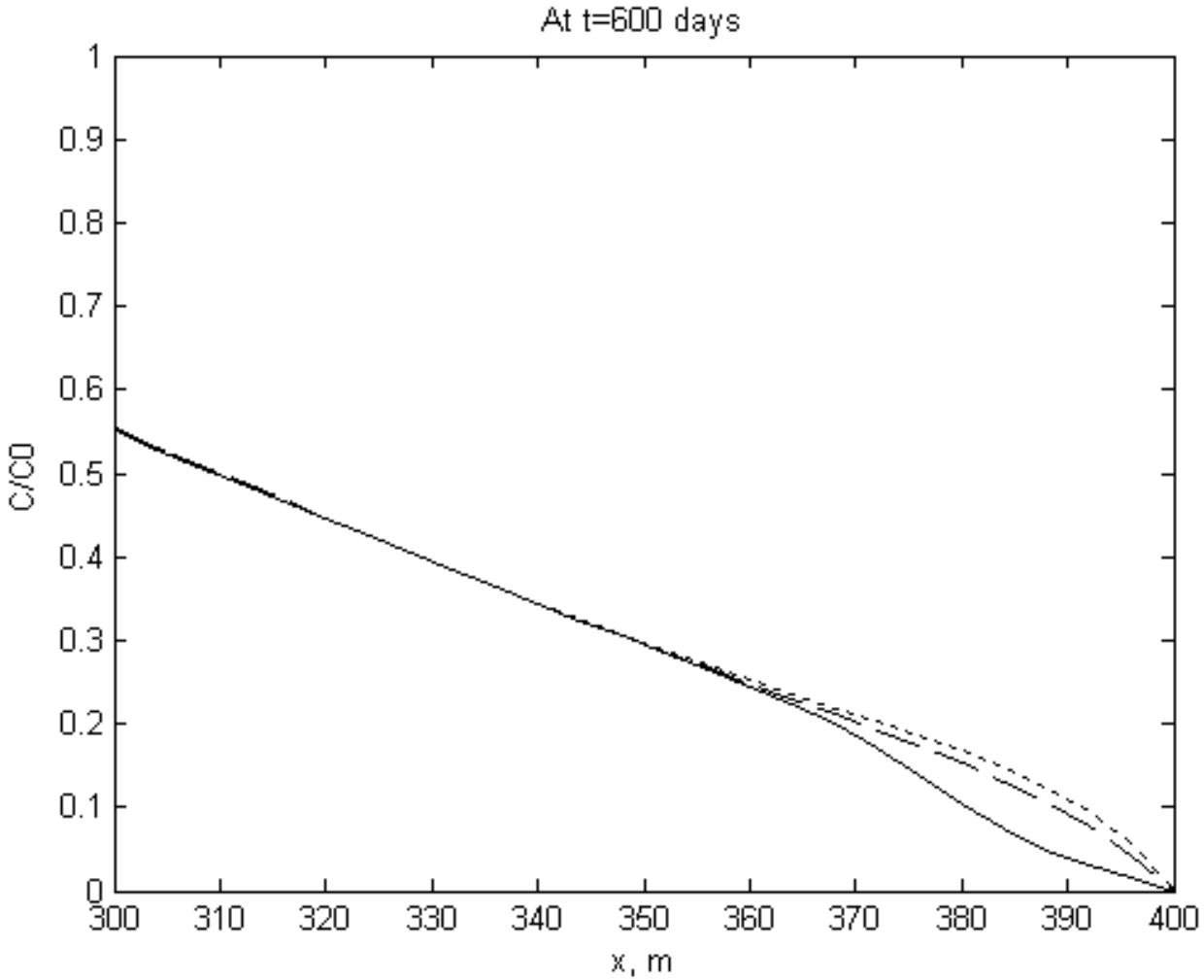

Legend: Dot-Baseline (without tidal effect), Solid-DM3, and Dash-DM6

Figure 5.37 Tidal Effect on Contaminant Distribution.

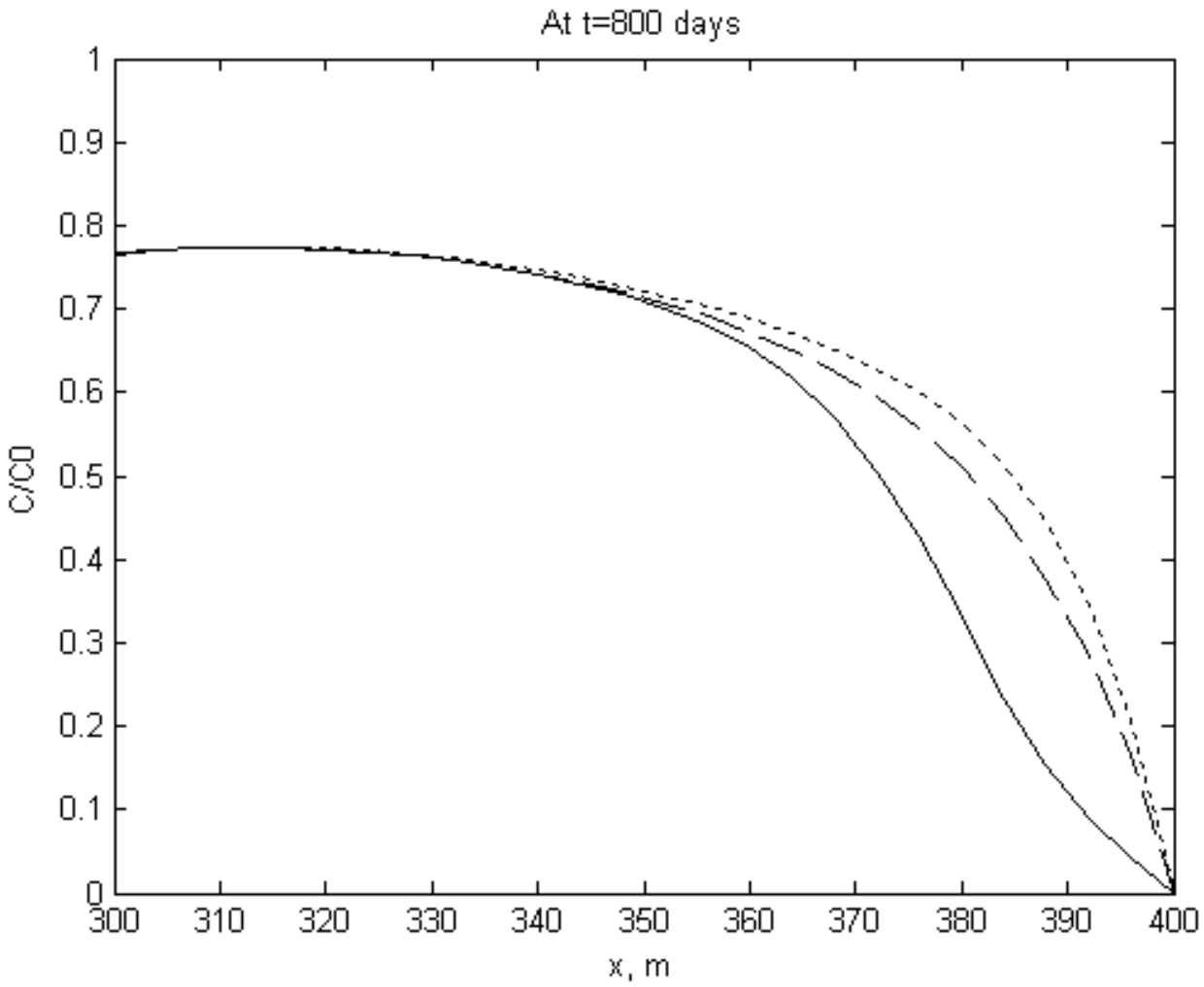

Legend: Dot-Baseline (without tidal effect), Solid-DM3, and Dash-DM6

Figure 5.37 Tidal Effect on Contaminant Distribution (Continued).

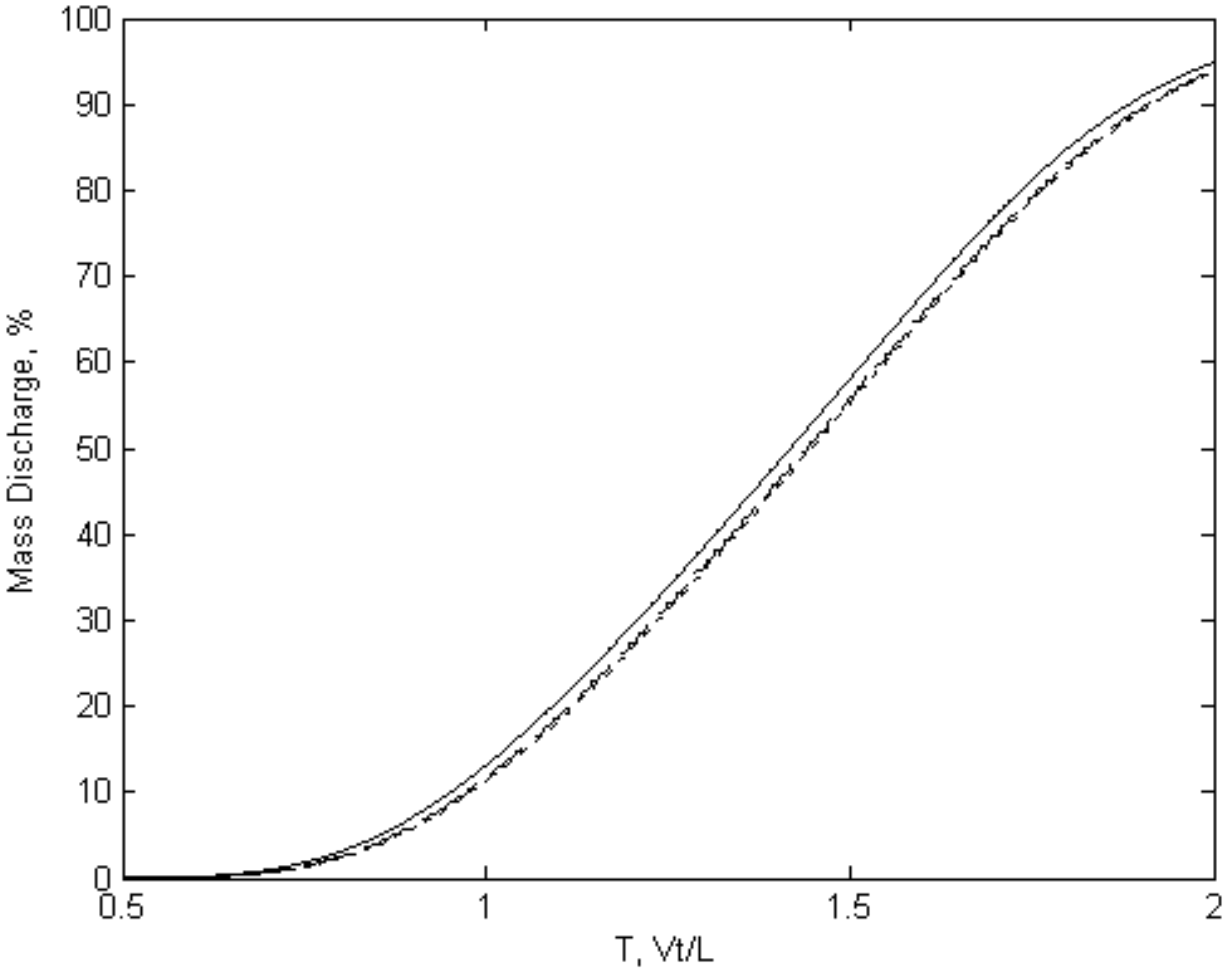

Legend: Dot-Baseline (without tidal effect), Solid-DM3, and Dash-DM6

Figure 5.38 Tidal Effect on Contaminant Discharge subject to Different Confining Status.

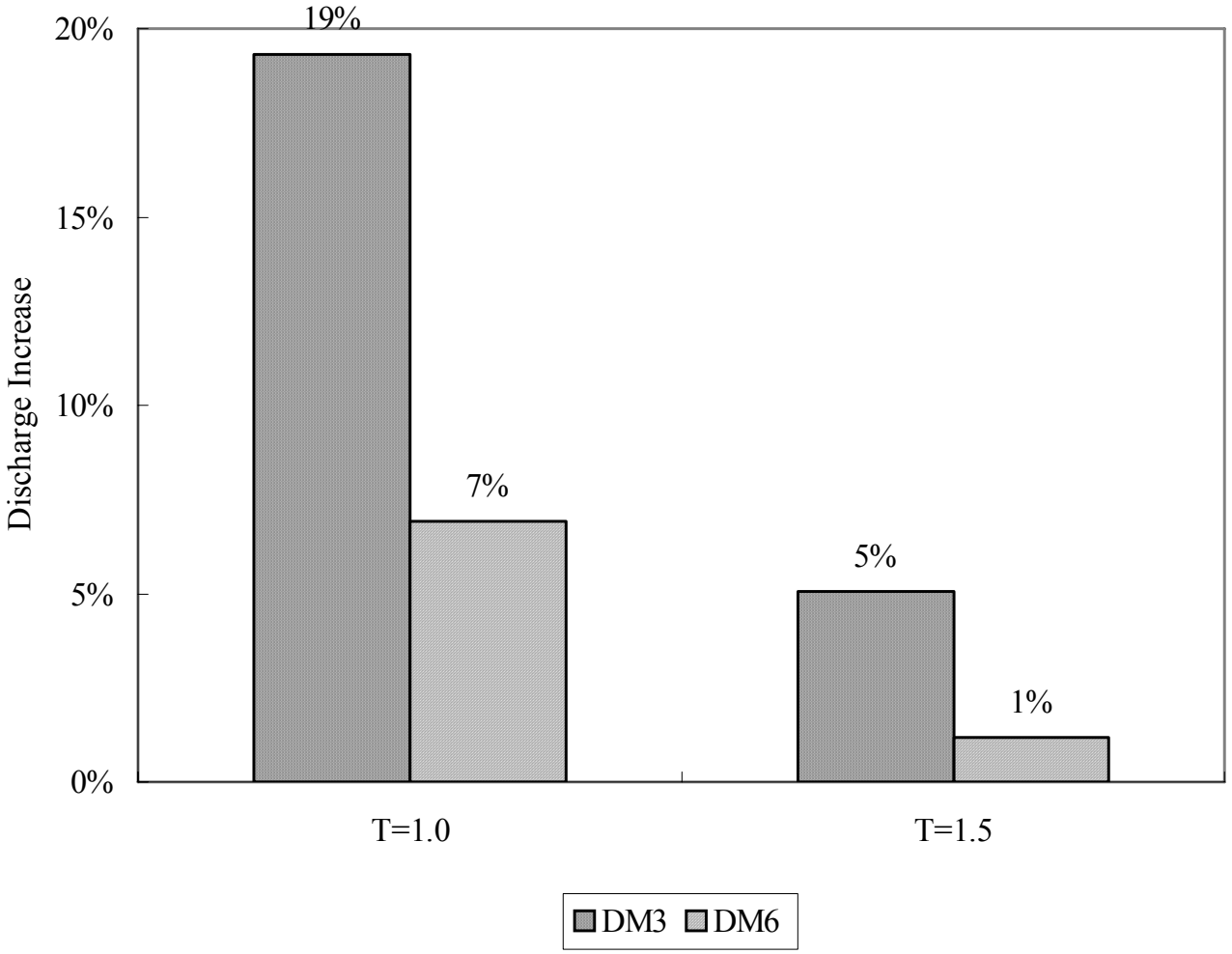

Figure 5.39 Tidal Effect on Contaminant Discharge subject to Different Confining Status.

5.5 Case Study

A case study is next conducted under the unconfined condition with an extremely low groundwater flow velocity (other conditions are the same as used in Table 5.1). The close-to-stagnant groundwater flow resulted from the assumed very small hydraulic gradient of 0.0002.

Due to the low flow velocity, contaminant transport through groundwater is also very slow: it takes tens of years for the contaminant to move through only a 100-meter long aquifer (see Figure 5.40). The comparison between the discharge profiles subject to, and not subject to, tides leads to an important and consistent conclusion: tidal fluctuations are extremely important under the low flow velocity condition. The tidal effect may cause the same amount of contaminant to be discharged out of the aquifer tens of years ahead of the case without tides. As shown in Figure 5.41, for example, 10 years after the contaminant has been released, there is almost no discharge if no tides present. However, discharge can reach over 10% of the total amount of contaminant released with tides of one-meter amplitude. This number can be even larger if the tides are more significant. Dramatic differences still exist after 20 years and 30 years have elapsed (Figure 5.41).

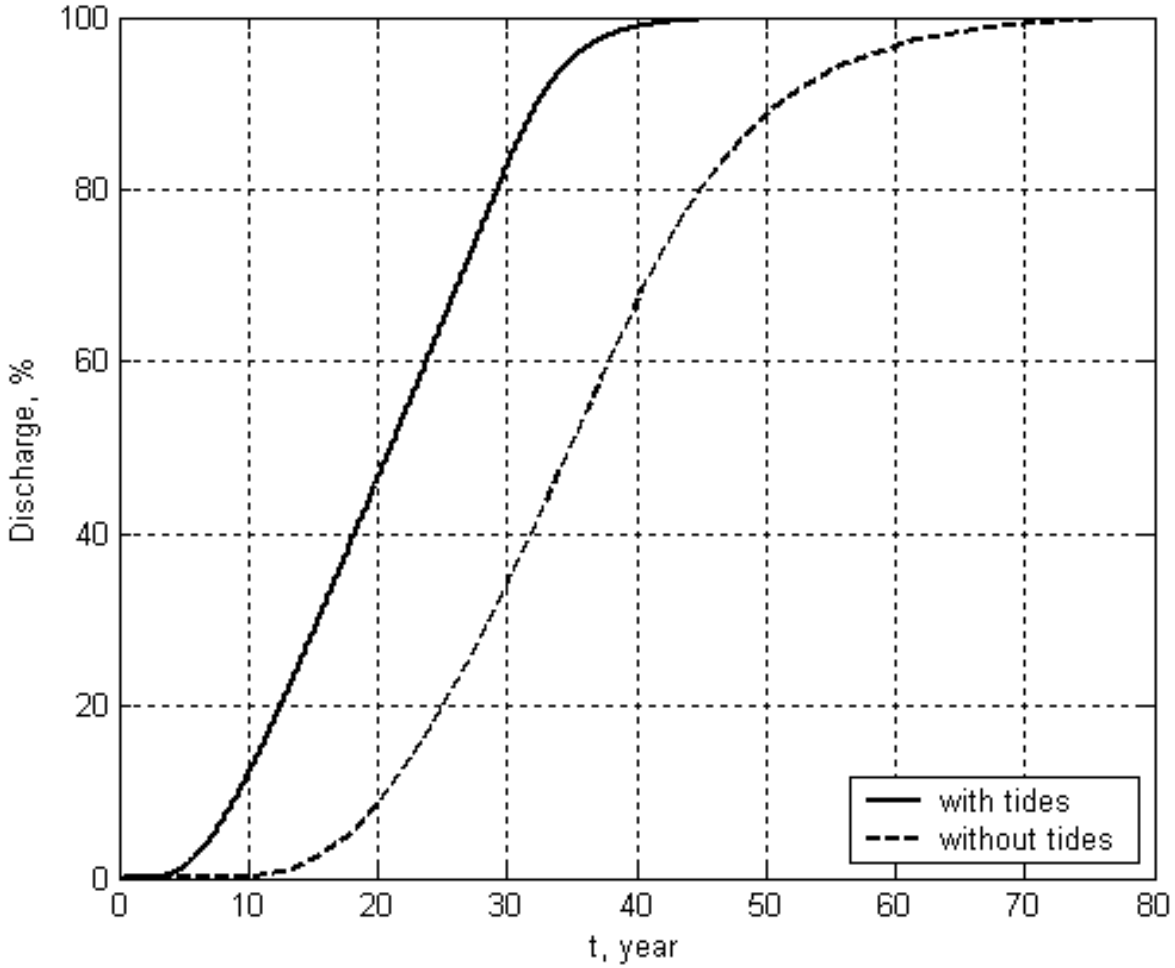

Figure 5.40 Case Study - Contaminant Discharge Profiles.

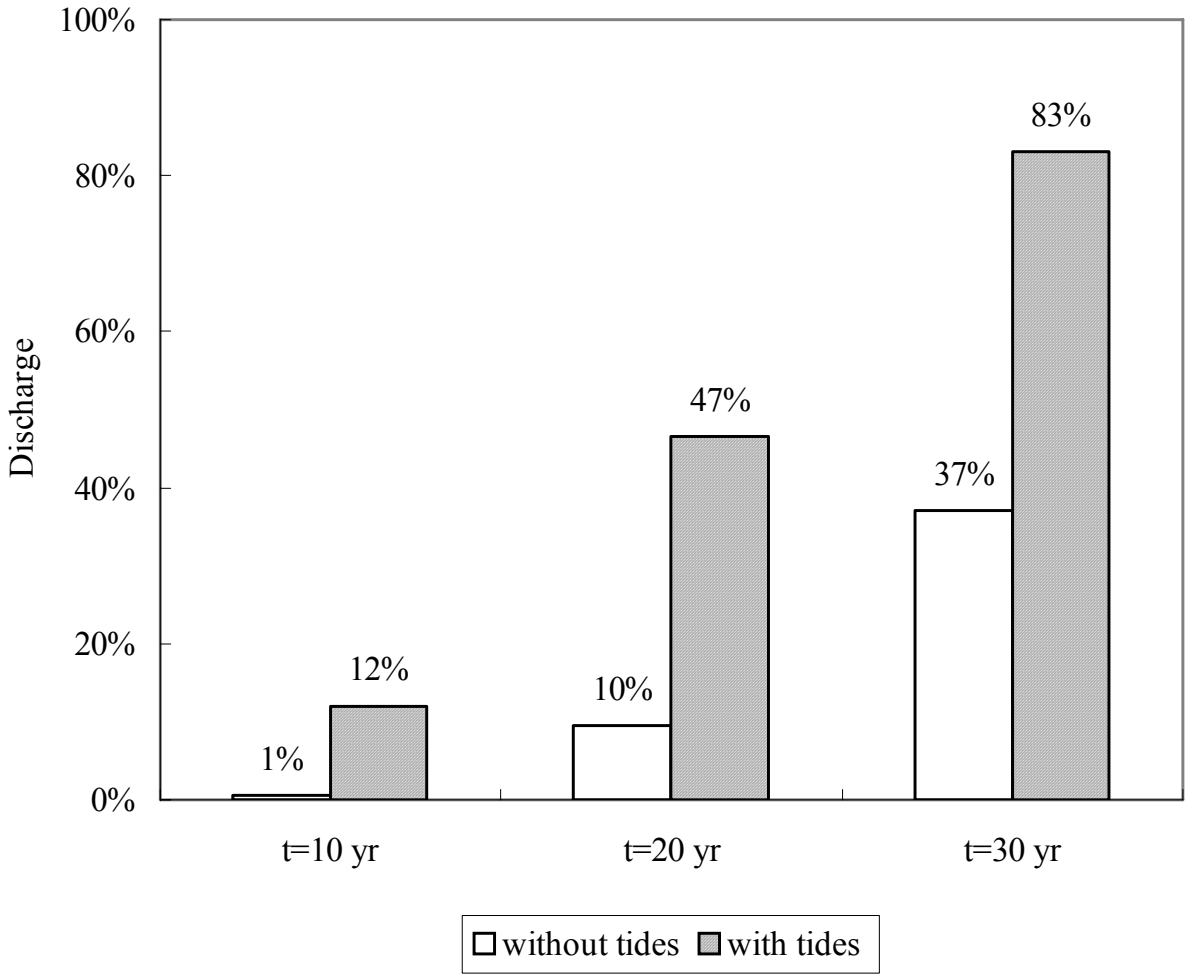

Figure 5.41 Case Study - Contaminant Discharge Comparison.

The tidal influence is also demonstrated in the contaminant concentration distribution as shown in Figure 5.42. It is worth noting that the concentration is highly diluted due in large part to the elongated transport time, which allows the contaminant to undergo extensive dispersion.

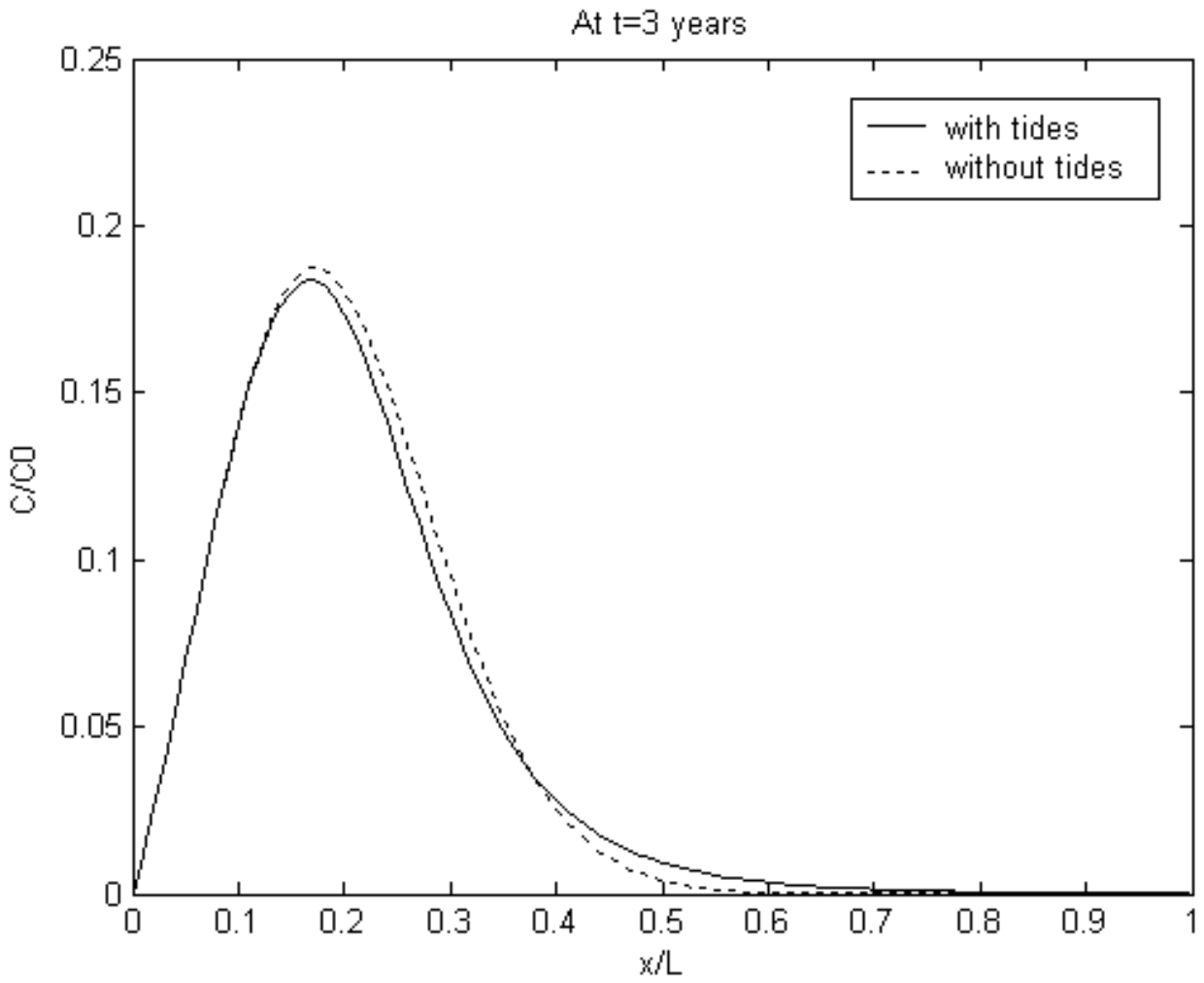

Figure 5.42 Case Study - Concentration Distribution.

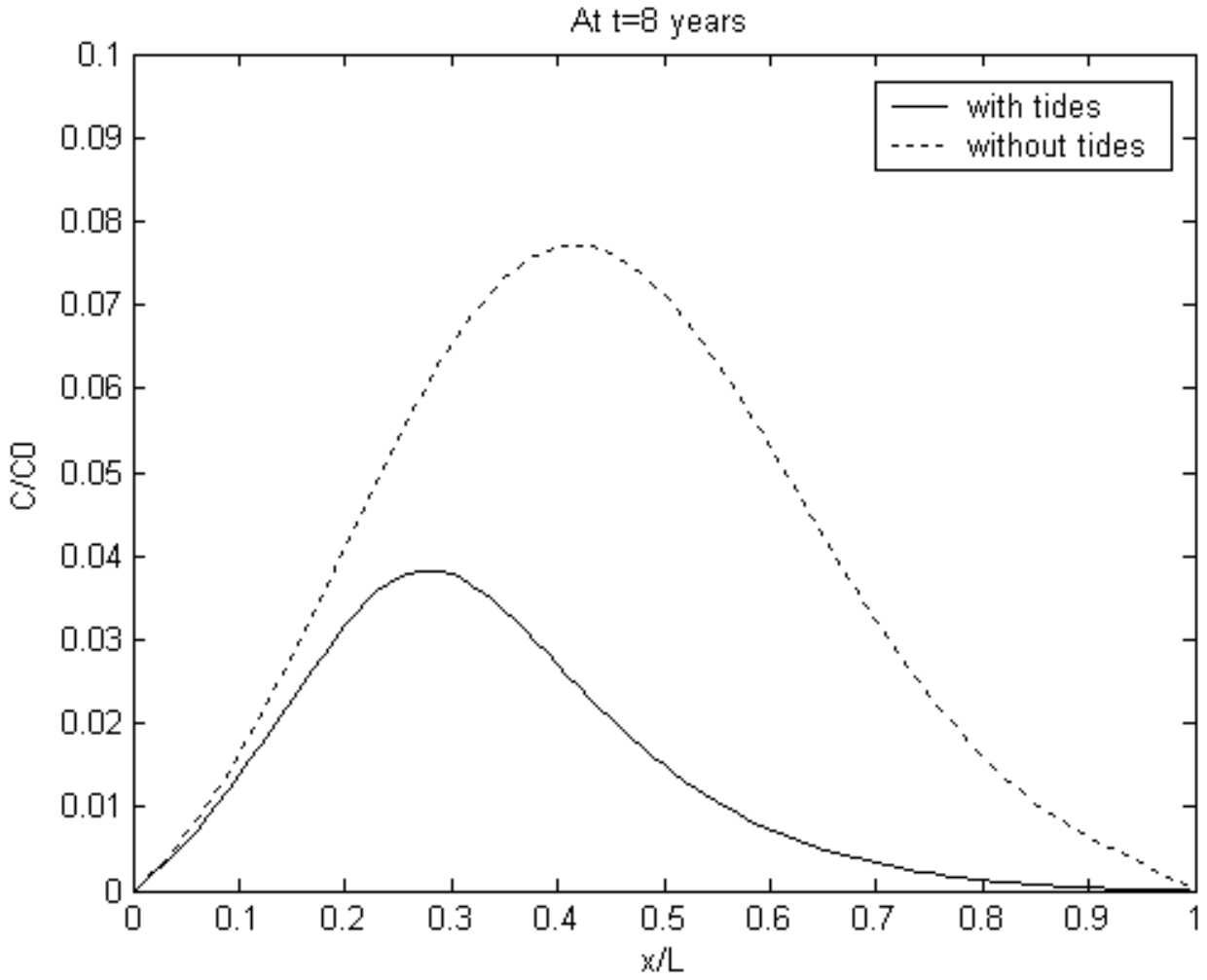

Figure 5.42 Case Study - Concentration Distribution (Continued).

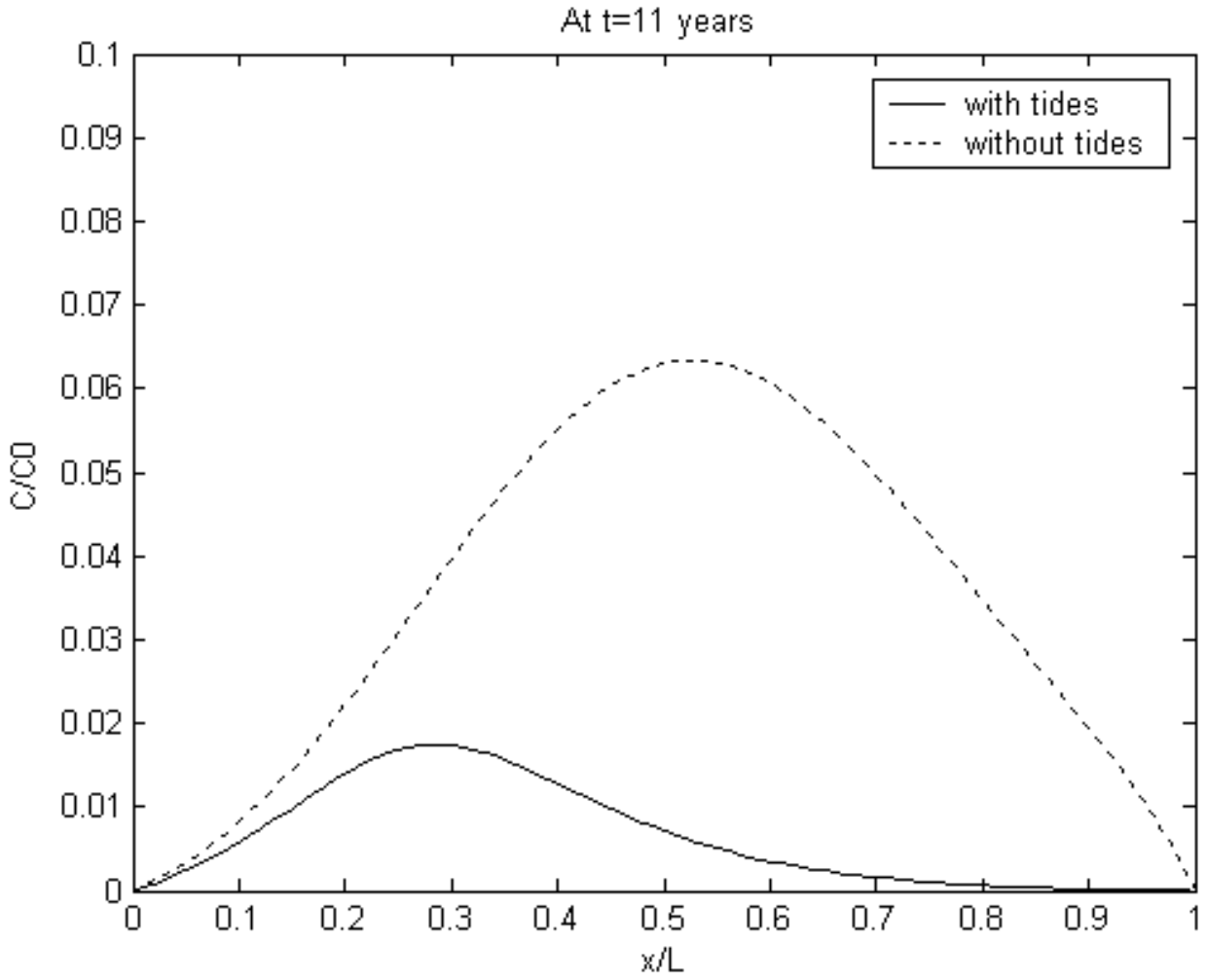

Figure 5.42 Case Study - Concentration Distribution (Continued).

5.6 Summary of Numerical Study

In the numerical study of tidal impact on contaminant transport in coastal aquifers, both unconfined cases and confined cases are considered. The tidal effect is evaluated in terms of both resulting fluctuations in hydraulic heads and fluctuations in contaminant transport. The significance of the tidal influence is quantified in terms of the scale of the potential effect zone, the degree by which the contaminant concentration is reduced, and the degree by which the discharge is enhanced. Tidal impact is also evaluated under conditions of varying tidal amplitude, groundwater flow velocity, retardation factor, decay constant, and aquifer dimension.

A summary regarding the effects of tidal influence on contaminant transport is as follows. First, tidal fluctuations may cause a significant acceleration of contaminant mass discharge, especially under unconfined conditions. Second, tidal fluctuations may result in a considerable decrease in contaminant concentration in areas adjacent to the coastline. And finally, in terms of the potential effect distance, the tidal influence on water level fluctuation is different from its effect on contaminant concentration and contaminant discharge in confined versus unconfined aquifers.

Table 5.12 further summarizes the numerical results concerning the potential tidal effect zone and the discharge affected.

A field application of the numerical simulation can be found in APPENDIX B of this text.

Table 5.12 Summary of Numerical Results with regard to Tidal Effect

Case No.	A m	V_x m/day	λ day^{-1}	R_f /	B* m	L m	[a] Effect Zone	[b] $T_{20\%}$ CC/BL	[c] $T_{40\%}$ CC/BL	[d] % At $T_{20\%}$	[e] % Increase At $T_{20\%}$	[f] % At $T_{40\%}$	[g] % Increase At $T_{40\%}$
Under Unconfined Conditions													
N3	[h] **1.0**	0.5	0.0	1.0	10	100	55m	0.81 / 0.91	1.05 / 1.20	13.6	47.1%	31.0	29.0%
N4	**2.0**	0.5	0.0	1.0	10	100	60m	0.75 / 0.91	0.99 / 1.16	10.7	86.9%	26.3	52.1%
R2	1.0	0.5	0.0	**10**	10	100	40m	4.80 / 5.70	6.10 / 7.10	10.3	94.2%	25.3	58.1%
R3	1.0	0.5	0.0	**100**	10	100	40m	44.0 / 53.0	56.0 / 66.0	9.5	110.5%	25.5	56.9%
DC2	1.0	0.5	**2×10^{-4}**	1.0	10	100	55m	0.81 / 0.91	1.06 / 1.20	13.6	47.1%	31.1	28.6%
DC3	1.0	0.5	**2×10^{-3}**	1.0	10	100	55m	0.85 / 1.00	1.20 / 1.35	12.0	66.7%	31.0	29.0%
DM2	1.0	0.5	0.0	1.0	10	**200**	54m	0.98 / 1.14	1.22 / 1.28	16.5	21.2%	35.0	14.3%
DM3	1.0	0.5	0.0	1.0	10	**400**	56m	1.09 / 1.12	1.31 / 1.34	17.0	17.6%	36.5	9.6%
DP1	1.0	0.5	0.0	1.0	**20**	100	55m	0.81 / 0.90	1.05 / 1.15	13.5	48.1%	32.0	25.0%
DP2	1.0	0.5	0.0	1.0	**30**	100	55m	0.81 / 0.91	1.06 / 1.16	14.0	42.9%	32.0	25.0%
N7	**1.0**	**2.0**	0.0	1.0	10	100	55m	0.86 / 0.90	1.11 / 1.16	17.0	17.6%	36.5	9.6%
N8	**2.0**	**2.0**	0.0	1.0	10	100	60m	0.81 / 0.91	1.06 / 1.16	14.0	42.9%	31.5	27.0%
N11	**1.0**	**0.2**	0.0	1.0	10	100	60m	0.72 / 0.90	0.97 / 1.16	9.5	110.5%	25.0	60.0%
N12	**2.0**	**0.2**	0.0	1.0	10	100	70m	0.67 / 0.90	0.90 / 1.16	6.5	207.7%	19.5	105.1%

*aquifer thickness.

[a] The potential effect zone by tides is measured as the distance between the coastline and the location inland where the concentration distribution deviates from the baseline by 5% or more.

[b] The time measured as the number of displaced pore volumes when the discharge reaches the amount equal to 20% of the total input with *CC* symbolizing the time for the current case and *BL* the time for the corresponding baseline.

[c] The time measured as the number of displaced pore volumes when the discharge reaches the amount equal to 40% of the total input with *CC* symbolizing the time for the current case and *BL* the time for the corresponding baseline.

[d] The percentage of discharge for the baseline case at the time when the discharge in the current case reaches the amount equal to 20% of the total input.

[e] The percentage increase in discharge due to tidal impact at the time when the discharge in the current case reaches the amount equal to 20% of the total input.

[f] The percentage of discharge for the baseline case at the time when the discharge in the current case reaches the amount equal to 40% of the total input.

[g] The percentage increase in discharge due to tidal impact at the time when the discharge in the current case reaches the amount equal to 40% of the total input.

[h] Value in **bond** font indicates the parameter specifically addressed in the comparison of tidal effect.

Table 5.12 Summary of Numerical Results with regard to Tidal Effect (Continued)

Case No.	A m	V_x m/day	λ day^{-1}	R_f /	B* m	L m	[a] Effect Zone	[b] $T_{20\%}$ CC/BL	[c] $T_{40\%}$ CC/BL	[d] % At $T_{20\%}$	[e] % Increase At $T_{20\%}$	[f] % At $T_{40\%}$	[g] % Increase At $T_{40\%}$
Under Confined Conditions													
N15	[h] **1.0**	0.5	0.0	1.0	10	100	50m	0.87 / 0.91	1.13 / 1.16	18.0	11.1%	37.5	6.7%
N16	**2.0**	0.5	0.0	1.0	10	100	67m	0.80 / 0.91	1.05 / 1.16	13.0	53.8%	31.0	29.0%
R6	1.0	0.5	0.0	**10**	10	100	35m	5.40 / 5.70	6.80 / 7.10	17.0	17.6%	36.5	9.6%
R7	1.0	0.5	0.0	**100**	10	100	60m	49.5 / 53.0	63.0 / 65.5	17.0	17.6%	36.3	10.2%
DC5	1.0	0.5	**2×10^{-4}**	1.0	10	100	50m	0.88 / 0.91	1.14 / 1.17	18.2	9.9%	37.6	6.4%
DC6	1.0	0.5	**2×10^{-3}**	1.0	10	100	45m	0.89 / 0.91	1.16 / 1.17	19.0	5.3%	39.0	2.6%
DM5	1.0	0.5	0.0	1.0	10	**200**	60m	1.02 / 1.14	1.26 / 1.28	18.5	8.1%	38.5	3.9%
DM6	1.0	0.5	0.0	1.0	10	**400**	52m	1.11 / 1.12	1.33 / 1.34	19.5	2.6%	39.5	1.3%
DP3	1.0	0.5	0.0	1.0	**20**	100	35m	0.90 / 0.91	1.15 / 1.16	19.5	2.6%	39.5	1.3%
DP4	1.0	0.5	0.0	1.0	**30**	100	0m	0.91 / 0.91	1.16 / 1.16	20.0	0.0%	40.0	0.0%
N19	**1.0**	**2.0**	0.0	1.0	10	100	0m	0.91 / 0.91	1.16 / 1.16	20.0	0.0%	40.0	0.0%
N20	**2.0**	**2.0**	0.0	1.0	10	100	27m	0.90 / 0.91	1.15 / 1.16	19.5	2.6%	39.5	1.3%
N23	**1.0**	**0.2**	0.0	1.0	10	100	70m	0.75 / 0.91	1.00 / 1.15	10.5	90.5%	27.0	48.1%
N24	**2.0**	**0.2**	0.0	1.0	10	100	85m	0.59 / 0.91	0.82 / 1.15	4.0	400.0%	14.0	185.7%

*aquifer thickness.

[a] The potential effect zone by tides is measured as the distance between the coastline and the location inland where the concentration distribution deviates from the baseline by 5% or more.

[b] The time measured as the number of displaced pore volumes when the discharge reaches the amount equal to 20% of the total input with *CC* symbolizing the time for the current case and *BL* the time for the corresponding baseline.

[c] The time measured as the number of displaced pore volumes when the discharge reaches the amount equal to 40% of the total input with *CC* symbolizing the time for the current case and *BL* the time for the corresponding baseline.

[d] The percentage of discharge for the baseline case at the time when the discharge in the current case reaches the amount equal to 20% of the total input.

[e] The percentage increase in discharge due to tidal impact at the time when the discharge in the current case reaches the amount equal to 20% of the total input.

[f] The percentage of discharge for the baseline case at the time when the discharge in the current case reaches the amount equal to 40% of the total input.

[g] The percentage increase in discharge due to tidal impact at the time when the discharge in the current case reaches the amount equal to 40% of the total input.

[h] Value in **bond** font indicates the parameter specifically addressed in the comparison of tidal effect.

The impact on hydraulic heads and contaminant transport by tidal activities observed in the numerical study can be summarized in detail as follows.

1. Tides have a greater influence in terms of tidal efficiency factor in confined aquifers compared with unconfined aquifers. The tidal amplitude is damped quickly in unconfined aquifers as it moves inland, while confined aquifers tend to have a much smaller capability of damping the tidal fluctuations. The distance whereby tides have a significant effect on water level is dramatically different for unconfined aquifers and confined aquifers. This distance, under the conditions considered in this study, is in the range of 200 to 300 meters inland for confined aquifers, which is almost one order of magnitude greater than that for unconfined aquifers, i.e., approximately 40 meters.

2. In sharp contrast to the conclusion concerning tidal impact on hydraulic heads, tidal effect on contaminant transport is generally greater in unconfined aquifers than in confined aquifers. The distance of potential influence by tides is within a range between 40 to 70 meters for the unconfined cases while it is between zero (no influence) and 85 meters for the confined cases. The potential influence zone regarding contaminant transport in unconfined aquifers is also typically smaller than that regarding hydraulic head fluctuation. The distance of potential influence is approximately 60 meters for unconfined cases under all of the various conditions. This distance under confined situations, however, changes in response to different tidal conditions, and may be smaller or larger than that in unconfined situations.

3. Tidal fluctuations vary the impact on contaminant transport from unconfined situations to confined ones in another perspective. For the unconfined cases, tidal impact is dramatic under most of the conditions considered. But the corresponding tidal effect may vanish under similar conditions in the confined cases as the retardation factor, decay factor, and aquifer length are varied (refer to the results in cases R6, DC6 and DM6).

4. Consistent with conclusions reached in the experimental study, the tidal effect is significant under certain conditions: a combination of low flow velocity, moderate to large tidal amplitudes, and certain retardation, decay, and aquifer domain conditions. Tidal influence is manifested to a greater extent in the concentration profiles in regions close to the coastal boundary, and in the discharge curves, particularly during the early stages in time after the contaminant begins to discharge into the aquifer.

5. The significance of the tidal effect is subject to tidal amplitude: the larger the tidal amplitude the more significant the tidal effect. The mass discharge, for example, is influenced by the magnitude of tides. The increase in mass discharge is approximately proportional to the magnitude of tidal amplitude. Under unconfined conditions (refer to cases N2, N3 and N4), doubling the tidal

amplitude from 0.5 m to 1.0 m to 2.0 m, for example, increases the mass discharge over the baseline after 100 days from 50% to 110% then to 207%, and after 200 days from 16% to 31% then to 50%.

6. The significance of the tidal effect is also subject to the hydraulic gradient or flow velocity. Groundwater flow velocity, and thus the speed at which the contaminant is transported, are both directly related to the average regional hydraulic gradient. A large flow velocity means a large convection component of contaminant transport. When the flow velocity rises to certain level, contaminant transport would be dominated by convection over dispersion, which would consequently dwarf the tidal effect. Also, observed in the unconfined cases is that the tidal influence is more significant under lower groundwater flow velocity. This is also true in terms of contaminant discharge. When the flow velocity is lowered to a certain level, less than 0.5 m/d for instance in this study, the tidal influence becomes significant.

CHAPTER 6

DISCUSSION AND CONCLUSIONS

6.1 Summary and Discussion

Serious contamination in estuarine and coastal water bodies has drawn tremendous public attention. Government authorities, together with industries and research groups, have recently exerted great effort to address the contamination and recovery issues. In order to pursue the parties responsible for the pollution and to prevent further contamination, the priority is to identify the various contamination sources. Conventional source identification processes have mainly focused on contaminant loadings to surface water such as rivers from point and nonpoint sources and atmospheric deposition, and little attention has been given to pollutant loadings through groundwater flow. A number of studies and reports, however, indicate that contaminant loadings through groundwater flow represent an important source to coastal water bodies, which leads to the author's interest in investigating in further detail contaminant transport and discharge through coastal aquifers. After an elaborate literature review of historic studies on contaminant transport in coastal aquifers, the author found that little work has been done so far on this issue, especially concerning the effect of tidal fluctuations, which are a signature characteristic of coastal aquifers.

This study includes two major components, numerical simulation including analytical analysis of boundary conditions, and laboratory experiments. The analytical analysis is intended to compare and thus select a boundary condition appropriately representative of the tidal boundary. Analytical results are also a useful basis for the evaluation of the numerical solution. The numerical simulation serves the purpose of

solving the transport equation incorporating tidal fluctuations, which is difficult for the analytical method to accomplish. The laboratory experiments, on the other hand, study the physical transport mechanism with tidal fluctuations, and the results are important to verify the validity of the analytical and numerical solutions.

From the comparative analysis, the first-type boundary condition (B.C.) is identified to better represent the coastal boundary, and thus is used in this study. Using this B.C. and the baseline solution based on it, the analysis of the tidal effect suggests that tide-induced contaminant transport fluctuations can be significant. The transport fluctuations appear to accelerate contaminant mass discharge into coastal waters, and result in noticeable differences in contaminant concentration distribution and mass discharge between confined aquifers and unconfined aquifers. The major conclusions are summarized in the next section.

6.2 Conclusions

The major conclusions that can be derived from the experimental and numerical results, based on the assumptions outlined earlier, include:

1. *The coastal boundary condition is more correctly represented by the first-type boundary condition than by the second-type boundary condition.* With different boundary conditions, and no dilution or high dilution, the contaminant concentration distribution and discharge show noticeable differences. These differences would have given a biased perspective with regard to the tidal effect if the case under the second-type boundary condition with no dilution was selected as the baseline in the experimental and numerical studies.

2. *Tides have a greater influence in confined aquifers in terms of tidal efficiency factor (or hydraulic head fluctuations).* This potential influence distance for confined aquifers is 200 to 300 meters extending inland, while it is only about 40 to 60 meters for unconfined aquifers.
3. *In sharp contrast to the above conclusion with regard to tidal impact on hydraulic heads, the tidal effect on contaminant transport is generally greater in unconfined aquifers than in confined aquifers.* The distance of potential influence by tides is around 60 meters in the unconfined cases under various conditions, with a similar distance effect range observed in the confined cases. This distance in the confined cases, however, is much smaller than the distance of potential effect in terms of hydraulic head fluctuations.
4. *Tidal fluctuations have greater impact on contaminant transport in unconfined situations than under confined ones in another perspective.* In the unconfined cases, tidal impact is dramatic under most of the conditions considered. But under similar conditions in the confined cases, the tidal effect may be very small.
5. *Consistently in both the experimental and numerical studies, the tidal effect is significant under certain conditions: a combination of low flow velocity, moderate to large tidal amplitudes, and certain retardation, decay, and aquifer domain conditions.* Tidal influence is manifested in the concentration profiles to a greater degree in regions close to the coastal boundary, and in the discharge profiles particularly during the early stages in time after the contaminant begins to discharge into the aquifer.

6. *The significance of the tidal effect is subject to tidal amplitude: the larger the tidal amplitude the more significant the tidal effect.*
7. *The significance of the tidal effect is also subject to flow velocity: the tidal influence is more significant under lower groundwater flow velocity.* When the groundwater flow is close to stagnant, as demonstrated in the CASE STUDY, the tidal impact is most apparent, leading to a significant discharge of the contaminant tens of years ahead of the case without tides.
8. *Under unconfined conditions, in general, retardation, decay, and aquifer domain have only a slight influence on the significance of tidal impact on contaminant transport. This is different under confined conditions, where high retardation, quick decay, and a large aquifer domain more easily cause the tidal impact to diminish.*

This study contributes to the understanding of tide-induced contaminant transport in coastal aquifers. The numerical and experimental results give rise to the observations of how tides influence contaminant discharge and concentration distribution patterns, the significance of tidal influence relative to other major factors such as hydraulic gradient, the scale of tide-influenced zone, and the tidal influence on contaminant transport in confined versus unconfined aquifers. These contributions, the authors believe, are an important offset to the limitations of prior work on tide-influenced contaminant transport and a significant extension of prior work on groundwater flow in coastal aquifers.

APPENDIX A

DERIVATION OF THE ANALYTICAL SOLUTION FOR 1-DIMENSIONAL CONTAMINANT TRANSPORT EQUATION SUBJECT TO DIRICHLET EFFLUENT BOUNDARY CONDITION

Equation Chapter 1 Section 1The 1-dimensional contaminant-transport equation with uniform flow is given in Chapter 3 as

$$R_f \frac{\partial C}{\partial t} = D_x \frac{\partial^2 C}{\partial x^2} - V_x \frac{\partial C}{\partial x} - \lambda R_f C \tag{A.1}$$

The initial condition is given as

$$C(x,t)\big|_{t=0} = f(x) = 0 \tag{A.2}$$

And the First-type boundary conditions are given as

$$C(x,t)\big|_{x=0} = C_0, \ and \ \ C(x,t)\big|_{x=L} = C_L \tag{A.3}$$

Change variables as

$$q = C \exp\left(-\frac{xV_x}{2D_x} + \frac{V_x^2 t}{4D_x} + \lambda t \right) \tag{A.4}$$

Then the original PDE becomes

$$\frac{\partial q}{\partial t} = D_x \frac{\partial^2 q}{\partial x^2} \tag{A.5}$$

And the I.C. and B.C. become the following accordingly

$$\begin{aligned} &q(x,0) = 0 \\ &q(0,t) = C_0 \exp\left(\frac{V_x^2 t}{4D_x} + \lambda \right) t = F_0(t) \\ &q(L,t) = C_L \exp\left(-\frac{V_x L}{2D_x} + \frac{V_x^2 t}{4D_x} + \lambda \right) t = F_L(t) \end{aligned} \tag{A.6}$$

Laplace transform (denoted by operator $\mathrm{L}\{\}$) of equation (A.5) leads to

$$s\bar{q} = D_x \frac{d^2\bar{q}}{dx^2} \tag{A.7}$$

With transformed B.C. becomes

$$\begin{aligned} \bar{q}(0,t) &= L\{F_0(t)\} = f_0(s) \\ \bar{q}(L,t) &= L\{F_L(t)\} = f_L(s) \end{aligned} \tag{A.8}$$

Solving (A.7) with the B.C. (A.8) gives (Churchill, 1971)

$$\bar{q}(x,s) = f_0(s)\frac{\sinh\left((L-x)\sqrt{\frac{s}{D_x}}\right)}{\sinh\left(L\sqrt{\frac{s}{D_x}}\right)} + f_L(s)\frac{\sinh\left(x\sqrt{\frac{s}{D_x}}\right)}{\sinh\left(L\sqrt{\frac{s}{D_x}}\right)} \tag{A.9}$$

Let

$$g_0(x,s) = \frac{\sinh\left((L-x)\sqrt{\frac{s}{D_x}}\right)}{s\cdot\sinh\left(L\sqrt{\frac{s}{D_x}}\right)},\ and\ g_L(x,s) = \frac{\sinh\left(x\sqrt{\frac{s}{D_x}}\right)}{s\cdot\sinh\left(L\sqrt{\frac{s}{D_x}}\right)} \tag{A.10}$$

Then solution (A.9) is simplified as

$$\bar{q}(x,s) = f_0(s)\cdot s\cdot g_0(x,s) + f_L(s)\cdot s\cdot g_L(x,s) \tag{A.11}$$

Let

$$G_0(x,t) = L^{-1}\{g_0(x,s)\},\ and\ G_L(x,t) = L^{-1}\{g_L(x,s)\} \tag{A.12}$$

where operator $L^{-1}\{\}$ denotes inverse Laplace transform. Then inverse Laplace transform gives

$$\begin{aligned} G_0(x,t) &= L^{-1}\{g_0(x,s)\} \\ &= \frac{L-x}{L} + \frac{2}{\pi}\sum_{n=1}^{\infty}\frac{(-1)^n}{n}\sin\frac{n\pi(L-x)}{L}\exp\left(-\frac{n^2\pi^2 D_x t}{L^2}\right) \end{aligned} \tag{A.13}$$

and

$$G_L(x,t) = L^{-1}\{g_L(x,s)\} = \frac{x}{L} + \frac{2}{\pi}\sum_{n=1}^{\infty}\frac{(-1)^n}{n}\sin\frac{n\pi x}{L}\exp\left(-\frac{n^2\pi^2 D_x t}{L^2}\right) \quad (A.14)$$

The terms $f_0(s)\cdot s$ and $f_L(s)\cdot s$ in equation (A.11) are

$$\begin{aligned} s\cdot f_0(s) &= L\left\{F_0'(t) + F_0(0)\right\} \\ s\cdot f_L(s) &= L\left\{F_L'(t) + F_L(0)\right\} \end{aligned} \quad (A.15)$$

By convolution theorem (Lee, 1999) it leads to

$$\begin{aligned} q(x,t) = {} & F_0(0)G_0(x,t) + \int_0^t F_0'(t-\tau)G_0(x,\tau)d\tau \\ & + F_L(0)G_L(x,t) + \int_0^t F_L'(t-\tau)G_L(x,\tau)d\tau \end{aligned} \quad (A.16)$$

with

$$\begin{aligned} F_0(0) &= C_0 \\ F_L(0) &= C_L\exp\left(-\frac{V_x L}{2D_x}\right) \\ F_0'(t-\tau) &= C_0\left(\frac{V_x^2}{4D_x}+\lambda\right)\exp\left[\left(\frac{V_x^2}{4D_x}+\lambda\right)(t-\tau)\right] \\ F_L'(t-\tau) &= C_L\left(\frac{V_x^2}{4D_x}+\lambda\right)\exp\left(-\frac{V_x L}{2D_x}\right)\exp\left[\left(\frac{V_x^2}{4D_x}+\lambda\right)(t-\tau)\right] \end{aligned} \quad (A.17)$$

Working on (A.13), (A.14), (A.16) and (A.17), leads to the solution of

$$q(x,t) = C_0 A(x,t) + C_L A(L-x,t) \quad (A.18)$$

with

$$\begin{aligned} A(x,t) = {} & \frac{L-x}{L}\exp(\beta t) - \frac{2}{\pi}\sum_{n=1}^{\infty}\frac{\sin(\eta x)}{n}\exp\left(-\eta^2 D_x\right) \\ & + \frac{2}{\pi}\sum_{n=1}^{\infty}\frac{\beta\sin(\eta x)}{n(\beta+\eta^2 D_x)}\left[\exp\left(-\eta^2 D_x\right) - \exp(\beta t)\right] \end{aligned} \quad (A.19)$$

where $\beta = \frac{V_x^2}{4D_x} + \lambda$ and $\eta = \frac{n\pi}{L}$.

Change variables back to

$$C = q \exp\left(\frac{xV_x}{2D_x} - \frac{V_x^2 t}{4D_x} - \lambda t\right) \tag{A.20}$$

Substituting into (A.18) it gives

$$C(x,t) = C_0 \exp\left(\frac{xV_x}{2D_x}\right) B(x,t) + C_L \exp\left(\frac{V_x(L-x)}{2D_x}\right) B(L-x,t) \tag{A.21}$$

with

$$\begin{aligned} B(x,t) = {} & \frac{L-x}{L} - \frac{2}{\pi}\sum_{n=1}^{\infty}\frac{\sin(\eta x)}{n}\exp\left[-(\beta + \eta^2 D_x)t\right] \\ & + \frac{2}{\pi}\sum_{n=1}^{\infty}\frac{\beta\sin(\eta x)}{n(\beta+\eta^2 D_x)}\left\{\exp\left[-(\beta+\eta^2 D_x)t\right] - 1\right\} \end{aligned} \tag{A.22}$$

where $\beta = \frac{V_x^2}{4D_x} + \lambda$ and $\eta = \frac{n\pi}{L}$.

The solution above is derived assuming a constant concentration at the influent boundary, which resembles the case with continuous contaminant input at the influent boundary. In a more realistic situation whereby contaminant input has duration of t_0, called pulse type input, it is represented by

$$C\big|_{x=0} = \begin{cases} C_0, & 0 < t < t_0 \\ 0, & t > t_0 \end{cases} \tag{A.23}$$

The solution of equation (A.1) can be derived by simply using linear superposition which gives

$$C(x,t) = \begin{cases} C_0 \exp\left(\frac{xV_x}{2D_x}\right) B(x,t) + C_L \exp\left(\frac{V_x(L-x)}{2D_x}\right) B(L-x,t), & as\ t \le t_0 \\ C_0 \exp\left(\frac{xV_x}{2D_x}\right)\left[B(x,t) - B(x,t-t_0)\right] + C_L \exp\left(\frac{V_x(L-x)}{2D_x}\right) B(L-x,t), & as\ t > t_0 \end{cases} \tag{A.24}$$

with B(x, t) is the same as represented by(A.22).

APPENDIX B

FIELD APPLICATION OF NUMERICAL SIMULATIONS

The numerical simulation outlined in Chapter 3 and Chapter 5 can be applied to realistic field conditions as exemplified by a case described in this appendix.

This field application considers a site located in central New Jersey bordering the Arthur Kill to the east, which is further subject to tidal fluctuations propagating from the Atlantic Ocean coast. The site and surrounding areas are characterized by a combination of industrial and petroleum storage facilities. Industrial operations on the site started almost a hundred years ago with the main contamination release occurred approximately 80 years ago. A contaminant-release duration of 5 years is assumed for this application. The primary contaminants include various dyestuffs and surfactants, but also other organic and inorganic compounds. A retardation factor of 10 and a decay constant of zero are estimated for this application. Table B.1 gives the parameter values based on field data (or otherwise estimated).

Table B.1 Parameters Considered in the Field Application Study

Parameters	Value
Aquifer Length, ft	200
Aquifer Thickness, ft	30
Hydraulic Gradient	0.01
Hydraulic Conductivity, ft/d	15.0
Porosity	0.30
Specific Yield	0.15
Tidal Amplitude, ft	3.0
Tidal Period, hour	12
Retardation Factor	10.0
Decay Constant, d^{-1}	0.0
Dispersivity, ft	20.0
Release Concentration, ppm	10.0

Based on these parameter values, numerical simulations, with time set to zero when the contaminants were released 80 years ago, give the contaminant distributions shown in Figure B.1. The simulation results reveal that the contaminant concentration distribution with tides starts to deviate from the condition without tides when the contaminant plume front reaches the boundary resulting from the tidal fluctuations. The deviation grows as the majority of the plume gets to the boundary.

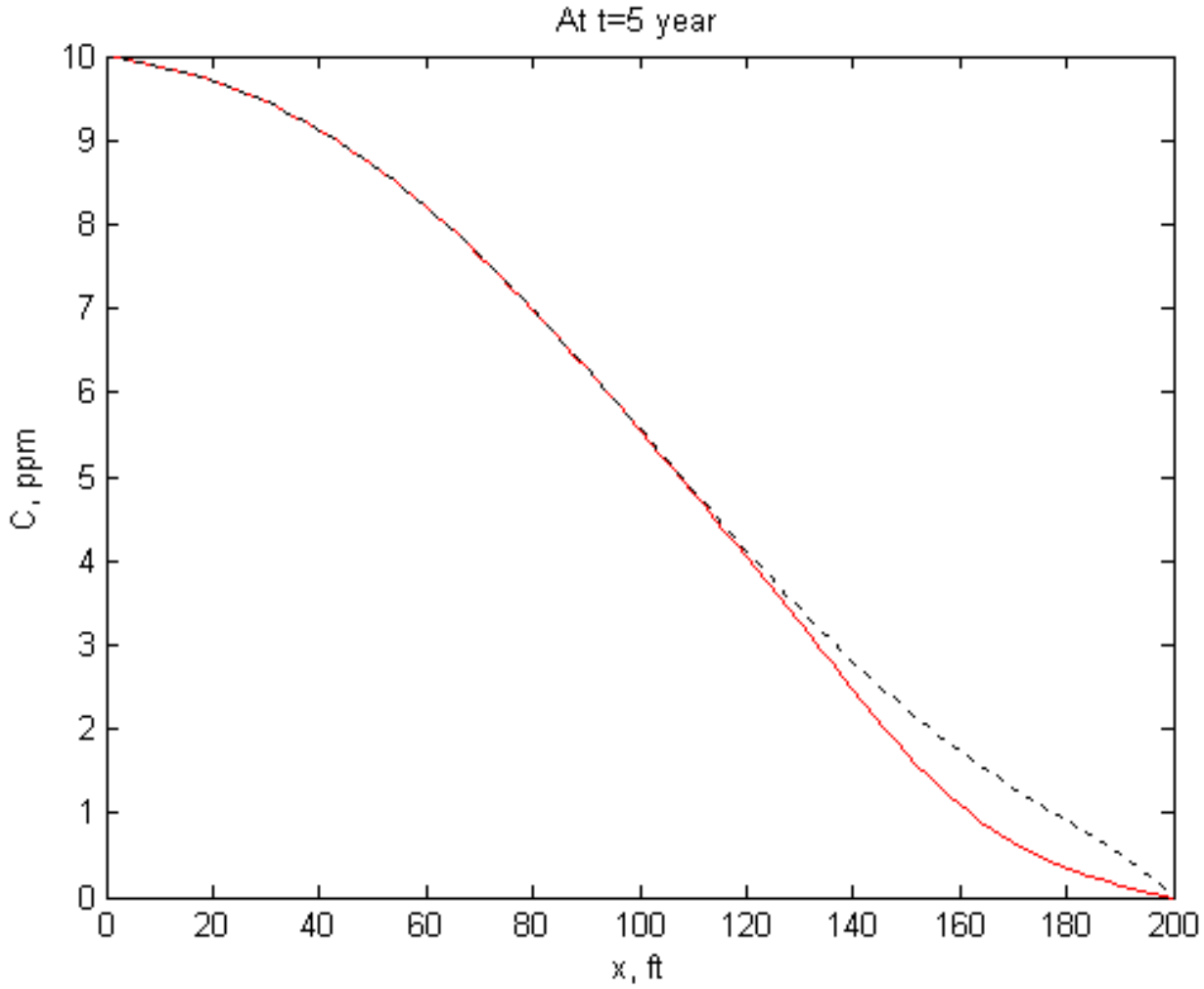

Figure B.1 Concentration Distribution in the Field Application Study.

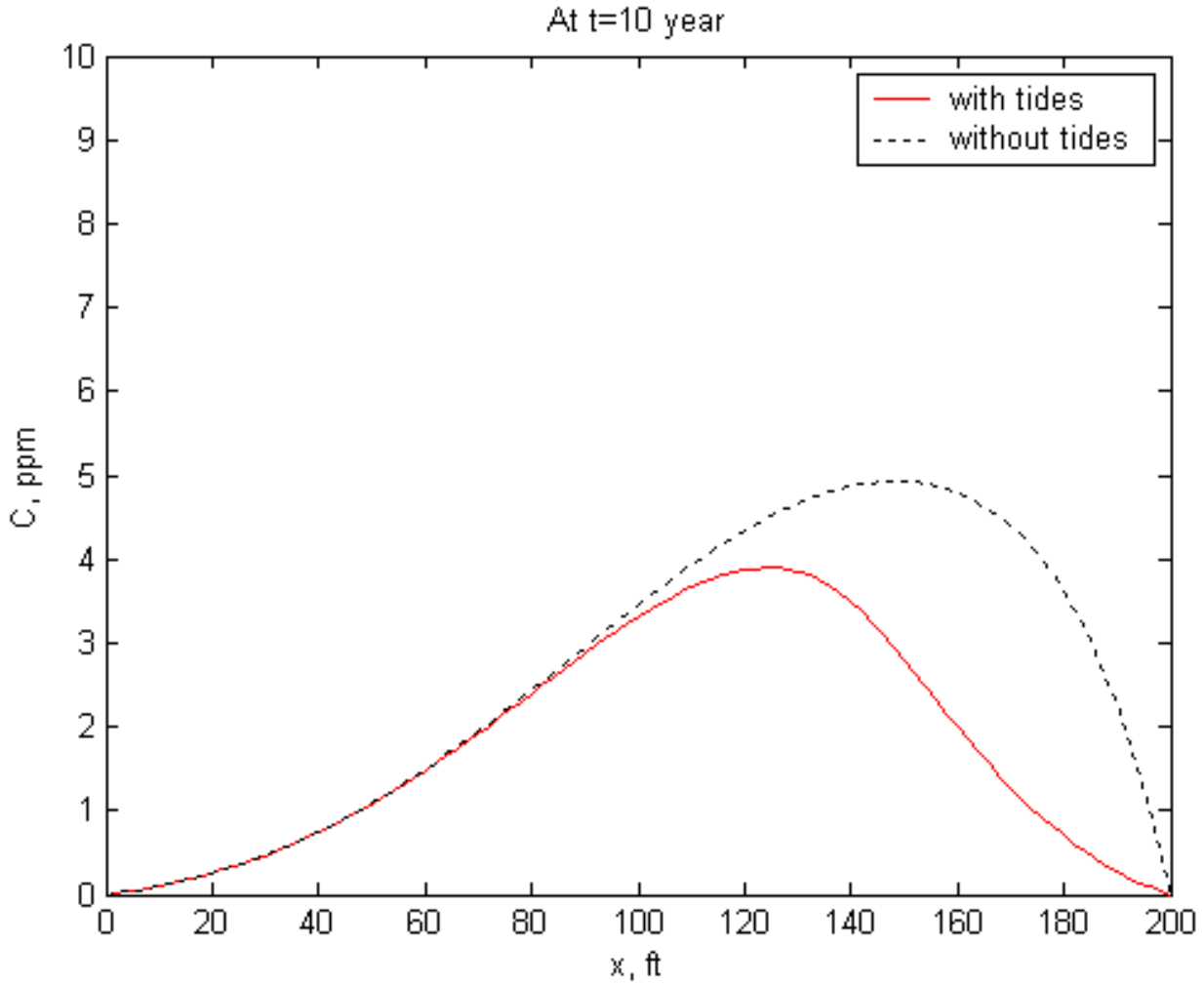

Figure B.1 Concentration Distribution in the Field Application Study (Continued).

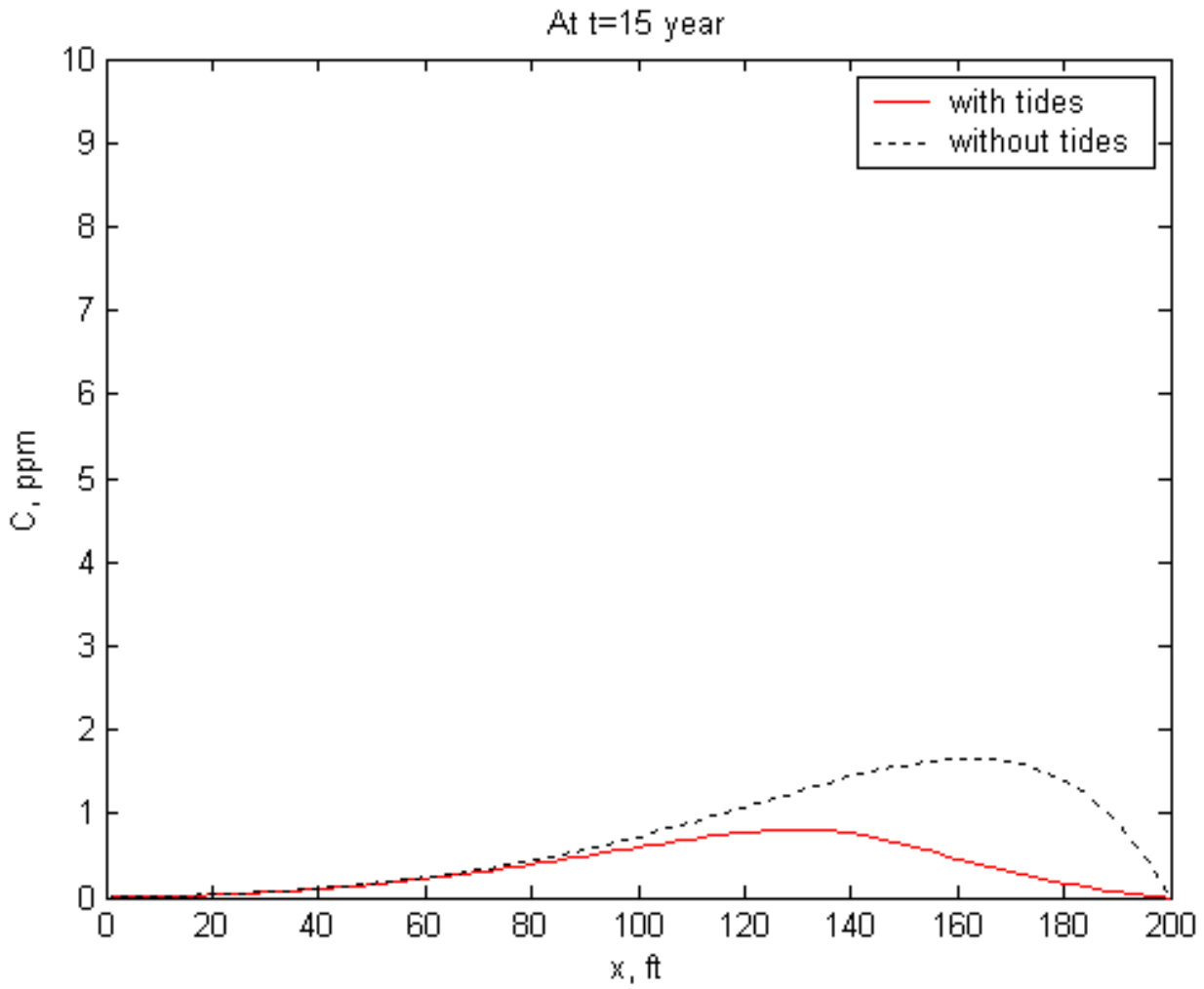

Figure B.1 Concentration Distribution in the Field Application Study (Continued).

Figure B.2 further gives the contaminant discharge profile with tides compared with the case subject to no tides. Because of the retardation, the contaminant plume takes years transporting from the release point inland to the tidal boundary. Specifically, only 36% (without tides) and 58% (with tides) of the total contaminant released discharges out of the system after 7.5 years since the start of the release. Tidal influence is also demonstrated in the discharge increase shown in Figure B.3. During the first half of the course of discharge, tidal fluctuations result in a significant increase in discharge (greater than 50 percent). This is especially true during earlier stage in discharge: discharge is increased by a factor of two after 5 years, and can still be accelerated by over 60 percent after seven and a half years.

This simulation serves as an example of utilizing the numerical solution to simulate the field contaminant transport problem. Similar applications can be accomplished using the numerical model under other conditions by simply changing the data to simulate the new conditions. Field application using the numerical simulation, however, has to proceed with due caution with regard to the assumptions made in the numerical model. In order for the numerical model to give sufficiently accurate predictions of contaminant transport, the field conditions have to closely match the assumptions made for the numerical model.

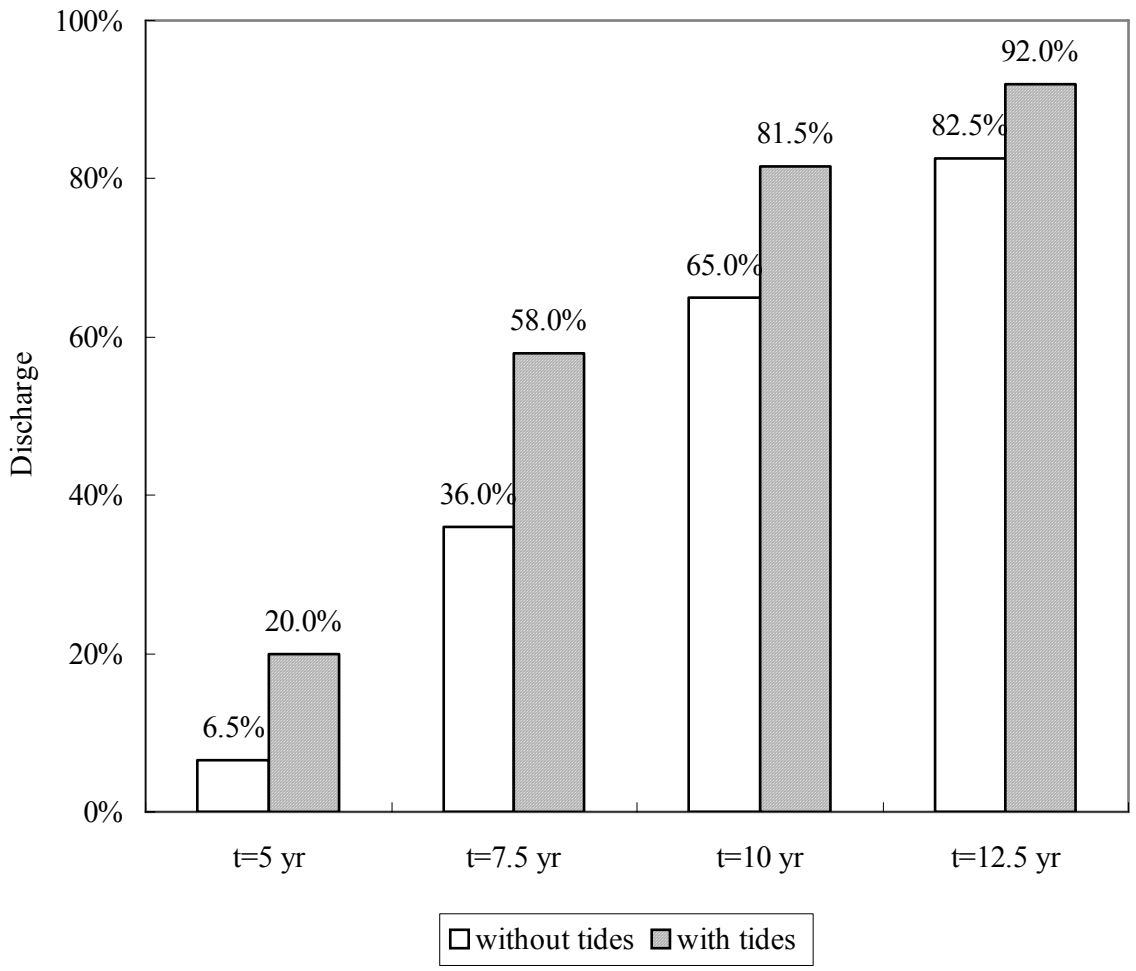

Figure B.2 Contaminant Discharge in the Field Application Study.

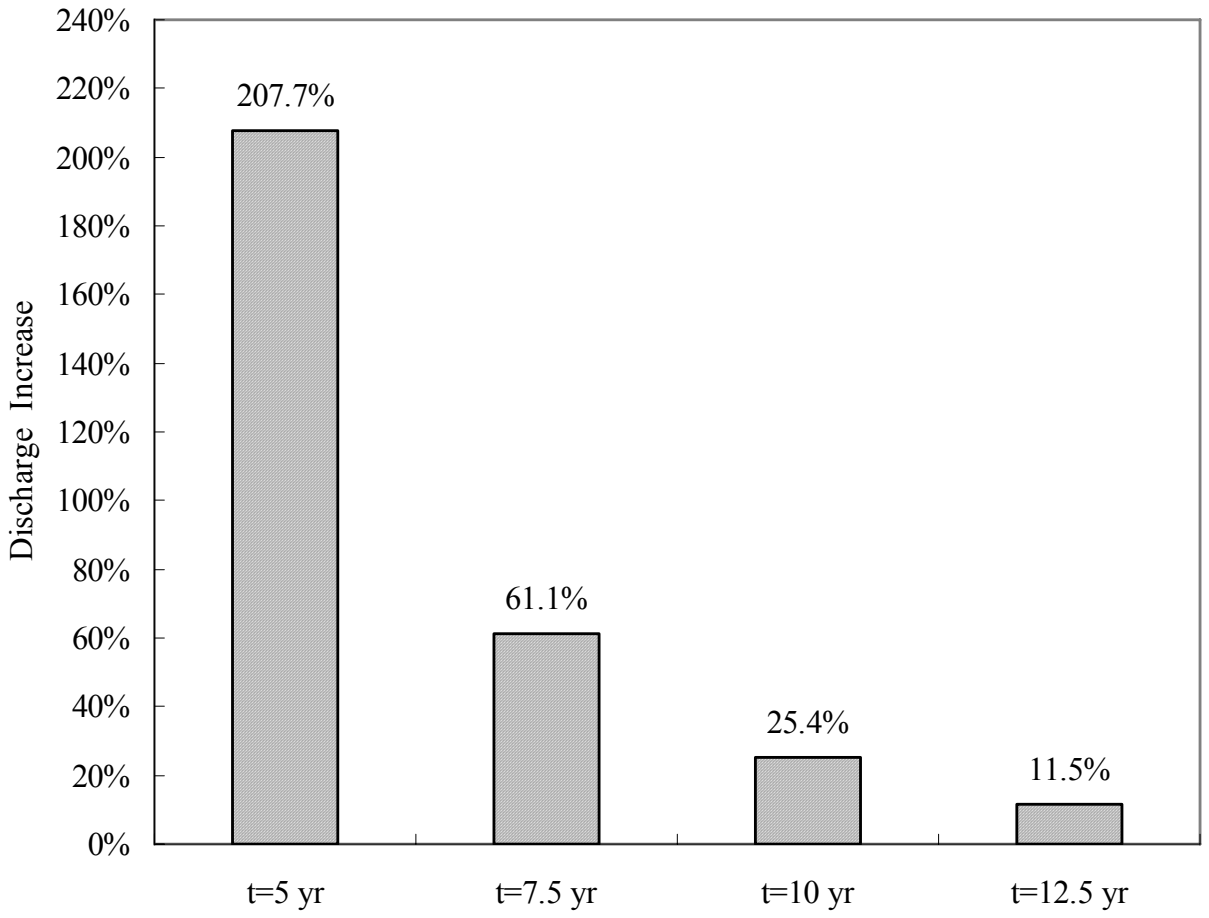

Figure B.3 Contaminant Discharge Increase in the Field Application Study.

REFERENCES

1. Adams, J.E. and M.L. Rhodes, 1960. Dolomitization by seepage refluxion. Bulletin of America Association of Petrologic Geology, 44, 1912-1920.

2. Anderson, M.P., 1984. Movement of contaminants in ground water: Groundwater transport-Advection and dispersion, in Groundwater contamination: Washington, D.C., National Academy Press, 37-45.

3. Ataie-Ashtiani, B., R.E., Volker and D.A. Lockington, 1999. Numerical and experimental study of seepage in unconfined aquifers with a periodic boundary condition. Journal of Hydrology, 222, 165-184.

4. Baird, A.J. and D.P. Horn, 1996. Monitoring and modeling groundwater behavior in sandy beaches. J. Coastal Res., 12 (3), 630-640.

5. Bakker, M., E.I. Anderson, T.N. Olsthoorn and O.D.L. Strack, 1999. Regional groundwater modeling of the Yucca Mountain site using analytic elements. Journal of Hydrology, 226(3-4), 167-178.

6. Barry, D.A., S.J. Barry and J.-Y. Parlange, 1996. Capillary correction to periodic solutions of the shallow flow approximation. In: Pattiaratch, C.B. (Ed.), Mixing Processes in Estuaries and Coastal Seas, Coastal Estuarine Studies, AGU, Washington, DC, 50, 496-510.

7. Baverman, C., L. Moreno and I. Neretnieks, 1995. A fast coupled geochemical and transport program and applications to waste leaching and contaminant transport. International Journal of Rock Mechanics and Mining Science & Geomechanics Abstracts, 32(7), 317A-318A.

8. Bear, J., 1972. Dynamics of fluids in porous media: New York, American Elsevier, 764 p.

9. Bear, J., 1979. Hydraulics of ground water: New York, McGraw Hill, 569 p.

10. Bower, J.W., L.H. Motz and D.W. Durden, 1999. Analytical solution for determining the critical condition of saltwater upconing in a leaky artesian aquifer. J. Hydrol., 221(1), 43-54.

11. Cambareri, T.C. and E.M. Eichner, 1998. Watershed delineation and ground water discharge to a coastal embayment. Ground Water, 36(4), 626-34.

12. Capone, D.G. and M.F. Bautista, 1985. A groundwater source of nitrate in near-shore marine sediments. Nature, 313, 214-216.

13. Carslaw, H.S. and J.C. Jaeger, 1959. Conduction of heat in solids. Oxford University Press, New York.

14. Chow, V.T., 1964. Handbook of Applied Hydrology. McGraw-Hill, New York, N.Y., 1418 p.

15. Churchill, R.V., 1971. Operational mathematics. McGraw-Hill, New York, N.Y.

16. Domenico, P.A. and F.W. Schwartz, 1997. Physical and Chemical Hydrogeology, second edition. John Wiley and Sons, 506 p.

17. Erskine, A.D., 1991. The effect of tidal fluctuation on a coastal aquifer in the UK. Ground Water, 29, 556-62.

18. Ferris, J.G., 1951. Cyclic fluctuations of water levels as a basis for determining aquifer transmissibility. Assemblee General De Bruxelles, Assoc. International D'Hydrologic Scientifique, 2, 148-155.

19. Fetter, C.W., 1994. Applied hydrogeology 3rd ed., Prentice Hall.

20. Finnemore, E.J. and J.B. Franzini, 2002. Fluid mechanics with engineering applications, 10th edition. McGraw-Hill, New York, N.Y., 790 p.

21. Fisher, H.B, E.J. List, R.C.Y. Koh, J, Imberger and N.H. Brooks, 1979. Mixing in inland and coastal waters, Academic Press, Inc., New York.

22. Freeze, R.A. and J.A. Cherry, 1979. Groundwater: Englewood Cliffs, N.J., Prentice-Hall, 604 p.

23. Gallagher, K.L., A.M. Dietrich, W.G. Reay, M.C. Hayes and G.M. Simmons Jr., 1996. Groundwater discharge of agricultural pesticides and nutrients to estuarine surface water. Ground Water Monitoring and Remediation, Winter, 1996, 118-129.

24. Gerke, H.H. and M.T. van Genuchten, 1996. Macroscopic representation of structural geometry for simulating water and contaminant movement in dual-porosity media. Advances in Water Resources, 19(6), 343-357.

25. Gershon, N.D., and A. Nir, 1969. Effects of boundary conditions of models on tracer distribution in flow through porous mediums. Water Resources Research, 5(4), 830-839.

26. Ghebart, B., Y. Jaluria, R.L. Mahajan and B. Sammakia, 1988. Buoyancy-induced flows and transport. Hemisphere/Harper and Row, New York.

27. Giblin, A.E. and A.G. Gaines, 1990. Nitrogen inputs to a marine embayment: The importance of groundwater. Biogeochemistry, 10, 309-328.

28. Glover, R.E., 1959. The pattern of fresh-water flow in a coastal aquifer. Journal of Geophysics Researches, 64(4), 457-469.

29. Gregg, D.O., 1966. An analysis of groundwater fluctuations caused by ocean tides in Glynn County, Georgia. Ground Water, 4(3), 24-32.

30. Herbert, A.W., C.P. Jackson and D.A. Lever, 1988. Coupled groundwater flow and contaminant transport with fluid density strongly dependent upon concentration. Water Resources Research, 24, 1781-1795.

31. Huber, Ludwig, 1993. Good laboratory practice-A primer. Hewlett-Packard Primer, publication number 12-5091-6259E.

32. Ippen, A.T., 1966. Estuary and coastline hydrodynamics. McGraw-Hill, New York.

33. Jiao, J.J., Z. Tang, 1999. An analytical solution of groundwater response to tidal fluctuation in a leaky confined aquifer. Water Resources Research, 35(3), 747-751.

34. Johannes, R.E., 1980. The ecological significance of the submarine discharge of groundwater. Marine Ecology Progress, series 3, 365-373.

35. Kim, J.M. and R.R. Parizek, 1997. Numerical simulation of the Noordbergum effect resulting from groundwater pumping in a layered aquifer system. Journal of Hydrology, 202(1-4), 231-243.

36. Kim, K., M.P. Anderson and C.J. Bowser, 2000. Enhanced dispersion in groundwater caused by temporal changes in recharge rate and lake levels. Advances in Water Resources, 23(6), 625-635.

37. Kohout, F.A., 1965. A hypothesis concerning cyclic flow of salt water related to geothermal heating in the Floridian aquifer. Trans. New York Academy Science Series, 2(28), 249-271.

38. Kolditz, O., R. Ratke, H.G. Diersch and W. Zielke, 1998. Coupled groundwater flow and transport: 1. Verification of variable density flow and transport models. Advances in Water Resources, 21(1), 27-46.

39. Lambrakis, N. and G. Kallergis, 2001. Reaction of subsurface coastal aquifers to climate and land use changes in Greece: modelling of groundwater refreshening patterns under natural recharge conditions. Journal of Hydrology, 245(1-4), 19-31.

40. Lanyon, J.A., I.G. Eliot, and D.J. Clarke, 1982. Groundwater level variation during semi-diurnal spring tidal cycles on sandy beaches. Australia Journal of Marine Freshwater Researches, 33, 377-400.

41. Lee, T.-C., 1999. Applied mathematics in hydrogeology. Lewis Publishers.

42. Li, H.L. and J.J. Jiao, 2003. Tide-induced seawater–groundwater circulation in a multi-layered coastal leaky aquifer system. Journal of Hydrology, 274, 211-224.

43. Li, L. and D.A. Barry, 2000. Wave-induced beach groundwater flow. Advances in Water Resources, 23, 325-337.

44. Li, L., D.A. Barry and C.B. Pattiaratchi, 1997. Numerical modeling of tide-induced beach water table fluctuations. Coastal Engineering, 30, 105-123.

45. Li, L., D.A. Barry, C. Cunningham, F. Stagnitti and J.Y. Parlange, 2000. A two-dimensional analytical solution of groundwater responses to tidal loading in an estuary and ocean. Advances in Water Resources, 23, 825-833.

46. Li, L., D.A. Barry, J.-Y. Parlange and C.B. Pattiaratchi, 1997. Beach water table fluctuations due to wave run-up: Capillarity effects. Water Resources Research, 33(5), 935-945.

47. Li, L., D.A. Barry, F. Stagnitti and J.-Y. Parlange, 1999. Submarine groundwater discharge and associated chemical input to a coastal sea. Water Resources Research, 35(11), 3253-3259.

48. Li, L., D.A. Barry, F. Stagnitti and J.-Y. Parlange, 2000a. Groundwater waves in a costal aquifer: A new governing equation including vertical effects and capillarity. Water Resources Research, 36(2), 411-420.

49. Li, L., D.A. Barry, F. Stagnitti, J.-Y. Parlange and D.-S. Jeng, 2000b. Beach water table fluctuations due to spring-neap tides: moving boundary effects. Advances in Water Resources, 23, 817-824.

50. Manheim, F.T., 1967. Evidence for submarine discharge of water on the Atlantic continental slope of the southern United States, and suggestions for further research. Trans. New York Academy Science Series, 2(29), 839-852.

51. Marsh, J.A. 1977. Terrestrial inputs of nitrogen and phosphates on the fringing reefs on Guam. Proceedings: Third International Coral Reef Symposium, 331-336. University of Miami, Miami, Florida.

52. Moore, W.S., 1996. Large groundwater inputs to coastal waters revealed by ^{226}Ra enrichments. Nature, 380, 612-614.

53. Moore, W.S., 1999. The subterranean estuary: A reaction zone of groundwater and seawater. Marine Chemistry, 65, 111-125.

54. Naji, A., D. Ouazar and A.H.D. Cheng, 1998. Locating the saltwater-freshwater interface using nonlinear programming and h-adaptive BEM. Engineering Analysis with Boundary Elements, 21(3), 253-259.

55. Nielsen, P., J.D. Fenton, R.A. Aseervathan and P. Perrochet, 1997. Water table waves in aquifers of intermediate depths. Advances in Water Resources, 20, 37-43.

56. Nielson, P., 1990. Tidal dynamics of the water table in beaches. Water Resources Research, 26(9), 2127-2134.

57. Nixon, S.W., C.A. Oviatt, J. Frithsen and B. Sullivan, 1986. Nutrients and the productivity of estuarine and coastal marine ecosystems. Journal of limnology society South Africa, 12, 43-71.

58. Oude Essink, G.H.P., 2001. Saltwater intrusion in 3D large-scale aquifers: a dutch case, Physics and Chemistry of the Earth, Part B: Hydrology, Oceans and Atmosphere, 26(4), 337-344.

59. Parker, J.C. and M.T. van Genuchten, 1984. Flux-averaged and volume-averaged concentrations in continuum approaches to contaminant transport. Water Resources Research, 20(7), 866-872.

60. Pinder, G.F. and H.H. Cooper, 1970. A numerical technique for calculating the gradient position of the saltwater front. Water Resources Research, 6(3), 875-882.

61. Portnoy, J.W., B.L. Nowicki, C.T. Roman and D.W. Urish, 1998. The discharge of nitrate-contaminated groundwater from developed shoreline to marsh-fringed estuary. Water Resources Research, 34(11), 3095-3104.

62. Reilly, T.E., and A.S. Goodman, 1985. Quantitative analysis of saltwater-freshwater relationships in groundwater systems-a historical perspective. Journal of Hydrology, 80, 125-160.

63. Ruan, F., D. Mclaughlin, and S.G. Li, 1999. A general technique for assessing the numerical accuracy of contaminant transport models. Water Resources Research, 35(12), 3961-3966.

64. Sandrin, S.K., F.L. Jordan, R.M. Maier and M.L. Brusseau, 2001. Biodegradation during contaminant transport in porous media: 4. Impact of microbial lag and bacterial cell growth. Journal of Contaminant Hydrology, 50(3-4), 225-242.

65. Schincariol, R.A. and F.W. Schwartz, 1990. An experimental investigation of variable density flow and mixing in homogeneous and heterogeneous media. Water Resources Research, 26(10), 2317-2329.

66. Sen, T.K., N. Nalwaya and K.C. Khilar, 2002. Colloid-associated contaminant transport in porous media: 2. Mathematical modeling. AIChE Journal, 48(10), 2375-2385.

67. Serfes, M.E., 1987. Interpretation of tidally affected groundwater flow systems in pollution studies. Proceedings of Petroleum Hydrocarbons and Organic Chemicals in Ground Water: Prevention, Detection and Restoration, November 17-19, 1987.

68. Serfes, M.E., 1991. Determining the mean hydraulic gradient of ground water affected by tidal fluctuations. Ground Water, 29, 549-555.

69. Serrano, S.E., 2001. Contaminant transport under non-linear sorption and decay. Water Research, 35(6), 1525-1533.

70. Sewell, P.L., 1982. Urban groundwater as a possible nutrient source for an estuarine benthic algal bloom. Estuarine coastal shelf Science, 15, 569-576.

71. Silliman, S.E., 1995. Particle transport through two-dimensional, saturated porous media: influence of physical structure of the medium. Journal of Hydrology, 167(1-4), 79-98.

72. Silliman, S.E., http://www.nd.edu/%7Esilliman/piez.html. Last update on November 13, 2003.

73. Silliman, S.E., L. Zheng and P. Conwell, 1998. The use of laboratory experiments for the study of conservative contaminant transport in heterogeneous porous media. Hydrogeology Journal, 6, 166-177.

74. Simmons, C.T. 1990. Submarine groundwater discharge abstracts from meeting of the North American Benthological Society, Virginia Polytechnic Institute, Blacksburg, Virginia, May 20-25, 1990. NABS Bulletin 7, 52.

75. Simmons, C.T., E. Miles, W.G. Reay and D.L. Gallagher. 1992. Submarine groundwater discharge quality in relation to land use patterns in the southern Chesapeake Bay. In Proceedings of the 1st International Conference on Groundwater Ecology. ed. J.A. Stanford and J.J. Simons, 341-350. Bethesda, Maryland: American Water Resources Association.

76. Simmons, C.T., T.R. Fenstemaker and J.M. Sharp, Jr., 2001. Variable-density groundwater flow and contaminant transport in heterogeneous porous media:

approaches, resolutions and future challenges. Journal of Contaminant Hydrology, 52(1-4), 245-275.

77. Simms, M., 1984. Dolomitization by ground water flow systems in carbonate platforms. Trans. Gulf Coast Association Geologic Society, 34, 411-420.

78. Teo, H.T., D.S. Jeng, B.R. Seymour, D.A. Barry and L. Li, 2003. A new analytical solution for water table fluctuations in coastal aquifers with sloping beaches. Advances in Water Resources, 26, 1239-1247.

79. Thomas, J.W., 1995. Numerical partial differential equations: finite difference methods. Springer-Verlag New York, Inc., 437 p.

80. Todd, D.K., 1959, Ground-water hydrology. New York, John Wiley and Sons, Inc., 336 p.

81. Todd, D.K., 1980. Groundwater hydrology, 2nd edition. New York, John Wiley and Sons, Inc., 535 p.

82. Townley, L.R., 1995. The response of aquifers to periodic forcing. Advances in Water Resources, 18(3), 125-146.

83. Valiela, I., G. Collins, J. Kremer and K. Lajtha, 1992. Couplings of watersheds and coastal waters: Sources and consequences of nutrient enrichment in Waquoit Bay, Massachusetts. Estuaries, 15, 443-457.

84. Valiela, I., J.M. Teal, S. Vkmann, D. Shafer and E.J. Carpenter, 1978. Nutrient and particulate fluxes in a salt marsh ecosystem: Tidal exchanges and inputs by precipitation and groundwater. Limnology Oceanography, 23(4), 798-812.

85. van Genuchten, M.T. and W.J. Alves, 1982, Analytical solutions of the one-dimensional convective-dispersive contaminant transport equation: U.S. Department of Agriculture Technical Bulletin 1661, 151 p.

86. Volker, R.E. and K.R. Rushton, 1982. An assessment of the importance of some parameters for seawater intrusion in aquifers and a comparison of dispersive and sharp-interface modeling approaches. Journal of Hydrology, 56, 239-250.

87. Volker, R.E., Q. Zhang and D.A. Lockington, 2002. Numerical modeling of contaminant transport in coastal aquifers. Mathematics and Computers in Simulation, 59, 35-44.

88. Voss, C.I., 1984. SUTRA: a finite element simulation model for saturated-unsaturated, fluid-density dependent groundwater flow with energy transport or

chemically reactive single species contaminant transport. U.S. Geological Survey, National Center, Reston, Virginia.

89. Waygal, R.J., 1963. Construction of models that simulate oil reservoirs. Journal of the Society of Petroleum Engineering, 281-286.

90. Wexler, E.J., 1992. Analytical solutions for one-, two-, and three-dimensional contaminant transport in groundwater systems with uniform flow. U.S. Geological Survey Techniques of Water Resources Investigations, Book 3, Chapter B7, 190 p.

91. Whitaker, F.F. and P.L. Smart, 1997. Groundwater circulation and geochemistry of a karstified bank–marginal fracture system, South Andros Island, Bahamas. Journal of Hydrology, 197(1-4), 293-315.

92. White, D.E., J.D. Hem and G.A. Waring, 1963. Data of geochemistry, sixth edition, chapter F. Chemical composition of subsurface waters. U.S. Geological Survey, Professional Paper, 440-F, 67 p.

93. White, J.K. and T.O.L. Roberts, 1994. The significance of groundwater tidal fluctuations. Proceedings of the International Conference Organized by the Institution of Civil Engineers, London, Wilkinson WB (ed.), 31-42.

94. Wrenn, B.A., M.T.Suidan, K.L. Strohmeier, B.L. Eberhart, G.J. Wilson and A.D. Venosa, 1997. “Nutrient transport during bioremediation of contaminated beaches: evaluation with lithium as a conservative tracer.” Water Research, 31(3), 515-524.

95. Yim, C.S. and M.F.N. Mohsen, 1992. Simulation of tidal effects on contaminant transport in porous media. Ground Water, 30(1), 78-86.

96. Zhang, Q., R.E. Volker and D.A. Lockington, 2001. Influence of seaward boundary condition on contaminant transport in unconfined coastal aquifers. Journal of Contaminant Hydrology, 49, 201-215.

97. Zhang, Q., R.E. Volker and D.A. Lockington, 2002. Experimental investigation of contaminant transport in coastal groundwater. Advances in Environmental Research, 6, 229-237.